UNIVERSITÉ DE STRASBOURG

ÉCOLE DOCTORALE des SCIENCES de la Vie et de la Santé **IGBMC –**

CNRS UMR 7104 – INSERM U1258

THÈSE présentée par :

Kamar GHAIBOUR

Soutenue publiquement le : **09 Septembre 2022**

Pour obtenir le grade de : **Docteur de l'Université de Strasbourg** Discipline/

Spécialité : Aspects moléculaires et cellulaires de la biologie

Unravelling the Role of Androgens in Skeletal Muscle Progenitor Cells and Myofibers

THÈSE dirigée par :

Dr. Metzger Daniel Directeur de recherches, IGBMC, Université de Strasbourg

RAPPORTEURS :

Dr. Buj Bello Ana Directrice de recherches, Université Paris Saclay

Prof. Tuckermann Jan Directeur de recherches, Université d'ULM

AUTRES MEMBRES DU JURY :

Dr. Plateroti Mechelina Directrice de recherches, Université de Strasbourg

---

INVITÉE : Dr. Duteil Delphine Chargée de recherches, IGBMC, Université de Strasbourg

In the memory of my father
Mohamed Kassem Ghaibour, Abu Kassem
For the love he gave
For the light he shed

Acknowledgments.

First and foremost, I would like to express my sincere appreciation for my jury members Prof. Jan Tuckermann, Dr. Ana Buj Bello, and Dr. Michelina Plateroti, for taking their time to evaluate my thesis and giving their valuable feedback.

I want to express my gratitude to my Ph.D. supervisor, Dr. Daniel Metzger, who guided me throughout this project, who was a true mentor, and taught me everything I know about critical thinking and scientific writing.

I would like to sincerely thank Dr. Delphine Duteil for her guidance and patience during the past five years, for answering every little question I had, and for her precious help with experiments.

I would also like to thank all my lab colleagues for the insightful discussions and feedback during my Ph.D., especially Dr. Mohamed AbouElmaaty and Dr. Daniela Rovito.

This project would not have been possible without the support of many people at IGBMC. Many thanks to Claudine Ebel, Muriel Philipps, Nadia Messaddeq, Erwan Grandgirard, Tao Ye, platforms, Mouse facility, Genomics, Flow cytometry, Histology, Electron microscopy, and Imaging.

I want to thank the fantastic trio Sandra, Ghina, and Syrine. Without their encouragement and love, I would've been unable to go through my Ph.D.

I wish to extend my special thanks to my IGBMC duo, Dounia, for always being there for me and making me laugh every day.

I wish to show my appreciation to my favorite student of all times, Joe, for his kindness, support, and fantastic help with writing.

I would like to sincerely thank everyone who felt I was worthy of their support and help since I arrived in France. So many names I need to mention many names here, and I'm grateful to have met each of them: Camille, Priscila, Laureen, Lucas, Lucile, Olivia, Myriam, and of course, my partner in crime since 2017, May Rahme.

I want to thank my family, my first and last inspiration and ambition source, for their support, for believing in me, and for being proud of me.

Impact of Covid19 pandemic on the project.

In October 2019, I started my Ph.D. thesis work on the role of the androgen receptor in muscle stem cells, the satellite cells. To this end, in the lab, we started breeding a mouse model in which the androgen receptor is selectively ablated in satellite cells using the Cre-LoxP system. Until the end of 2019, I had received one cohort in which we explored the regeneration capacity of tibialis muscles upon injury. Unfortunately, the early 2020 Covid19 pandemic hit. The country underwent confinement, and our institute was closed for two months; for this reason, we had to stop all mice breeding and sacrifice newborn offspring.

At the beginning of May 2020, we returned to our laboratories and started animal breeding. However, the changing in the environment and the routine of mice during the lockdown affected their energy. The mice were not collaborative and many research teams, including ours, faced problems restarting their animal models.

While waiting for my mouse model, I used this time to collaborate with some of my colleagues and learn valuable techniques like ChIP-seq and FACS sorting, resulting in a co-authorship published in the prestigious journal of nucleic acid research (see Annexes). Finally, in October 2020, I received my first post-covid cohort of mice and started over my project. The results presented in this thesis were obtained between October 2020 and April 2022.

Table of Contents

Table of figures

Introduction

Discussion

Introduction

List of abbreviations

AA : Amino Acid

ACh : Acetylcholine

ADAM : Androgen Deficiency in the Aging Male

AF-1 : transactivation function 1

AF-2 : transactivation factor 2

AMP : Adenosine Monophosphate

AMPK : AMP-activated protein kinas

Ang1 : Angiopoitin 1

AR : Androgen Receptor

ARE : Androgen Response Elements

BCKAs : Branched-Chain α-Keto Acids

BCKDH : Branched-Chain α-Keto Acid Dehydrogenase complex

CALCR : Calcitonin Receptor

CD : Cluster of differentiation

CDKIs : Cyclin-Dependent Kinase Inhibitors

CDKs : Cyclin-Dependent Kinases

CFZS : Carey-Fineman-Ziter Syndrome

CK : Creatine Kinase

Col: Collagens

Cpt1 : Carnitine palmitoyl transferase I

CXCR4 : C-X-C chemokine receptor type 4

DAG : Dystrophin Associated Group

DBD : DNA Binding Domaine

DHPR : Dihydropyridine receptors

Dll4 : Delta like 4

DMD : Dystrophin

DNA : Deoxyribonucleic acid

DRIP : Vitamin D Receptor Interacting Protein

ECM : Extracellular Matrix

EGF : Epidermal Growth Factor

eMHC : Embryonic Myosin Heavy Chain

eMHCI : Slow Embryonic Myosin Heavy Chain

eMHCII : Fast Embryonic Myosin Heavy Chains

ER : Estrogen Receptor

ETC : Electron Transport Chain

FAD2+ : Flavin adenine dinucleotide

FAPs : Fibro-Adipogenic Progenitors

FGF : Fibroblast Growth Factor

FN : Fibronectin

FSH : Follicle-Stimulating Hormone

FST : Follistatin

Fzd7 : Frizzled-7

G-CSF : Granulocyte Colony-Stimulating Factor

GLUT4 : Insulin Responsive Glucose Transporter 4

GnRH : Gonadotropin-Releasing Hormone

GR : Glucocorticoid Receptor

HGF : Hepatocyte Growth Factor

IGF1 Insulin-like Growth Factor 1

IL : Interleukin

Itga7 : Integrin Alpha 7

Itgb1 : Integrin beta 1

JNK : c-Jun N-terminal kinas

Klf7 : Kruppel-Like Factor 7

Lama : Laminin

LBD : Ligand Binding Domaine

LGMDR23 : Muscular Dystrophy, Limb-Girdle, autosomal recessive 23

LH : Luteinizing Hormone

Lipolysis : Triglyceride lipase

LPL : Enzyme lipase

Mcad : M-cadherin

MCK : Muscle Creatine Kinase

MDC1A : Muscular Dystrophy, Congenital Merosin-Deficient 1a

MRF4 : Myogenic Regulatory Factor 4

MRFs : Myogenic Regulatory Factors

MSTN : Myostatin

mtDNA : mitochondrial DNA

mTOR : the mammalian Target Of Rapamycin

Myf5 : Myogenic factor 5

MYMK : Myomaker

MyoD : Myoblast determination protein

MYODRIF : Myopathy, Congenital, With Diaphragmatic Defects, Respiratory Insufficiency, And Dysmorphic Facies

Myog : Myogenin

MYOSCO Progressive Congenital Myopathy with Scoliosis

NAD+ : Nicotinamide adenine dinucleotide

N-cam : Neural cell adhesion molecule

NCAM : Neural Cell Adhesion Molecule

NEFA : Non-esterified fatty acids

NLS : Nuclear Localization Signal

NMJ : Neuromuscular Junction

NO : Nitric Oxide

NRs : Nuclear Receptors

NTD : N-terminal Domain

PADAM : Partial Androgen Deficiency in the Aging Male

Pax3 : Paired box 3

Pax7 : Paired box 7

P-creatine : Phosphorylated creatine

PI3K : Phosphoinositide 3-kinases

PPARα : Peroxisome Proliferator activated Receptor alpha

PR : Progesterone Receptor

ROS : Reactive Oxidative Species

RYR : Ryanodine receptors

SARM : Selective Androgen Receptor Modulator

SatC : Satellite cells

SBMA : Spinal and Bulbar Muscular Atrophy

SCA1 : Stem Cell Antigen 1

scRNAseq : Single-Cell Ribonucleic acid Sequencing

Sdf1 : Stromal derived factor 1

SERCA : Sarco endoplasmic reticulum Ca2+ ATPase

Spry1 : Sprouty1

SR : Sarcoplasmic reticulum

StAR : Steroidogenic Activator protein

Syn3/4 : Syndecan 3 and 4

TCA cycle : Krebs cycle's oxidation

TGF-β : Transforming growth factor beta

Tie2 : endothelium-specific receptor tyrosine kinase2

TNF-a : Tumor Necrosis Factor alpha

TNNT : Troponin

TPM1 : Tropomyosin

TRAP : Thyroid Hormone Receptor-Associated protein

T-tubules : Transversal tubules

VEGF : Vascular Endothelial Growth Factor

WISP1 : Wnt1-inducible signaling pathway protein 1

1 Skeletal muscles

Skeletal muscles represent up to 40 % of the adult body weight of mammals and are composed of striated multinucleated myofibers. Skeletal muscles play a fundamental role in breathing, posture, and energy production, although their primary role is movement via the contraction of muscle fibers. This chapter will summarise the common knowledge and recent discoveries regarding skm.

1.1 Embryonic development of skeletal muscles

During embryogenesis, skeletal muscles drive from the paraxial mesoderm that segments into somites on both sides of the neural tube and notochord. The ventral part of the somites, named sarcolemma, generates the bones and cartilages, whereas the dorsal region, also called dermatomyotome, gives rise to the back derma from its epaxial extremity and skeletal muscles of the body and limbs from the hypaxial part (Figure 1) (Buckingham et al., 2003).

Limb muscle progenitors expressing the transcription factors Paired box 3 (PAX3) and 7 (PAX7) delaminate from the dermatomyotome and migrate into the limb bud. Of note, only the early embryonic muscle of the myotome forms in the absence of both PAX3 and PAX7 with no advanced stages of muscle development (Relaix et al., 2005). Once in position, muscle precursors express myogenic factor 5 (MYF5) and myoblast determination protein (MYOD) transcription factors and undergo extensive proliferation and generate myoblasts. The latter differentiate and express myogenin-forming myocytes that fuse to give rise to myotubes and, ultimately, multinucleated myofibers (Buckingham et al., 2003). Noteworthy, MYF5/MYOD null mice embryos do not form limbs, and precursors adopt another cell fate (Rudnicki et al., 1993).

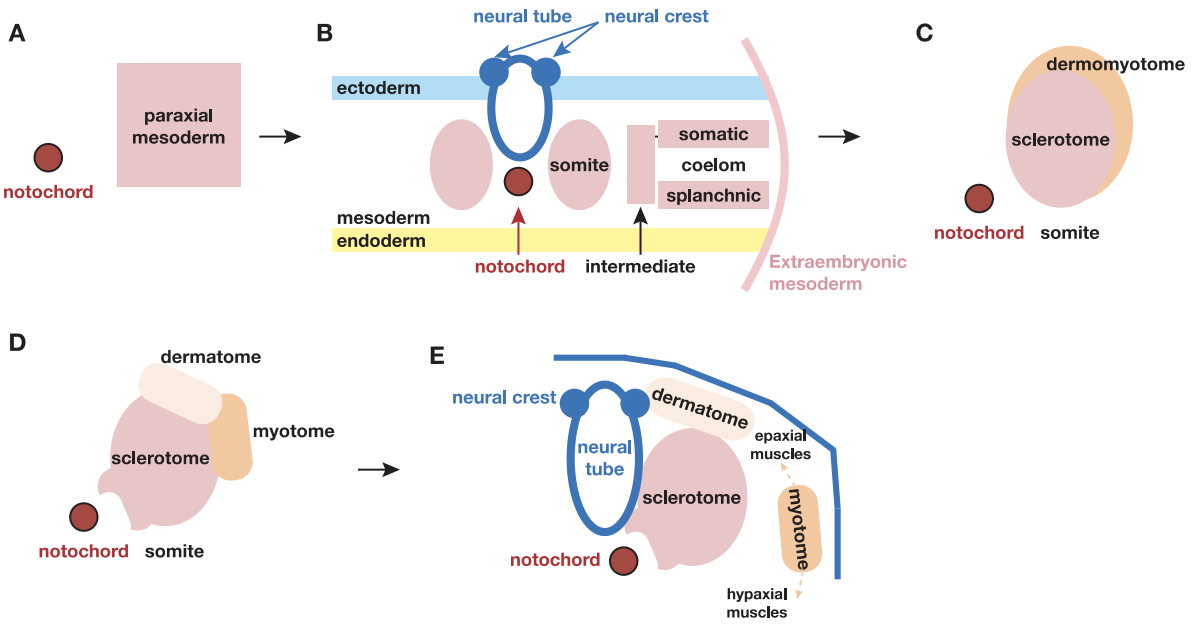

Figure 1: Embryonic development of skeletal muscles (adapted from Buckingham et al., 2003).

The first muscle fibers, known as primary fibers, appear in mice at about embryonic day (E) 11-14, expressing slow embryonic myosin heavy chain (eMHCI), yet secondary fibers form when limb innervation begins to be established around E 14.5-17.5. Initially, secondary myotubes are smaller than primary, but later they increase in size and emerge to express fast embryonic myosin heavy chains (eMHCII) A, B, and X (Buckingham et al., 2003). It has been proposed that approximately 5 % of myoblasts remain quiescent in the limb and form muscle stem cells, also known as the satellite cells (SatC). SatC participate in the pre-and postnatal development of skeletal muscles as well as in their regeneration upon injury (Almeida et al., 2016).

1.2 Structure of skeletal muscles

Skeletal muscles are composed of several highly organized bundles of myofibers. Each myofiber is covered by the endomysium and is formed by the assembly of myofibrils containing the basic contracting unit of skeletal muscles, the sarcomere (Figure 2). Each myofiber bundle is surrounded by connective tissue called perimysium to form a muscle fascicle, and the ensemble of fascicles is gathered via a dense connective tissue named epimysium (Figure 2). Connective tissues link individual myofibers to the tendons and provide a pathway for blood vessels, lymphatics, and nerve fibers (Figure 2).

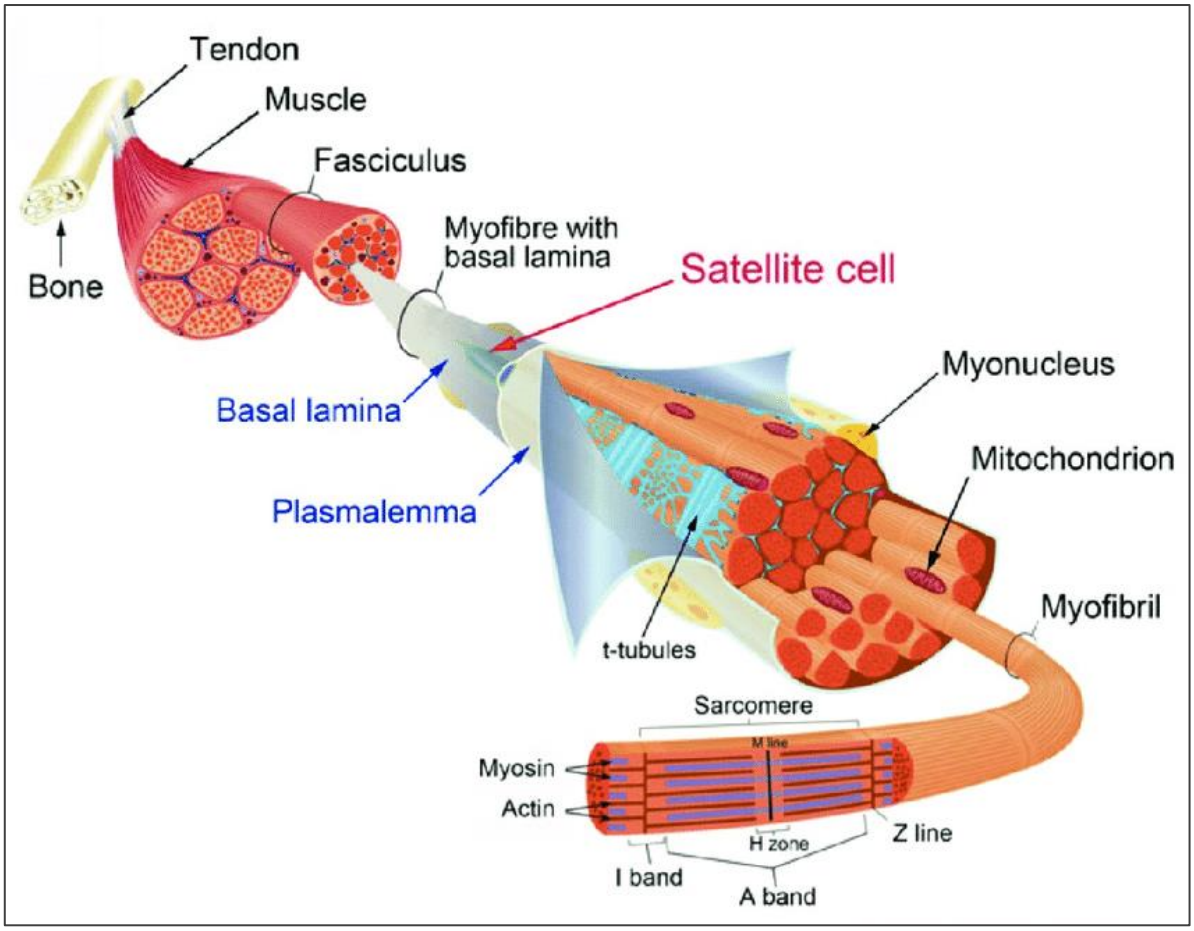

Figure 2: Skeletal muscle structure (adapted from Buckingham et al., 2003).

1.2.1 Myofibers

A myofiber is about 100 µm in diameter and spans the entire muscle length. Myofiber cell membrane is named sarcolemma, and its cytoplasm is called sarcoplasm (Figure 3) (Mukund & Subramaniam, 2020). The sarcolemma invaginates regularly, forming tubular structures known as the transversal tubules (T-tubules). On both sides of the T-tubule, the fiber sarcoplasmic reticulum (SR) is located, where the intracellular calcium Ca^{+2} is stored (Mukund & Subramaniam, 2020).

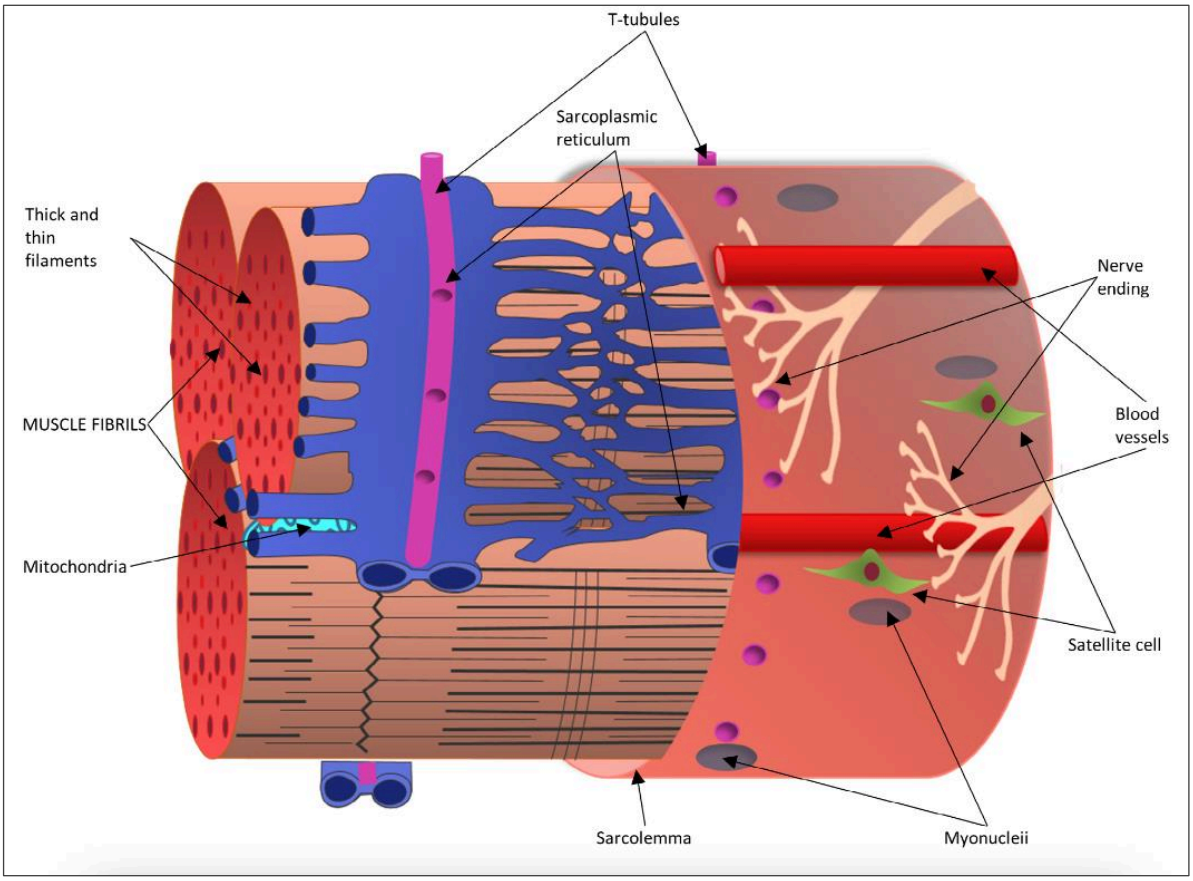

Figure 3: Myofiber structure (adapted from Mukund & Subramaniam, 2020).

1.2.2 Myofibrils, the contractile unite

Myofibrils represent up to 80 % of muscle fiber mass and are cylindric structures with a diameter of around 1-2 µm and extend all along the muscle length (Figure 2). They are formed of repeated contractile structures called sarcomeres (Figure 2). Sarcomeres, the contractile unit of skeletal muscles, are composed of two main types of protein filaments, thick, which is formed of myosin heavy chains, and thin, which is comprised of polymerization of globular actin molecules. When viewed under a microscope, the sarcomere exhibits two distinct bands: a dark band known as A-band, where the thin and thick filaments overlap, and a light band named I-band, where a portion of thin filaments is located (Figures 2 and 4). The alteration between the dark and the light bands leads to the striation appearance of skeletal muscles

(Figure 4) (Gollapudi et al., 2014). The dark region is connected by the M-line, where the thick filaments originate (Figure 4). Moreover, the light I-band is bound by the Z-disc, and a giant protein links both lines termed titin (Figures 4 and 5). The area between two Z-lines is called the sarcomere, which can produce force by interacting with the various proteins (Mukund & Subramaniam, 2020).

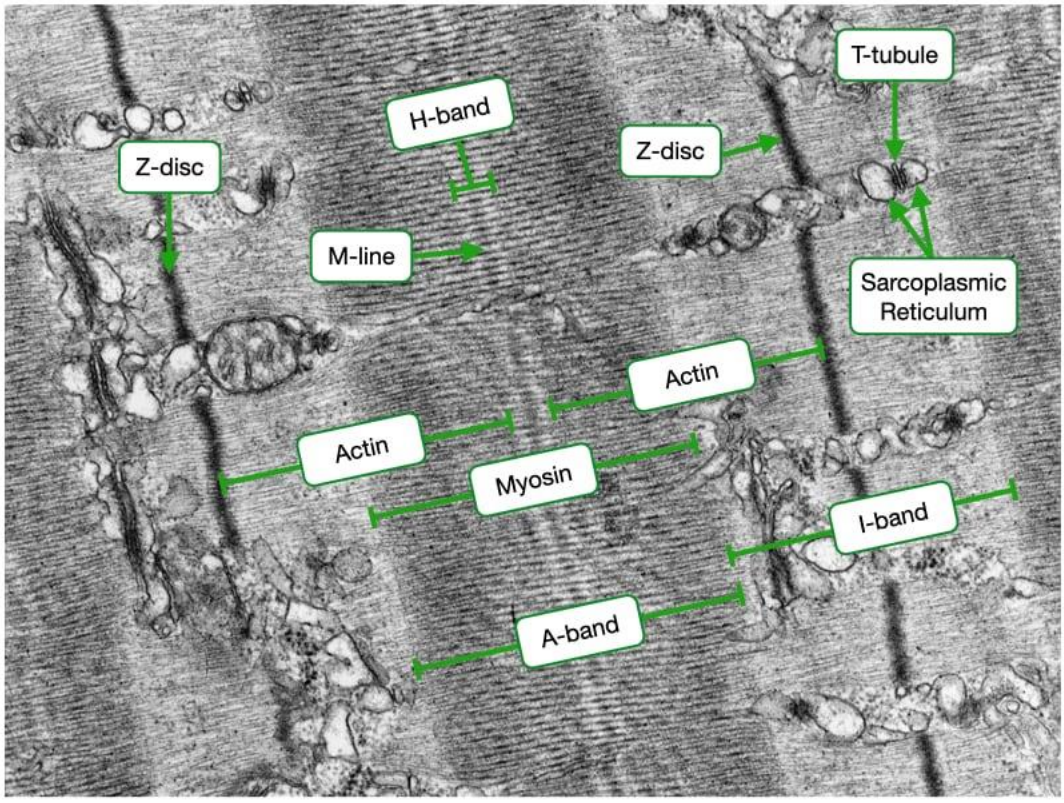

Figure 4: Ultrastructural image of a skeletal muscle fiber highlighting the Sarcomeres.

(adapted from: http://medcell.org/tbl/structure_and_function_of_muscle_and_nerves/reading.php)

1.2.2.1 Thin filaments

The main component of this region is the actin filaments formed by the polymerization of globular actin molecules and spiral around a structural protein termed nebulin (Figure 5). Each actin monomer contains a binding site for the myosin protein, the main component of the thick filaments. The main feature of this region is the polarization of the actin filaments toward the M-line, which allows the thick filaments to direct the force of contraction towards the center of the sarcomere (Figure 5) (Mukund & Subramaniam, 2020).

Another essential protein in this region is the troponin complex (TNNT), which contains three protein subunits: TNNTc, TNNTi, and TNNTt (Rasmussen & Jin, 2021). The TNNTc is the calcium-binding subunit that is the trigger for muscle contraction. The TNNTi is the inhibitory subunit of the TNNT complex that ensures muscle relaxation when the Ca^{+2}

level decreases. The TNNTt is the binding site to another essential filamentous protein, the tropomyosin (TPM1) (Figure 5). In the absence of calcium (Ca^{+2}), the TNNTt holds the TPM1 in a configuration that physically blocks the interaction between the myosin and the actin, rendering the contraction impossible (Barua et al., 2012). Once the Ca^{+2} is released from the SR, it binds to the TNNTc, and upon a cascade of interaction between the TNNT and TPM1, TPM1 moves and exposes the actin-myosin interaction site (Figure 5) (Mukund & Subramaniam, 2020).

1.2.2.2 Thick filaments

The main component of the thick filament is myosin II (two myosin heads); each myosin consists of two identical myosin heavy chains. Myosin-II is structured in the form of an ax, containing a globular head and a tail region. The tails of up to 300 myosin-II proteins polymerize to form the thick filament of the sarcomere. Myosin heads are polarized towards the Z-line on both sides of the M-line. This opposite orientation of Myosin-II filaments ensures contraction force directed toward the center of the sarcomere (Figure 5) (Mukund & Subramaniam, 2020). Each globular myosin-II contains an ATP and an actin-binding site. The energy produced from hydrolyzing ATP molecules induces the rotation of the myosin head to interact with the actin protein in the thin filament, which results in force production and shortening of the sarcomere.

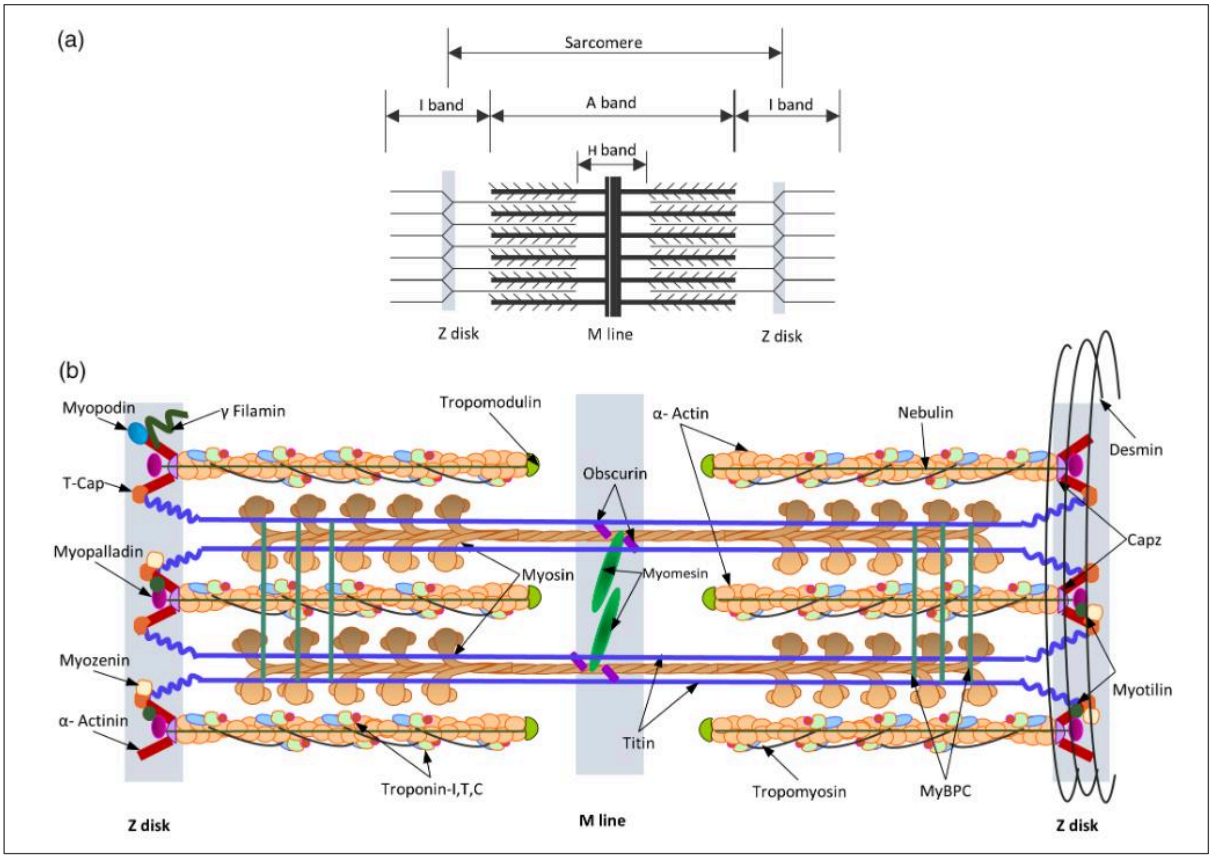

Figure 5: Schematic representation of the striated skeletal muscle sarcomere (adapted from Mukund & Subramaniam, 2020).

(a) Schematic representation of the arrangement of thick and thin filaments in the sarcomere and the bands of overlap between them. (b) Schematic diagram of the sarcomere demonstrating the organization and location of major sarcomeric proteins. Cytosolic Ca^{2+} induces conformational changes of troponin C, exposing the myosin binding sites. Myosin heads bind and crawl along the length of actin, causing sarcomeric contraction. Titin and nebulin maintain the length of the thick and thin filaments, respectively. The desmin intermediate filaments support the structure of the muscle cell by forming transverse links between adjacent myofibrils.

1.2.3 Non-contractile cytoskeleton

The noncontractile cytoskeleton provides the connection on the one hand between myofibrils, allowing coordination of contraction throughout the contractile apparatus, and on the other hand between myofibrils and the extracellular matrix (ECM), reinforcing the resistance of the cell structure to contraction. It can be divided into three groups:

- A peri-sarcomeric cytoskeleton is a group of proteins that form the shape and maintain the architecture of the myofibrils.

It is a group of proteins located within the sarcomeres, such as titin and nebulin. Titin is a giant protein of approximately 1 μm that runs from the Z-line to the M-line and ensures longitudinal stability to the sarcomere by providing resistance to overstretching. Myomesin connects titin to thick filaments. At the Z-line, myotilin is also found, which binds actin filaments and thus contributes to the stability of sarcomeres. Actin globular polymerization surrounds nebulin, ensuring its stability (Figure 5) (Mukund & Subramaniam, 2020).

- The inter-myofibrilla cytoskeleton connects adjacent myofibrils.

It is composed of non-contractile γ-actin and intermediate desmin filaments. Desmin is concentrated around the Z line in the myofibrillar space and thus establishes a link between adjacent myofibrils (Figure 6). It coordinates the contraction of the different myofibrils (Hnia et al., 2015). Of note, there is a category of myopathy in humans named desmin-related myopathies, in which accumulation of protein aggregates occurs between the myofibrils and affects muscle function, suggesting more roles to desmin than structure, probably related to the cellular integrity (Hnia et al., 2015). Vimentin, nestin, synemin, and paranemin are also involved in the composition of intermediate filaments, but their role is less well established (Figure 6).

- The sub-sarcolemma cytoskeleton forms a group of proteins that connect the contractile apparatus to the sarcolemma and indirectly to the extracellular matrix (Figure 6) (Csapo et al., 2020; Mukund & Subramaniam, 2020; Henderson et al., 2017) .

These proteins can be classified into three groups according to the physical interactions they establish between them: integrins from the ECM, spectrin (proteins that span the intracellular side of the cellular membrane in eukaryotic cells), and the dystrophin-associated group (DAG) (Figure 6). Noteworthy, defects in these proteins are the leading cause of

myopathies in humans. The absence of dystrophin, for example, is the cause of Duchenne muscular dystrophy (Duan et al., 2021).

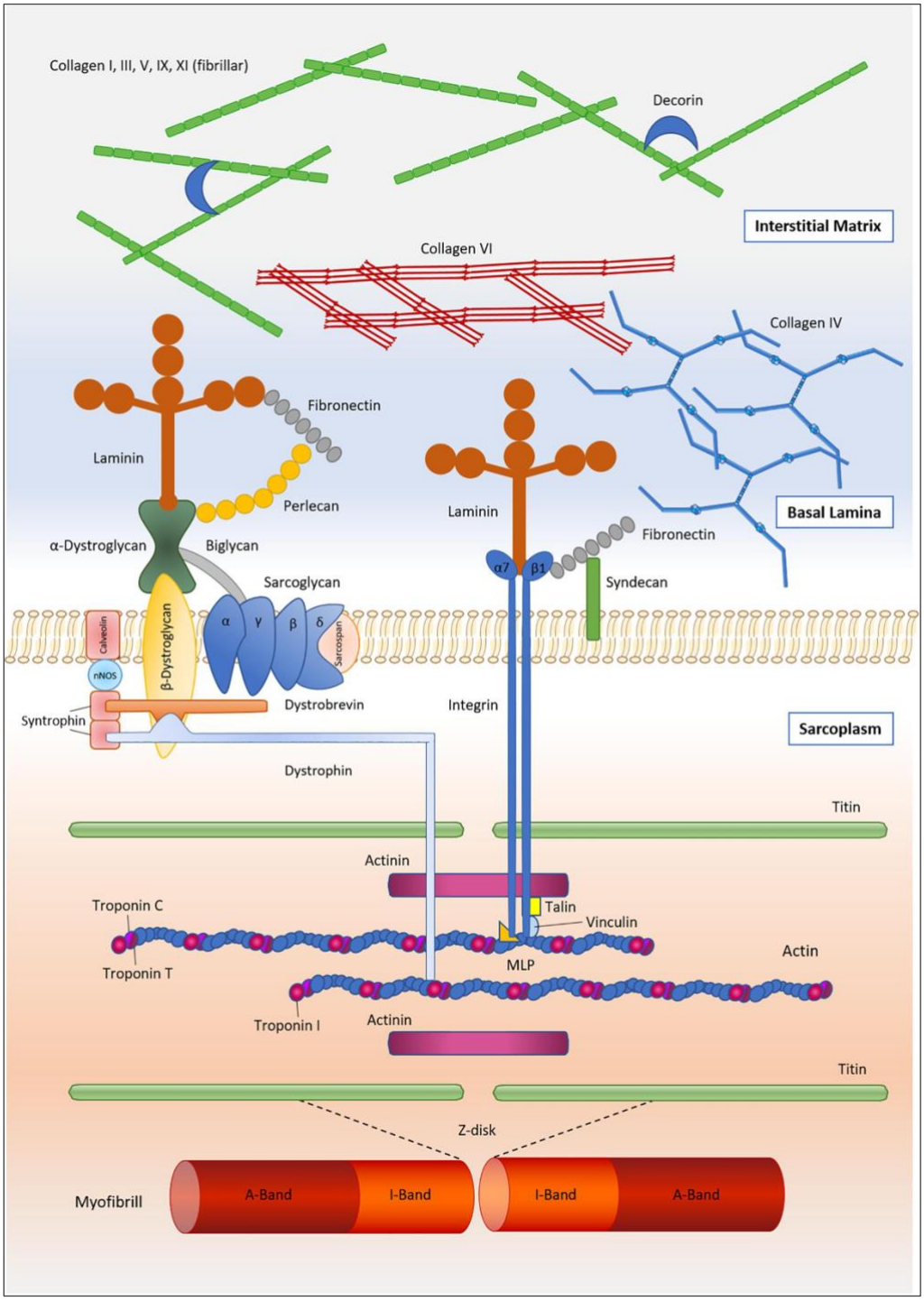

Figure 6: Schematic representation of the sub-sarcolemma cytoskeleton (adapted from (Csapo et al., 2020).

1.2.4 Sarcoplasmic reticulum and T tubules

The sarcoplasmic reticulum (SR) is the membranous sac that spans and envelops each myofibril. This membranous system has the function of intracellular calcium regulation and participates in the control of the muscle contraction (Al-Qusairi & Laporte, 2011). The T-tubules are transversal invaginations of the SR into the sarcolemma, and the portions near the T-tubules are called internal cisternae. The area where the T-tubule and sarcoplasmic reticulum meet, where the membranes are close together, is called the triad (Figure 7) (Al-Qusairi & Laporte, 2011).

Dihydropyridine receptors (DHPR) and ryanodine receptors (RYR) are located and, upon activation, allow the release of Ca^{+2} from the SR to the sarcoplasm, which provokes muscle contraction. This structure is responsible for providing the Ca^{+2} necessary for muscle contraction.

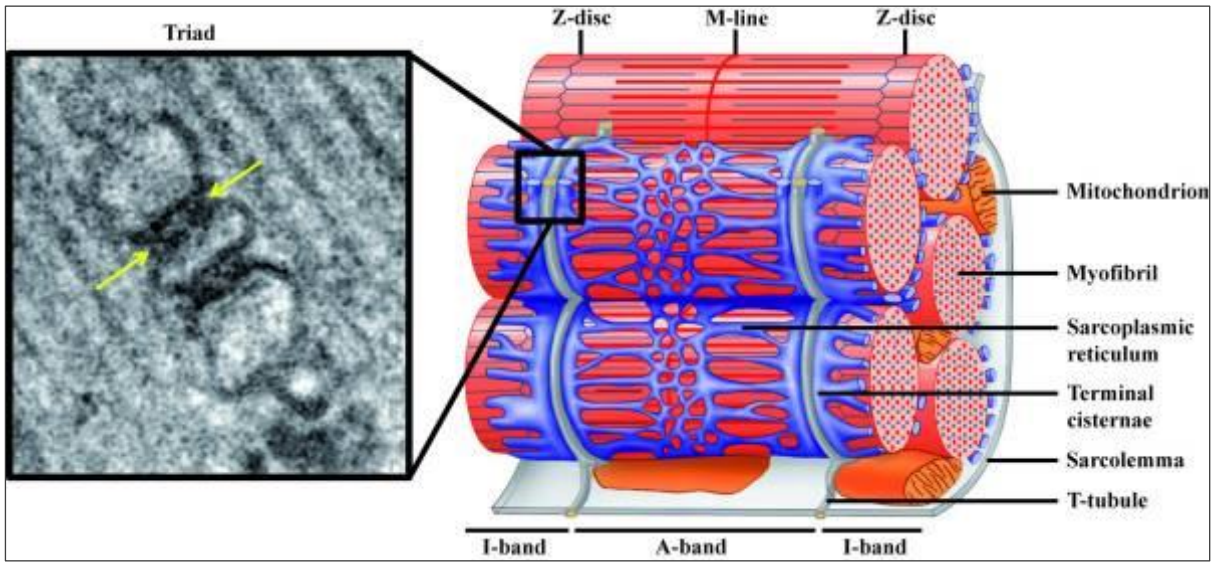

Figure 7: Triad structure (adapted from Al-Qusairi & Laporte, 2011).

Yellow arrows point at triad structure.

1.2.5 The neuromuscular junction and the action potential

Innervation is essential for muscle contraction since the moto-neuron delivers action potential to the fiber. Each mature muscle fiber is innervated by a single axon. The α-motoneuron innervates several muscle fibers via axonal branches, and a motor unit is a group of muscle fibers innervated by a single motor neuron (Rodríguez Cruz et al., 2020). The neuromuscular junction (NMJ) is a synapse located between the motor nerve terminal and the surface of a muscle fiber sarcolemma.

Action potentials arrive at the axon terminal, causing the opening of voltage-gated calcium channels. The influx of calcium into the pre-synaptic cytoplasm leads to the fusion of synaptic vesicles containing acetylcholine (ACh) and the release of their contents into the synaptic cleft. ACh receptors are located on the surface of the post-synaptic membrane (Figure

8). The binding of ACh to its receptor results in depolarization of the muscle fiber membrane, and the propagation of this depolarization is dependent on the amount of ACh released into the synaptic cleft (Figure 8) (Castets et al., 2020; Mukund & Subramaniam, 2020).

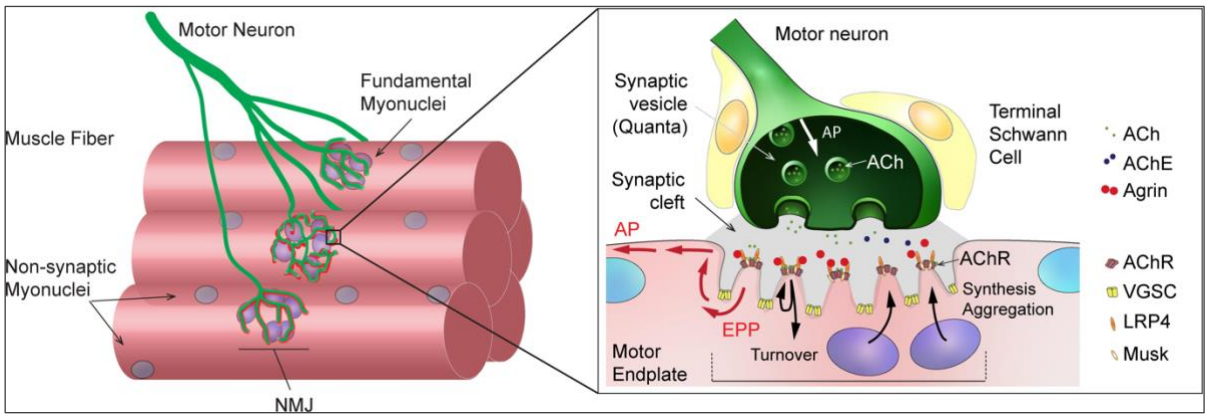

Figure 8: Schematic representation of the neuromuscular junction, adapted from (Castets et al., 2020).

If the amount of ACh released reaches a certain threshold, an action potential is generated. Massive entry of Na^+ ions into the cell causes the depolarization of the membrane (Rodríguez Cruz et al., 2020). The action potentials that originate at the neuromuscular junction propagate along the fiber and, within the fiber, along the T-tubules leading to the depolarization of the latter membrane and the release of Ca^{+2} from the SR (Mukund & Subramaniam, 2020).

1.3 Contraction of skeletal muscles

1.3.1 Types of muscle contraction

The force of muscle contraction depends on the mechanical conditions in which the muscle is placed. Several types of contractions are distinguished:

- Isometric contraction during which the muscle develops force at a constant length. This type of contraction is essential because it is the muscle state that stabilizes joints (Figure 9A).

- Isotonic contraction, during which the muscle shortens or lengthens to develop a constant force. There are two types of isotonic contractions: i) concentric, during which the muscle shortens (Figure 9B), and ii) eccentric, during which the muscle lengthens while exerting force (Figure 9C).

- Auxotonic contraction occurs at varying load and length.

Most human activities involve these different types of contraction.

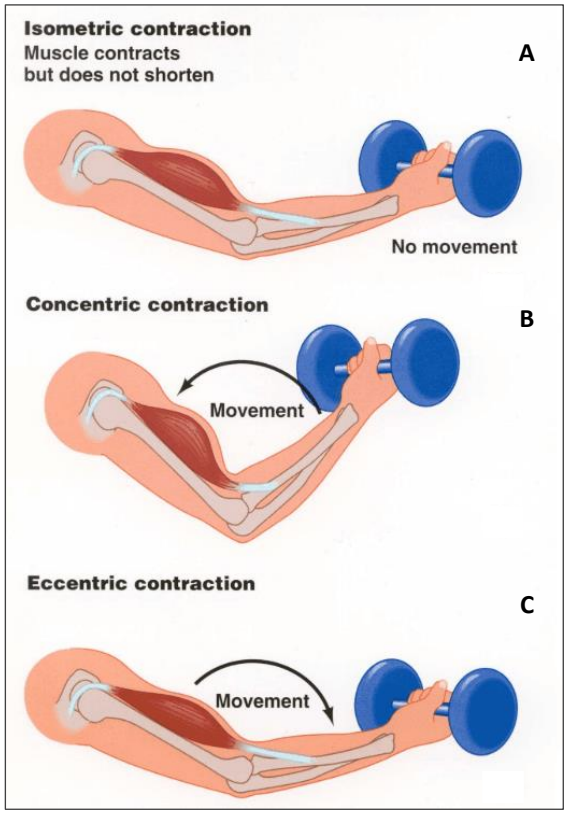

Figure 9: Types of muscle contraction.

(Adapted from https://www.ebtofficial.com/build-muscle/eccentric-vs-concentric/).

1.3.2 Dynamics of skeletal muscle contraction

The action potential in the T-tubules activates voltage-sensitive receptors that cause the release of calcium from the terminal cisterna of the sarcoplasmic reticulum into the cytosol. This mechanism is called excitation-contraction coupling (Figure 10) (Calderón et al., 2014).

The T-tubule contains L-type voltage-dependent calcium channels, also known as dihydropyridine receptors (DHPR), whose action is blocked by the calcium channel blocker, dihydropyridine (Figure 10) (Calderón et al., 2014). The sarcoplasmic reticulum membrane has ryanodine receptors (RyRs) because of their sensitivity to ryanodine, an alkaloid of plant origin. Two DHPRs on the T-tubule face a RyR on the sarcoplasmic reticulum (Figure 10) (Calderón et al., 2014). The DHPR senses changes in the membrane potential and responds to depolarization with a conformational change resulting in the opening of the RyR (Calderón et al., 2014).

Calcium released from the sarcoplasmic reticulum binds to troponin C (TnC), causing a conformational change that displaces tropomyosin so that actin-myosin binding sites are uncovered.

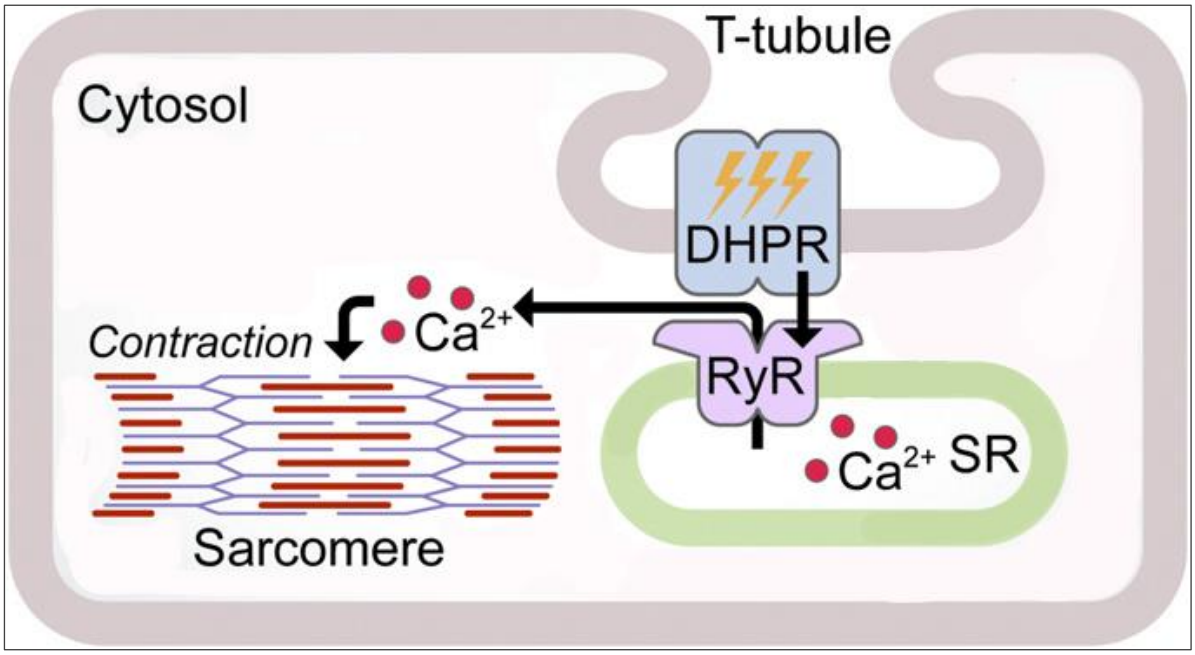

Figure 10: Excitation contraction coupling (adapted from Nelson et al., 2013).

Myosin head swings out toward thin actin filament in a stiff state at a 45° angle. ATP binds to myosin at this position, briefly dissociating it from actin (Figure 11). The ATPase activity of myosin hydrolyzes the ATP to ADP and Pi (free phosphate), causing a weaker binding to actin at the 90° angles, forming what is known as a cross-bridge (Figure 11). The release of Pi initiates the power stroke (Figure 11). The myosin head then rotates on its hinge, pushing the actin filament past it towards the M-line. At the end of the power stroke, the myosin head releases ADP and regains its firm state (Mukund & Subramaniam, 2020; Squire, 2019).

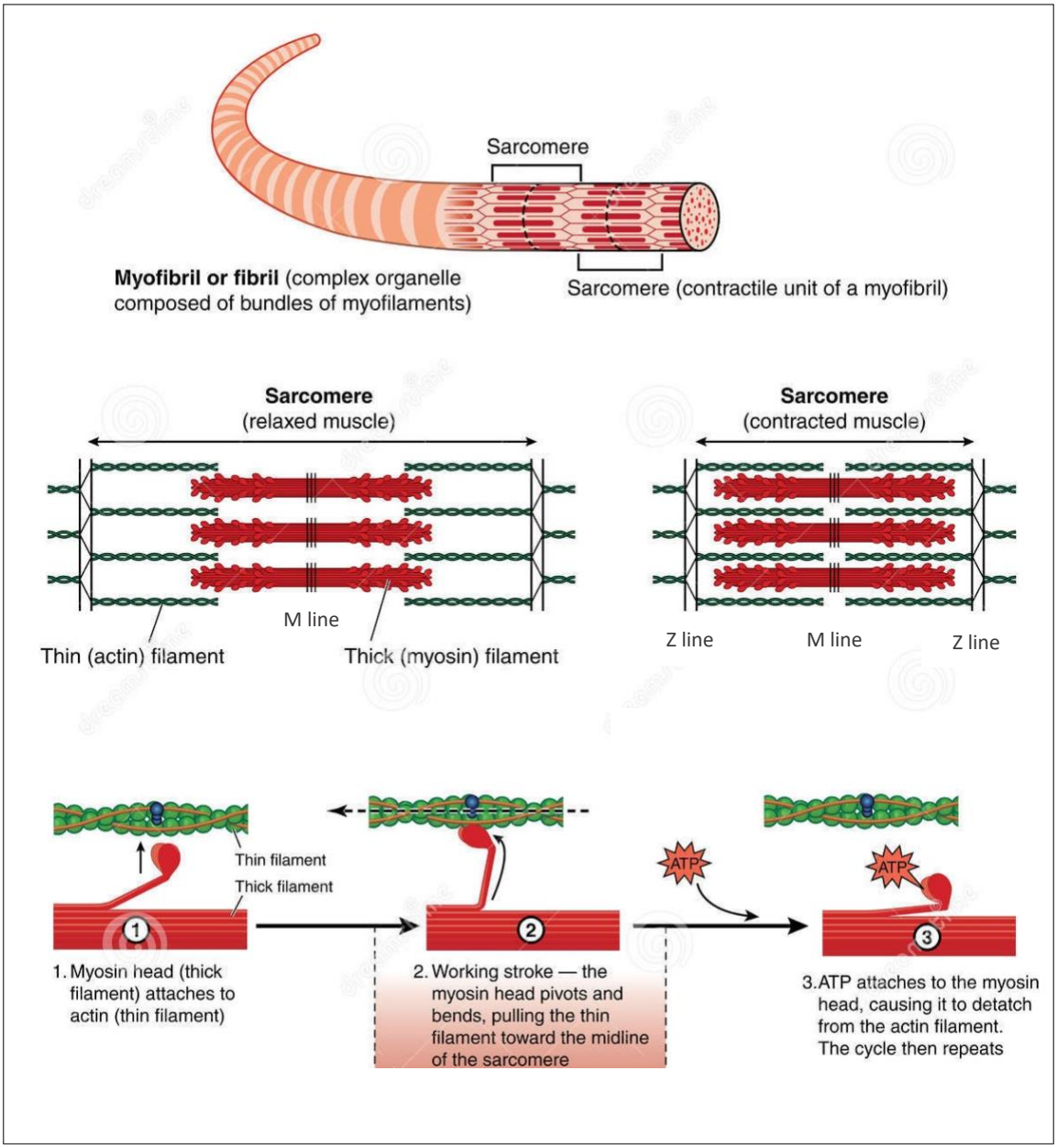

Figure 11: Mechanisms of muscle contraction.

(adapted from https://www.dreamstime.com/stock-illustration-mechanism-muscle-contraction-detail-

Once contraction is complete, calcium dissociates from troponin and is repumped into the sarcoplasmic reticulum by an ATP-dependent process (Figure 12). It is the protein called Sarco endoplasmic reticulum Ca^{2+} ATPase (SERCA), present in the sarcoplasmic reticulum, that allows calcium recovery (Figure 12) (Rahate et al., 2020). This protein belongs to the family of P-type ATPases.

Three isoforms of the protein exist: SERCA1 expressed in fast skeletal muscles, SERCA2 expressed in the heart and slow skeletal muscles, and SERCA3 in lymphoid cells and endothelial cells (Rossi & Dirksen, 2006).

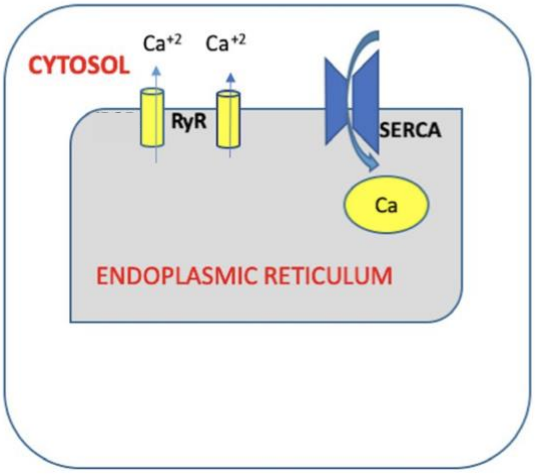

Figure 12: Mechanisms of calcium exchange in and out the endoplasmic reticulum (adapted from Rahate et al., 2020).

1.4 Energy production

ATP is the energy unit produced, stored, and consumed by skeletal muscles; however, the storage of ATP in myofibers is low (5 to 6 mmol/kg of muscle). For this reason, rapid energy production is essential in skeletal muscles to provide the ATP necessary for muscle activity, especially during exercise (Westerblad et al., 2010).

Lipids, carbohydrates, and amino acids are the three major nutrients for mammals (Figure 13). After their oxidation and breakdown, they supply energy in various ways to maintain the body's activities. Skeletal muscles exert aerobic and anaerobic metabolisms (Figure 13), and either pathway is preferred, dependent on the type of activity and muscle fiber (Westerblad et al., 2010).

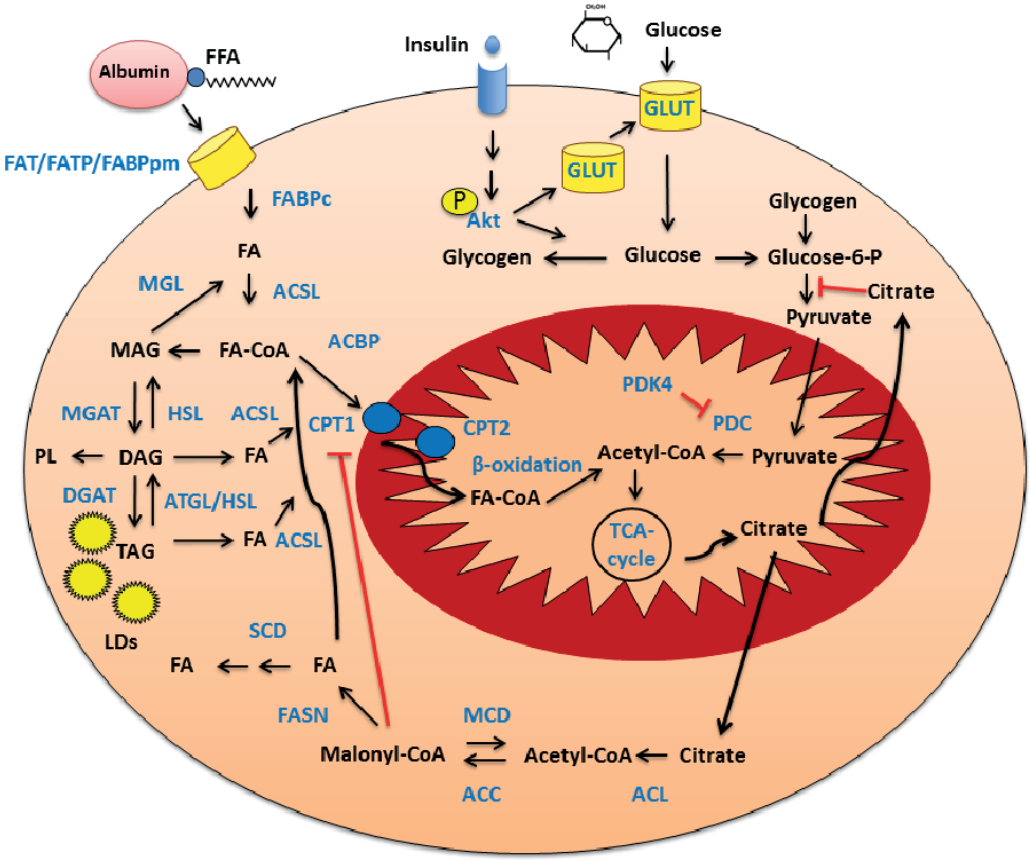

Figure 13: Metabolic pathways in skeletal muscle fibers.

(adapted from https://www.semanticscholar.org/paper/Regulation-of-energy-metabolism-in-skeletal-muscle-Feng/ae0878ec6c8788f0c7cab6d569b7ef0e542c830c).

1.4.1 Anaerobic metabolism.

During an intensive exercise, the muscle prefers the anaerobic metabolic pathway as it rapidly produces ATP via phosphocreatine hydrolyzation and degradation of stored glycogen.

1.4.1.1 Creatine usage

Creatine can be endogenously synthesized from amino acids in the liver and released into the bloodstream. In an average 70 kg human, the total creatine reserve reaches up to 120 g, with 2 g/day productions. Circulating creatine can be absorbed by skeletal muscles and phosphorylated by a creatine kinase (CK) in the presence of ATP to be stored until needed (Figure 14). At rest, 80 % of the creatine in skeletal muscles is found in the form of phosphorylated creatine (P-creatine), and the energy produced from dephosphorylating it is of short burst (Koch et al., 2014).

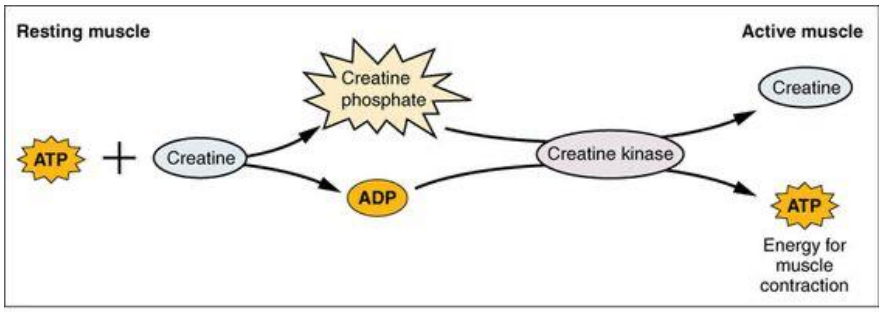

Figure 14: Creatin utilization for rapid ATP production.

(adapted from: https://www.differencebetween.com/difference-between-aerobic-and-anaerobic-muscles/).

1.4.1.2 Glucose metabolism

In mammalians, skeletal muscles are the major storing tissue of glucose in the form of glycogen. Muscle fibers have different capacities for glucose storage according to their main metabolic activity. Indeed, type II fibers have a more important glycogen storage capacity than type I.

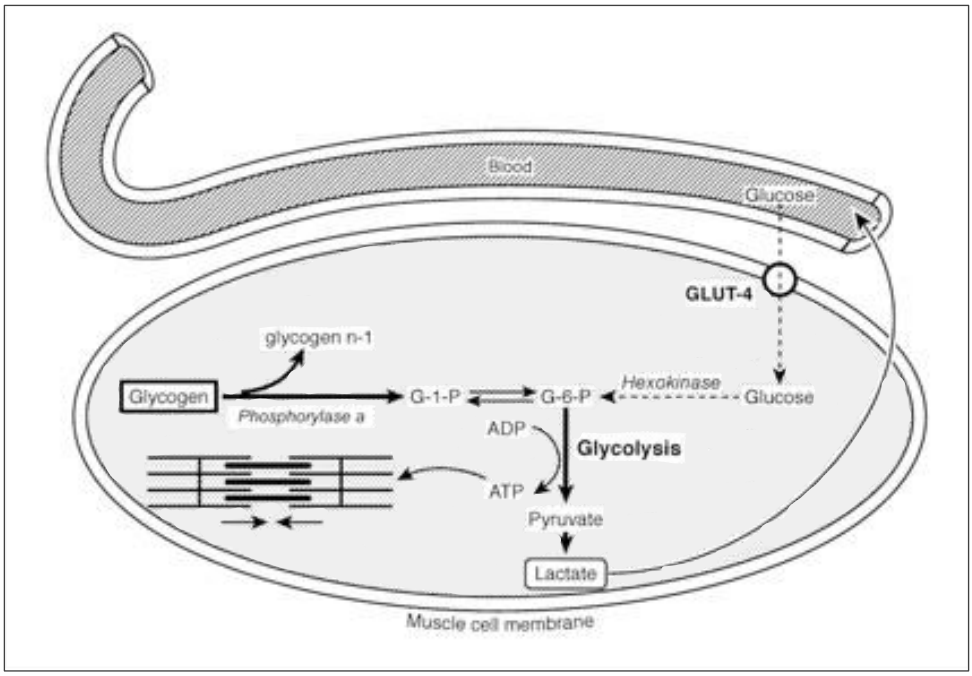

Figure 15: Anaerobic glycolysis catalyzed in the sarcoplasm.

Glucose is taken up by glucose transporters (GLUT4) or stored glycogen are metabolized to pyruvate (generating 2 ATPs/molecule of glucose). This pathway produces lactic acid, which is released into the extracellular matrix.

At rest, glucose incorporation into the fiber is mainly mediated by insulin-responsive glucose transporter 4 (GLUT4) transmembrane receptor, a mechanism controlled by the circulating insulin levels. Once glucose is inside the cytoplasm, it is phosphorylated to 6-glucose by hexokinase II, then enrolled in the glycogen synthesis pathway (Figures 15 and 16). During exercise, adenosine monophosphate (AMP)-activated protein kinase (AMPK) signaling stimulates the translocation of GLUT4 from the cytoplasm to the membrane due to ATP shortage. Upon incorporation, glucose or glycogen enters a series of chemical reactions in a metabolic pathway called glycolysis, producing 2 ATP molecules from hydrolyzing 1 glucose molecule (Ohlendieck, 2010).

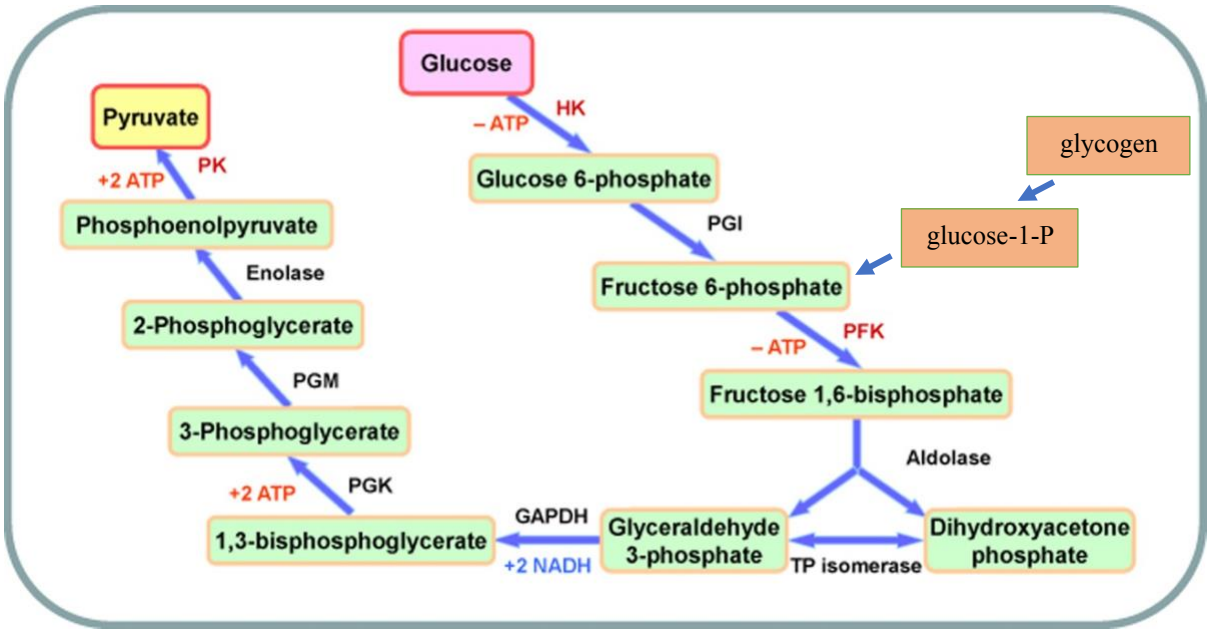

Figure 16: Metabolism of stored glycogen and uptaken glucose for energy production (adapted from Li et al., 2015)

1.4.2 Aerobic metabolism

1.4.2.1 Carbohydrate metabolism

Pyruvate from glycolysis enters the mitochondria, either decarboxylated to oxaloacetate, an intermediate of the Krebs cycle, or converted to acetyl-CoA (Figure 17) (Martínez-Reyes & Chandel, 2020). Of note, acetyl-CoA is also the entry point of fatty acids and amino acids into the Krebs cycle in the mitochondria.

The critical components of the mitochondria are, on the one hand, the enzymatic reactions of energetic substrate oxidation and, on the other hand, the electron transport chain or respiratory chain (Figure 17). The Krebs cycle substrates reduce nicotinamide adenine dinucleotide (NAD+) to NADH and flavin adenine dinucleotide (FAD2+) to FADH2. These intermediates are called reducing equivalents and provide electrons to the respiratory chain. The latter comprises five complexes: complex I or NADH dehydrogenase, complex II or succinate dehydrogenase, complex III or ubiquinol cytochrome c reductase, complex IV of cytochrome c oxidase, and complex V or ATP synthase (Figure 17) (Martínez-Reyes & Chandel, 2020).

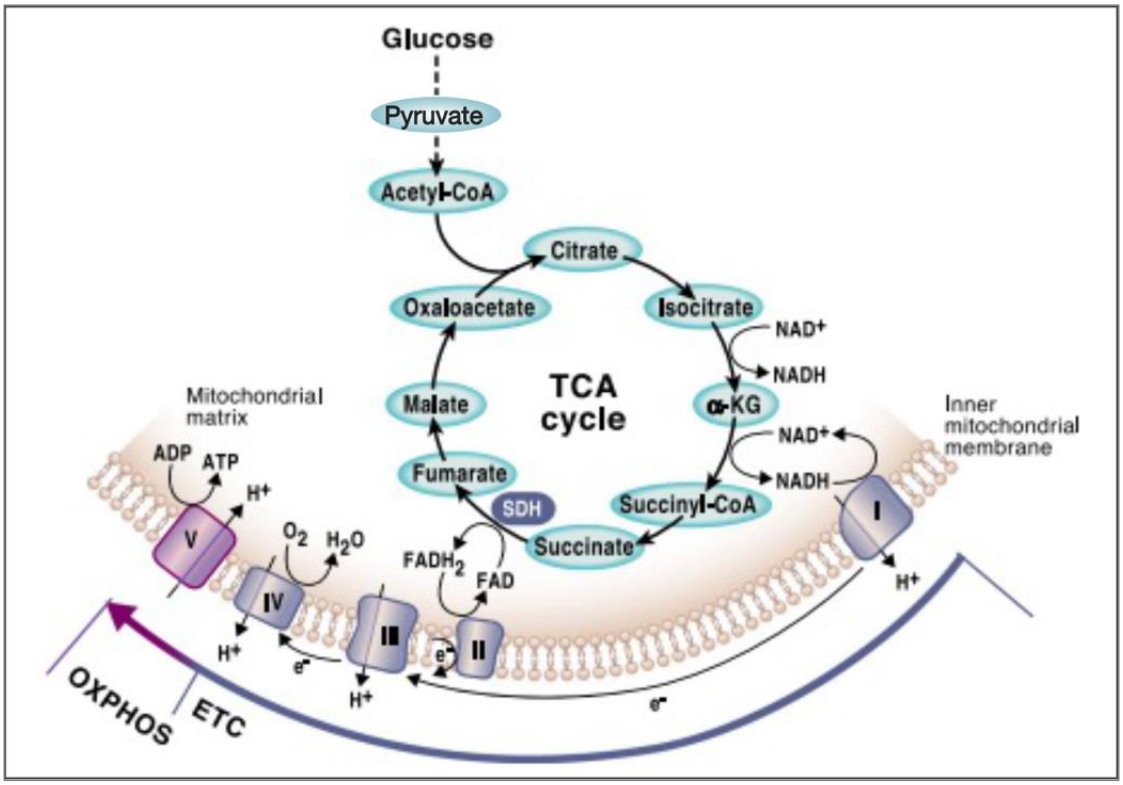

Figure 17: Aerobic carbohydrate metabolism (adapted from Martínez-Reyes & Chandel, 2020).

In the presence of oxygen, pyruvate is metabolized to carbon dioxide and water through oxidative phosphorylation (OXPHOS) inside the mitochondria, producing 34 molecules of ATP.

Of note, all are composed of several protein subunits, and only complex II is entirely encoded in the nucleus. In contrast, the other complexes result from the association of proteins encoded by nuclear and mitochondrial DNAs (Taylor & Turnbull, 2005). Pyruvate oxidation varies with the type of fiber. For example, type I fibers have a higher oxidation capacity than type II glycolytic fibers (Westerblad et al., 2010).

1.4.2.2 Fatty acid metabolism

Skeletal muscle is the primary site of fatty acid (FA) oxidation at rest or during exercise. FAs are the sour energy used predominantly at rest or again after fasting. FA oxidation is increased during low-intensity exercise and reduced during high-intensity exercise. Free fatty acids are stored in adipose tissue as triglycerides. During increased energy requirements, triglycerides are hydrolyzed by triglyceride lipase (lipolysis) and transported bound to albumin via the vascular system to skeletal muscle. Lipolysis occurs under the control of hormones. It is stimulated by epinephrine and inhibited by the insulin (Langlois et al., 2021).

Non-esterified fatty acids (NEFA) are derived from triglycerides via the activity of enzyme lipase (LPL) and transported to the sarcoplasm via transporters such as cluster of differentiation 36 (CD36) (Figure 18). After their cleavage to form FA-acyl-CoA, they are imported into the mitochondria via the transporter carnitine palmitoyl transferase I (Cpt1) to undergo β-oxidation (Figure 18) (Langlois et al., 2021).

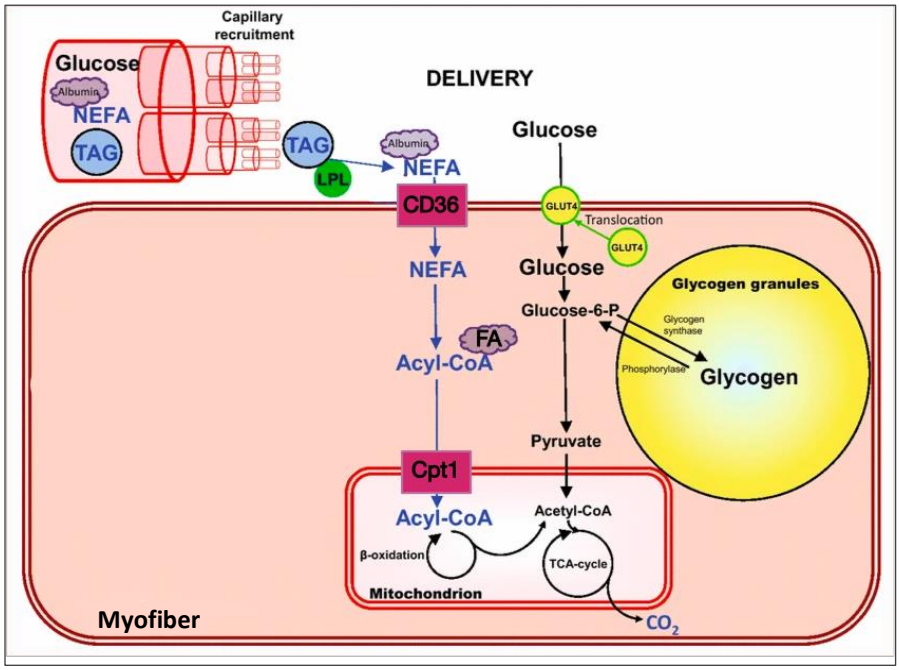

Figure 18: Aerobic β-oxidation and glucose metabolism (adapted from van Hall, 2015).

β-oxidation is a sequence of four reactions that converts acyl-CoA to acetyl-CoA (Figure 19). The first step is the dehydrogenation of acyl-CoA in the presence of FAD. This reaction is catalyzed by an oxidoreductase (acyl-CoA dehydrogenase). Then, the l'action of crotonase leads to β-hydroxyacylCoA, which will then be dehydrogenated in the presence of NAD. Finally, the cleavage of the carbon chain leads to the release of acetyl-CoA, which can then enter the Krebs cycle (Figure 19) (H. Chen et al., 2019). The Krebs cycle oxidation (TCA cycle) of substrates and β-oxidation results in the reduction of NAD+ to NADH and FAD2+ to FADH2, which provide electrons to the respiratory chain in the mitochondria (Langlois et al., 2021).

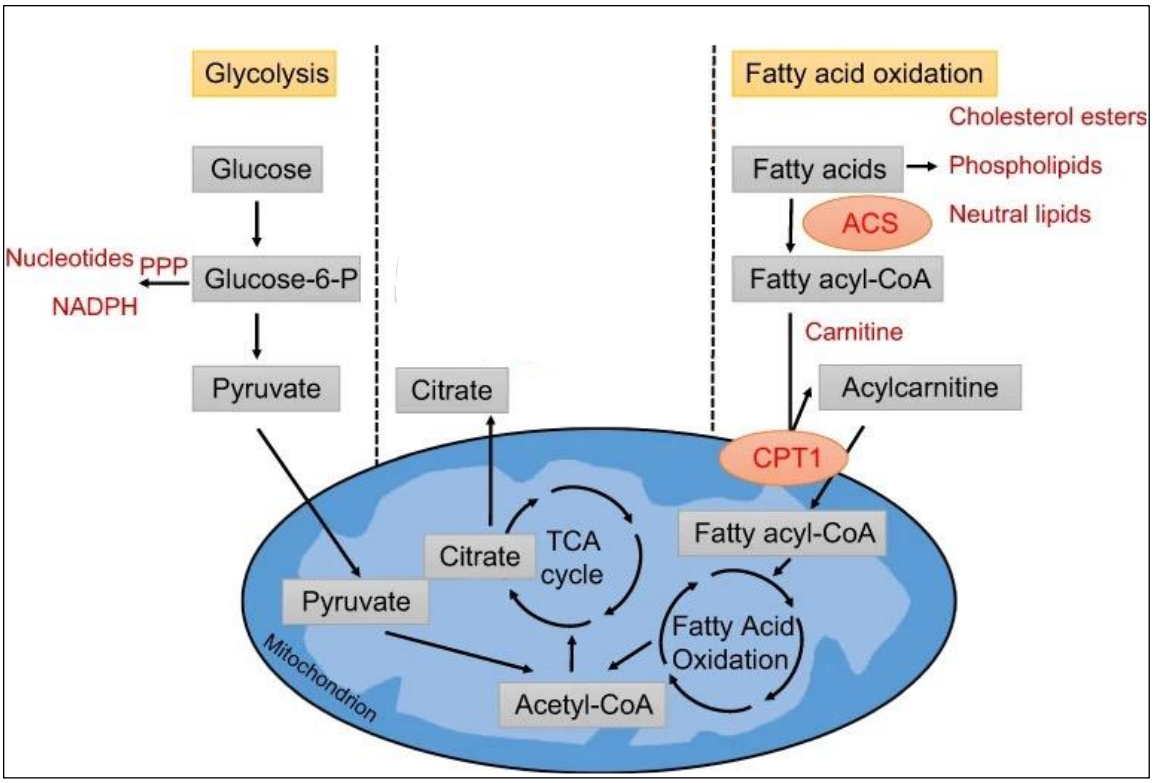

Figure 19: Schematic representation of fatty acid beta oxidation and glycolysis (adapted from H. Chen et al., 2019).

1.4.2.3 Protein and amino acid metabolism

Skeletal muscle protein synthesis and degradation (protein turnover) is relatively slow, ensuring a stable balance of the protein pool in healthy individuals at rest (Wagenmakers, 1998). Feeding or starvation affects the protein pool of muscles in healthy individuals (Wagenmakers, 1998). Skeletal muscle is also an important amino acid (AA) storage unit since, on average, they contain 130 grams of free intramuscular AA in adult individuals. In comparison, only 5 grams are free in the blood circulation (Wagenmakers, 1998).

For energy production in rat and human resting muscles, six amino acids can be metabolized, including branched-chain amino acids BCAAs (i.e., leucine, isoleucine, valine -), as well as asparagine, aspartate, and glutamate (Figure 20). While only leucine and a part of isoleucine can be turned into acetyl CoA in the mitochondria (Figure 20) (Mann et al., 2021), asparagine, aspartate, and glutamate can be transformed into intermediates of the TCA-cycle (Figure 20).

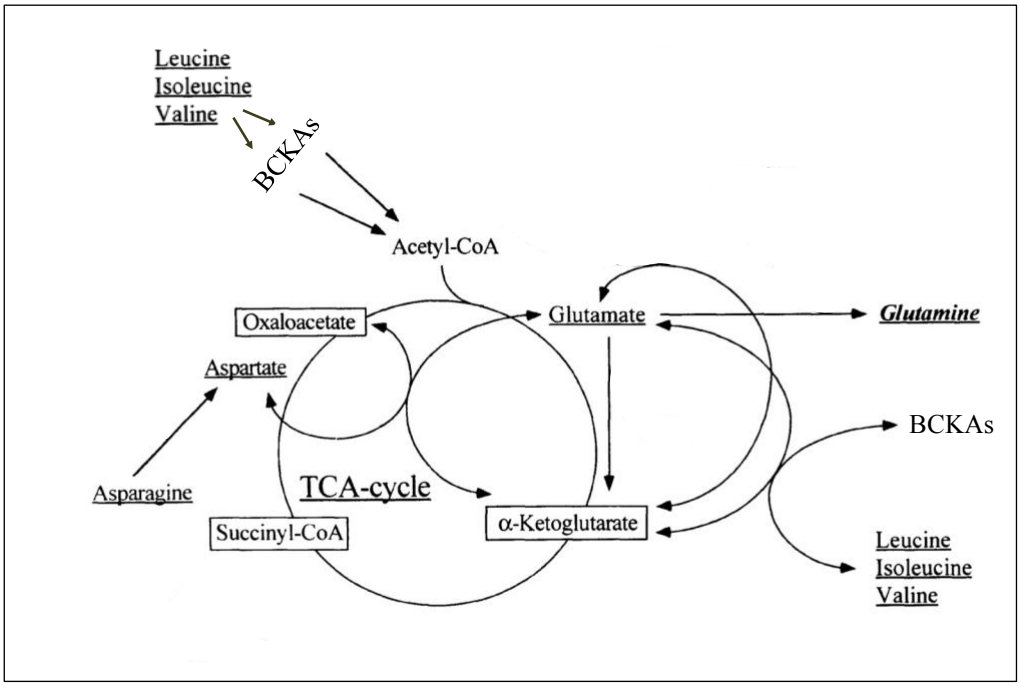

Figure 20: Schematic representation of amino acids metabolism in skeletal muscles (adapted from Wagenmakers, 1998).

BCAAs first undergo reversible transamination in the mitochondria to form the corresponding branched-chain α-keto acids (BCKAs). The branched-chain α-keto acid dehydrogenase complex (BCKDH) then catalyzes the oxidative decarboxylation of BCKAs to form the related acetyl-CoA derivatives (Figure 21) (Mann et al., 2021).

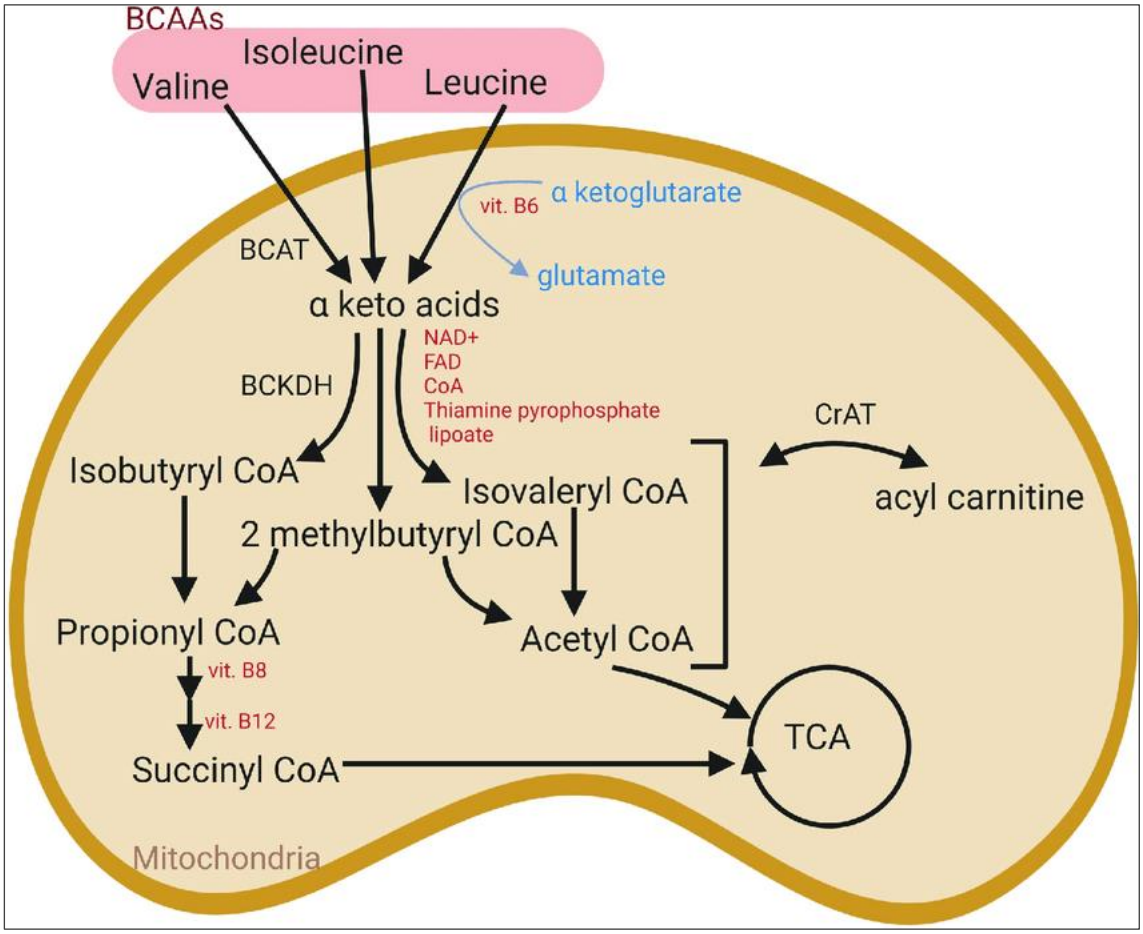

Figure 21: BCAA metabolism in muscles mitochondria (adapted from Mann et al., 2021).

Experiments performed to study protein synthesis during exercise following the incorporation of labeled L[I)3C]leucine showed that the ratio of protein synthesis-degradation becomes negative without increased protein oxidation (Wagenmakers, 1998). Moreover, evidence showed that during exercise, there is increased oxidation of BCAA in the mitochondria of skeletal muscles (Figure 20) (de Meeûs d'Argenteuil et al., 2021; Wagenmakers, 1998). Noteworthy, excessive BCAA activity produces an increased amount of ammonium (NH_4^+) which is toxic to the cell (Mann et al., 2021).

1.4.3 Types of muscle fibers

The body's musculature is composed of different skeletal muscles; some appear red like the soleus, and some appear pale in color like the quadriceps. Each muscle is characterized by a major muscle fiber type that differs in biochemical properties, physiology, and metabolic parameters.

Several classifications based on the revelation of contractile or metabolic properties have been established for muscle fibers. The ATPasic activity of the fibers was first used to classify them according to their contraction rate. Combining several pHs of the fibers according to the method of Brooke and Kaiser (Green et al., 1982), three types of fibers were distinguished: type I (slow contraction), IIA, and IIB (fast contraction). Other authors have combined the revelation of contractile type by ATPase activity with metabolic type by analysis of oxidative metabolism activity such as succinate dehydrogenase (Peter et al., 1972).

Thus, type I fibers are slow with oxidative metabolism, IIA fibers are intermediate to fast-tending with oxidoglycolytic metabolism, and IIB is fast with glycolytic metabolism. Finally, the use of antibodies directed against MHCs allowed the identification of the fourth type of intermediate type fibers, the IID or IIX fibers (Galpin et al., 2012). The classification of the fibers and their properties are summarized in Table 1

Type of fiber/MHC	I	IIA	IIX	IIB
Contraction	**Slow**	**Rapid**		
ATPase activity	**Weak**	**high**		
Metabolism	**Oxidative**	**Oxidative/Glycolytic**		**Glycolytic**
Fatigue resistance	**+++**	**++**	**+**	**+**
Mitochondria riche	**+++**	**++**	**+**	**+**

Table 1: Types of skeletal muscle fibers.

In addition to these four types of so-called pure fibers, anti-MHCs antibodies have revealed hybrid fibers that can simultaneously express two to four isoforms of MHCs (Medler, 2019; Termin et al., 1989). These mixed fibers result from the transition of the MHCs expression, which in mammals occurs in the following sequence: I→IIa→IId→IIb. These transitions occur with age but also under various factors such as exercise (Medler, 2019).

1.5 Role of skeletal muscles in the development of type II diabetes

In the body, skeletal muscle has two leading roles, the mechanical one. If this function is impaired, it leads to severe pathologies such as myopathies. The second is a metabolic one, which, when deregulated, can lead to metabolic disorders such as type II diabetes or obesity.

In patients with type 2 diabetes, insulin levels are normal or even high, but organs such as the liver, skeletal muscles, and adipose tissues become resistant to this hormone. Insulin signaling stimulates glucose uptake in skeletal muscles, the major glucose regulator tissue in the body (Bouzakri et al., 2005). Upon activation of the insulin receptor, GLUT4 is recruited to the plasma membrane and incorporates blood glucose into the sarcoplasm (Figure 22) (Rose & Richter, 2005). When the muscle loses its insulin sensitivity, blood glucose level stays high, and this contributes to the development of type II diabetes. Indeed, disruptions in the insulin signaling pathway (Krook et al., 2000) and defects in GLUT4 recruitment to the membrane in the muscle (Ryder et al., 2000) are associated with insulin resistance.

Hickey and colleagues have shown a correlation between the stimulation of glucose uptake by insulin in the muscles and the percentage of slow fibers. They reported that the decrease in the number of oxidative fibers leads to an insulin resistance (Hickey et al., 1995). In addition, Song et al. have shown that slow oxidative fibers are more sensitive to insulin than fast glycolytic fibers (Song et al., 1999). Also, in obese individuals, skeletal muscle has reduced oxidative capacity with decreased type I fibers and increased glycolytic capacity (Tanner et al., 2002). Therefore, muscle function activity and fiber composition changes are involved in the development of type II diabetes.

Patients with type II diabetes are often advised to exercise and follow a strict diet. Exercise and acute muscle contraction promote insulin-mediated glucose uptake in skeletal muscles, improving disease symptoms, including glucose circulating levels (Figure 22) (Stanford & Goodyear, 2014; Rose & Richter, 2005).

Many hormones, including androgens, are significant regulators of skeletal muscles. It is therefore essential to study the function of these hormones and their receptors in this tissue to develop, in the long term, compounds for the treatment of different pathologies.

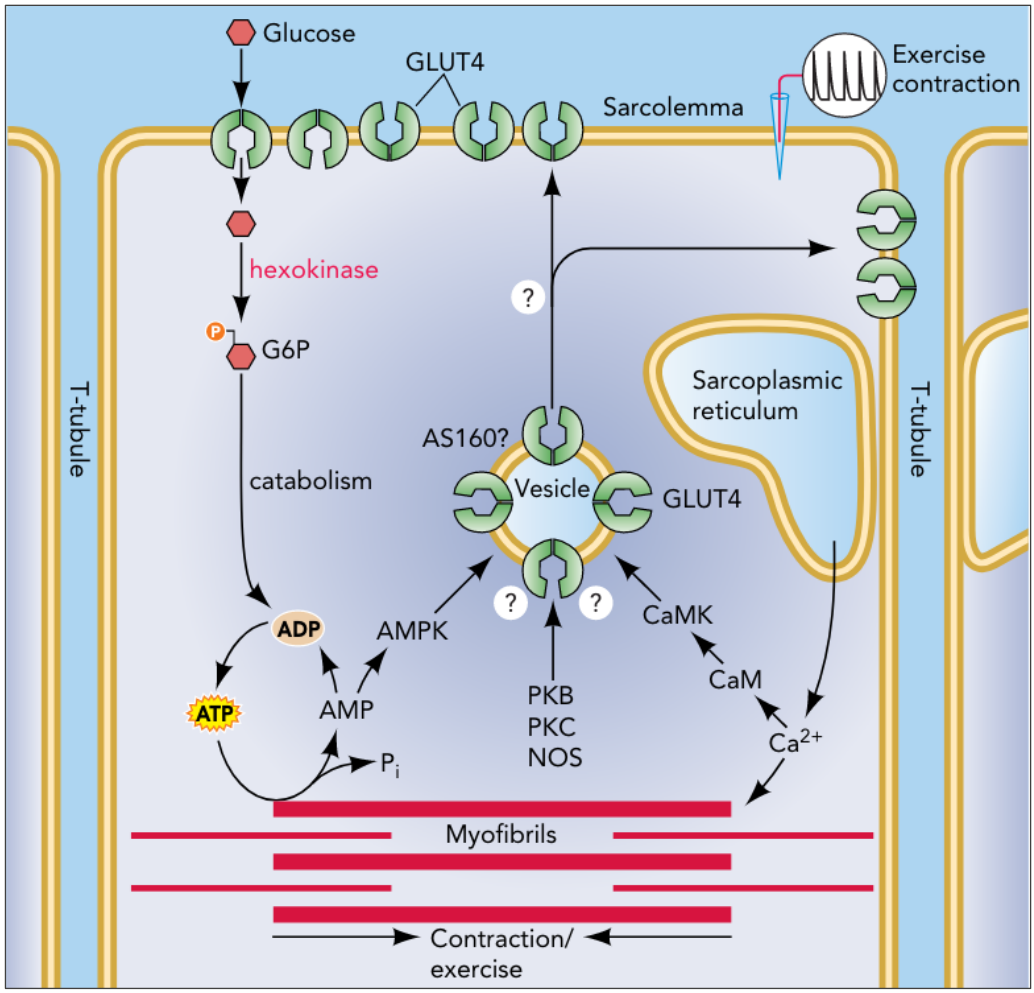

Figure 22: Potential regulation of glucose uptake and GLUT4 translocation in skeletal muscle during exercise/contractions (adapted from Rose & Richter, 2005).

More important glucose uptake by skeletal muscles occurs due to increased presence of glucose transport protein (GLUT4) in plasma membranes. The mechanisms by which exercise induce glucose transport are unclear but may involve different kinases that sense the changes in the intracellular environment during contractions (i.e., elevated Ca2+, AMP concentrations). The question marks refer to the unknown signalling and structural molecules that could be involved.
CaM, calmodulin; PKC, protein kinase C; G6P, glucose-6-phosphate; AS160, Akt substrate of 160 kDa; AMPK, AMP-activated protein kinase; CaMK, Ca2+-CaM dependent protein kinase; PKB, protein kinase B (also known as Akt); NOS, nitric oxide synthase.

2 Muscle stem cells

2.1 Satellite cell discovery and identification

In 1960, Alexander Mauro was the first to identify a muscle stem cell population after observing their particular position between the sarcolemma of the host fiber and the basal lamina (Mauro, 1961). Mauro named them the satellite cells (SatC) due to their shape and alignment along the fiber (Figure 23). They account for approximately 5 % of adult skeletal muscle nuclei in 8-week-old mice (Ontell et al., 1984). Slow muscle fibers contain three to four times more satellite cells than fast muscle fiber (Schmalbruch & Hellhammer, 1977).

SatC reside in a quiescent state in a highly specialized microenvironment (niche) on the periphery of the muscle fibers (Sinha-Hikim et al., 2003; Yin et al., 2013). They are easily distinguished from myonuclear since they are located under the basal lamina (Figure 23A-red arrows) and above the sarcolemma (Figure 4A-yellow arrows), harboring their cytoplasm (Figure 23A). Myoculei are also located under the basal lamina (Figure 23B-red arrows) but within the sarcolemma and do not have their cytoplasm (Figure 23B).

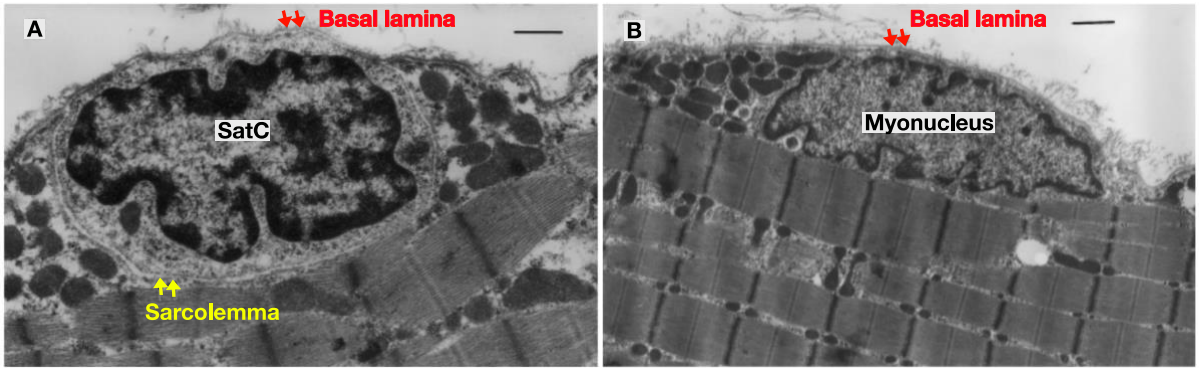

Figure 23: Electron microscopy of a muscle satellite cell (A) and a typical myonucleus (B) (adapted from Sinha-Hikim et al., 2003).

(A) Muscle satellite cells (SatC) are located inside the basal lamina (red arrows) and outside the sarcolemma (yellow arrows). (B) A myonucleus is found inside the sarcolemma and red arrows show the basal lamina. Scale bar: 1 µm.

SatC are primarily responsible for post-natal muscle regeneration and growth. They are classified under the adult unipotent stem cell category, indicating that they exist in adulthood and can undergo asymmetric division to generate one type of stromal cells in muscles termed myocytes while auto-renewing the population (Kuang et al., 2007).

In addition, SatC can also undergo symmetric division to expand the stem cell population or symmetric differentiation to generate a higher number of progenitor cells, which in the long-term could lead to the loss of the population (Cossu & Tajbakhsh, 2007; Kuang et al., 2007; Motohashi & Asakura, 2014). This will be further discussed in section **3.2.1**.

2.2 Characteristics of the satellite cell population

The expression of the transcription PAX7 is a significant characteristic of SatC (Figure 24) (Yin et al., 2013). The indispensable role of PAX7 in SatC homeostasis and physiological function has mainly been studied using different approaches, including constitutive (Oustanina et al., 2004; Seale et al., 2000) or conditional genetic modifications (Günther et al., 2013; Lepper et al., 2009; von Maltzahn et al., 2013). The role of PAX7 in SatC will be further detailed in the next section. SatC can also express the PAX3 transcription factor (a PAX7-paralogue), mainly in the trunk and forelimb muscles, but not the hindlimb (Relaix et al., 2006).

The primary markers that characterize SatC are used to study to isolate them, as shown in Figure 24. The most known among these markers are the M-cadherin (Mcad, also called CDH15) (Irintchev et al., 1994), integrin alpha 7 (Itga7) (Burkin & Kaufman, 1999), cluster of differentiation 34 (CD34) (Beauchamp et al., 2000), C-X-C chemokine receptor type 4 (CXCR4) (Ratajczak et al., 2004), Neural cell adhesion molecule (N-cam also named CD56) (Illa et al., 1992), and syndecan 3 and 4 (Syn3/4) (Cornelison et al., 2001).

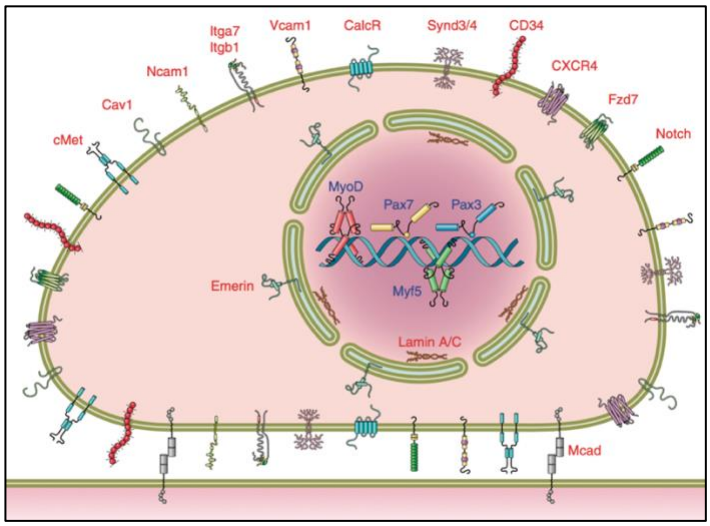

Figure 24: Satellite cell markers, adapted from (Yin et al., 2013).

Some markers are mainly expressed in quiescent stem cells and not activated ones, such as the calcitonin receptor (Fukada et al., 2007) and the Notch receptor (Baghdadi et al., 2018). Size and granularity features could be added to the aforementioned trans-membrane markers to isolate the SatC population (Montarras et al., 2005). Moreover, SatC exhibit cellular axon-like elongations called protrusions that help the cells sense their micro-environment. Blake et al. showed that the higher number of protrusions are more dormant, and cells with fewer protrusions are more responsive to activation (Blake, 2022). These elongations could also be observed in culture since SatC has a fibroblast-like shape with extensions.

MYF5 and MYOD1, two transcription factors involved in myogenesis, can also be expressed in SatC, and this will be further discussed in section **3.2.2**.

2.3 Satellite cell quiescence and niche

SatC dormancy is essential for conserving the stem cell population throughout life. SatC niche is a complex microenvironment constituting diverse signaling molecules and factors, as well as cell types residing and influencing cell quiescence and homeostasis. Each SatC niche component contributes to its homeostasis, and in this paragraph, we will discuss the known main factors and their roles. New studies providing single-cell RNA sequencing (RNAseq) analysis unraveled the presence of various cell types residing in and influencing the SatC niche, including tendon cells, immune cells, by a mesenchymal stem cell subtype named fibro-adipogenic progenitors (FAPs), the host fiber, and endothelial cells (Figure 25) (Christov et al., 2007; Evano & Tajbakhsh, 2018; Montarras et al., 2013; Yin et al., 2013). Thus, the SatC niche encompasses anatomical and functional dimensions (Figure 25).

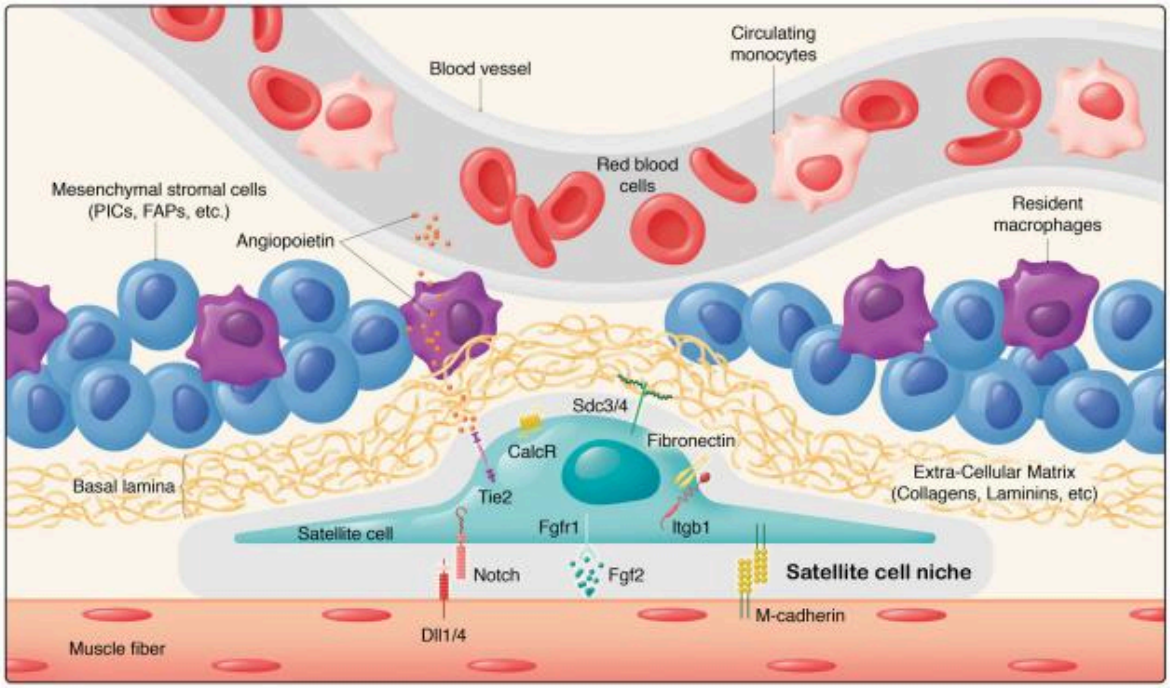

Figure 25: Satellite cell niche composition (adapted from Brendan Evano and Shahragim Tajbakhsh et al., 2018).

2.3.1 Satellite cell-intrinsic factors

It has been shown that PAX7 plays a crucial role in SatC quiescence and maintenance; it also protects cells from the apoptosis (Evano & Tajbakhsh, 2018; Florkowska et al., 2020). Indeed, PAX7 null mice die at two weeks of age and exhibit reduced muscle mass and complete absence of SatC (Seale et al., 2000). In addition, upon PAX7 ablation in adulthood, SatC displays cell-cycle arrest and dysregulation of myogenesis (von Maltzahn et al., 2013). Of note, PAX7 is also expressed in proliferating SatC but at lower levels, and its transcripts are rapidly downregulated in the myogenic differentiation (Seale et al., 2000; von Maltzahn et al., 2013). Genome-wide analysis performed in FACS-isolated SatC established a detailed signature of quiescence, including M-cad, Itga7, and CD34 (Figure 24) (Cho & Doles, 2017). SatC can also

proliferate while remaining in limited numbers, thus expanding the stem cell pool by inhibiting differentiation (Yin et al., 2013).

The Notch signaling is required to maintain SatC in the quiescent state (Baghdadi et al., 2018; Bjornson et al., 2012; Mourikis et al., 2012). Indeed, Notch3 signaling inhibits *Myod1* expression and, therefore, cell activation and differentiation (Kuroda et al., 1999). Also, Klf7, a member of the Kruppel-like transcriptional regulator family involved in cell stemness and proliferation induces SatC quiescence downstream of the Notch 3 pathway (Wang et al., 2016).

2.3.2 Extrinsic factors to satellite cells

A study combining single-cell transcriptomics and CyTOF mass cytometry revealed a new tenocyte cell type constituting the niche. These cells contribute to the remodeling of the ECM and the maintenance of new muscle fibers in the tendon through collagen secretion and thus collaborate with FAPs during the muscle regeneration (Giordani et al., 2019). Also, recent RNAseq data revealed the presence of several types of immune cells, mainly macrophages and neutrophils, reside within the cell niche (Bentzinger, Wang, Dumont, et al., 2013), which may play a role in SatC activation upon injury.

ECM plays a vital role in preserving SatC quiescence (dormant state), the components of which include collagens (e.g., Col6a1, Col5a1), laminins (e.g., lama2, lamb1), and fibronectin (Fn1) are mainly secreted by FAPs (Chapman et al., 2017). ECM deposition defines niche stiffness, which in turn impacts SatC self-renewal, proliferation, and differentiation (Ishii et al., 2018; Rayagiri et al., 2018). SatC are attached to the basal lamina by integrins (Figure 25), and Itgb1/integrin-a7 interactions with laminin-211 (laminin- $\alpha 2\beta 1\gamma 1$) from the basal lamina sustains cell adhesion and protects SatC from apoptosis (Burkin & Kaufman, 1999). Also, integrin beta 1 (Itgb1) deficient SatC lose their dormancy and stemness potential (Rozo et al., 2016a).

Attaching to the ECM is crucial for SatC homeostasis. Indeed, Syndecan-4 (Sdc4, a plasma membrane proteoglycan), and Frizzled-7 (Fzd7, a receptor of the secreted glycoprotein Wnt), form a co-receptor complex in SatC that binds fibronectin (FN) and stimulates stem cell symmetric expansion (Figure 25) (Bentzinger, Wang, von Maltzahn, et al., 2013). Additionally, a cluster of differentiation 34 (CD34) promotes the interaction of SatC with the ECM and, consequently, the cell quiescence (Beauchamp et al., 2000). Interestingly, it has been shown that the Notch pathway stimulates the production of collagen V by SatC that binds to the calcitonin receptor expressed on the SatC membrane. Collagen V depletion leads to a progressive decrease in the stem cell stock (Baghdadi et al., 2018).

Adjacent fiber, another contributor to the niche, plays a role in the physiological functions of the SatC niche. It has been shown that the fiber secretes Wnt4, which activates the non-canonical signaling pathway of Wnt in SatC to maintain their quiescence (Figure 26) (Eliazer et al., 2019). Myofibers also secrete myostatin (MSTN), a TGF-β (Transforming growth factor beta) family member and a negative regulator of muscle mass (Saunders et al., 2006), which prevents SatC activation (McCroskery et al., 2003) and activates the cell-cycle

suppresser p21 *in vitro* (Thomas et al., 2000). In addition, Notch3 ligand (a transmembrane receptor protein), Delta-like 4 (dll4), is expressed in myofibers (Figure 26) (Low et al., 2018).

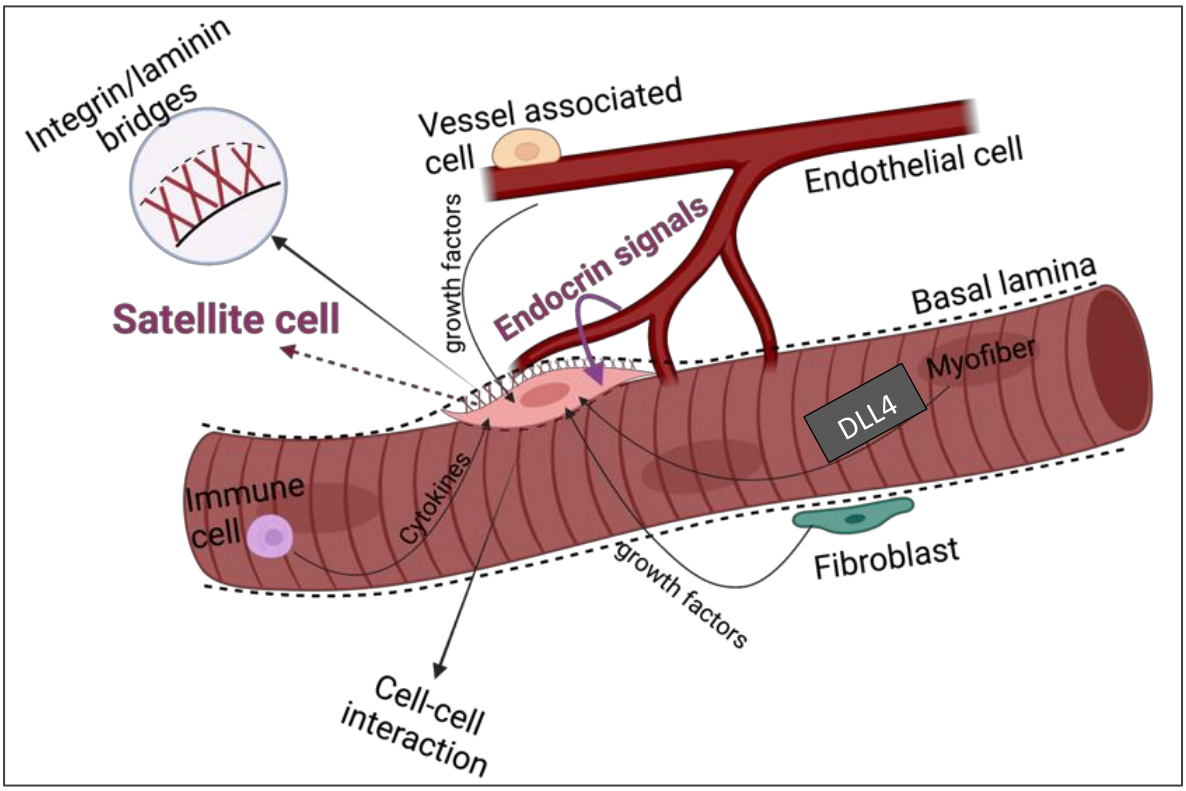

Figure 26: Schematic representation of satellite cell interaction with its niche.

The microvascular network provides an essential supply of nutrients and oxygen to the muscle cells, whose function is mainly dependent on it. Up to 80 % of SatC niches lie in the vicinity of capillaries, suggesting the importance of the vascularization for SatC activity (Figure 25) (Christov et al., 2007). SatC secrete vascular endothelial growth factor (VEGF) to promote angiogenesis by recruiting endothelial cells (Abou-Khalil et al., 2009; Verma et al., 2018). In addition, DLL4 is predominantly secreted by endothelial cells to endorse satellite cell quiescence and self-renewal after muscle injury (Verma et al., 2018). Endocrine signals delivered by the vascular system to the niche modulate cell homeostasis since sex hormones induce SatC quiescence by promoting the Notch signaling (J.-H. Kim et al., 2016a). Although the exact molecular targets of sex hormones are unknown in SatC and their mechanisms are still to be unraveled.

Pericytes, a cell type found in the basal lamina of the capillary endothelium, control the proliferation and survival of endothelial during angiogenesis and the assembly of the basement membrane (Franco et al., 2011). These cells influence the behavior of myogenic cells differentiation through secretion of the growth hormone-insulin-like growth factor 1 (IGF1) and quiescence via Ang1 (Kostallari et al., 2015).

In conclusion, through SatC-surrounding cell and SatC-myofiber interactions, a complex set of molecules diffuse into the niche, such as Wnt, Notch, VEGF, and IGF either to maintain SatC quiescence, activation, or proliferation and differentiation (Figure 27). However, many studies investigated and revealed signaling pathways regulating SatC function; a lot is still to be uncovered using this era's molecular cutting-edge technologies.

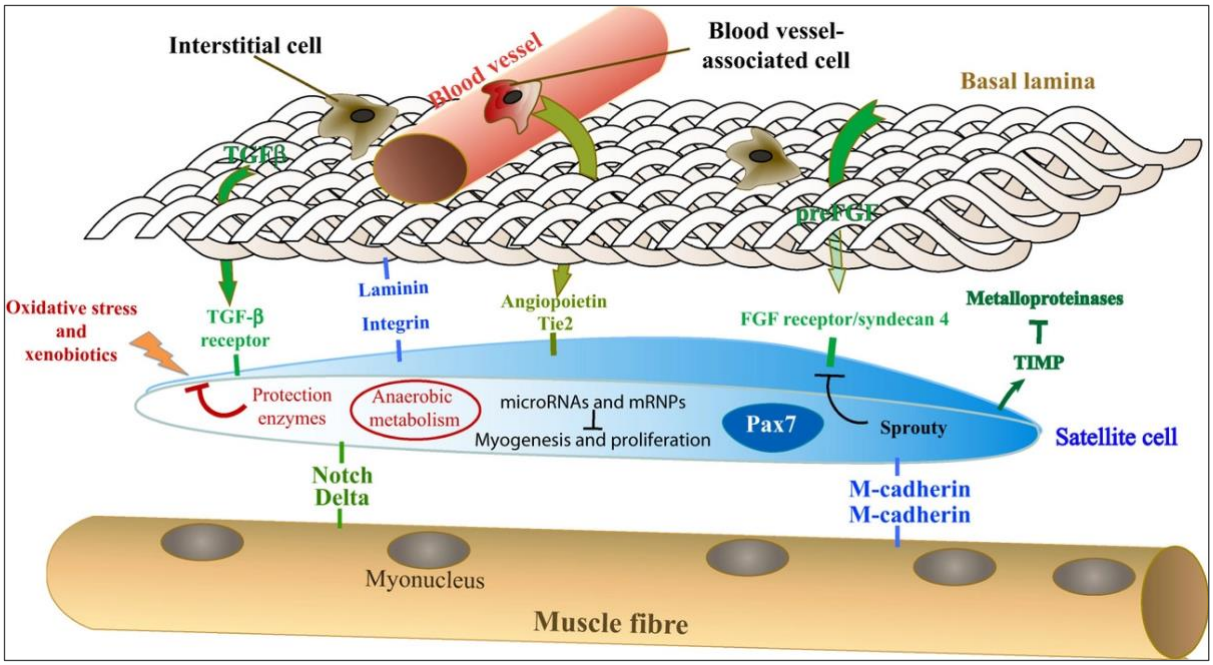

Figure 27: Signaling within the satellite cell niche (adapted from Montarras et al., 2013).

2.4 Heterogeneity of the satellite cell population

SatC are considered to be a heterogeneous stem cell population according to their genetic signature (Cho & Doles, 2017), deoxyribonucleic acid (DNA) template origin (Rocheteau et al., 2012; Shinin et al., 2006), proliferation rate (Ono et al., 2012), asymmetric division, myogenic differentiation capacity as well as transplantation potential (Kuang et al., 2007).

Recent findings suggest that SatC form functionally heterogeneous sub-populations characterized by the expression of other markers along with *Pax7*. These cells exhibit variable capacities to activate, divide and self-renew (Cho & Doles, 2017). Indeed, the scRNA-seq analysis showed the transcriptional heterogeneity of the SatC pool since cells were grouped into two different clusters: one enriched for genes associated with quiescence (i.e., PAX7 and the calcitonin receptor-CALCR), and the other containing genes involved in the early stage of activation (MYOD, MYF5) (Dell'Orso et al., 2019). Such differences reflect differential "stemness" potential and activation states of SatC.

The heterogeneity of the SatC population is also dependent on the cell cycle. The cell cycle is a four-phase process in which the cell increases in size (G1-phase), copies its DNA template (S-phase), prepares to divide (G2-phase), and then divides to generate two cells (mitosis, M-phase). The G0 phase corresponds to the quiescent state of the cells (Figure 28), which is a reversible cellular state representing a non-cycling cell. SatC self-renew, i.e., replenish the stem cell pool, by returning to the quiescent state (W. Chen et al., 2020a; Yin et al., 2013). Moreover, recent studies have shown intermediate states between quiescence (G0) and activation.

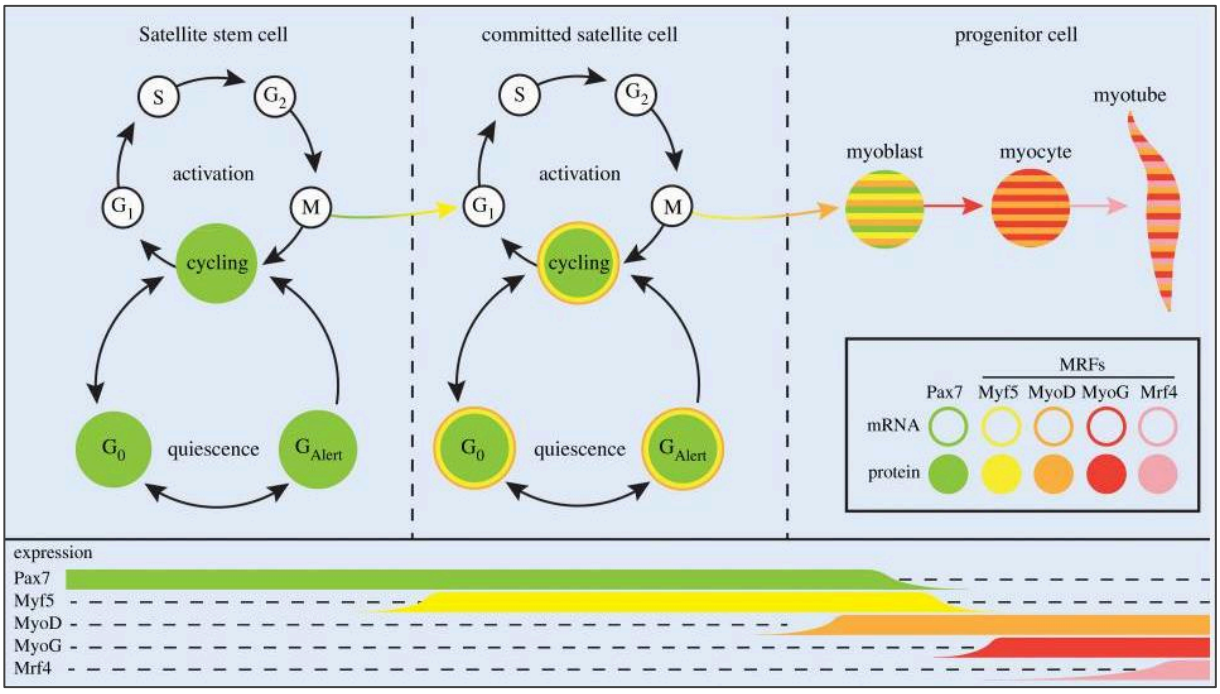

Figure 28: Cell cycle heterogeneity of satellite cells (adapted from Chen et al., 2020).

Rodgers et al. described an "alert" state [Phase G(alert)] that was similar to, but still distinguished from, quiescence, lying between the G0 and G2 phases (Figure 28) (Rodgers et al., 2014). G(alert) phase can be activated in case of a signal muscle injury or environmental stress (toxins, dioxins) to counter aberrant proliferation (Figure 28) (Rodgers et al., 2014). SatC in G(alert) phase are slightly larger, ready for the first division, and show increased mitochondrial activity (Rodgers et al., 2014). Of note, chronic damage accumulation derive an irreversible arrest of the G1 phase of SatC, a state also known as cellular senescence (W. Chen et al., 2020a).

SatC heterogeneity has also been observed in the regenerating environment. Single-cell mass cytometry analysis conducted on isolated SatC after acute injury revealed that cells express a novel combination of surface markers cluster of differentiation 9 (CD9) and 104 (CD104) in the transition toward the differentiation program (Porpiglia et al., 2017). The decision between cell cycle progression or differentiation is made during the G1 phase (Figure 28). Cell cycle regulation of SatC depends on the expression of several factors, including myogenic regulatory factors (MRFs) such as MYF5 and MYOD1, as well as cyclin-dependent kinases (CDKs), cyclin-dependent kinase inhibitors (CDKIs), and the retinoblastoma protein Rb (Kitzmann & Fernandez, 2001) (Figure 28). Thus, SatC form a heterogeneous population differing in genetic signature, stemness potential, quiescence status, and cell cycle progression, all of this leading to varying myogenic capacity and subsequently myofiber formation capability.

3 Regeneration of skeletal muscles

3.1 Overview of the regeneration process

Injuries to skeletal muscle in humans or rodents can result from exposure to myotoxic agents (e.g,. Cardiotoxin-Ctx, Notexin-Ntx), sharp or blunt trauma such as puncture or contusion, ischemia, exposure to hot or cold temperatures (Figure 29) (Baghdadi & Tajbakhsh, 2018), burst and continuous muscle contraction during excessive sports activities, and diseases such as dystrophies.

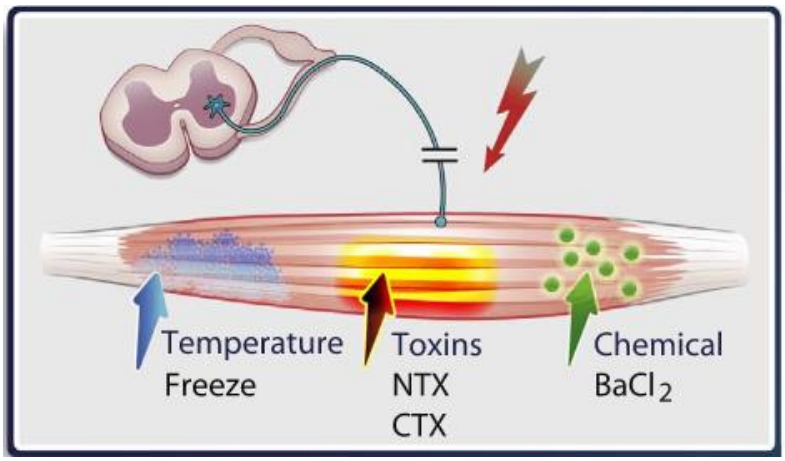

Figure 29: Injury models in skeletal muscles (adapted from Baghdadi & Tajbakhsh, 2018).

SatC are mandatory and sufficient for the adult muscle repair (Lepper et al., 2011). The process of skeletal muscle regeneration can be divided into five phases: fiber necrosis, inflammation, SatC activation/differentiation, remodeling of newly regenerated tissue, and the maturation of newly formed myofibers (Figure 30) (Musarò, 2014).

Muscle regeneration recapitulates in many aspects the embryonic development, particularly the expression of main MRFs during the differentiation of progenitor cells to form uni-nucleated muscle cells named myocytes.

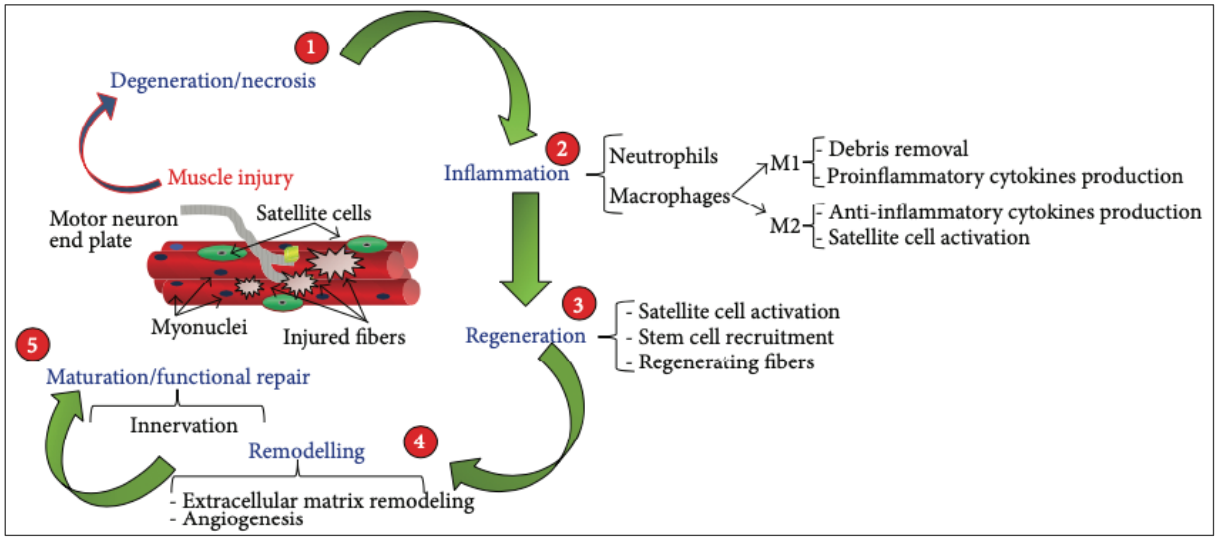

Figure 30: Muscle regeneration phases upon injury (adapted from Musarò, 2014).

The latter then fuse to generate cylindric multi-nucleated structures called muscle fibers (Musarò, 2014). Skeletal muscle repair is a process that involves different cellular and molecular responses (Musarò, 2014). Although the repair process is similar after different injuries, the kinetics and amplitude of each phase depend on the particularity of the damage, the extent of the damage, or the damage model used (Chargé & Rudnicki, 2004; Musarò, 2014).

Initially, there is rapid necrosis of the myofibers, characterized by the disruption of the sarcolemma of muscle fibers and thus an increase in permeability and calcium ion influx, loss of myonuclei, contractile material, and cellular organelles dissolution. Necrotic fibers upon haematoxylin and eosin staining (H&E) appear pale (Figure 31A) and enlarged with altered internal architecture (Figure 31B) with the presence of internal nuclei, which can reflect the invasion of macrophages to eliminate debris (Figure 31C-D) (Chargé & Rudnicki, 2004; Musarò, 2014).

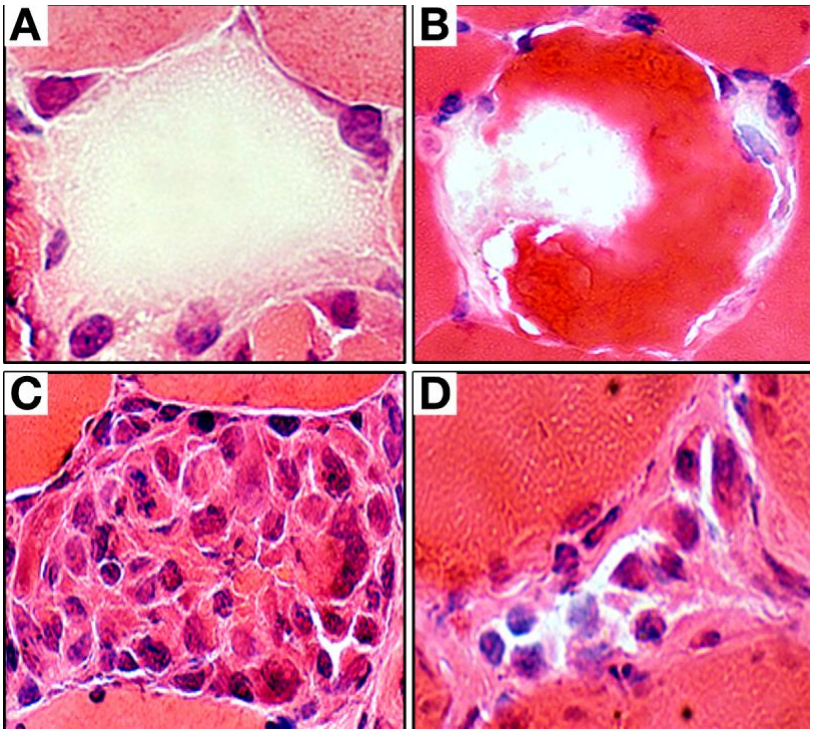

Figure 31: H&E staining demonstrating different stages of myofiber necrosis.

Fiber necrosis stages revealed with H&E staining showing (A) pale cytoplasm, (B) disrupted sarcolemma, and (C) macrophages invasion to remove cellular debris followed by (D) complete collapse of the fiber.
(adapted from: https://neuromuscular.wustl.edu/pathol/necrosis.htm)

As a result of muscle injury, quiescent SatC become activated (Figure 32). Five days after injection of Ctx in tibialis muscles of rodents, regenerating muscles exhibit mostly mononuclear cells (satellite cells, immune cells, etc.) and some multinucleated myotubes expressing the embryonic devMHC (Figure 32). Two days later (day 7), muscles are mainly composed of newly formed centri-nucleated myotubes, some of which maintain the expression of eMHC (Figure 32-red). Myotubes later mature into multinucleated myofibers on day 21 (Figure 32). Of note, the nuclei of intact myofibers are located at the periphery (Day 0), while newly regenerating myofibers are characterized by centrally located myonuclei (Day 5, 7, and 21). During the maturation process, the myonuclei migrate to the periphery (Schmidt et al., 2019).

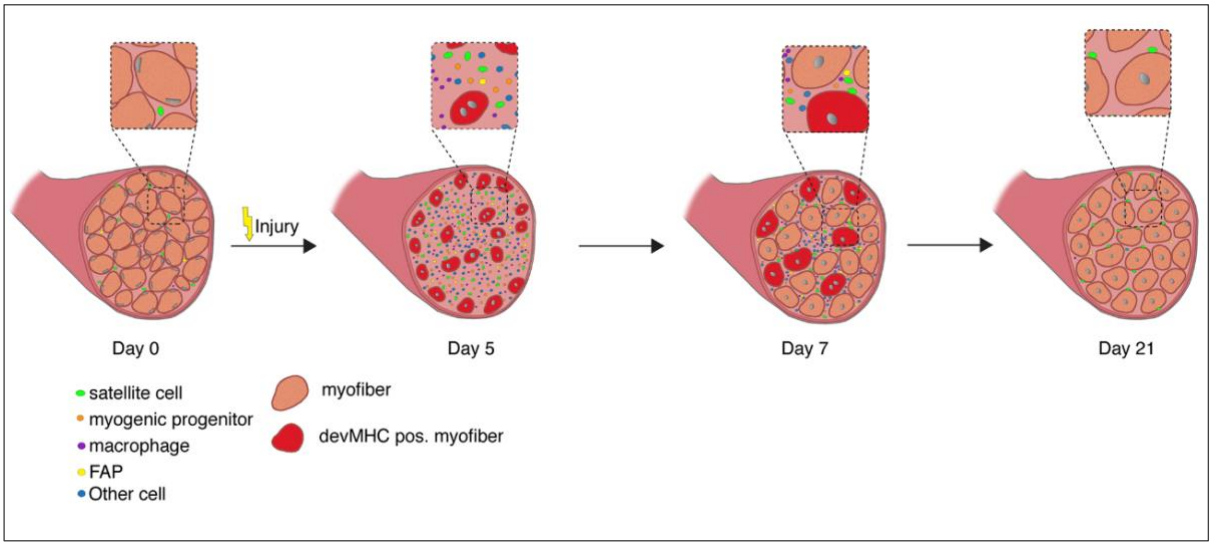

Figure 32: Time course of muscle regeneration upon cardiotoxin (Ctx) injury (adapted from Schmidt et al., 2019).

3.2 Role of satellite cells in muscle regeneration

3.2.1 Activation/division of satellite cells

Upon injury, SatC receive various signals released from necrotic myofibers, immune infiltration, fibroblasts, etc. that induce their activation and cell cycle entry (Chargé & Rudnicki, 2004; Dumont et al., 2015; Fu et al., 2015; Musarò, 2014). Damages to the basal lamina destroy the collagen–laminin network, where SatC anchor via α7/β1 integrins, which disturbs cell quiescence (Figure 26) (Burkin & Kaufman, 1999; Liu et al., 2008; Loreti & Sacco, 2022). Nitric oxide (NO) released by necrotic fibers diffuses through the membrane of quiescent SatC and induces their activation (Wozniak & Anderson., 2006). Interestingly, the expression of *Pax7*, as well as targets of Notch signaling, are reduced before the entry of SatC into cell cycle, allowing MYOD protein accumulation (Evano & Tajbakhsh, 2018). Other factors from the microenvironment play critical roles in SatC activation and differentiation that will be discussed further in section **3.3**. Muscle regeneration relies on the capacities of SatC to

activate and proliferate, giving rise to a population of transient amplifying myogenic precursor cells that express *Pax7* along with the transcription factors *Myf5* and MyoD (Yin et al., 2013).

After activation, SatC quit their G0 dormancy state and re-entered cell cycle (Fu et al., 2015). Classically, SatC is able to undergo symmetric or asymmetric divisions during muscle regeneration (Figure 33), and the molecular detriments controlling SatC choice between both paths remain unclear (Cossu & Tajbakhsh, 2007). Indeed, PAX7+ primary muscle cell divide to generate a PAX7+/MYF5+ progenitor, which expresses later MyoD and differentiate into myocytes, and a PAX7+/MYF5- daughter cell that re-enter quiescence to replenish the stem cell niche (Kuang et al., 2007), which makes MYF5 a significant marker of SatC asymmetric division (Kuang et al., 2007). Notch signaling was also shown to take action in SatC asymmetric division since Notch ligand (Delta-1) was only spotted in one daughter cell, while the other cell harbored the Notch3 receptor (Kuang et al., 2007).

Not only signals but also localization plays an important role in the asymmetric division of SatC since planar orientation division along the basal lamina is symmetric and generates identical daughter stem cells (Figure 33). In contrast, SatC divisions in an apical-basal orientation are asymmetric and give rise to a stem cell at the basal surface and a committed daughter cell destined for differentiation on the apical surface (Figure 33). It has been reported that 3 days post muscle injury with Ntx, SatC rather undergo symmetric division, expanding the population; however, two days later, cells switch to asymmetric division, generating myoblasts to form myofibers while maintaining the stem cell pool (Evano et al., 2020).

Importantly, SatC isolated from mice muscles with Duchenne dystrophy displays accelerated differentiation and impaired asymmetric division (Yablonka-Reuveni & Anderson, 2006). These data suggest that under pathological conditions, SatC undergo strictly symmetric differentiation, and the balance between stem cells and committed progenitors within the SatC compartment is disturbed (Figure 33).

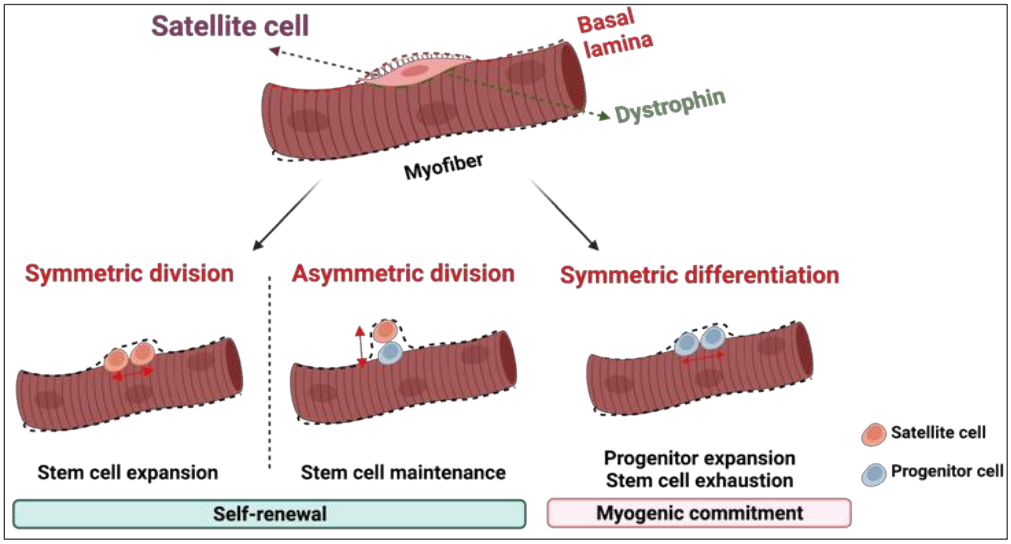

Figure 33: A schematic representation of satellite cell symmetric, asymmetric division and symmetric differentiation.

3.2.2 Satellite cells differentiation

SatC differentiation is an orchestrated process that requires the timely regulated expression of myogenic markers called MRFs (Figure 34), namely *Myf5*, *MyoD*, Myogenin (*Myog*), and myogenic regulatory factor 4 (MRF4) transcription factors (Figure 34) (Gattazzo et al., 2020; Smith et al., 1994). It has been shown that quiescent and activated SCs express PAX7; however, the up-regulation of MYF5, followed by MYOD launchs the myogenic differentiation program. PAX7 controls the entry of SatC into the myogenic differentiation program, and activation of the MyoD gene allows differentiation into the myoblasts (Seale et al., 2000).

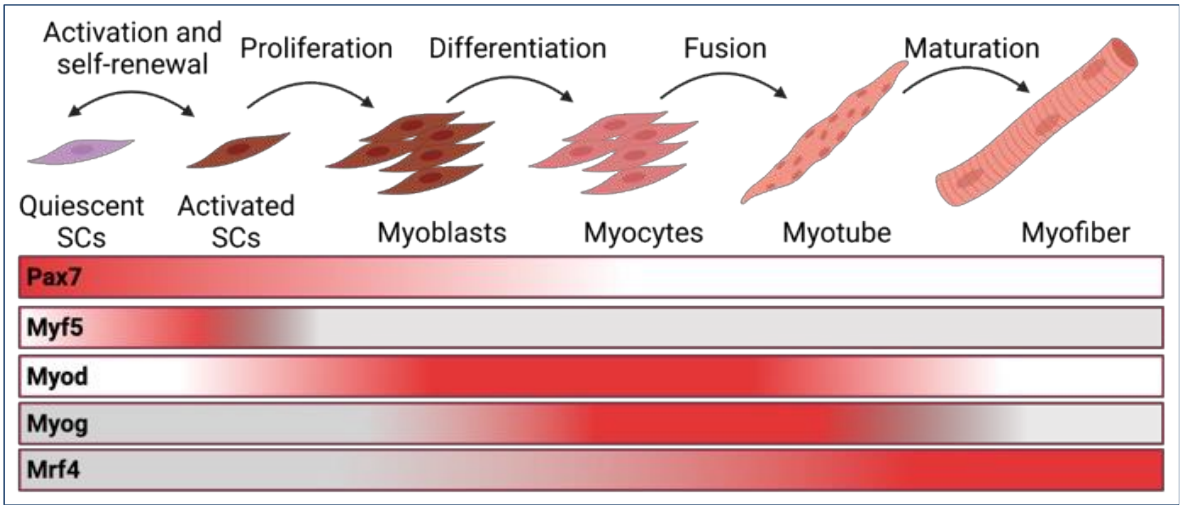

Figure 34: Myogenic regulatory factor expression during satellite cell differentiation.

In the absence of MYOD, SatC proliferate slowly, and differentiation is delayed (Sabourin et al., 1999). The myogenic determination gene *Myf5*, mainly expressed in activated SatC, induces the expression of the differentiation factor MYOG and directly triggers the myogenesis process (Zammit, 2017). MYOG is a crucial transcription factor mainly expressed in myocytes. The latter fuse to each other or existing myofibers (Figure 34 and 35) (Baghdadi & Tajbakhsh, 2018; Ganassi et al., 2018).

In the late myotube state, MRF4 is induced for the final maturation of the regenerative fibers (Figure 34). Mice mutant for Mrf4 show deficit myotome differentiation, defects in intercostal muscle morphology, and a decreased ability of cells to migrate to the cartilage, suggesting a specific role for MRF4 in the establishment of overall tissue structure (Vivian et al., 2000).

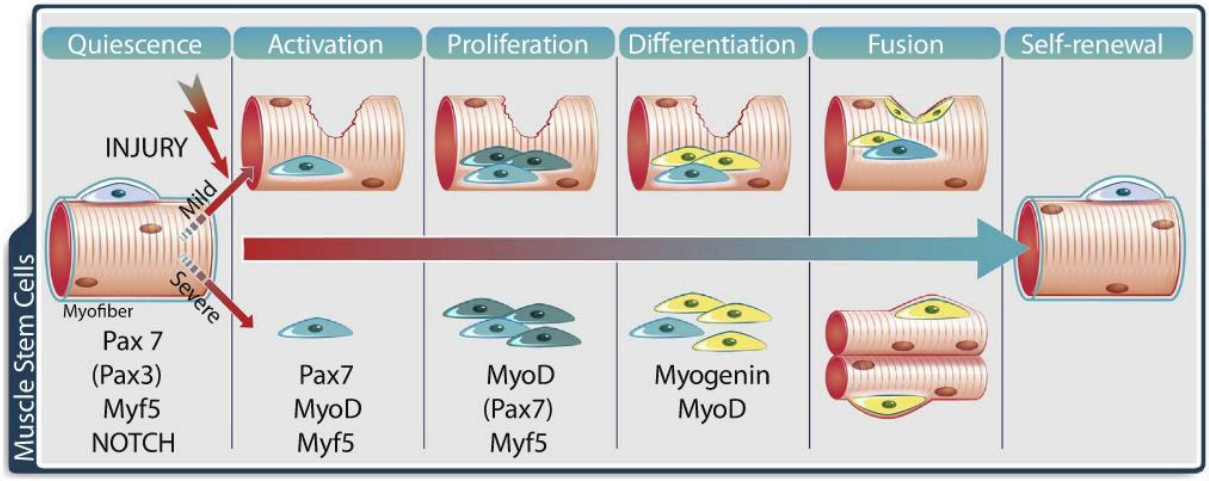

Figure 35: Stages of satellite cell differentiation during muscle regeneration (adapted from Baghdadi & Tajbakhsh, 2018).

3.2.3 Myoblast fusion

Myoblast fusion results from an orchestrated sequence of events, including clustering, cell alignment, the establishment of close cell-cell contacts, and fusion of plasma membranes (Sampath et al., 2018). Myoblasts can fuse with pre-existing muscle fibers to repair them or fuse with each other to form new fibers (Figure 35) (Yablonka-Reuveni., 2011).

Multiple proteins are involved in regulating myocyte cell fusion and can be located intracellularly or at the membrane. Indeed, it has been shown that Zebrafish muscles lacking MYOG remain predominantly mononuclear (Ganassi et al., 2018). In addition, the mitogen p38 signaling in SatC inhibits the c-Jun N-terminal kinase (JNK) pathway leading to cell cycle exit and allowing myoblast differentiation (Perdiguero et al., 2007). Likewise, treatment with a P38 inhibitor prevents myocyte fusion and myofiber formation (Lluís et al., 2006; Segalés et al., 2016).

Trans-membrane proteins such as Itga7 and M-cad play an essential role in intercellular recognition and fusion (McClure et al., 2019). Other integrins have also shown a role in fusion, including Itgα3 and Itgα7, as well as the CD9 tetraspanin (Przewoźniak et al., 2013). Interestingly, stromal-derived factor 1 (Sdf1), a ligand of CXCR4, induces the expression of CD9 to control myoblast fusion (Figure 36) (Leikina et al., 2018; Millay et al., 2014). It has been reported that the tight regulation of CD9 is crucial for normal myocyte fusion and muscle fiber formation upon injury (Charrin et al., 2013).

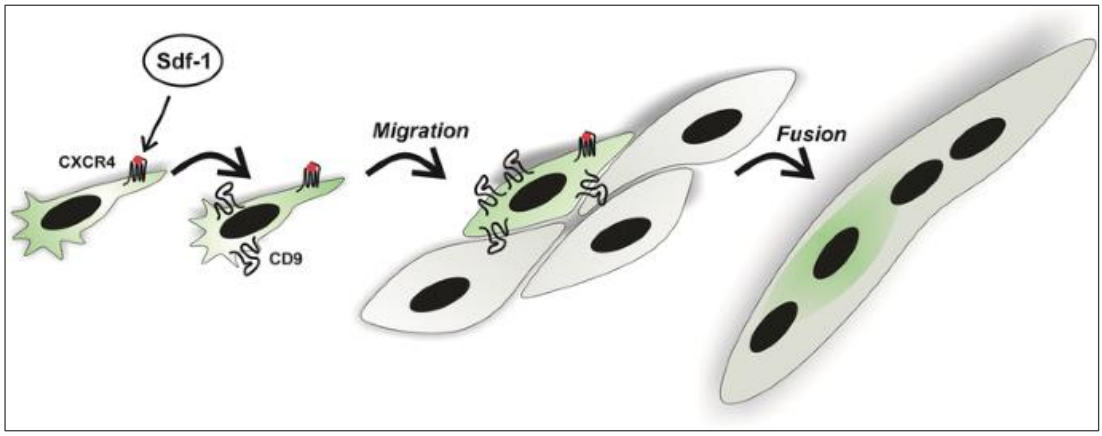

Figure 36: Sdf1 via CXCR4 induces CD9 expression promoting myocyte migration and fusion (adapted from Brzoska et al., 2015).

Other transmembrane proteins play critical roles in myoblast fusion, namely, Myomaker (MYMK) and Myomerger [, since they are both considered skeletal muscle fusogenic -glycopeptides involved in the cell fusion (Leikina et al., 2018; Millay et al., 2014), and are independently engaged in distinct stages of fusion]. Myomaker is essential for the early stage of cell fusion involving the transition to hemifusion - the connection of the two cell membranes (Figure 37) (Leikina et al., 2018; Millay et al., 2014; Petrany & Millay, 2019). Genetic deletion of myomaker abolished muscle regeneration in mice, resulting in severe muscle destruction after injury (Millay et al., 2014). Intriguingly, MYOG is required for the

protein expression of the MYOMAKER (Ganassi et al., 2018). MYOMERGER, also known as MYOMIXER or MINION, is required to complete cell fusion by altering membrane conformations to form a fusion pore (Figure 37) (Quinn et al., 2017). Interestingly, MYOMAKER and MYOMERGER do not require physical interaction between them.

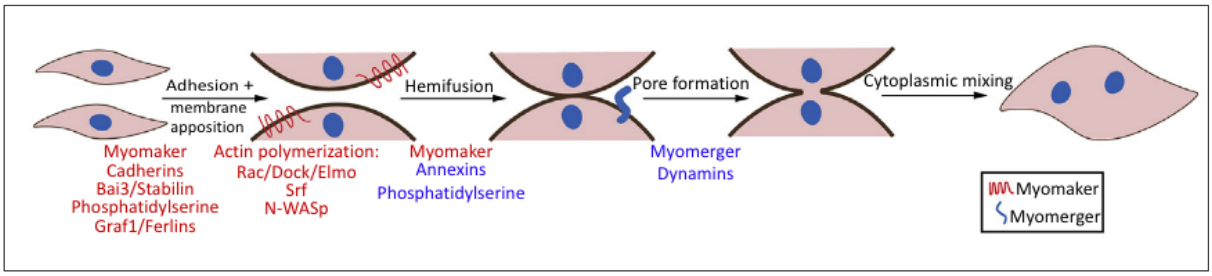

Figure 37: Myocyte fusion controlled by Myomaker and Myomerger (adapted from Petrany & Millay, 2019).

The actin cytoskeleton plays an important role during the myoblast fusion (Shilagardi et al., 2013). Still, it is not defined whether the functions of CXCR4, CD9, MYOMAKER, and MYOMERGER are upstream or downstream of actin rearrangements associated with the cell fusion process. Notably, the new fibers are characterized by the expression of the eMHC (Schiaffino et al., 2015).

3.2.4 Re-establishing the stem cell niche

After activation and differentiation of SatC and at the end of the regeneration process, cells should undergo quiescence again to replenish the niche (Figure 38). *In vitro* experiments showed that multiple signalling pathways actively promote SatC quiescence. Indeed, activation of the Ang1/endothelium-specific receptor tyrosine kinase2 (Tie2) signaling pathway promotes the return to dormancy of myoblasts (Abou-Khalil et al., 2009). Interestingly, in humans and mouse, Tie2 is mainly expressed in quiescence SatC.

Our understanding of reversion back to quiescence *in vivo* is limited to (Yin et al., 2013); nevertheless, it has been reported that Notch3 null mice exhibit hyperplasia of muscles and out-of-control proliferation of SatC (Kitamoto & Hanaoka, 2010). Moreover, SatC deficient for Sprouty1 (Spry1), a negative regulator of receptor tyrosine kinase, cannot return to quiescence and undergo apoptosis, leading to a diminished progenitor cell pool. These data demonstrate an essential role of Spry1 in reviving satellite cell pool size after injury (Shea et al., 2010). The microenvironment plays a vital role in SatC reverse quiescence since MSTN secreted by myoblasts and myofibers was shown to negatively regulate the cell cycle of SatC (M. Thomas et al., 2000). However, additional *in vivo* analysis and genetic approaches targeting satellite cells will clarify the signal cascades that regulate the quiescence and the return to quiescence from the proliferation state (Figure 38).

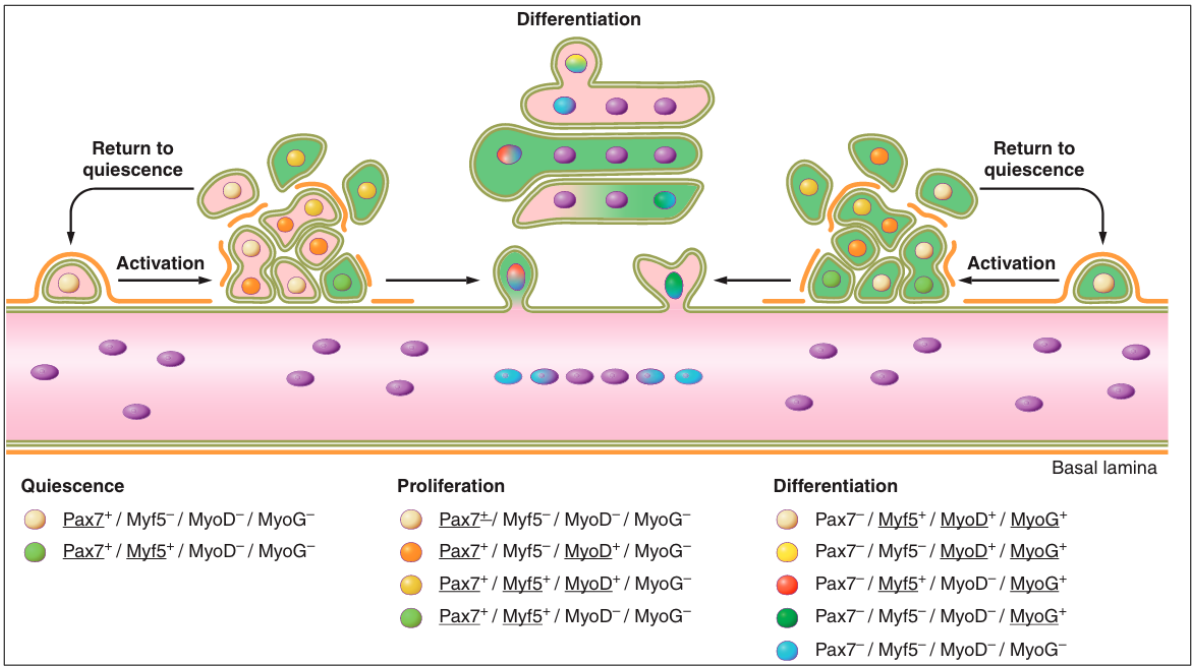

Figure 38: Satellite cell activation, differentiation, and return to quiescence upon muscles injury (adapted from Yin et al., 2013).

Quiescent PAX7+ satellite cells undergo differentiation upon activation by expressing various MRFs, including Myf5, MyoD, and Myog. At the end of the regeneration process, satellite cells return to quiescence to replenish the stem cell niche.

3.3 Role of the microenvironment in muscle regeneration

The muscle microenvironment is a key factor affecting the efficiency and outcome of myofiber regeneration. There are several cell types directly involved in SatC function and muscle formation upon injury, and we will discuss main cell types implicated.

3.3.1 Endothelial cells (CD31+)

The vascular system provides SatC with oxygen and nutriments and it is no surprise that the majority of the niches are localised close to capillaries (Christov et al., 2007). In the case of extensive damage to the blood supply of the injured area, regeneration can only take place when new angiogenesis occurs. Indeed, endothelial cells (CD31+) promote SatC proliferation through IGF1, fibroblast growth factor (FGF), and hepatocyte growth factor (HGF) secretion (Pannérec et al., 2012). They stimulate myogenesis *in vitro* (Latroche et al., 2017), and VEGF promotes myoblasts migration and survival *in vivo* (Germani et al., 2003). In turn, myoblasts promote angiogenesis via the secretion of vascular growth factors including VEGF and Ang1 (McClung et al., 2015).

3.3.2 Immune cells (CD45+)

Early phases of muscle injury are accompanied by infiltration of the damaged area by the first wave of inflammatory cells expressing CD45, mainly neutrophils and pro-inflammatory macrophages expressing F4/80 and Ly6c (also named M1) (Figure 39) (Loreti & Sacco, 2022; Yang & Hu, 2018). The number of infiltrated neutrophils culminates in 6 to 24 hours after injury and declines rapidly 72 to 96 hours. Pro-inflammatory macrophages number reach a peak at 48 h (Loreti & Sacco, 2022; Yang & Hu, 2018). Damaged myofibers participate by secretes factors to regulate the recruitment of inflammatory cells and activation SatC (Zhou et al., 2020).

After infiltration, M1 phagocytose cellular debris and remove disrupted myofilaments, other cytosolic structures, and damaged sarcolemma. In addition, M1 macrophages activate SatC proliferation and inhibit their premature differentiation by secreting various cytokines including tumor necrosis factor alpha (TNF-a), as well as interleukin 6 (IL-6) and interleukin 1-beta (IL-1β) (Loreti & Sacco, 2022; Saclier et al., 2013), and coordinate the angiogenesis/myogenesis coupling promoting muscle regenerating upon damage (Latroche et al., 2017). Endothelium and macrophages secrete granulocyte colony-stimulating factor (G-CSF) that stimulates the proliferation, differentiation, and survival of muscle cells (Hara et al., 2011). Interestingly, injured muscles are characterized by intra-tissue glutamine restriction. Low glutamine levels confer on macrophages the metabolic capacity to secrete glutamine, and macrophage-derived glutamine importation by SatC activates the mammalian target of rapamycin (mTOR) signaling and promotes cell proliferation and differentiation (Shang et al., 2020).

The second wave of infiltration occurs around 96h upon injury. M1 macrophages are replaced with anti-inflammatory macrophages expressing F4/80 and CD206 (also called M2) (Figure 39), which promote SatC myogenesis and myofiber formation via the secretion of growth factors such as TGF-ß (Arnold et al., 2007; Loreti & Sacco, 2022). In addition, neutrophils and T-reg cells (CD8+) infiltrate the muscles during the second wave, and secret growth factors like Amphiregulin promoting muscle formation (Burzyn et al., 2013) (Figure 39).

Despite their beneficial effects on muscle regeneration, extensive recruitment of the pro-inflammatory natural killer cells (NK1-1+) during the first infiltration stage negatively impacts muscle formation capacity (Larouche et al., 2022). Also, chronic inflammation negatively impacts muscle regeneration and the SatC function (Perandini et al., 2018).

3.3.3 Fibro-adipogenic progenitors (SCA1+)

FAPs, a mesenchymal stem cell population expressing the stem cell antigen 1 (SCA1), play an essential role during muscle formation since the balance between FAPs-mediated adipogenesis and SatC-dependent myogenesis is responsible for the normal muscle regeneration (Joe et al., 2010). Upon muscle injury, FAPs enter a phase of expansion provoked by eosinophils to contribute to ECM production through the deposition of collagen, laminin, and fibronectin which are necessary for the SatC function (Heredia et al., 2013). Moreover, FAPs- generated fibroblasts secrete growth factors, such as FGF, follistatin (FST), and the glycoprotein NCAM (Neural Cell Adhesion molecule or CD56) to promote regeneration (Figure 39) (Biferali et al., 2019; Joe et al., 2010).

Upon accomplishment of their role, FAPs are removed by M2 macrophages to clean the site for newly regenerated fibers (Biferali et al., 2019). Noteworthy, extensive fibrosis is a hallmark of several dystrophies impacting muscle and SatC homeostasis and function (Mahdy, 2019).

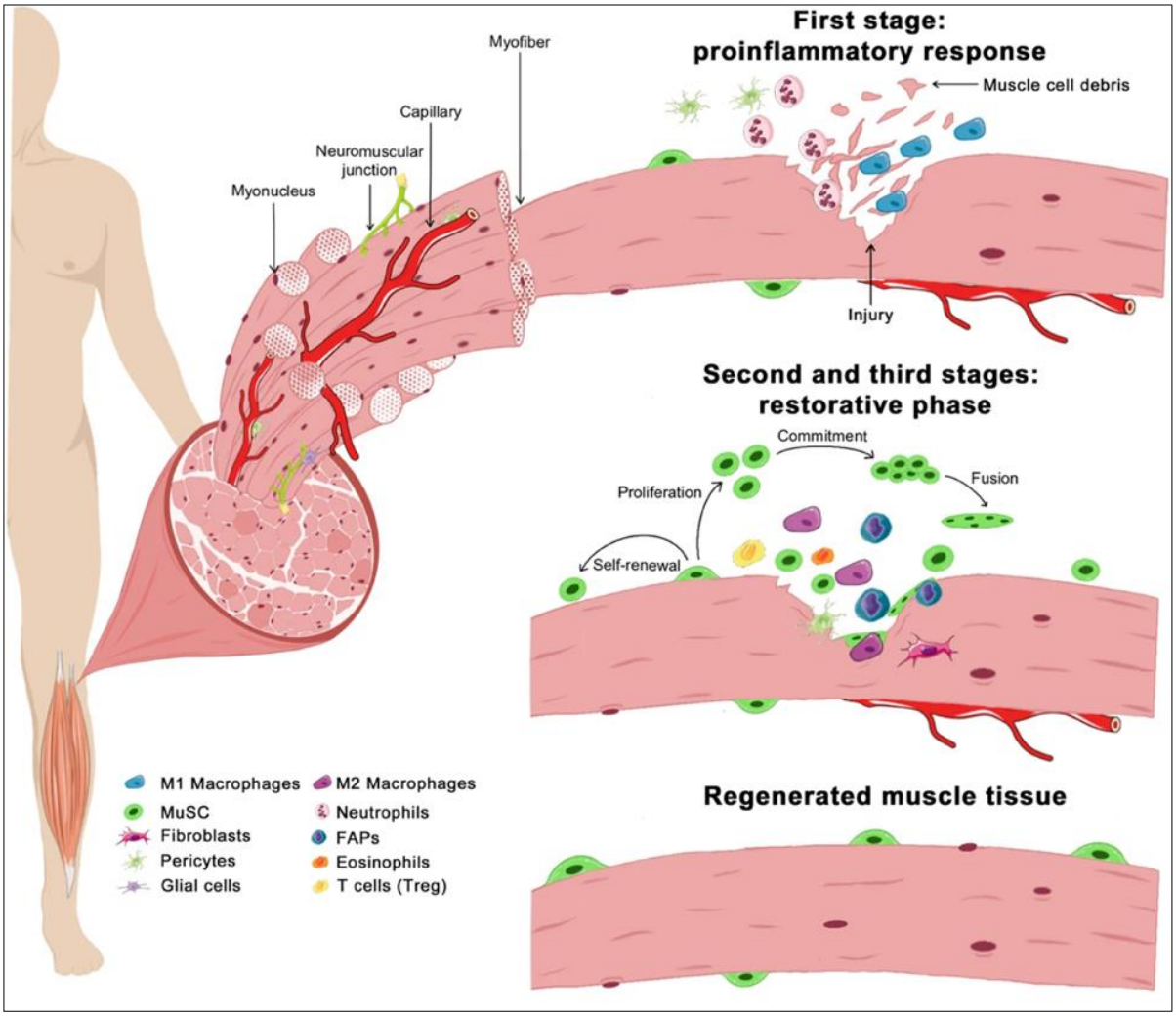

Figure 39: Microenvironment role in muscle regeneration (adapted from Loreti & Sacco, 2022).

3.4 Final touches of muscle regeneration

Although the initial phases of muscle regeneration do not depend on neural function, the following growth and maturation of regenerating muscle fibers necessitate the company of the nerve (Musarò, 2014). Interestingly, SatC and daughter cells play an essential role guiding and promoting the formation of moto-neuron in muscle injury (Daneshvar et al., 2020; Tatsumi et al., 2009).

The remodeling of connective tissue and angiogenesis highlight the final stage of the regenerative process (Grounds, 2008) (Figure 40). This stage is characterized by the activation of fibroblasts, leading to the production of several types of collagens, fibronectin, laminin, etc., which serves to stabilize the tissue, act as a support for the newly regenerated fibers, and guide the formation of neuromuscular junctions (Lluri et al., 2006). It is worth mentioning that the newly regenerated myofibers are only functional when the muscle becomes innervated. Within two weeks of damage, newly formed NMJs can be identified between the surviving axons and the regenerated muscle fibers (Musarò, 2014). After this stage, repositioning the centri-nuclei to the periphery of the myofiber occurs (Cadot et al., 2015). The mechanisms behind this movement of nuclei is still unknown, although a recent study reported the importance of myofiber microtubules in this process (J. Liu et al., 2020).

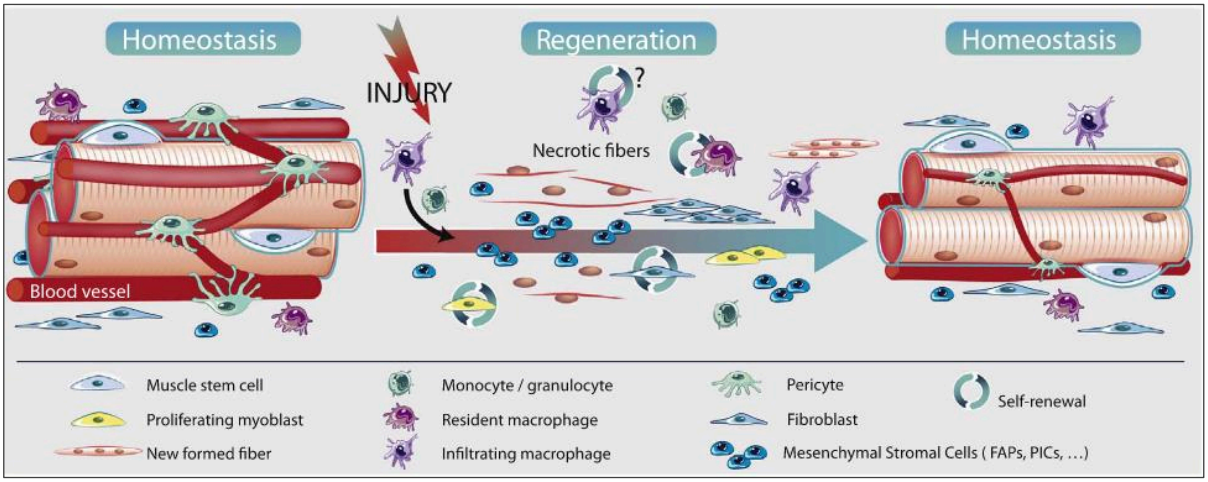

Figure 40: Schematic representation of the muscle regeneration process (adapted from Baghdadi & Tajbakhsh, 2018).

4 Muscle satellite cellopathies

Myopathies are a hereditary heterogeneous group of diseases mainly impacting skeletal muscle structure, metabolism, or channel function. They are usually characterized by muscle weakness and altered physiology, which affect patients' daily lives. Among these diseases, two genetically inherited major categories named muscular dystrophies and myopathies, both globe genetic mutations that result in muscle weakness and structural defects. While inherited myopathies exhibit disorganized myofibre structure, muscular dystrophies are distinguished by repeated cycles of myofibre degeneration and regeneration, leading to continuing substitution of muscle tissue with fat, immune infiltrates, and fibrosis (Cardamone et al., 2008). Noteworthy, while histopathological characteristics are usually different, a poor regeneration capacity is usually mutual to both muscular dystrophies and myopathies, which might shed light on SatC function and ability to regenerate fibers on demand.

To characterize the potential contribution of SatC to different myopathies and dystrophies, a recent study combined data collected on 116 myopathogenes involved in muscular dystrophies, congenital muscular dystrophies, congenital myopathies, and distal myopathy and designated two main categories : (i) primary and (ii) secondary satellite cellopathies (Ganassi et al., 2022).

4.1 Primary satellite cellopathies

Primary cello-pathies were characterized by the direct mutation in genes essential for SatC homeostasis, activation, differentiation, and myoblast fusion, including PAX7, MYOD, and MYOMAKER.

4.1.1 Pax7 mutations

Due to its essential role in SatC function, it is unsurprising that mutations in the *Pax7* gene leads to muscular dystrophies. Indeed, recently an inherited myopathy was designated to *Pax7* mutation, which was accompanied by scoliosis named progressive congenital myopathy with scoliosis (MYOSCO) (Feichtinger et al., 2019).

These patients have a global hypotonia, a growth deficit, and concomitant weakness in the diaphragm that leads to respiratory deficiency (Feichtinger et al., 2019). In addition, muscle biopsies showed the presence of atrophic fibers and fibro adipose tissue substitution (Figure 41), along with the absence of necrosis. Interestingly, lack of *Pax7* expression was accompanied by exhaustion of the SatC pool (Figure 41) (Feichtinger et al., 2019).

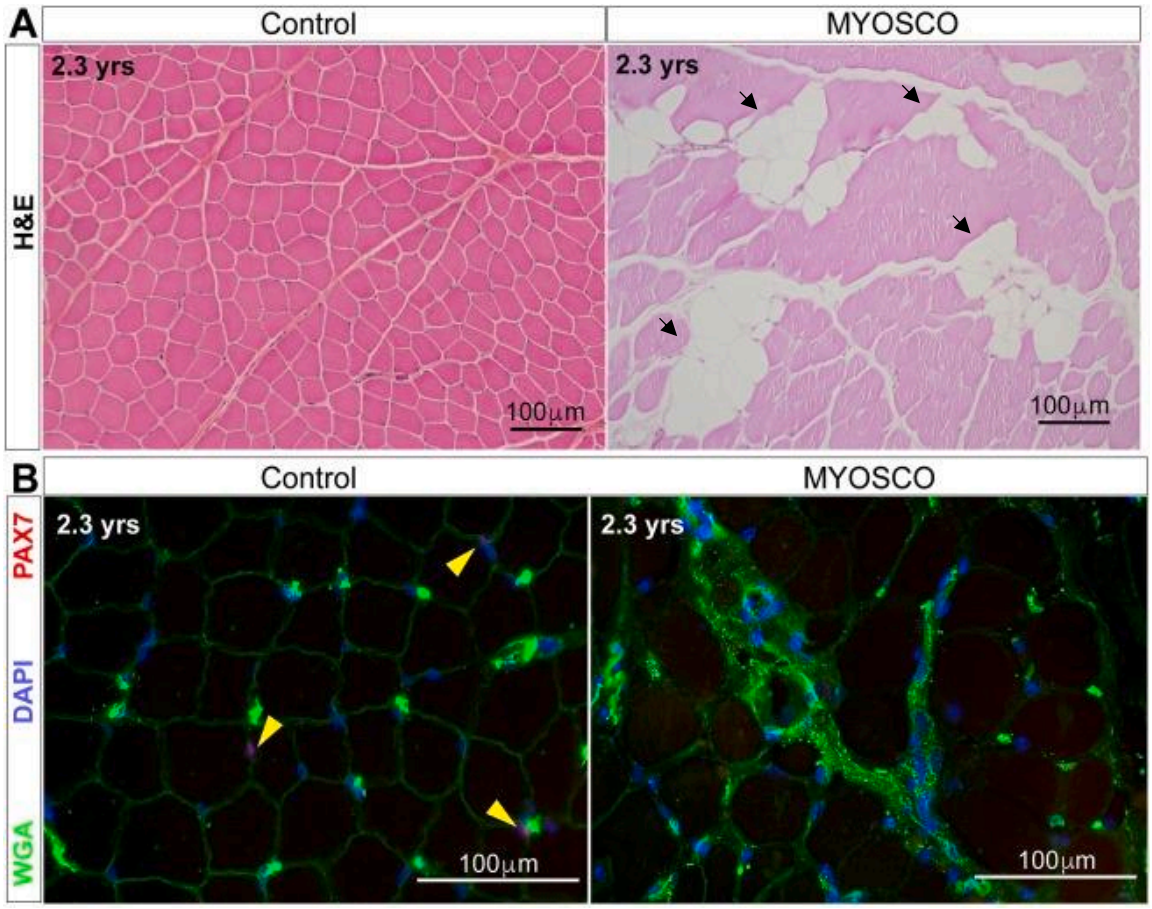

Figure 41: MYOSCO muscle dystrophy histological analysis, adapted from (Feichtinger et al., 2019).

A. *Hematoxylin and Eosin (H&E) staining of MYOSCO quadriceps muscle biopsy exhibiting myopathology, including intermyofibrillar of lipid accumulation (black arrows), compared to age-matched healthy muscle (Control).* ***B.*** *Immunofluorescence detection of PAX7 demonstrating complete abolishment of PAX7-positive satellite cells (red color) highlighted by yellow arrowheads in Control muscle sections compared to age-matched MYOSCO muscle. Myofibres are marked by Wheat germ agglutinin (WGA, green) and nuclei stained with DAPI (blue).*

4.1.2 MyoD mutations

Since responsible and mandatory for SatC differentiation and myoblast specification, *MyoD* mutation is related to primary cellopathies. Indeed, *MyoD* mutation is designated to rare myopathies named MYODRIF (Myopathy, Congenital, With Diaphragmatic Defects, Respiratory Insufficiency, And Dysmorphic Facies). Patients with MYODRIF exhibit severe respiratory failure concomitant with muscle weakness, hypotonia, and motor delay (Lopes et al., 2018, p. 1; A. Shukla et al., 2019). The extremely limited number of individuals harboring these diseases renders further characterizing the symptoms impossible and suggests that loss-of-function MYOD is incompatible with life.

4.1.3 Myomaker mutations

As discussed in section **3.2.3**, MYOMAKER (MYMK) is essential for myoblast fusion and muscle fiber formation. MYMK mutations are associated with the congenital myopathy Carey-Fineman-Ziter Syndrome (CFZS) (Di Gioia et al., 2017). Disease manifests as static hypotonia, muscle weakness, facial weakness, and respiratory distress, most probably due to a weak diaphragm. Muscle biopsies exhibit myofibre hypertrophy, likely resulting from dysregulated, even lack of myoblast fusion (Di Gioia et al., 2017).

4.2 Secondary satellite cellopathies

Secondary satellite cell-opathies emerge from mutations in genes involved in both SatC and myofibre function, leading to chronic injury/repair cycles and continuing decline of the extracellular microenvironment quality and muscle function. These diseases include myopathies related to a mutation in laminin and dystrophin.

4.2.1 Laminin mutations

Laminin is structural proteins that serve as myofiber-ECM connection and are also involved in SatC polarization. Laminin subunits alpha two also named 211os, the predominant isoform expressed in skeletal muscles. Complete loss of Lama2 causes muscular dystrophy, and congenital merosin-deficient 1a (MDC1A), while partial deficiency of the protein leads to LGMDR23muscular dystrophy (Limb-Girdle, autosomal recessive 23) (Gavassini et al., 2011, p. 2). MDC1A patients suffer from muscle weakness, hypotonia, and respiratory distress. Muscle histology exhibits dystrophic features such as necrosis, muscle fiber size variation, and fat/fibrotic infiltrations, indicating myofiber stability and regeneration defects.

Interestingly, MDC1A exhibits disruption in SatC quiescence and function (Barraza-Flores et al., 2020), In addition, up to 80 % of SatC isolated from (129 RJ dy/dy) laminin ,deficient mouse muscles failed to fuse and form myotubes *in vitro* (Summers & Parsons, 1981).

4.2.2 Dystrophin mutations

Dystrophin (DMD) is an essential structural protein supporting muscle fiber and connecting it to the ECM. Duchenne muscular dystrophy is a known disease arising from a mutation in the DMD gene. Recent studies suggest Duchenne muscular dystrophy might also be a secondary satellite cellopathy. Duchenne myopathy manifests in early childhood and develops progressively to induce severe muscle weakness and wasting (Duan et al., 2021). Muscle biopsies show extensive necrosis, fibrosis, and fat infiltration, chronic rounds of muscle degeneration and regeneration, and initially elevated number of SatC, which declines drastically with advanced stages of the disease (Kottlors & Kirschner, 2010).

5 Muscle aging

5.1 Sarcopenia

Sarcopenia defines a state of skeletal muscle wasting with age affecting humans starting with the fourth decade of their lives (McCormick & Vasilaki, 2018). Aged muscle is characterized by deficits in the protein synthesis (Welle et al., 1993), accumulation of T-tubules aggregates as well as lipid, immune, and connective tissue infiltration (Addison et al., 2014; Brack et al., 2007), mitochondrial dysfunction (Short et al., 2005), neuromuscular changes (Piasecki et al., 2016), reactive oxidative species (ROS) production (McCormick & Vasilaki, 2018) and loss of SatC number (Shefer et al., 2006; Tajbakhsh, 2013) (Figure 42).

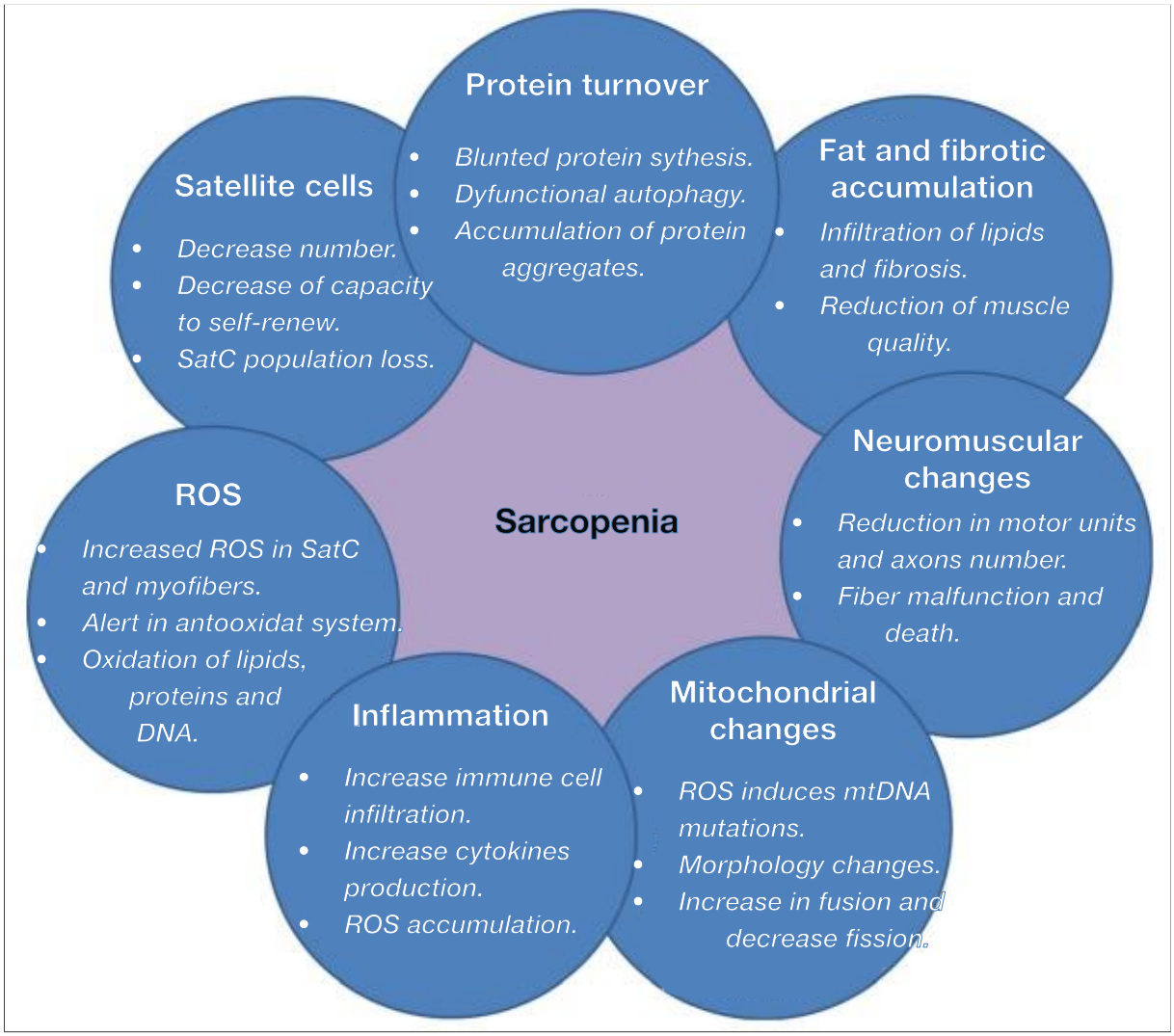

Figure 42: Schematic representation of age-related defects in skeletal muscles (adapted from McCormick & Vasilaki, 2018).

Since several studies reported contradicting results regarding the difference in muscle protein content between young and older individuals, protein synthesis capacity was studied

after protein ingestion or exercise. Researchers reported a significant decrease in muscle capacity to synthesize proteins with age upon exercise or protein ingestion Field (Fry et al., 2011; Wall et al., 2015), a phenomenon also named anabolic resistance.

ROS production increases with aging and accumulates in muscles fiber in rest (Palomero et al., 2013). ROS are eliminated by the antioxidant system, a group of compounds obstructing the chemical reactions that can produce free radicals, which was shown to be over-activated in aged muscles (Palomero et al., 2013). ROS accumulation results in the oxidation of DNA, proteins, and lipids, and is essential for autophagy since treatment with antioxidative agents abolishes the formation of autophagosomes and the consequent degradation of proteins (*Scherz-Shouval et al., 2007*).

The role of the mitochondria and the effect of ROS on sarcopenia was proposed in the 80s by (Miquel et al. 1980). This study suggested that mitochondrial dysfunction in aged muscles occurs from the increase in ROS production and weak antioxidant defenses, leading to mutations in the mitochondrial DNA (mtDNA). mtDNA mutations result in dysfunctional electron transport chain (ETC) and consequently in compromised oxidative phosphorylation, which induces a further rise in ROS, causing a vicious circle that aggravates the aging phenotype (Miquel et al. 1980). This hypothesis was confirmed in skeletal muscles by studies showing an increase in ROS, mtDNA, and mitochondrial dysfunction with aging, which were associated with skeletal muscle atrophy in humans and other species (Bua et al., 2006). Interestingly, the release of damaged mitochondrial particles into the ECM correlates with increases in inflammatory cytokines in the bloodstream of elderly humans (Pinti et al., 2014). The function and morphology of mitochondria changes during aging could affect its performance (Leduc-Gaudet et al., 2015). Inflammation of the aged muscles also contributes to increased ROS production by the myofibers (Li et al., 1998), which promotes fiber apoptosis (Marzetti et al., 2008). In addition, inflammation plays a role in anabolic resistance, and high levels of inflammation have been linked to catabolism of skeletal muscles (McCormick & Vasilaki, 2018).

Another characteristic of sarcopenia is fibrosis and adipocyte infiltration into skeletal muscles (Song et al., 2004; Serrano & Muñoz-Cánoves, 2010). This decrease in muscle tissue quality is believed to contribute to the age-related impairment in force generation and lateral force transmission from active fiber to muscle surface (Ramaswamy et al., 2011). This accumulation of ECM content, particularly collagen, could result from impaired muscle repair following injury (Serrano & Muñoz-Cánoves, 2010).

Neuromuscular changes are also observed in muscles with sarcopenia (Deschenes et al., 2010). The decrease of motor unit connectivity is thought to be one of the first characteristics of aged skeletal muscles in mice since tissue size and contractility are associated with motor innervation number and quality (Sheth et al., 2018). Indeed, upon moto-neuron connectivity loss, the quality of reinnervation of fibers in aged muscles decreases compared to young individuals, which eventually could lead to myofiber cell death (Vasilaki et al., 2016).

5.2 Aging effects on satellite cells

Muscle aging is one of the causes that disrupt SatC homeostasis and self-renewal capacity, which induces a decline in SatC pool with age (Figure 43) (Henze et al., 2020; McCormick & Vasilaki, 2018). Interestingly, aging in humans leads to particularly type II muscle fiber atrophy accompanied by a specific decline in type II fiber SatC content (Verdijk et al., 2014).

Many intrinsic factors of SatC impact their function with age. Indeed, geriatric muscle stem cells exhibit elevated p38αβ/MAPK signaling activity fail to undergo asymmetric division, self-renew or maintain the stem cell population (Bernet et al., 2014), and correction of this defect restores cell homeostasis and function (Bernet et al., 2014; Cosgrove et al., 2014). Moreover, the expression levels of main genes involved in myogenesis, such as *MyoD1* and *Myog*, increase in aged muscles, referring to the elevated rates of commitment and differentiation of SatC with aging in mice and human (Chakkalakal et al., 2012; Hameed et al., 2003; Raue et al., 2006). Additionally, since SatC are dormant, their metabolic and autophagy activity is decreased, therefore, they are incapable of eliminate altered proteins or organelles aggregates (Henze et al., 2020). Geriatric SatC exhibit defected autophagy resulting in protein and organelles aggregates accumulation, inducing stress and ROS production (García-Prat et al., 2016; Henze et al., 2020). ROS production is increased in the SatC with aging, which may contribute to the loss of regeneration capacity in muscles of older animals and humans (Figure 43) (Minet & Gaster, 2012). Restoring autophagy and protein degradation activities in old mice restores SatC function and improves muscle regeneration (García-Prat et al., 2016).

The geriatric muscle microenvironment may also negatively affect SatC homeostasis. It has been reported that aged muscle fiber in mice overexpresses FGF2 under homeostatic conditions, driving a subset of SatC to break quiescence, lose self-renewing capacity, and thus decline in number (Figure 43) (Chakkalakal et al., 2012), which is concomitant with loss of neuromuscular junctions (W. Liu et al., 2017). Although, SatC isolated from young and old mice proliferate similarly *in vitro* even when supplemented with FGF. Thus suggesting an essential role of other micro-environment changes affecting SatC function (Figure 43) (Shefer et al., 2006). Also, it has been shown that aged FAPs fail to produce a Wnt1-inducible signaling pathway protein 1 (WISP1), which is required for SatC expansion and differentiation (Figure 43) (Lukjanenko et al., 2019). Other studies focused on the effect of the anti-aging hormone Klotho on SatC delivered to the niche by the vascular system. For instance, Ahrens et al. showed that klotho serum levels decline with aging is correlated with mitochondrial damage in SatC and impacts muscles regeneration, and restoring its levels in geriatric mice rescues mitochondrial integrity in progenitor cells. It improves regeneration capacity (Figure 43) (Ahrens et al., 2018).

Together, these findings suggest that aging impacts SatC homeostasis and function with intrinsic and extrinsic factors. Conducting more studies in the future will help decipher other factors and conditions that could be modified to improve the life experience of elderlies.

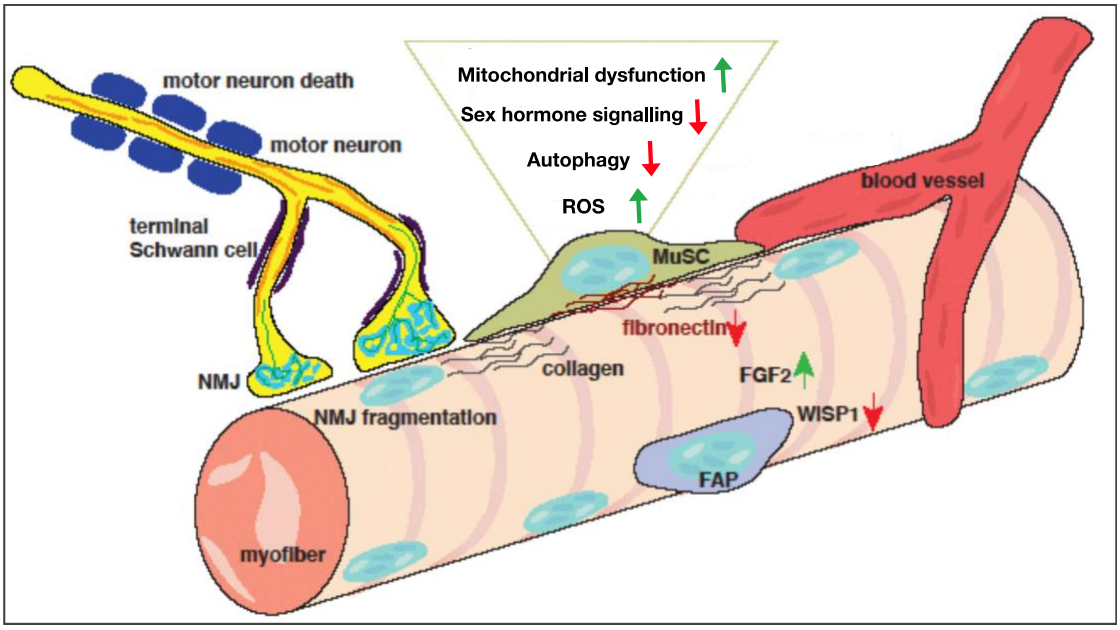

Figure 43: Effect of aging on SatC niche (adapted from Henze et al., 2020).

5.3 Aging effects on muscle regeneration

Skeletal muscle regenerative capability declines with aging (Domingues-Faria et al., 2016), and age-related changes within the lean muscle tissue and the host environment affect SatC function in response to injury (Grounds, 1998). Indeed, aged SatC are more prone to undergo senescence or apoptosis than young ones, which could explain the loss of the stem cell population with aging (Jejurikar et al., 2006). These geriatric SatC proliferate less rapidly, and their pre-senescent state could represent a point of no return (McCormick & Vasilaki, 2018).

In the context of acute muscle injury, symmetric and asymmetric cell divisions promote the expansion and maintenance of the SatC population, respectively. Changes in the microenvironment with age increase the growth factors TGFβ and FGF leading to a decline in Notch activity, which in turn decreases the regenerative and self-renewing capacities of SatC (McCormick & Vasilaki, 2018). Notch pathway defects in aged muscles lead to impairment of SatC division capacity resulting in the blunt generation of myoblasts necessary for muscle regeneration (Conboy et al., 2003). Moreover, aged muscles are characterized by increased methylation and, therefore inhibition of the SPRY1 locus leading to an impairment of the self-renewal capacity of the stem cells and loss of the SatC pool (Bigot et al., 2015).

Noteworthy, advancing in age is also concomitant with changes in whole body physiology, including disruptions of hormones secretion and regulation, particularly sex hormones.

6 Nuclear receptors

Nuclear receptors (NRs) are a multigene family of transcription factors present in all metazoans. In the human genome, 48 genes have been identified (Table 1) (P. Chambon, 2005; Germain et al., 2006), 49 in the mouse genome, 21 in Drosophila melanogaster, and 270 in Caenorhabditis elegans (Robinson-Rechavi et al., 2005). NRs are involved in many physiological processes, including embryogenesis, differentiation, apoptosis, and metabolism,byh regulating the transcription of a multitude of target genes (Gronemeyer et al., 2004).

NRs bind to DNA, and 2/3 are activated by binding to small hydrophobic molecules that enter or are synthesized in the target cell. Ligands, such as steroid hormones, vitamin A derivatives, thyroid hormones, or vitamin D, act as regulatory signals that modify the transcriptional activity of NRs. For most of these receptors, an interaction with a ligand is necessary for their activation. However, for some, no ligand has been identified yet, and for this reason, they are called orphan receptors. Through the study of the phylogeny and structure of NRs, it has been shown that some receptors have acquired the ability to bind a ligand during evolution (Escriva et al., 2000).

The property of NRs to bind ligands affecting their transcriptional activity makes them critical pharmacological targets for treating major pathologies such as cancer, diabetes, obesity, or hormone resistance syndrome.

6.1 Structure

Nuclear receptors are organized in 6 domains designated A to F from N-terminal to C-terminal (Figure 44) (Fruchart et al., 2019; Germain et al., 2006). These regions will be detailed in the section on androgens.

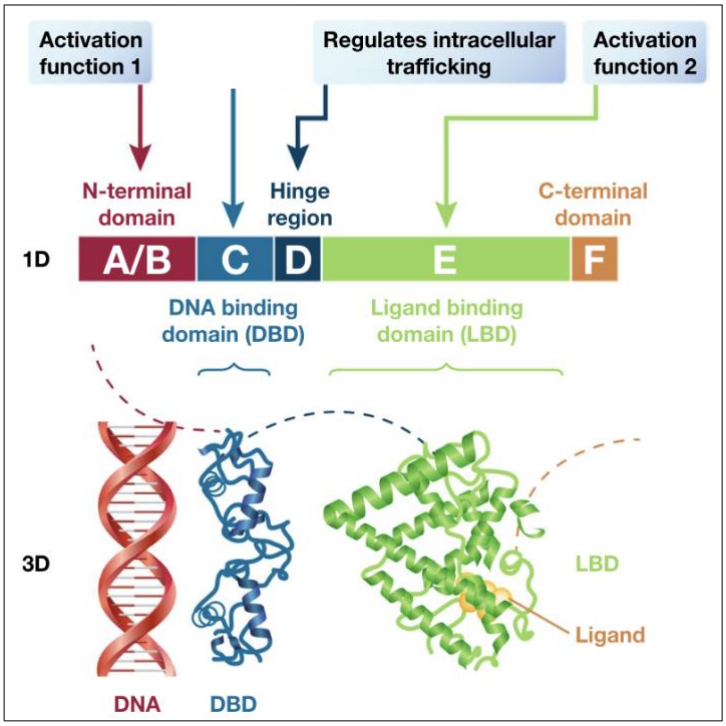

Figure 44: Structural organization of nuclear receptors (adapted from Fruchart et al., 2019).

As for mice, humans are classified into 6 groups based on phylogenic analyses and sequence alignments (Escriva et al., 2000; Thornton and DeSalle, 2000). The most conserved regions among the multigene family of nuclear receptors are the C (DBD) and E (LBD) regions, involved in DNA and ligand binding, respectively. The sequence and size of the A/B, D, and F regions are variable. Most NRs have two transactivation functions: AF-1 (N-terminal, ligand-independent) and AF-2 (C-terminal of the E domain, ligand-dependent). All nuclear receptors have a nuclear localization signal (NLS) located at the hinge domain (Figure 44) (Fruchart et al., 2019; Germain et al., 2006).

6.2 Gene expression regulation

In the absence of ligand, the NRs are localized in the cytoplasm or the nucleus. In the cytoplasm, steroidal NRs are associated with a large multiprotein chaperone complex, including Hsp90 and Hsp56 (Pratt & Toft, 1997). Ligand binding will induce dissociation of the complex, homodimerization of the NR, and its translocation into the nucleus, activating the transcription of target genes. Most other NRs are localized in the nucleus and bound to DNA in the absence of ligands. In the absence of ligands or in response to antagonistic or agonistic ligands, these NRs will repress or activate transcription by recruiting multi-protein complexes to the promoter of their target genes.

NRs can have non-genomic effects, too, through kinases that activate signaling cascades from the cytoplasm. These non-genomic effects appear within minutes of NRs activation. Moreover, inhibition of transcription (such as actinomycin D) or translation (like cycloheximide) does not affect these signaling pathways, suggesting that these activities are independent of the transcription activity of NRs. These activities are described for several steroid receptors such as the glucocorticoid (GR), progesterone (PR), estrogen (ER), and androgen (AR) receptor (Levin, 2008). Some nuclear receptors can also interact with other transcription factors such as AP-1 or NF-κB, like GR. Glucocorticoids exert their anti-inflammatory effect by inhibiting the NF-κB pathway by their receptor GR (K.M. Reeves et al., 2012).

6.3 Nuclear receptors co-regulators

Co-regulators are proteins that interact with NRs and other transcription factors in the regulatory region of target genes to activate or repress the transcription (Glass & Rosenfeld, 2000). Co-regulators can be classified into two groups: co-activators (p160 family, CBP/p300) and co-repressors (such as SMRT) that activate and repress transcription of target genes, respectively. Some co-integrators facilitate the interaction of NRs with the transcriptional machinery. Chromatin decondensation by co-activators allows the recruitment of the basal transcriptional machinery. NRs recruit via interaction with members of the mediator complex, TRAP/DRIP (Thyroid Hormone Receptor-Associated protein / Vitamin D Receptor Interacting Protein). This complex allows the assembly of the pre-initiation complex and serves as a

molecular bridge that connects transcriptional activators or other regulatory elements to the RNA polymerase II (Larivière et al., 2012).

6.4 Post-translational modifications of nuclear receptors

Nuclear receptors can undergo several post-transcriptional modifications, such as phosphorylation, acetylation, sumoylation, or ubiquitination.

- Kinases phosphorylate some receptors on a residue in the A/B, C, and E domains. In general, phosphorylation stimulates the transcriptional activity of NRs by promoting co-activator recruitment. However it has been shown that it can also negatively impact the movement of NRs by inducing their dissociation from DNA, decreasing their binding affinity for the ligand, or inducing their degradation (Lalevée et al., 2010).

- Acetylation on the lysine residues of NRs negatively or positively affects their transcriptional activity (C. Wang et al., 2011). It has been widely described for steroid receptors (Faus & Haendler, 2006).

- Sumoylation, which requires the covalent binding of small polypeptides called SUMO (Small Ubiquitin-like Modifier) to a specific lysine residue of the target protein, affects the transactivation potential and DNA binding ability of NRs (W. Liu et al., 2021). This mechanism has also been widely described for steroid receptors (Faus & Haendler, 2006).

- Ubiquitination is the conjugation of ubiquitin, a 76 amino acid polypeptide, to a substrate. Mono-ubiquitination is involved in transcriptional regulation, while poly-ubiquitination leads to protein degradation via the ubiquitin-proteasome signaling pathway. Several nuclear receptors such as ER, AR, PPARα (Peroxisome Proliferator activated Receptor alpha), GR, RARγ, RXRα, and TR are regulated by the ubiquitin-proteasome system (El Hokayem et al., 2017).

In response to ligand binding, NRs regulate target gene expression, including interaction with DNA and cofactors, posttranscriptional modifications, or communication with other transcriptional factors.

7 Androgens

Androgens are steroid hormones responsible for male characteristics in mammals. Testosterone is the major circulating androgen in men. The Leydig cells of the testis synthesize up to 95% of the total testosterone produced, which reaches up to 6-7 mg of testosterone per day in men. The adrenal cortex also synthesizes a part of the testosterone (Jordan & DonCarlos, 2008). In women, androgens are synthesized in the ovaries.

7.1 Synthesis

Androgens are formed from cholesterol, either synthesized de novo from acetate or extracted from plasma lipoproteins and cell membranes. Cholesterol is transported to the mitochondrial membrane by a luteinizing hormone (LH)-dependent mechanism that is regulated by a transfer protein called steroidogenic activator protein (StAR) (Manna et al., 2016). Once in the mitochondria, cholesterol is cleaved to pregnenolone by cytochrome p450scc (side chain cleavage - encoded by the CYP11A gene) (Figure 45).

Inactivated pregnenolone, released into the endoplasmic reticulum, is converted to progesterone or 17α-hydroxypregnenolone by P450c17 encoded by the CYP17 gene. The side chain of progesterone is cleaved by P450c17 to produce dehydroepiandrosterone or DHEA. DHEA is converted to Androstenediol by the action of 17β-hydroxysteroid dehydrogenase (17β-HSD). Then, Androstenediol is converted to testosterone by the action of 3β-HSD. In addition, Pregnenolone is converted by 3β-HSD to progesterone which is then hydroxylated by P450c17 to 17 hydroxyprogesterone. The latter is cleavage by P450c17 to form androstenedione. Finally, testosterone is formed by the action of 17β-HSD. Testosterone can be converted to estradiol by P450 aromatase and dihydrotestosterone (DHT) by 5α-reductase at the level of target tissues (Figure 45) (Diotel et al., 2018).

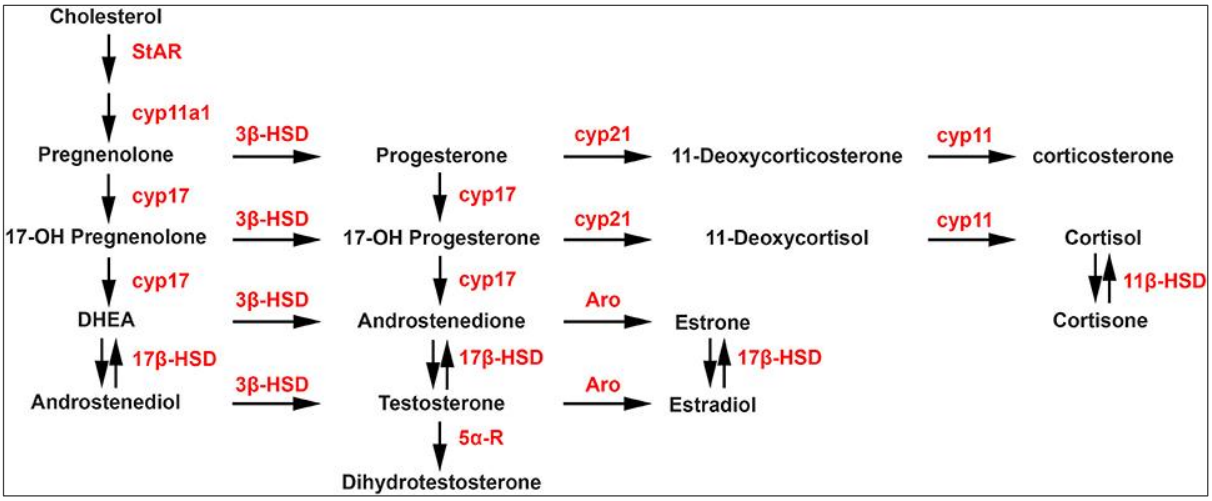

Figure 45: Biosynthesis of androgens (adapted from Diotel et al., 2018).

Production and secretion of testosterone are tightly regulated by the hypothalamic–pituitary–testicular axis (Loveland et al., 2021). Secretion of LH stimulates the production of androgens by the Leydig cells. LH is a hormone produced by the hypothalamus-pituitary axis. The hypothalamus is responsible for the pulsative secretion of GnRH (Gonadotropin-Releasing Hormone) that reaches the pituitary gland via the pituitary portal system, which is a system of blood vessels in the microcirculation at the base of the brain, connecting the hypothalamus with the anterior pituitary. The adenohypophysis releases LH and follicle-stimulating hormone (FSH) in smaller quantities. Negative feedback also regulates this production. If too much testosterone is released, it will inhibit the secretion of GnRH in the hypothalamus and LH in the pituitary gland. This will lead to a decrease in its production by the Leydig cells (Figure 46) (Loveland et al., 2021). See section **7.3**.

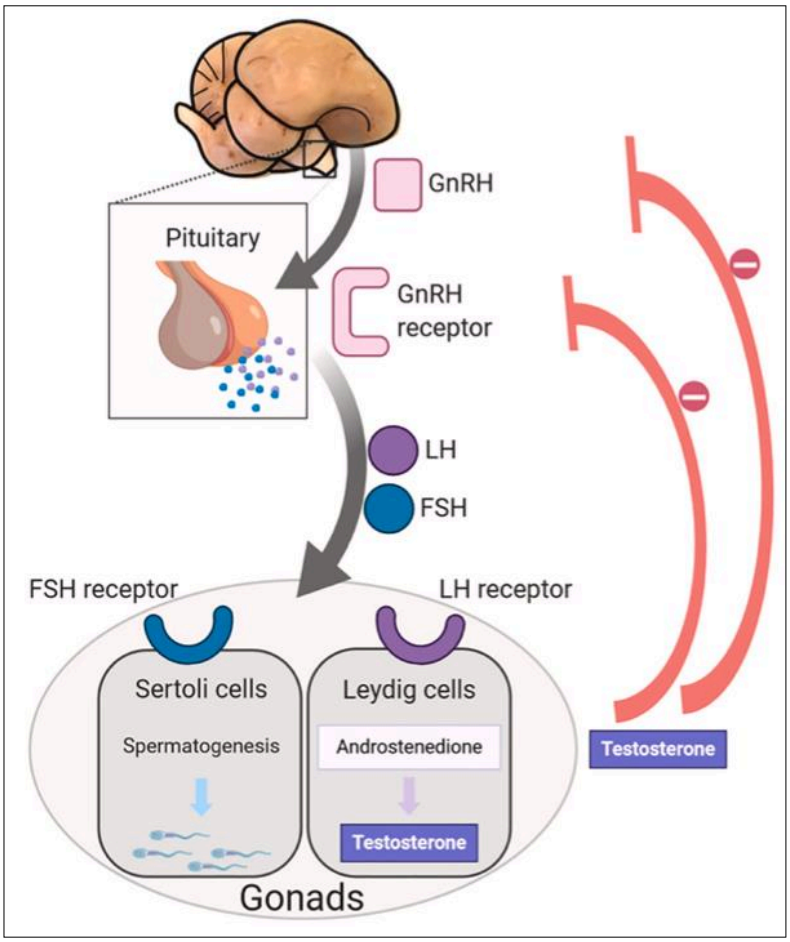

Figure 46: Secretion axis of androgens (adapted from Loveland et al., 2021).

7.2 Functions of androgens

The main of androgen's actions on target tissues is relayed by a nuclear receptor, the androgen receptor (AR).

7.2.1 Spermatogenesis

During puberty, the production of androgens, LH, and FSH increases, allowing the formation of seminiferous tubules and the differentiation of germ cells into spermatozoa. In

adulthood, androgens and FSH act on Sertoli cells in the testes to will enable the production of sperm (L. B. Smith & Walker, 2014).

7.2.2 Fat accumulation

Androgens may be the main reason men have less fat accumulating in their bodies since they inhibit the ability of some adipocytes to store fat by blocking a signal pathway that supports regular adipogenesis (Blouin et al., 2008; R. Singh et al., 2006). Andropause in men, which reflects a decline in circulating androgen levels with age, is concomitant with visceral obesity and metabolic syndromes (Tchernof et al., 2018).

7.2.3 Brain

Circulating androgens can influence human behavior since some neurons are steroid hormone-sensitive. Androgen plays a crucial role in regulating human aggression (Scarth & Bjørnebekk, 2021). Androgens have a positive effect on hippocampal neurogenesis in preadolescents that may be related to depressive symptoms (Duarte-Guterman et al., 2019).

7.2.4 Effects in women

In women, androgens are synthesized in the ovaries, adrenal glands, and fat cells. In adult women, androgens are mandatory for estrogen synthesis and play a key role in preventing osteoporosis and sexual desire. Moreover, androgens are thought to affect myometrial relaxation in a non-genomic,signalingling pathway-independent manner, preventing premature uterine contractions during pregnancy (Makieva et al., 2014). However, an excess of androgens can harm the female body since it is believed to play a vital role in the development of polycystic syndrome (Walters et al., 2019).

7.2.5 Skeletal muscle mass

Androgens promote skeletal muscle cell mass growth and act on several cell types in lean muscle tissue. Higher levels of androgens increase AR protein levels (Sinha-Hikim et al., 2004a). In addition, androgens via the androgen receptor control limb muscle strength (C. Chambon et al., 2010). See section **8**.

7.3 Androgen receptor

The androgen receptor (AR) belongs to the superfamily of nuclear receptors. It is a member of the steroid hormone receptor class along with the glucocorticoid (GR), mineralocorticoid (MR), estrogen (ER), and progesterone (PR) receptors. The gene encoding AR is located in humans on the X chromosome and has 8 exons (Davey & Grossmann, n.d.). It generates a 919 amino acids protein with a 110 kDa molecular mass (Lubahn et al., 1988). AR relies in the cytoplasm and is believed to have ligand dependant and independent functions and binds to the DNA as a homo- or heterodimer (Figure 47) (G. C. Shukla et al., 2016). In Figure 47, there is the representation of critical cellular signaling pathways that modulates AR transactivation function independent of androgens. Among many extracellular growth factors, cytokines, G-protein-coupled receptors, and multiple kinases have been implicated in AR androgen-independent function.

7.3.1 Ligand-dependent activity

Due to binding to heat shock protein 90 (HSP90) and p23 and tetratricopeptide repeat motif-containing co-chaperones of HSP90, AR resides in the cytoplasm in an inactive form. During the ligand-dependent transactivation, AR binds to the testosterone directly or its active metabolite DHT (Figure 47). After dissociation from HSP, conformational changes occur to AR conformational, forming a homodimer via the NH2-and COOH-termini interactions. Afterward, the AR homodimer undergoes phosphorylation by MAPK and translocates to the nucleus via an intrinsic nuclear localization signal. AR interacts with DNA sequences containing a palindromic region known as androgen response elements (ARE) (Figure 47) (Shukla et al., 2016).

7.3.2 Ligand independent activity

AR may be translocated to the nuclei independently of the ligand; indeed, several cellular pathways could induce this effect, and the key ones involved are indicated in Figure 47.

Extracellular growth factors, G-protein-coupled receptors, cytokines, and multiple kinases, are implicated in AR androgen-independent function (Shukla et al., 2016). Among cytokines, interleukin-6 (IL-6) and interleukin-8 (IL-8), which are expressed in multiple cell types, were shown to induce AR translocation and activity (Figure 47) (Blaszczyk et al., 2004; Seaton et al., 2008). Interestingly, this effect of IL-6 was independent of MAPK or AKT pathways. In addition, several paracrine-regulated growth factors such as IGF, epidermal growth factor (EGF), and FGF also promote prostate epithelial cell proliferation by AR modulation (Figure 47) (Shukla et al., 2016). Transactivation of AR via this manner leads to the activation of genomic targets and signaling pathways involving various coactivators, cyclic AMP, and kinases. Several putative steps in these pathways remain uncharacterized.

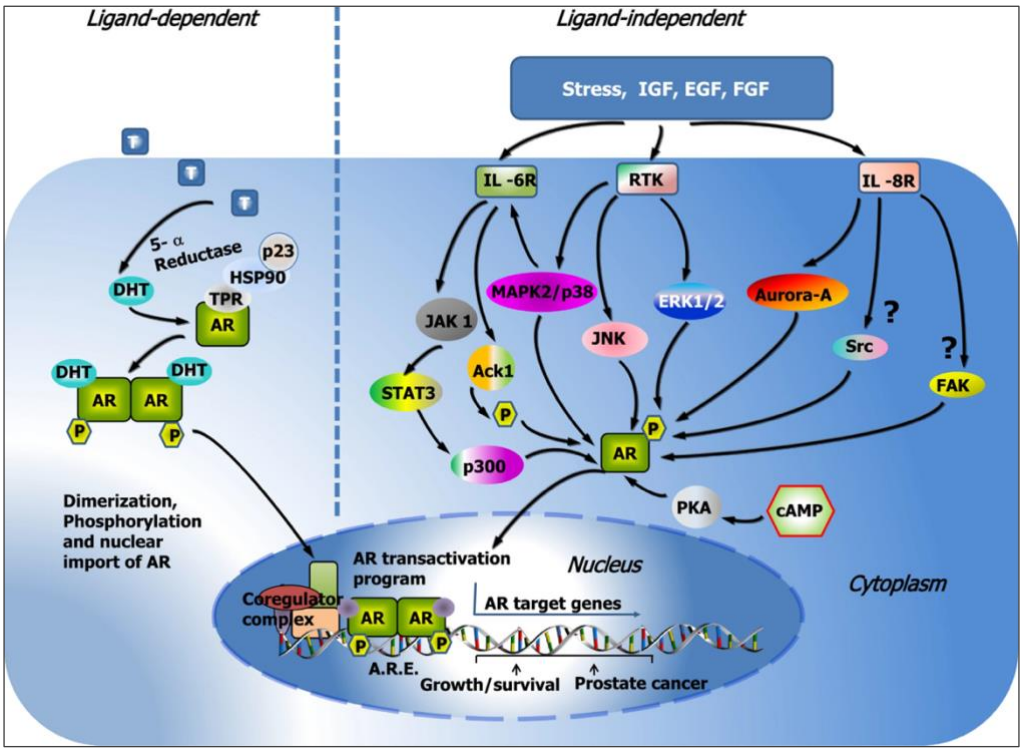

Figure 47: Schematic representation of Ligand-dependent and -independent androgen receptor (AR) transactivation (adapted from Shukla et al., 2016).

7.3.3 Structure

AR consists of three major functional domains: 1) the N-terminal domain (NTD), 2) the DNA binding domain (DBD), and 3) the C-terminal ligand binding domain (LBD) (Figure 48). DBD is highly conserved, and it tethers the AR to regulated regions by direct DNA binding to allow the activation of the NTD and LBD to promote the transcription of target genes. The activation function 1 (AF1) in the NTD is constitutively active, whereas the activation function 2 (AF2), a hydrophobic region composed of helices 3, 4, and 12 located in the LBD, is ligand dependent. Of note, there is no structural information for the full-length AR receptor yet. However, the DBD and LBD structures have been solved separately (Tan et al., 2015).

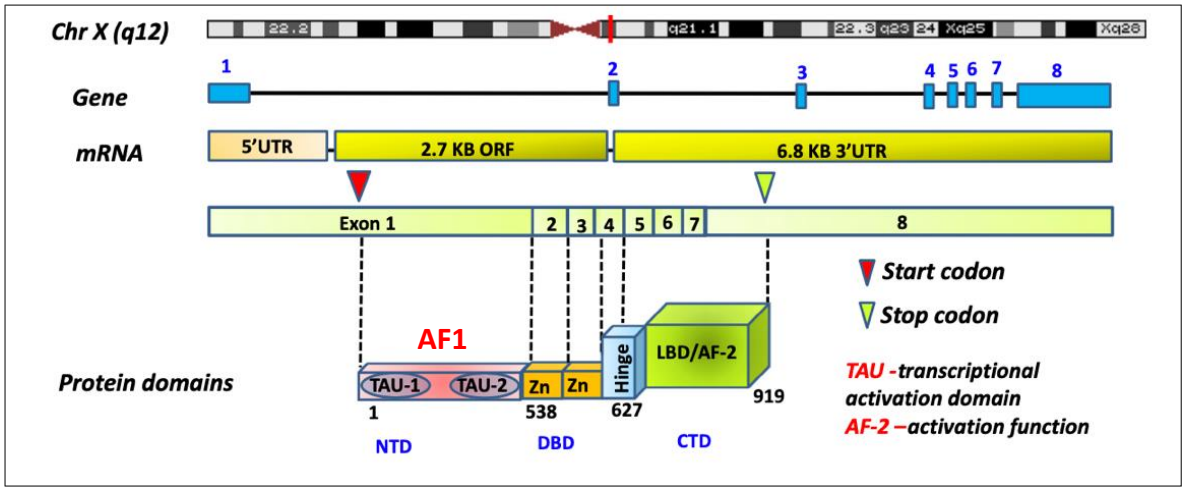

Figure 48: Structure of the human androgen receptor (adapted from Shukla et al., 2016).

The androgen receptor gene containing 8 exons is coded on X chromosome region Xq11-12 covering up to 180 kb region. Nearly 10.6 kb long AR transcript contains an unusually long 6.8 kb untranslated region (UTR) in addition to a 1.1 kb UTR. Almost 75% of the AR transcripts code for noncoding UTRs, and only 25% account (2.7 kb) for the coding region or open reading frame (ORF).

7.3.3.1 N-terminal domain (NTD)

The NTD accounts for half of AR size panning along the whole first exon (exon 1) and is responsible for the protein-protein interaction function (Figure 49). This region's length affects AR's folding and structure and is highly variable in humans. Interestingly, the longest the NTD, the lower the transcriptional activity is. Several deletion studies showed the essential role of a specific region in AR function, which was named the activation function 1 (AF1). Importantly, AF1 contains Tau-1 and Tau-5 domains that are mandatory for the ligand-dependent, interdomain interactions between the NTD and the LBD of the receptor (Figure 49) (Shukla et al., 2016).

7.3.3.2 DNA binding domain (DBD) and hinge

The DBD binding domain is highly conserved among steroid hormone receptors and has a core composed of two Zn fingers; each one consists of four cysteine residues that manage a zinc ion.

The Z finger from the NTD side is involved in the DNA sequence (half-site ARE) recognition, which consists of 5′-AGAACA-3′, while the other Z finger from the CTD site is responsible for the dimerization of AR (Figure 50) (Shukla et al., 2016).

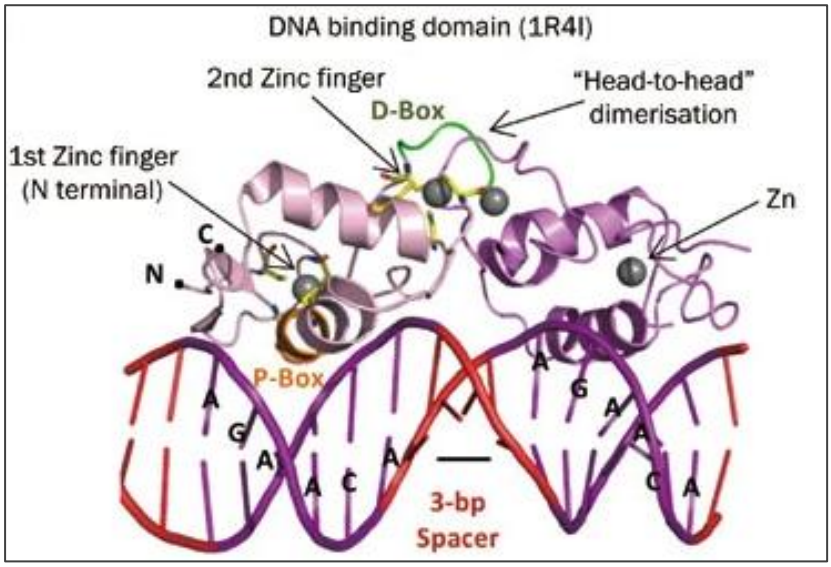

Figure 49: Crystal structure of the AR DBD (pink) binding to the DNA (purple) (adapted from Shukla et al., 2016).

7.3.3.3 Ligand binding domain (LBD)

AR LBD consists of 11 a-helices and a 4 β-strands forming two antiparallel sheets. The first layer consists of the H1 and H3 helices. The middle layer is formed by the H4 and H5 helices and H8 and H9 from B-sheet, and the third layer is formed by H10 and H11.

The ligand binding domain is located between the H3, H5 and H11, and H12, which forms the core activation site of AF2 (Shukla et al., 2016).

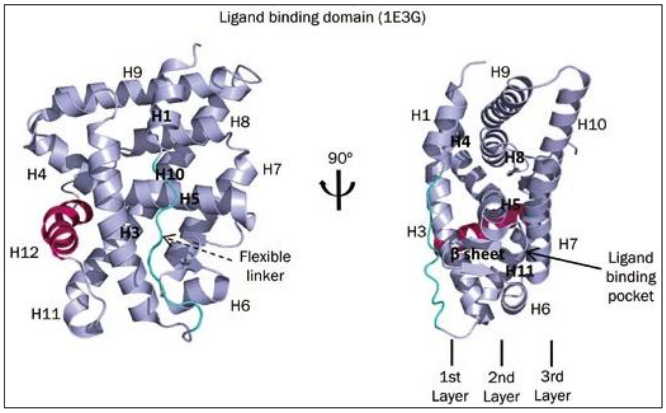

Figure 50: Crystal structure of the ligand binding domain of AR (adapted from Shukla et al., 2016).

7.4 Diseases caused by defects in androgens

Mutations in the AR cause many pathologies:

1. Androgen insensitivity syndrome, a rare X-related disease due to mutations in AR. Individuals with this syndrome exhibit several degrees of insensitivity. If the insensitivity is complete, the male individuals have female external genitalia, or if partial, the phenotype may be gradient depending on the extent of this insensitivity (Hughes et al., 2012).

2. Prostate cancer is the second most common cancer in men and in which androgens appear to be a risk factor. This can be explained by the fact that androgens, via their receptor, can stimulate cell proliferation and that AR mutations increase with the progressive stage of the cancer (Tan et al., 2015).

3. Kennedy disease or SBMA (spinal and bulbar muscular atrophy), which is an X-linked genetic disease characterized by progressive and particularly severe muscle weakness in the bulbar and proximal limb muscles (Breza & Koutsis, 2019).

7.5 Androgens decline with age.

Andropause is the name given to the decline in testosterone levels in men with age, also known as ADAM (Androgen Deficiency in the Aging Male) or PADAM (Partial Androgen Deficiency in the Aging Male). From the age of 30, testosterone levels decrease by about 1% per year. By the age of 60, 20% of men have an androgen deficiency. This percentage increases to 50% by age 80 (Brawer, n.d.; P. Singh, 2013).

8 Androgens and skeletal muscles

Androgens play different roles in limbs and in highly responsive perineal muscles, and several studies reported contradictive results.

8.1 Androgens during embryonic muscle development

In male mice, androgens are mandatory for the formation of perineal muscle. Howeverr, they are dispensable for the formation of limb muscles but not for their growth (MacLean et al., 2008). Of note, female mice deficient in AR exhibit normal muscle development and function (MacLean et al., 2008).

8.2 Androgens administration in adulthood

At puberty, a peak of androgens occurs, leading to a nearly 30-fold increase in testosterone production. In perineal muscles, the administration of supraphysiological doses of testosterone to adulrodentsnt increased fiber cross section area and satellite cell number (Dalbo et al., 2017a).

In limb muscles, supraphysiological levels of androgens activate IGF-1, Phosphoinositide 3-kinases (PI3K)/Akt, and follistatin (FST- an antagonist of MSTN) pathways stimulating protein synthesis and muscle hypertrophy. It also inhibits the MSTN/SMAD and FOXO3 catabolic pathway (Seo et al., 2019). In addition, re-supplementation upon inhibition of androgens significantly increased muscle size and the expression of IGF1, FST, and HGF, while decreasing the expression of the glucocorticoid receptor (GR) (MacKrell et al., 2015) that is known to induce muscle atrophy (Schakman et al., 2008).

Contrarily, our laboratory using the HSA-Cre mouse model in which AR is selectively ablated in myofibers in adulthood report no effect on muscle size or fiber CSA (C. Chambon et al., 2010). This highlights that our knowledge regarding androgens regulation of skeletal muscles is still shallow. This will be further discussed in the “general discussion and conclusion” section.

Interestingly, testosterone administration improves skeletal muscle regeneration upon injury in young and old mice by increasing the number and cross-section area of newly formed fibers (Figure 51) (Serra et al., 2013a).

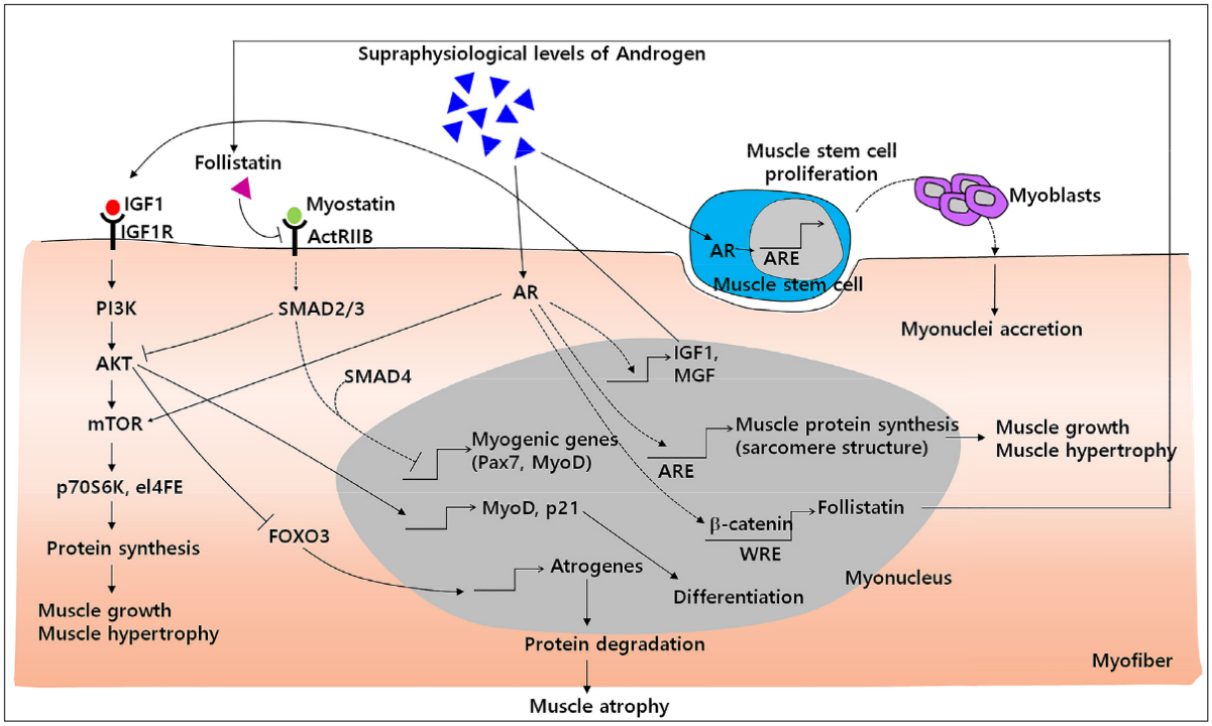

Figure 51: Supraphysiological levels of androgens-associated signaling pathways on skeletal muscles (adapted from Seo et al., 2019).

Supraphysiological levels of androgen treatment activate anabolic effects via the IGF-1, PI3K/Akt and follistatin pathways. They blunt the catabolic effects by inhibiting the myostatin/SMAD and Foxo3 pathways. In addition, androgens induce the expressions of IGF1, FST and sarcomeric proteins leading to muscle protein synthesis and hypertrophy. The role of androgens in SatC is still deliberated, it was shown that androgens also can activate muscle stem cells to proliferate and stimulate myonuclei accretion in pre-existing myofibers.

8.2.1 Androgens as a potential treatment

In young individuals, the benefits of supraphysiological effects of testosterone with or without (weightlifting) exercise on muscle size and strength have been studied (Bhasin et al., 1996). The results show that lean mass, muscle size, and strength increase, even more when exercise is combined with testosterone treatment. Thus, exercise may increase the effect of androgens on the muscle. Additionally, testosterone replacement in hypogonadal men or in patients with androgen insufficiency caused by disease and aging rescues muscle wasting by increasing tissue density, and protein synthesis capacity and subsequently improves pthe hysical fitness of individuals (Zitzmann & Nieschlag, 2003).

Androgen replacement in aging men is an idea that is strongly emerging. More and more researchers are showing support for administrating androgens to older individuals to improve aging symptoms summarized in sarcopenia, osteoporosis, sexual incapacity, and even psychological symptoms. However, testosterone administration is known to play a major role in prostatic cancer development in men (Myers & Meacham, 2003).

However, recent studies are raising the red flag regarding abusers of androgens and calling it the “next public health problem” of this century (Kanayama et al., 2018). Indeed, it has been shown that prolonged consumption of androgens leads to cardiovascular toxicity. Withdrawal of androgens upon long-term use results in hypogonadism in men. Supraphysiologic doses were shown to induce irritability, aggression, and violence, and withdrawal might cause depression (Kanayama et al., 2018).

Altogether, despite the significant side effect of androgen replacement, it is still considered a potential treatment for hypogonadal men and older individuals, which shows the importance of unraveling tissue-specific targets of these hormones. Of note, an ongoing clinical trial on a selective androgen receptor modulator (SARM) is showing an improvement in individuals' body mass but inconclusive results regarding muscle strength and function (Fonseca et al., 2020).

8.3 Castration at adulthood

Castration of adult mice induces atrophy of perineal muscles, while testosterone administration rescued the phenotype (Axell et al., 2006). White et al. reported that androgen deficiency in mice by castration in adulthood induces limb muscle mass and strength decrease (White et al., 2013), while another study by Davidyan and colleagues do not describe diminution in limb muscle mass upon castration (Davidyan et al., 2021). Interestingly, White et al. also showed that androgens regulate muscle protein synthesis and degradation through Akt/mTORC1/FoxO3a pathway (White et al., 2013), which was further confirmed by (Figure 52) (Jiao et al., 2009).

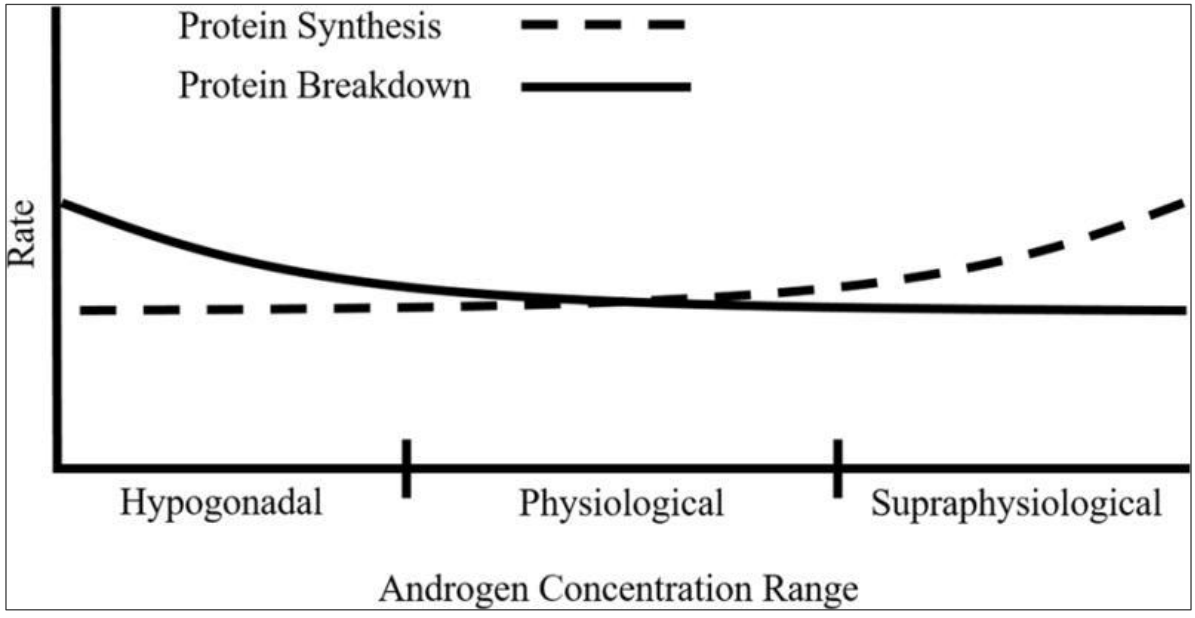

Figure 52: Effect of androgen levels on muscle protein regulation (adapted from Rossetti et al., 2017).

In humans, prostate cancer patients are treated with anti-androgen molecules after chemotherapy to ameliorate their chance of survival, also known as chemical castration. However, these patients exhibit a higher incidence of all grades of fatigue and musculoskeletal pain compared to the placebo group (Scher et al., 2012).

8.4 AR mutation or ablation in skeletal muscles

Mice carrying a CAG/glutamine expansion in AR (polyQ AR) (Figure 53A), a mutation causing SBMA, show diminished glycolysis, altered mitochondria, impaired response to exercise, and loss of muscle mass (Figure 53A) (Giorgetti et al., 2016). In addition, the reduction of androgen levels with age or AR blocking inhibits fat metabolism in skeletal muscle by suppressing cluster of differentiation 36 (CD36) expression, the primary fatty acid transporter in the myofibers (Kim et al., 2019).

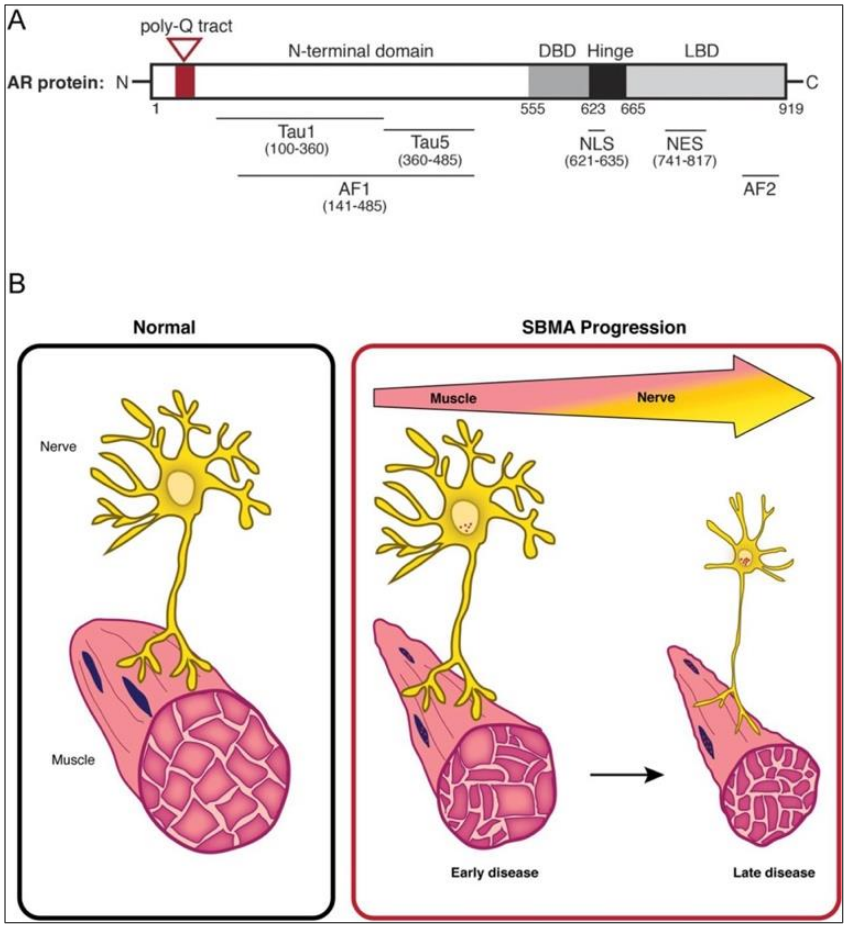

Figure 53: AR mutant mouse model of SBMA disease (adapted from Giorgetti et al., 2016).

A. *Schematic representation of AR structure and the mutation localization in the N-term (poly-Q, red box), and* ***B.*** *SBMA effect on skeletal muscle mass.*

Our team demonstrated that selective ablation of myocytic AR in adulthood, using the HSA-Cre mouse model (Miniou, 1999), affects only contraction strength but not the mass of limb muscles (C. Chambon et al., 2010). However, using a muscle creatine kinase (MCK)-Cre mouse-model deficient of postmitotic myocyte-AR, Ophoff et al. reported that androgens via their receptor control limb muscle mass and fiber type regulation but not strength or fatigue resistance (Ophoff et al., 2009). Of note, AR knock-out during embryonic development generates skeletal muscles containing 10 % more type I and 10 % less type II fibers in adulthood with decreased contraction strength (Dubois et al., 2014a).

Altogether, these studies show an evident influence of androgen on all aspects of skeletal muscles, including development, mass, contraction force, fatigue resistance, protein synthesis ,and metabolism; however, whether these effects are driven by AR or what the exact molecular mechanism is still a mystery.

9 Androgens and satellite cells

Androgens play critical roles in various stages of SatC physiological function at different age stages (Figure 54). Noteworthy, AR protein level is upregulated in SatC treated with androgens in the humans (Sinha-Hikim et al., 2004b).

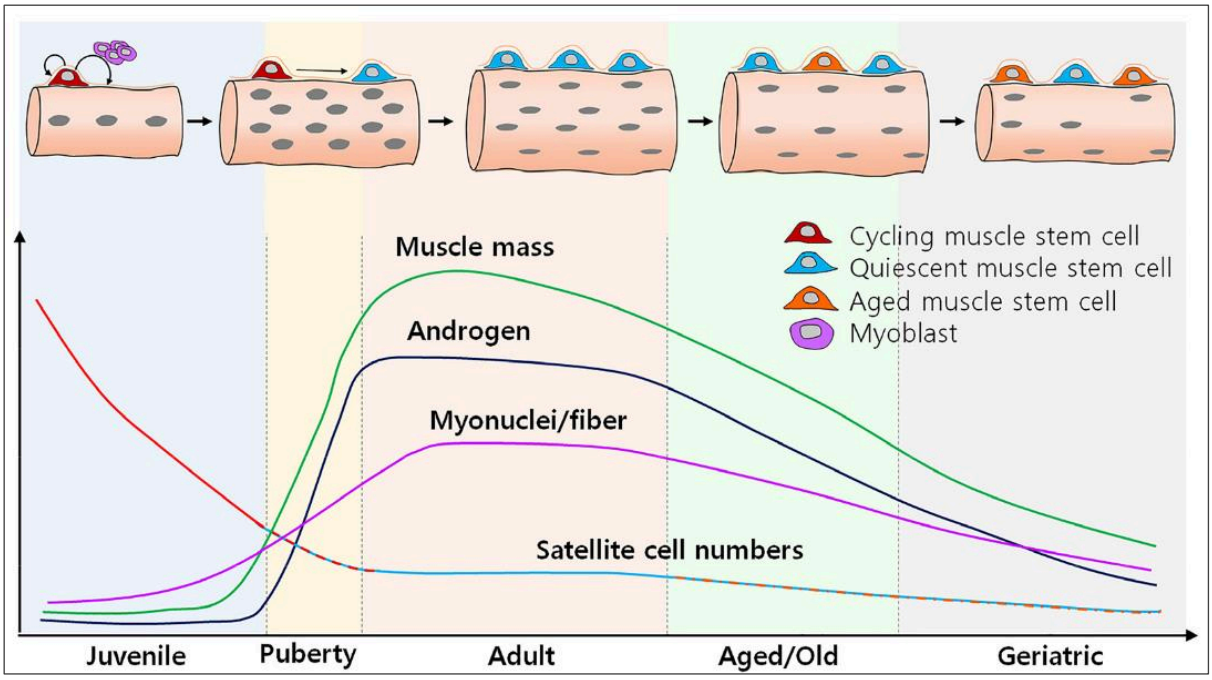

Figure 54: Dynamics of Satellite cells, limb muscle mass, and androgen levels in different age stages (adapted from Seo et al., 2019).

9.1 Role in homeostasis/quiescence

A study by Kim and colleagues showed that sex hormones peak at puberty establishes a reserve pool of SatC by promoting Notch signaling, consequently deriving cells from proliferation to quiescence (Kim et al., 2016b). Moreover, castration induces SatC break of quiescence and activation in the absence of external stimuli (Klose et al., 2018).

Intriguingly, AR knock-out in SatC of perineal muscles negatively impacts the expression levels of the MSTN (Dubois et al., 2014a). Also, inhibition of androgen signaling results in the decline of *Pax7* and *MyoD* expressions in levator ani muscle SatC of rats *in vitro* (MacKrell et al., 2015). Together, in homeostatic conditions, androgens promote SatC quiescence and protect its dormancy.

9.2 Role in activation/proliferation

Testosterone administration increase SatC number without elevating myonuclei count in myofibers in perineal muscles of adult rodent (Dalbo et al., 2017b) and promotes SatC activation in perineal muscles of rats (Nnodim, 2001). In addition, testosterone treatment

enhances SatC proliferation and differentiation in young and old mice during limb muscles regeneration (Serra et al., 2013b).

Additionally, AR knock-out in C2C12 and L6 myoblasts impaired proliferation *in vitro*, and its overexpression reversed the phenotype (S. Fu et al., 2021). Of note, C2C12 is derived from female mouse muscles suggesting a role of AR in muscle regulation in females.

9.3 Role in differentiation/myoblast fusion

C2C12 myoblast differentiation is stimulated by androgens administration, accompanied by MSTN and PAX7 modulation (Diel et al., 2008), and AR recruitment promotes the expression of myogenic genes and myoblast fusion *in vitro* (Vlahopoulos et al., 2005).

SBMA patients with an AR PolyQ mutation exhibit impaired myotube fusion and altered contractile structures. Interestingly, in contrast to healthy individuals, androgens administration to SatC isolated from SBMA patients did not increase the number of myonuclei in *vitro* generated myotubes (Malena et al., 2013).

In addition, muscle biopsies from steroid-treated athletes show an increase in central nuclei, indicating activation and proliferation of satellite cells to form new fibers (Kadi et al., 1999).

Thus, androgens play essential roles in SatC dormancy in homeostatic conditions and in their activation, proliferation, and differentiation in case of injury. However, the precise molecular targets and whether AR is involved are still unknown.

Objectives

Modern studies using combinatorial chemistry, rational drug design, and mass chemical screening aim to develop selective AR modulators (SARMs). The ideal SARM should be an AR agonist in muscle, adipose tissues, and bone but inactive in the reproductive and other nontarget organ systems. Recent years have seen a surge in patents for nonsteroidal androgens that aim to increase bone and muscle mass with minimal effects on reproductive and other tissues (Fonseca et al., 2020; Solomon et al., 2019). Indeed, the diversity of pre-and post-receptor mechanisms involved in androgens action provides scope for opportunities to be discovered and exploited to develop SARMs that are genuinely selective for anabolic effects on muscles and bones. To this end, more precise cell and tissue targeting of pharmacological androgen action require greater insight into the mechanisms of androgens' effects on mature skeletal muscle.

Main *in vitro* and animal studies have focused on developmental action in skeletal muscles, showing that androgens protect satellite cells (SatC) quiescence (muscle stem cells) (Klose et al., 2018; J.-H. Kim et al., 2016b; Sinha-Hikim et al., 2004b), enhance myogenic cell commitment, and proliferation of myogenic progenitors (Dubois et al., 2014; Serra et al., 2013b; Vlahopoulos et al., 2005; Sinha-Hikim et al., 2003; Nnodim, 2001), as well as myofiber hypertrophy and protein accretion (MacLean & Handelsman, 2009; Herbst & Bhasin, 2004; Sinha-Hikim et al., 2003). However, decisive *in vivo* physiological studies on androgen action in mature muscles are hindered by difficulties in defining cell-specific mechanisms within the tissue since no AR cistrome was published in mature myofiber or SatC, as well as the inability to separate effects mediated via AR and those via ER when using ligands (such as testosterone). In this context, the development of genetic mouse models, notably providing the ability to inactivate specific molecules within a targeted cell population, offer powerful new tools to investigate the physiological actions of androgens.

The original gene knockout approach using homologous recombination to inactivate a gene can eliminate that gene and its protein from the cell, thereby providing exceptional insight into its function. However, this cannot identify effects mediated within different cells in a given tissue. Hence, the development of the Cre/LoxP technique allowed the timely specific inactivation of a gene within a targeted cell type *in vivo* and has expanded the horizon of experimentation. To decipher the molecular mechanisms by which androgens via their receptor (AR) control skeletal muscle fiber and SatC population homeostasis in physiological and regeneration conditions, we generated two mouse models. In our animal models AR is selectively ablated in muscle myofibers and SatC using HSA-Cre (Miniou et al., 1999) and Pax7-CreER^{T2} (Lepper et al., 2009), respectively. Understanding the molecular underpinnings by which AR regulates myofiber and SatC population might open new perspectives to develop a variety of specific SARMS and therapeutic strategies for injury caused by trauma or degeneration in muscle dystrophies and aging.

Results

Chapter I

Objectives and contribution to this part.

Skeletal muscles are a major metabolic tissue regulating glucose and other energy sources in the body. Metabolic disorders such as type II diabetes is characterized by major changes in skeletal muscle metabolic activity.

Androgens were reported throughout history to exert anabolic effects on skeletal muscles. In this part, we investigated the role of the androgen receptor in muscle myofiber homeostasis in physiological conditions at adulthood that affect their metabolic activity.

This project initially started in 2007 with Dr. Céline Chambon, a former Ph.D. student of our lab. Her results deciphered that myocytic AR controls limb muscle strength but not mass. These results were published in the PNAS journal (C. Chambon et al., 2010). However, the molecular mechanisms behind those observations were still unknown. For this reason, another former Ph.D. student Dr. Mélanie Schuh continued working on this project, and her results deciphered severe metabolic defects in skeletal muscle lacking AR. Beginning 2021, I was introduced to this project, and we started working on it along with Dr. Delphine Duteil. We managed to connect all the dots and plan future experiments to answer the questions we had.

Interestingly, we noticed that mice deficient for AR in skeletal muscles had a higher glucose serum level and developed early type II diabetes. To identify the mechanisms behind our observation, we performed chromatin immune precipitation on limb muscles of adult male mice. Our data revealed a set of genes in which AR is directly recruited and involved in glycolysis. Transcriptomic analysis unveiled the downregulation of these genes in the absence of AR in limb muscles and others implicated in fatty acid oxidation. Interestingly, our data also revealed the upregulation of the branched-chain amino acids metabolic pathway. BCAA over-activation led to ammonia accumulation and ROS production, which is very toxic for the cells, consequently inducing cell death via apoptosis.

Manuscript in preparation

Myofiber androgen receptor coordinates muscle metabolism and contractile properties

Kamar Ghaibour[1*], Mélanie Schuh[1*], Sirine Souali-Crespo[1], Céline Chambon[1], Anouk Charlot[2], Daniela Rovito[1], Anna-Isavella Rerra[1], Nadia Messadeq[1], Joffrey Zoll[2], Delphine Duteil[1#], Daniel Metzger[1#]

[1] Université de Strasbourg, CNRS UMR7104, INSERM U1258, IGBMC, F-67400 Illkirch, France

[2] Centre de recherche en biomédecine de Strasbourg, CRBS, F-67000 Strasbourg, France

* These authors equally contributed

Correspondence: metzger@igbmc.fr and duteild@igbmc.fr

Running title: Myofiber AR is instrumental for muscle homeostasis

Abstract

Androgens are steroid hormones that exert pleiotropic effects in mammals by binding to the androgen receptor (AR), a member of the ligand-dependent nuclear receptor superfamily. However, despite numerous studies performed in men and in rodents, the effects of androgens on muscle metabolic functions and the underlying molecular mechanisms remain poorly understood. To characterize androgen signaling in skeletal muscles, we combined cistrome and transcriptome analyses with metabolomics and mouse phenotyping, and showed that AR controls a vast number of genes involved in energy metabolism, myofiber cytoskeleton and regulation of transcription in male mice. Loss of myofiber AR impairs glycolytic activity and fatty acid usage of limb muscles, which is compensated by amino acid consumption. This metabolic switch generates oxidative stress, ammonia production, thereby affecting mitochondrial functions. Altogether, these dysregulations contribute to decreased muscle contraction and accelerate the development of type-2 diabetes. Thus, our data demonstrate that myofiber AR is instrumental for skeletal muscle contractile and metabolic activities.

Keywords

Skeletal muscle / metabolism / androgen receptor / type-2 diabetes / genomics

Introduction

Skeletal muscle is a dynamic tissue that accounts for about one third of the body mass in mammals. It is essential for posture, locomotion and energy balance (Hawley et al., 2018). Skeletal muscles are composed of myofibers with different contractile and metabolic properties. Slow-twitch muscles, such as soleus, preferentially use fatty acids as a source of acetyl-coA via beta-oxidation, and fast-twitch ones, like extensor digitorum longus (EDL), mainly use glucose as source of pyruvate via glycolysis (Schiaffino, 2010). However, most of limb muscles (e.g. gastrocnemius, tibialis, quadriceps) are composed of various combination of oxidative and glycolytic fibers, and have the capacity to switch between oxidative and glycolytic metabolism according to environmental demands. For instance, endurance exercise induces muscle fiber type switching from fast-glycolytic to slow-oxidative and increases BCAA oxidation (Handschin et al., 2007; Xu et al., 2017), while sedentariness decreases muscle oxidative capacities (Figueiredo et al., 2009; Xu *et al.*, 2017), associated with oxidative stress (Porter et al., 2015), as well as obesity and type-2 diabetes (Duteil et al., 2010; Schuler et al., 2006). Energy production in muscles also relies on amino acid metabolism, including branched-chain amino acids (BCAA: leucine, isoleucine and valine) that can be converted to acetyl-CoA, as well as asparagine, aspartate and glutamate that can be transformed into intermediates of the tricarboxylic acid (TCA) cycle (Kamei et al., 2020).

Muscle metabolic plasticity is also triggered by hormones, such as thyroid hormones (Nicolaisen et al., 2020), glucocorticoids (Kuo et al., 2013) and sex hormones (Haizlip et al., 2015; Ueberschlag-Pitiot et al., 2017). In particular, testosterone deficiency in men leads to obesity, dyslipidemia, hypertension, hyperglycemia and insulin resistance (Kelly and Jones, 2013). Furthermore, testosterone-induced cardiomyocyte hypertrophy is associated with increased glycolytic activity (Troncoso et al., 2021). Testosterone and dehydroepiandrosterone (DHEA) also activate glucose metabolism in skeletal muscle (Sato et al., 2008; Troncoso *et al.*, 2021), and insulin resistance negatively correlates with serum testosterone (Pitteloud et al., 2005).

Androgen effects are mediated by the androgen receptor (AR, NR3C4), which belongs to the nuclear receptors' superfamily (Lubahn et al., 1988). Reduced androgen levels with age or AR inhibition impairs fat metabolism in skeletal muscle by reducing the expression of the fatty acid transporter CD36 (Kim et al., 2019). Conversely, selective overexpression of AR in male rat and mouse skeletal muscles increases lean mass and reduces fat mass. This shift in body composition is associated with type IIb myofiber hypertrophy, decreased adipocyte size, and enhanced muscle mitochondrial activity (Fernando et al., 2010). Our previous study of mice in

which AR is selectively ablated in myofibers ($AR^{skm-/y}$ mice) showed that the androgen-dependent postnatal hypertrophy of perineal muscles is mediated by myofiber AR, whereas that of limb muscle fibers androgen is myocytic AR-independent (Chambon et al., 2010). However, AR deficiency in limb myocytes impairs myofibrillar organization of sarcomeres and decreases muscle strength, demonstrating that myocytic AR controls critical pathways required for maximum force production (Chambon *et al.*, 2010; Ophoff et al., 2009b). Nevertheless, despite numerous studies performed in men and rodents, the molecular and cellular mechanism by which androgens via their receptor affect myofiber homeostasis remains poorly understood. Here we show that myofiber AR controls muscle fiber contraction and metabolism by direct binding at genes encoding the key enzymes from these pathways.

Results

Loss of myofiber AR impairs glycolysis and promotes type-2 diabetes

Sedentary male mice initiate a metabolic transition between 15 to 30 weeks of age, during which their muscles undergo an oxidative-to-glycolytic switch (Duteil *et al.*, 2010), associated with glucose intolerance and insulin insensitivity (**Figures S1A and S1B)**. Western blot analysis of gastrocnemius muscles of male mice revealed that AR levels culminate just after puberty (**Figure 1A**). To determine the role of myofiber AR in muscle metabolism, we analyzed $AR^{skm-/y}$ mice, in which AR is selectively knocked-out in myofibers (Chambon *et al.*, 2010). In agreement with previous results, immunofluorescent analysis revealed that AR was efficiently ablated in skeletal muscle fibers, but not in PAX7-positive satellite cells (**Figures S1C and S1D**).

Remarkably, blood glucose levels were higher in $AR^{skm-/y}$ mice than in control littermates at 10 to 25 weeks (**Figure 1B**). Moreover, intraperitoneal glucose tolerance tests (IPGTT) showed that mice lacking myofiber AR became glucose intolerant at 15 weeks of age (**Figure 1C**). In addition, blood insulin levels were higher in $AR^{skm-/y}$ mice than in control mice at 15 and 25 weeks (**Figure 1D**), and intraperitoneal insulin sensitivity tests (IPIST) revealed that $AR^{skm-/y}$ mice became insulin resistant earlier than their control littermates (**Figure 1E**), indicating that muscle glycolytic activity is impaired in the absence of myofiber AR. Interestingly, hexokinase activity in quadriceps muscles was decreased by 20% at 15 weeks in the absence of myofiber AR (**Figure 1F**). Of note, Western Blot analysis showed that protein levels of HK2, the rate limiting enzyme of glycolysis, follow those of AR with age, reaching a peak between 11 and 15 weeks (**Figure 1A**).

To provide further insights on the role of AR in glucose metabolism, we evaluated glucose uptake in C2C12 myotubes. The incorporation of 2-deoxyglucose (2-DG), a glucose analog that cannot be metabolized, was enhanced by 1.7-fold by 5α-Androstan-17β-ol-3-one (DHT), and lowered by 1.3-fold by the anti-androgen flutamide (**Figures 1G and S1E**). Moreover, extracellular acidification rate (ECAR) measurements revealed that glycolysis, maximal glycolytic capacities and glycolytic reserve were increased by DHT (**Figures S1F and S1G**), whereas flutamide had an opposite effect (**Figures 1H and 1I**), demonstrating that androgens via AR stimulate the glycolytic activity in C2C12 myotubes.

Food and water intake (**Figure S1H**), as well as lean and fat content (**Figure S1I**) were similar in $AR^{skm-/y}$ and control mice at the age of 15 weeks. Moreover, body weight of $AR^{skm-/y}$ male mice was similar to that of their control littermates over a 30-week period (**Figure S1J**). Altogether, our data show that defective AR functions in myofibers impair glucose uptake and glycolytic capacities, and accelerate the development of type-2 diabetes (T2DM), without impacting adiposity.

Figure 1.

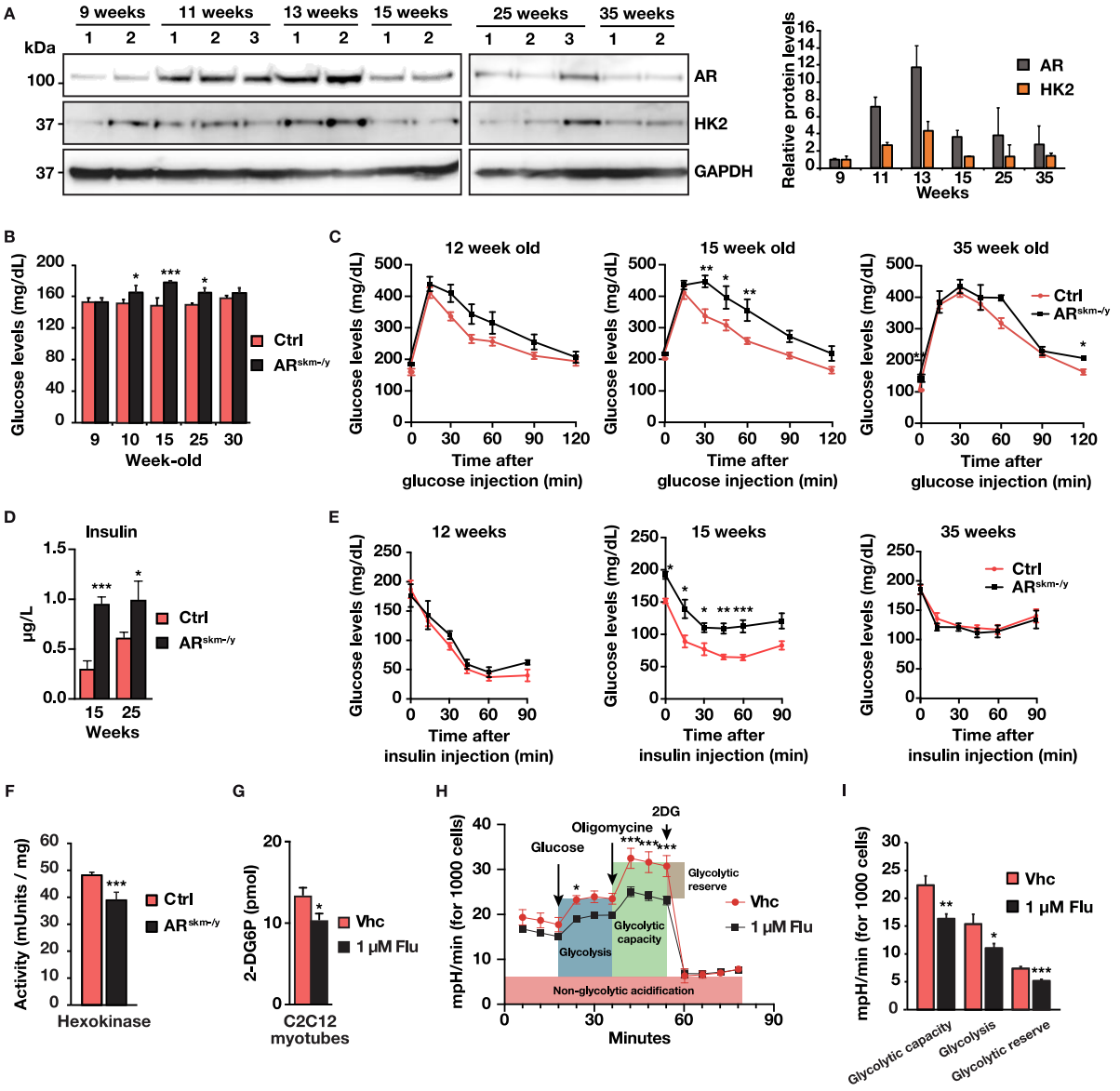

Figure 1: Role of AR in glucose metabolism. *A. Representative Western blot analysis and quantification of androgen receptor (AR) and hexokinase 2 (HK2) protein levels in gastrocnemius muscles of 9 to 35-week-old C57/Bl6 mice. GAPDH was used as a loading control. B-E. Basal glucose levels (B), glucose tolerance test (IPGTT) (C), blood insulin levels (D) and insulin sensitive test (IPIST) (E) of control and AR$^{skm-/y}$ mice at indicated ages. F. Hexokinase activity in quadriceps muscles of control and AR$^{skm-/y}$ mice at 15 weeks of age. G-H. 2-deoxyglucose (2-DG) uptake (G), representative extracellular acidification rate (ECAR) (H), and maximal glycolytic capacity, glycolysis and glycolytic reserve deduced from ECAR (I) in C2C12 myotubes treated with 1 µM flutamide (Flu) or with vehicle (Vhc). A: n=2-3 mice in duplicate, B: n= 8 control and 12 AR$^{skm-/y}$ mice, C, E: n=7 mice, D: 7 control and 12 AR$^{skm-/y}$*

*mice at 15 weeks, and 12 control and 8 AR$^{skm-/y}$ mice at 27 weeks. F: n=4, G: n=3, H-I: n=6. A, B, D, F, G, I: mean + SEM. C, E, H: mean ± SEM. *, p<0.05; **, p<0.01; ***, p < 0.001.*

Impaired glycolysis is not compensated by oxidative metabolism in AR$^{skm-/y}$ mice

Even though glucose metabolism was altered in AR$^{skm-/y}$ mice, their cholesterol and triglyceride blood levels were similar to those of control mice from 15 to 25 weeks (**Figures S2A and S2B**). Free fatty acid (FFA) levels were similar in control and AR$^{skm-/y}$ mice at 15 weeks, and increased by two-fold between 15 and 25 weeks in control mice, but not in AR$^{skm-/y}$ mice (**Figure 2A**). Interestingly, transcript levels of the fatty acid transporter *Cd36* were 1.3-fold higher in gastrocnemius muscles of 15-week-old AR$^{skm-/y}$ mice than in those of age-matched control mice (**Figure 2B**), indicating that FFA uptake might be increased in muscles of AR$^{skm-/y}$ mice. After import by CD36, fatty acids (FA) are processed by lipases and converted to FA-CoA. Interestingly, the expression and activity of the triglyceride hydrolase LPL were decreased in AR$^{skm-/y}$ mice (**Figures 2B and 2C**), as well as transcripts levels of *Pnpla2* (ATGL, that catalyzes the conversion of TAG to DAG) (**Figure 2B**), which is in favor of decreased lipolysis and decreased production of FA-CoA. To be processed by beta-oxidation, FA-CoA are complexed with carnitine in the cytoplasm, and imported in the mitochondria by CPT1A, the activity of which is inhibited by malonyl-CoA. Malonyl-CoA is produced from acetyl-CoA by the acetyl-CoA carboxylase (ACC). When phosphorylated, ACC activity is inhibited, leading to a reduction in production and increased CPT1A activity. Metabolomic analysis revealed increased levels of free carnitine (i.e. not complexed with FA) in myofibers lacking AR (**Figure 2D)**. In addition, Western blot analysis unveiled that the ratio between phosphorylated and total ACC was decreased by two-fold (**Figures 2E-2G**), indicating that CPT1A activity is impaired, leading to altered fatty acid import to the mitochondria (Hoehn et al., 2010). Interestingly, ultrastructure analyses revealed the presence of higher number and larger lipid droplets in myofibers of AR$^{skm-/y}$ mice than in control mice (**Figure 2H**). Together, these data show that FA are less efficiently metabolized in skeletal muscles of AR$^{skm-/y}$ mice and accumulate in their cytoplasm, despite increased transcript levels of genes encoding key enzymes of beta-oxidation (**Figure 2B**).

Interestingly, histochemical staining of the reduced form of nicotinamide adenine dinucleotide (NADH) dehydrogenase (mitochondrial respiratory complex I) activities in fast-twitch muscles showed that the proportion of darkly stained oxidative fibers was higher in 15-week-old AR$^{skm-/y}$ mice (**Figures 2I and S2C**). Moreover, mitochondrial content, determined by qPCR on mitochondrial and genomic DNA, was higher in quadriceps and tibialis muscles of AR$^{skm-/y}$

mice (**Figures 2J and S2D**). Nevertheless, mitochondrial activity determined by oxygen consumption in saponin-skinned gastrocnemius fibers from 15-week-old mice in the presence of the mitochondrial substrates' pyruvate/malate, showed that O_2 consumption was 40% lower in $AR^{skm-/y}$ compared to control mice in the absence of ADP (V0-Leak, **Figure S2E**), thus demonstrating a higher proton leak. In addition, Vadp, determined after exogenous ADP addition (complex I, III, IV and V activity), was decreased by 33 % in $AR^{skm-/y}$ mice (**Figure 2K**), as well as the maximal speed of respiration assessed by succinate supplementation (**Figure 2K**, Vsucc) and Vrot (Complex II to V), determined after blocking complex I with rotenone (**Figure 2K**, Vrot), indicating that the activity of terminal complexes might be affected. Staining for Cox activity (complex IV) in quadriceps muscle revealed that the percentage of dark fibers was decreased in the absence of myofiber AR (**Figure 2L**). Moreover, transmission electron microscopy analyses unveiled mitochondrial structural abnormalities in 10-20% of AR deficient myofibers (**Figure S2F**), including megamitochondria with normal cristae density (**Figure 2M**, red arrow), mitochondrial swelling with reduced cristae content (**Figure 2F**, blue arrow), or even mitochondria devoid of material (**Figure 2M**, white arrow), confirming that mitochondria of $AR^{skm-/y}$ mice are dysfunctional. Together, our data show that $AR^{skm-/y}$ mice fail to switch their metabolism from carbohydrate to lipid consumption, due to impaired FA usage and mitochondrial respiration.

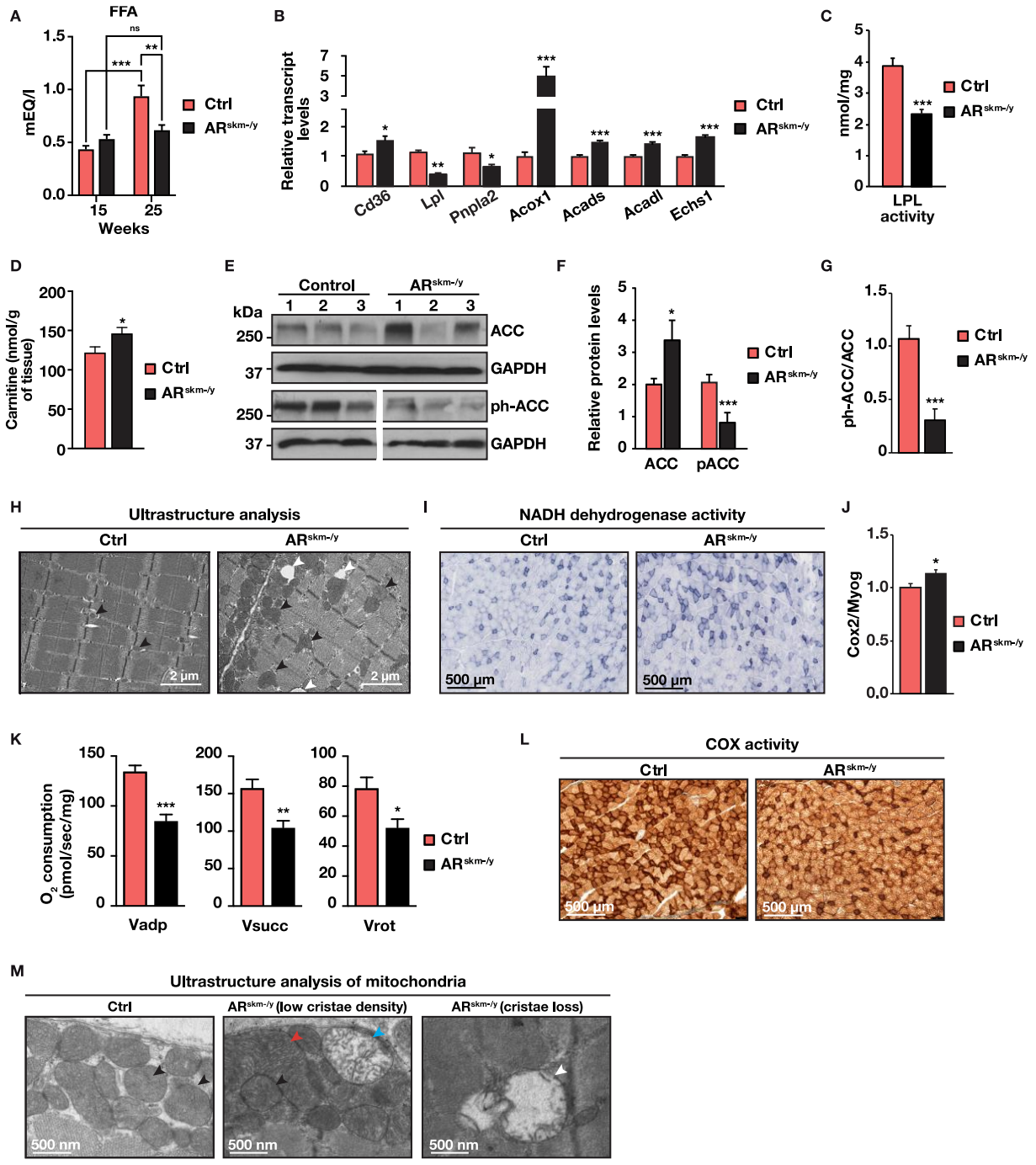

Figure 2: Role of AR in oxidative metabolism *A. Blood free fatty acid (FFA) content in control (Ctrl) and AR$^{skm-/y}$ mice at indicated ages. B. Relative transcript levels of indicated genes in gastrocnemius muscles of 15-week-old Ctrl and AR$^{skm-/y}$ mice. C. LPL activity in quadriceps muscles of Ctrl and AR$^{skm-/y}$ mice at 15 weeks of age. D. Free carnitine levels in gastrocnemius muscles of 15-week-old Ctrl and AR$^{skm-/y}$ mice. E-G. Representative Western blot analysis of total and phosphorylated ACC (E), corresponding protein quantification (F) and ratio between the phosphorylated and total ACC protein content (G) in gastrocnemius muscle of 15-week-old*

*Ctrl and AR$^{skm-/-}$ mice. GAPDH was used as a loading control. H. Ultrastructure of tibialis muscles from representative 15-week-old Ctrl and AR$^{skm-/y}$ mice. White arrow heads show lipid accumulation. Scale bar: 2 µm. I. Histochemical staining of NADH dehydrogenase activity in quadriceps muscle of 15-week-old Ctrl and AR$^{skm-/y}$ mice. Three different fiber types are distinguished. Oxidative and intermediate fibers are darkly and moderately stained, respectively; glycolytic fibers are unstained. The scale bar represents 500 µm. J. Quantification of mitochondrial content in quadriceps muscles of 15-week-old Ctrl and AR$^{skm-/y}$ mice by qPCR amplification of the Cox2 mitochondrial gene and the Myog nuclear gene. K. Oxygen consumption in saponin-skinned gastrocnemius fibers of 15-week-old control and AR$^{skm-/y}$ mice in the presence of ADP (Vadp), succinate (Vsucc, maximal respiration), and rotenone (Vrot, complex II). L. Histochemical staining of COX activity in quadriceps muscle of 15-week-old control (Ctrl) and AR$^{skm-/y}$ mice. Oxidative and intermediate fibers are darkly and moderately stained, respectively; glycolytic fibers are unstained. Scale bar: 500 µm. M. Ultrastructure analysis of mitochondria of quadriceps muscles from 15-week-old Ctrl and AR$^{skm-/y}$ mice. Black, red, blue and white arrow heads show normal mitochondria, megamitochondria and mitochondria swelling, respectively. A: 7 Ctrl and 12 AR$^{skm-/y}$ mice at 15 weeks, and 12 Ctrl and 8 AR$^{skm-/y}$ mice at 25 weeks, B, I, J, L, K: n=6 mice, C: n=4 mice, D: n=3 mice, E-G: n=7 mice, H: n= 10 mice, M: n=6, 30 fields / mouse. Mean + SEM. *, p<0.05; **, p<0.01; ***, p < 0.001.*

Loss of myofiber AR promotes amino acid catabolism and ROS production

Metabolomic analysis of the amino acid content in gastrocnemius muscles of 15-week-old AR$^{skm-/y}$ mice revealed decreased levels of lysine and of the branched-chain amino acids (BCAA) leucine, isoleucine and valine, even though the latter did not reach statistical significance (**Figures 3A and S3A**). In agreement with these results, transcript levels of *Bcat2*, *Echs1*, *Acads* and *Hadhb*, encoding enzymes involved in BCAA and lysine degradation, were increased in mutant muscles (**Figures 2B and 3B)**.

In addition to its contribution to the production of acetyl-CoA that is processed by TCA cycle, muscle metabolism of BCAAs also generates ammonia (NH_3), via glutamate dehydrogenase (GLUD1) enzymatic reactions, that is funneled into glutamine by glutamine synthetase (GLUL) (Mann et al., 2021). Interestingly, NH_3 content in quadriceps muscle was two-fold higher in AR$^{skm-/y}$ than in control mice (**Figure 3C**). Moreover, RT-qPCR analyses unveiled that *Glud1* levels were increased in the absence of AR (**Figure 3B**), and metabolomics analysis revealed

that glutamate levels were 1.8-fold higher in muscles of $AR^{skm-/y}$ mice than those of control mice, whereas glutamine levels were similar (**Figures 3D and S3A**).

Alternatively, glutamate is converted into ornithine via ALDH18A1 and OAT, and integrates the polyamine pathway (Chattopadhyay and Tabor, 2013). Even though *Aldh18a1* transcript levels were similar in muscles of control and $AR^{skm-/y}$ mice, those of *Oat* and those encoding most of the key enzymes involved in polyamine interconversion (i.e. *Odc1*, *Smox* and *Amd1*) were decreased by more than 2-fold in the absence of myofiber AR (**Figure 3B**), and thus might contribute to increased glutamic acid levels.

Metabolomics studies also uncovered variations in the levels of several biogenic amines. Indeed, levels of carnosine, a dipeptide of beta-alanine and histidine that scavenges ROS and buffers pH in muscle cells, were decreased in gastrocnemius muscles of $AR^{skm-/y}$ mice (**Figure 3E**), whereas those of methionine sulfoxide (MetO), the oxidized form of the amino acid methionine, were increased (**Figure 3F**). Of note, transcript levels of *Msrb3*, which encodes the most abundant isoform of the methionine sulfoxide reductase (MSR) in skeletal muscle, and catalyzes the enzymatic reduction and repair of oxidized methionine residues, were decreased in the absence of AR (**Figure 3B**). Moreover, muscle fluorescence intensity of dihydroethidium (DHE, a fluorescent probe for the detection of ROS), and H_2O_2 production by mitochondrial respiration were enhanced in the absence of myofiber AR (**Figures 3G and 3H**). Myofibers in which most of the mitochondria were swollen presented nuclear condensation, as well as chromatin clumps and marginalization (**Figures 3I and S2F**), which are characteristic of cell necrosis. Hematoxylin and eosin as well as Gomori trichrome staining of transversal muscle sections revealed the presence of almost 1% of necrotic myofibers (**Figures 3J, S3B and S3C**), characterized by the expression of the necrosis markers FADD, RIPK3 and PUMA (**Figure 3J**), associated with macrophage infiltration (**Figure 3J**). Various stages of metabolic necrosis were observed: (i) fibers with a pale cytoplasm, (ii) sarcolemma membrane disruptions, and (iii) phagocytic necrosis where myofibers are replaced by macrophages (**Figures 3J, S3B and S3C**).

Together, these data show that AR loss in muscle fibers leads to increased lysine and BCAA catabolism, glutamate accumulation, decreased polyamine biosynthesis, ammonia and ROS accumulation, mitochondrial damages, and necrosis of highly affected fibers.

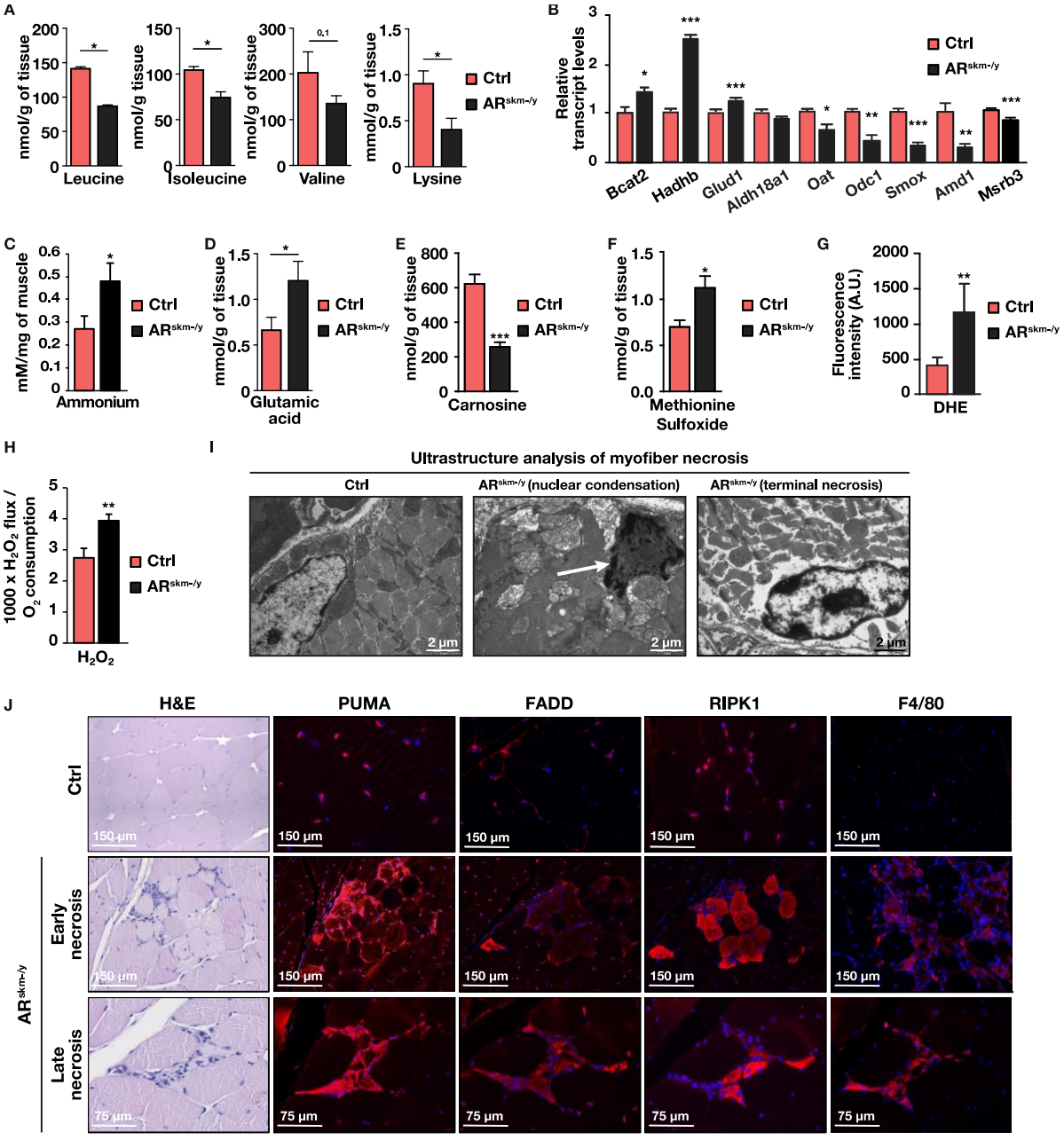

Figure 3: Role of AR in amino acid metabolism *A. Levels of indicated amino acids in gastrocnemius muscles of 15-week-old control (Ctrl) and AR$^{skm-/y}$ mice. B. Relative transcript levels of the indicated genes in gastrocnemius muscles of 15-week-old Ctrl and AR$^{skm-/y}$ mice. C. Ammonium content in quadriceps muscles of 15-week-old Ctrl and AR$^{skm-/y}$ mice. D-F. Levels of glutamic acid (D), carnosine (E) and methionine-sulfoxide (F) in gastrocnemius muscles of 15-week-old Ctrl and AR$^{skm-/y}$ mice. G-H. Fluorescent detection of ROS production by quantification of DHE staining intensity (G) and measurement of H_2O_2 production relative to oxygen consumption determined in the presence of ADP (H) on gastrocnemius fibers of 15-week-old Ctrl and AR$^{skm-/y}$ mice. I. Ultrastructure of myofiber necrosis of quadriceps nuclei*

*from 15-week-old Ctrl and AR$^{skm-/y}$ mice. White arrow shows necrotic nucleus. Scale bar: 2 µm. J. Hematoxylin and eosin (H&E) staining and PUMA, FADD, RIPK1 and F4/80 immunofluorescent detection of quadriceps muscles of 15-week-old Ctrl and AR$^{skm-/y}$ mice. Nuclei are stained with DAPI. Scale bars: 75 and 150 µm, as indicated. B, C, H-J: n=6 mice, A, D-F: n=3, G: n=6, 30 fields / mouse. Mean + SEM. *, p<0.05; **, p<0.01; ***, p < 0.001.*

AR in myofibers controls the expression of numerous metabolic enzymes, structural proteins and transcription factors

To characterize the molecular players that account for the phenotype of AR$^{skm-/y}$ mice, we performed a transcriptome analysis of gastrocnemius muscles from control and mutant mice at the age of 9 weeks. Our data unraveled 1092 down- and 1046 upregulated genes (reads more than 50 and p-value less than 0.05). Pathway analysis revealed that genes up-regulated upon myofiber AR loss are involved in amino acid metabolism, nitrogen metabolism and fatty acid beta-oxidation (**Figure 4A**). In agreement with our RT-qPCR and metabolomic analyses, the transcript levels of genes encoding enzymes involved in BCAA degradation, (e.g. *Bcat2*, *Bckdhb*, *Dbt*, *Ivd*, *Aldh7a1*, *Hadha*, *Hadhb*, *Echs1*, *Acads*, *Acadsb*, and *Acaa2*), as well as those involved in lysine degradation (e.g. *Aldh7a1*, *Gcdh*, *Echs1*, and *Hadha*) were upregulated in AR$^{skm-/y}$ mice (**Figures 4B and S4A-S4D)**. Our analysis also confirmed the up-regulation of transcripts encoding enzymes involved in nitrogen metabolism, such as *Glud1* and *Glul*, as well as the decrease in those encoding enzymes involved polyamine pathway, such as *Oat*, *Azin2*, *Odc1*, *Amd1*, *Amd2* and *Smox* (**Figures S4E-S4G**).

Moreover, pathway analysis revealed that genes down-regulated in AR$^{skm-/y}$ mice are involved in muscle contraction, which is in line with our previous studies (Chambon *et al.*, 2010). We also identified metabolic pathways such as insulin signaling, fatty acid biosynthesis and glycolysis (**Figure 4C**). In particular, we observed a decrease in transcript levels of the glucose transporter *Glut3* (*Slc2a3*), the main isoform responsible of insulin-independent basal glucose uptake into the muscles (Copland et al., 2007; Stuart et al., 2000), of *Hk2* and various genes involved in anaerobic glycolysis, as well as *Pcx*, that converts pyruvate to oxaloacetate (**Figures 4D, S4H and S4I**), thereby showing that AR is instrumental for pyruvate entry in the TCA cycle. Furthermore, the transcript levels of genes involved in fatty acid beta-oxidation, such as *Acox1*, *Acadl*, *Acads* and *Hadha* were decreased after AR loss in myofibers, whereas those promoting *de novo* fatty acid synthesis, including *Lpl*, *Acly*, *Fasn* and *Scd1*, were decreased (**Figures 2B, 4E and S4J**).

To identify direct AR targets, hind limb muscle chromatin from 11-week-old mice was immunoprecipitated with antibodies directed against AR, followed by massive parallel sequencing (ChIP-seq). Our analysis uncovered 3457 peaks, mainly located at intronic and intergenic regions (**Figure S4K**). HOMER motif search unveiled that AR is recruited to DNA via AREs (21.2%) and AR half-sites (33.6%) (**Figure 4F**), as exemplified for *Tead4* (**Figure S4L**). An analysis of the genomic distribution revealed that peaks are equally distributed between far up-stream and down-stream regions (-100 kb to -50 kb and 50 kb to 100 kb), intermediate locations (-50 kb to -20 kb and 20 kb to 50 kb), and DNA segments encompassing the TSS (-10 kb to -2 kb, -2 kb to 2 kb and 2 kb to 10 kb) (**Figure 4G**). About 10% of the differentially expressed genes in $AR^{skm-/y}$ mice were bound by AR as determined by a nearest TSS analysis (**Figure S4M**). A gene centric analysis using TSS coordinates showed that AR is recruited to 350/1092 of genes down-regulated in $AR^{skm-/y}$ mice within a 100 kb window (**Table S1**), indicating that AR regulates target genes via enhancers located at far up/down stream regions. Interestingly, we found that AR directly controls genes involved in metabolic processes including *Hk2*, *Fbp2* and *Slc2a3* for glycolysis, *Aacs*, *Abca2*, *Acot11*, *Pgc1a* and *Scd1* for lipid metabolism, *Azin2*, *Odc1* and *Smox* for the polyamine biosynthesis, and *Msrb3* for ROS scavenging. Our analysis also unveiled that AR directly controls the expression of numerous genes encoding skeletal muscle cytoskeleton, cell-adhesion and calcium flux, including *Acta2*, *Cnn1*, *Lmod1*, *Lmod3* and *Tnni2* of the contractile cytoskeleton *Cav3*, *Col17a1*, *Dmd* and *Dtnb* of the non-contractile cytoskeleton, *Itgb5* and *Lama5* from the extra-cellular matrix, and *Cacnai* and *Cacng7* encoding subunits of calcium voltage-gated channels, also known as dihydropyridine receptors (DHPR).

Interestingly, immunofluorescence analysis revealed that whereas the DHPR beta (DHPRB) and the sarcoplasmic reticulum Ca^{2+} transport ATPase SERCA1 were expressed at similar levels on longitudinal sarcoplasmic reticulum of control and $AR^{skm-/y}$ mice, protein levels of DHPRA and RYR1 were strongly decreased in the absence of myofiber AR (**Figures 4H and S4N**). In addition, the DHPRA, DHPRB, RYR1 and SERCA1 were misallocated (**Figures 4I and S4N**). In agreement, ultrastructure analyses revealed 10-20% of myofibers with dilatation and unparalleled T-tubules to the Z-lines upon AR loss (**Figure 4A**), indicating an altered connection between sarcolemma and endoplasmic reticulum, thus showing that AR is instrumental for proper triad organization.

In addition, we identified various transcription factors and co-regulators as direct targets of AR in skeletal muscle [e.g. *Atf4*, *Cux2*, *Irx3*, *Kdm2b*, *Kdm4b*, *Med25*, *Nr1d1* (*Rev-ErbAalpha*), *Smarca2*, *Smyd2*, *Tgif*, *Trp53* and *Trp63*], some of which are involved in muscle development

(e.g., *Myod1*, *Naca*, *Tcf15* and *Tead4*) (**Figure S4L and Table S1**). Altogether, combined cistrome and transcriptome analysis show that myofiber AR directly controls genes involved in glycolysis, fatty acid processing, polyamine biosynthesis and ROS scavenging. AR also regulates various components of skeletal muscle cytoskeleton, as well as a number of transcription factors.

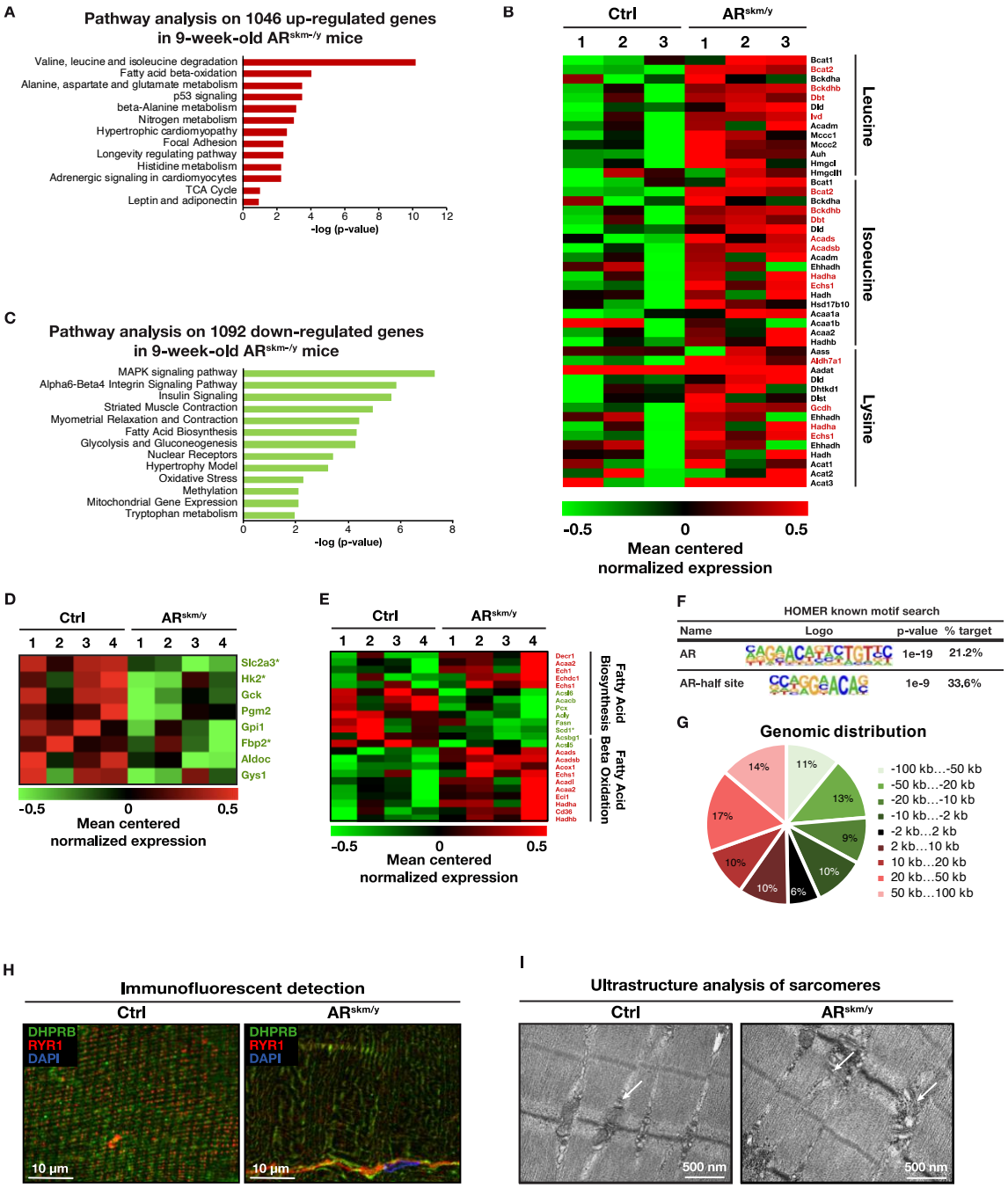

Figure 4: Analysis of AR functional targets in skeletal muscle A. Pathway analysis of up-*regulated genes in gastrocnemius muscle of 9-week-old AR$^{skm-/y}$ mice. B. Heatmap depicting the*

mean centered normalized expression of genes involved in branched chained amino acid metabolism, obtained by RNA-seq analysis performed in gastrocnemius muscle of 9-week-old Ctrl and AR$^{skm-/y}$ mice. Genes significantly up-regulated in AR$^{skm-/y}$ mice are marked in red. C. Pathway analysis of down-regulated genes in gastrocnemius muscle of 9-week-old AR$^{skm-/y}$ mice. D-E. Heatmaps depicting the mean centered normalized expression of genes involved in glycolysis (D), and fatty acid synthesis and beta-oxidation (E) obtained by RNA-seq analysis performed in gastrocnemius muscle of 9-week-old Ctrl and AR$^{skm-/y}$ mice. Genes significantly down- and up-regulated in AR$^{skm-/y}$ mice are marked in green and red, respectively. F. HOMER known motif analysis of AR-bound DNA sequences in skeletal muscles. G. Pie chart depicting the AR peak distribution in the genome of skeletal muscles. H. Immunofluorescent detection of the RYR1 (red) and DHPRB (green) in quadriceps muscles of 15-week-old control and AR$^{skm-/y}$ mice. Nuclei are stained with DAPI. Scale bar: 10 µm. I. Ultrastructure of quadriceps sarcomeres from 15-week-old Ctrl and AR$^{skm-/y}$ mice. White arrow points to a T-tubule. Scale bar: 500 nm. H: n=4, I: n=10.

Discussion

Despite the large number of studies investigating androgen action on skeletal muscles (De Gendt and Verhoeven, 2012), a comprehensive picture of the role of AR on myofiber homeostasis remained elusive at the molecular level.

Using a mouse model in which AR was selectively ablated in myofibers, we demonstrate that AR deficiency leads to decreased muscle glucose uptake and glycolytic activity. Previous studies showed that testosterone supplementation in adult male rats induces *Hk2* and *Pfk2* mRNA levels in cardiomyocytes (Troncoso *et al.*, 2021), and increases GLUT-4 (SLC2A4) protein expression and translocation, as well as PFK and HK activities in cultured skeletal muscle cells (Sato *et al.*, 2008). Moreover, androgens promote the expression of glucose transporter 1 (*Glut1, Slc2a1*) and 3 (*Glut3, Slc2a3*), as well as hexokinase 1 (*Hk1*) and 2 (*Hk2*), and phosphofructokinase (*Pfk1*) (Vaz et al., 2016) in various cell-types. To our knowledge, none of the above-mentioned genes was identified as direct AR targets. Our genome-wide analyses unravel that myofiber AR directly promotes the expression of *Slc2a3*, *Hk2* and *Fbp2*, thereby enhancing the uptake and conversion of glucose to glyceraldehyde-3P. In addition, we identified the lipase *Lpl* as a direct AR target. As our results show interfibrillar lipid droplet accumulation, decreased LPL activity and reduced *Pnpla2* levels in muscles of AR$^{skm-/y}$ mice are likely to impair FA cleavage to fatty-acyls. Moreover, increased ACC activity might limit CPT1A-dependent FA import in the mitochondria. In contrast to the age-dependent decreased

lipid oxidation (ref), the transcript levels of genes encoding fatty acid transporter *Cd36* and beta-oxidation enzymes are enhanced in $AR^{skm-/y}$ mice, probably through a compensatory mechanism. Interestingly, we found that PGC1A, one of the main coordinators of muscle oxidative metabolism (Schuler *et al.*, 2006), is also a direct target of AR, and that its transcript levels are decreased in $AR^{skm-/y}$ mice. Thus, reduced *Pgc1a* levels might contribute to impaired FA catabolism in AR-deficient fibers. In addition, we identified *Scd1* and *Fasn*, encoding two enzymes of *de novo* lipogenesis, as direct AR targets, in agreement with studies showing that androgens stimulate glycolysis for *de novo* lipid synthesis in prostate cancer cells (Moon et al., 2011). This indicates that AR stimulates glycolysis and fatty acid cleavage to provide substrate for the TCA, and promotes *de novo* lipogenesis to store energy upon excess of the food supplies. Combined metabolomics and transcriptome analyses showed that BCAA and lysine degradation is induced upon AR loss to generate acetyl-CoA that can be processed by the TCA cycle. To date, only little is known about the role of androgen in BCAA metabolism. The transcription factors and co-regulators identified as AR direct targets in skeletal muscle might contribute to the increased transcript levels of the enzymes involved in BCAA degradation. In particular, it is well established that BCAA catabolism is activated by the glucocorticoid pathways (Liu et al., 2017). Since we found that GR transcript levels were augmented by 1.5-fold in $AR^{skm-/y}$ mice, increased levels of BCAA degradation enzymes such as *Bcat2*, that catalyzes the first step of BCAA oxidation, is most likely mediated by enhanced GR-dependent transcription. In the transamination reaction, BCAT transfers an amino group to a-ketoglutarate to produce glutamate (Goto et al., 2005). In the mitochondria, glutamate is processed by GLUD1 to generate a-ketoglutarate that enters the TCA cycle and ammonia (NH_3) (Mann *et al.*, 2021). In agreement with increased *Bcat2* transcripts, glutamate and NH_3 levels were higher in $AR^{skm-/y}$ mice compared to their control littermates.

Previous studies showed that ammonia excess impairs skeletal muscle mitochondrial activity (Davuluri et al., 2016). We show that respiration was lower in the presence of pyruvate and malate, with increased H_2O_2 production, despite an increased NADH oxidase activity and higher mitochondrial DNA content. Electron microscopy analysis revealed hypertrophic mitochondria with normal cristae and normal matrix density, that might account for higher NADH oxidase activity. Megamitochondria formation is an adaptative response to decrease intracellular ROS levels by reducing oxygen consumption (Wakabayashi, 2002). If cells cannot cope with excess amounts of free radicals, megamitochondria become swollen (Wakabayashi, 2002). In the absence of myofiber AR, we observe such defective organelles randomly distributed at interfibrillar and subsarcolemmal areas. Therefore, ammonia production resulting

from amino acid degradation in myofibers of $AR^{skm-/y}$ mice leads to ROS accumulation and impaired mitochondrial functions, ultimately causing necrosis of highly affected fibers.

We and other previously showed that hindlimb muscle strength was reduced in AR-null male mice (MacLean et al., 2008; Ophoff et al., 2009a) and skeletal muscle-specific AR knockout mice (Chambon *et al.*, 2010; Dubois et al., 2014; Ferry et al., 2014; Fraysse et al., 2014; Ophoff *et al.*, 2009b; Rana et al., 2016). In agreement with a recent paper that identified *myosin light-chain kinase 4* (*Mylk4*) as a target of AR that accounts for strength defects in skeletal muscles of $AR^{skm-/y}$ female mice supplemented or not with DHT (Sakakibara et al., 2021), we found that *Mylk4* transcript levels were decreased in the absence of myofiber AR in males. Our previous electron microscopy of various muscles from 15-wk-old $AR^{skm-/y}$ mice revealed disruptions of myofibrils in about 10% of the sarcomeres from $AR^{skm-/y}$ mice, with loss of myofilaments, rupture of Z lines, and enlarged sarcoplasm (Chambon *et al.*, 2010). In this study, our omics data unveiled that AR directly controls the expression of various genes of the contractile cytoskeleton including *Acta2* and *Tnni2*, of the non-contractile cytoskeleton such as *Cav3*, *Dmd* and *Dtnb*, and the calcium channel subunits *Cacnai* and *Cacng7*. Moreover, combined ultrastructure and immunofluorescence analyses revealed sarcoplasmic reticulum malformation $AR^{skm-/y}$ mice. As calcium flux stimulates aerobic metabolism and ATP production, impaired calcium conduction caused by decreased expression of calcium channel subunits and triad disorganization might contribute to mitochondrial dysfunction in $AR^{skm-/y}$ mice.

The metabolic muscle alterations of $AR^{skm-/y}$ mice were associated with increased blood glucose levels and an accelerated development of type-2 diabetes (T2DM), without impacting adiposity. Previous studies of AR-null male mice showed that insulin sensitivity of young mice was not altered, despite increased muscle transcript levels of *Slc2a4*, *Hk1*, *Pfk* and *Pkm*, as well as decreased energy expenditure and lipolysis with late-onset obesity (Fan et al., 2005). Another study revealed a progressive reduced insulin sensitivity and impaired glucose tolerance in AR-null mice, accompanied with accelerated weight gain, hyperinsulinemia, and hyperglycemia, and increased triglyceride content in skeletal muscle and liver (Lin et al., 2005). Epidemiological studies have shown that low testosterone levels are associated with obesity, impaired glucose tolerance, insulin resistance, an adverse lipid profile, decreased V_{O2max} and oxidative phosphorylation gene expression (Pitteloud *et al.*, 2005). Conversely men with metabolic syndrome and type-2 diabetes have a high prevalence of hypogonadism (Muraleedharan and Jones, 2010). Altogether, these data indicate that the development of T2DM upon AR loss is mainly caused by its deficiency in myofibers, whereas dyslipidemia and obesity might result from disruption of androgen signaling in adipose tissue and/or liver.

Patients with Kennedy's disease (KD), also known as spinal and bulbar muscular atrophy (SBMA), a X-linked recessive neuromuscular disease caused by CAG/glutamine expansions in exon 1 of the AR encoding for the AF1 domain, suffer from metabolic changes (e.g. glucose intolerance and hyperlipidemia) (Pradat et al., 2020), reduced muscle force, associated with a switch in fiber-type composition, disrupted muscle striation, altered calcium dynamics in response to muscle contraction, and aberrated expression of excitation-contraction coupling (ECC) machinery genes (Chivet et al., 2019). Corresponding poly-Q expansions in mice impaired glycolysis with decreased *Hk2* expression, and altered mitochondrial functions in their muscles (Giorgetti et al., 2016), which resembles the phenotype of $AR^{skm-/y}$ mice. This data indicate that the defects induced by the poly-Q-AR are mainly due to impaired AR activity in skeletal muscle and not to the toxicity of the misfolded protein.

By directly coordinating the expression of a large number of genes, myofiber AR stimulates glycolysis and fatty acid cleavage. In AR-depleted myofibers, ammonia production resulting from amino acid degradation to compensate for impaired glucose and fatty acid metabolism leads to ROS accumulation and impaired mitochondrial functions, ultimately causing necrosis of highly affected fibers. Combined structural and metabolic alterations result in strength reduction and accelerate the development of T2DM. Therefore, androgen signaling via AR is instrumental for optimal metabolic capacities and energy production of limb muscles of male mice.

Materials and Methods

Generation of $AR^{skm-/y}$ mice

$AR^{skm-/y}$ mice were previously described (Chambon *et al.*, 2010). In brief, $AR^{L2/y}$ mice were intercrossed with HSA-Cre mice that express the Cre recombinase selectively in skeletal muscle myofibers (Schuler et al., 2005), to generate control ($AR^{L2/y}$) and $AR^{skm-/y}$ mutant mice. All mice were on a C57/Bl6J background.

Mouse studies

Mice were maintained in a temperature- and humidity-controlled animal facility, with a 12-hours light/dark cycle. Water and standard rodent chow (2800 kcal/kg, Usine d'Alimentation Rationelle, Villemoisson-sur-Orge, France) were provided *ad libitum*. Breeding and maintenance of mice were performed according to institutional guidelines. All experiments were done in an accredited animal house, in compliance with French and EU regulations on the use of laboratory animals for research. Intended manipulations were submitted to the Ethical committee (Com'Eth, Strasbourg, France) for approval and to the French Research Ministry (MESR) for ethical evaluation and authorization according to the 2010/63/EU directive under the APAFIS numbers 2012-025, 2012-027, 2012-028 and 23910.

The body weight from our various cohorts was measured every week. Food and water consumption were measured with a Labmaster system (TSE, www.TSE-Systems.com) at 26 min intervals for 24 h. Body lean and fat content were recorded in anaesthetized mice by qNMR (PIXIMUS, GE Medical Systems) according to the manufacturer's instructions (Duteil *et al.*, 2010).

Animals were sacrificed by cervical dislocation, and tissues were immediately collected, weighed, and frozen in liquid nitrogen or processed for biochemical and histological analysis.

Blood and serum analyses

Experiments were performed as described (Duteil *et al.*, 2010). Basal glucose levels were determined on 6 h-starved mice by blood collection from the tail vein. Intraperitoneal glucose tolerance test (IPGTT) and insulin sensitive tests (IPIST) were performed after 6 hours fasting. Following measurement of the basal glucose level (time 0), mice were intraperitoneally injected with 20 % glucose in sterile saline solution (0.9 % NaCl) at a dose of 2 g per kg body weight for IPGTT, and with porcine insulin (Sigma) at 0.5 U/kg for IPIST. Blood was collected from the tail vein after 15, 30, 45, 60, 90 and 120 min for glucose determination.

For serum glucose, insulin, cholesterol, triglyceride and free fatty acid levels measurements, blood was collected from retro orbital sinus after a 6-hour fast, and was analyzed as described (Duteil *et al.*, 2010).

Histological analyses

Hematoxylin and eosin, as well as Gomori's trichrome staining, were performed as described (Biancalana et al., 2021; Duteil *et al.*, 2010).

For NADH staining, 10 µm cryosections were incubated with staining solution [0.2 M Tris pH 7.4, 1.5 mM NADH (Roche, 10128015001) and 1.5 mM nitroblue tetrazolium (Sigma-Aldrich, N-6876)], dehydrated in an ascending ethanol gradient, incubated twice with xylene and mounted as described (Duteil *et al.*, 2010).

For COX staining, 10 µm cryosections were incubated for 1 hour with staining solution [50 mM phosphate buffer solution pH 7.2 (35% of H_2PO_4 solution at 6.9 mg/mL and 65% of $Na_2H_2PO_4$ at 17 mg/mL) containing 2 mg/mL diaminobenzidine, 2 mg/mL Cytochome C, 7.5 mg/mL sucrose and 2% catalase], dehydrated in an ascending ethanol gradient, incubated twice with xylene and mounted.

For immunofluorescent detection, tissues were fixed in 4% PFA and embedded in paraffin. Five µm paraffin sections were deparaffinized and rehydrated. Immunofluorescence analysis was performed with AR (C-terminal, #3299, IGBMC), PAX7 (PA1117, Fisher Scientific SAS), RIPK1 (17519-1-AP-20UL, Proteintech Europe Ltd), PUMA (55120-1-AP-20UL, Proteintech Europe Ltd), FADD (14906-1-AP-20UL, Proteintech Europe Ltd), F4/80 (70076S, OZYME SAS), DHPRA (AB81980, ABCAM), DHPRB (VD21B12, Developmental Studies Hybridoma Bank), RYR1 (HPA056416, Sigma-Aldrich), SERCA (MA3-911, Fisher Scientific SAS) antibodies as described (Rovito et al., 2021). Mouse or rabbit IgGs were used as controls.

For ultrastructural analyses, skeletal muscle samples were fixed by immersion in 2.5 % glutaraldehyde and 2.5 % paraformaldehyde in cacodylate buffer (0.1 M, pH 7.4) and washed in cacodylate buffer for 30 minutes and kept at 4 °C. Post-fixation was performed with 1 % osmium tetraoxide in 0.1 M cacodylate buffer for 1 hour at 4 °C and dehydration through graded alcohol (50, 70, 90 and 100 %) and propylene oxide for 30 minutes each. Samples were oriented longitudinally or transversally, and embedded in Epon 812. Ultrathin sections were cut at 70 nm and contrasted with uranyl acetate and lead citrate, and examined at 70 kV with a Morgagni 268D electron microscope. Images were captured digitally by a Mega View III camera (Soft Imaging System).

RNA extraction and quantification

Muscles were homogenized in TRIzol reagent (Life Technologies, Darmstadt, Germany). RNA was isolated using a standard phenol/chloroform extraction protocol, and quantified by spectrophotometry (Nanodrop, Thermo Fisher). cDNA was prepared by reverse transcription of 2 µg of RNA using SuperScript IV (Life Technologies) and oligo(dT) primers according to the supplier's protocol. cDNA was diluted hundred times and quantitative PCR was performed with a Lightcycler 480 II (Roche) using the SYBR® Green PCR kit (Roche) according to the supplier's protocol (2 µl cDNA, 4.8 µl H_2O, 5 µl Syber Green 2x mix and 0.2 µl of 100 µM primer mix). Primers are described in Table S2. *Hprt*, *36b4* and *18S* were used as internal controls. Data were analyzed using the standard curve (Bookout et al., 2006) and ΔΔCt (Livak and Schmittgen, 2001) methods. Primer efficiency was calculated as *Eff* = 100*10^((-1/The Slope Value)-1). Results obtained with *36b4* housekeeping gene and the standard curve method are presented.

For RNA-seq, RNA integrity was determined by Bioanalyzer, cDNA library prepared, and sequenced with the standard Illumina protocol (HiSeq 4000, single-end, 50 bp) following the manufacturer's instructions. Image analysis and base calling were performed using RTA 2.7.7 and bcl2fastq 2.17.1.14. Adapter dimer reads were removed using DimerRemover. The quality of the sequencing was determined with FastQC 0.11.2 (http://www.bioinformatics.babraham.ac.uk/projects/fastqc/). Reads were mapped to the mouse mm10 genome (NCBI Build 38) using Bowtie2 2.3.4.3 (http://bowtie-bio.sourceforge.net/bowtie2/index.shtml/) (Langmead and Salzberg, 2012). Only uniquely aligned reads were retained for further analyses. Quantification of gene expression was performed HOMER. For comparison among datasets, the transcripts with more than 50 raw reads were considered. Differentially expressed genes (DEGs) were identified using the Bioconductor libraries EdgeR and DESeq (Love et al., 2014; Robinson et al., 2010). A p-value $< 10^{-5}$ and reads >50 were used as a threshold for DEGs that were further submitted for pathway analysis in WebGestalt (Wang et al., 2013) using the Over-Representation Analysis (ORA) method 5. Heatmaps were generated by centering and normalizing expression values with Cluster 3.0 (de Hoon et al., 2004) and importing them to MultiExperiment Viewer (MeV, http://mev.tm4.org/#/welcome) (Saeed et al., 2006). Genes were clustered according to the hierarchical method (HCL clustering) using gene tree, the Pearson correlation and average linkage.

Bioinformatics parameters: RNA-seq parameters were set as default, with the exception of the following:

DimerRemover parameters: -a AGATCGGAAGAGCACACGTCTGAACTCCAGTCAC
HOMER: --format bam, --fragLength given -o auto, --strand both -count genes –d -norm (total read count)

Metabolic enzyme activity measurements

Hexokinase and LPL activity, as well as ammonium content were assessed by the Hexokinase Colorimetric Assay Kit (MAK091, Sigma-Aldrich), the LPL Activity Assay kit (MAK109, Sigma) and the Ammonia Assay Kit (ab83360/K370-100, ABCAM), respectively. All activities were measured using 10-50 mg of quadriceps muscle according to the manufacturer recommendations.

Quantification of mitochondrial and nuclear DNA

Quadriceps, tibialis, gastrocnemius and soleus muscles were digested with Proteinase K overnight, and DNA was extracted by a phenol-chloroform method. Mitochondrial and nuclear DNA was amplified by quantitative PCR using *Cox2* and *Myog* primers (Table S2), respectively, and their ratio was determined to evaluate the mitochondria DNA content.

Metabolomic analysis.

Gastrocnemius muscles from 15-week-old mice were harvested and frozen at -80°C. Metabolites were extracted from gastrocnemius muscles and placed in an ice-cold ultrasonic bath for 5 minutes. Then samples were centrifuged, and the supernatant was used for further analyzes. The Biocrates kit (Biocrates) was used for the quantification of amino acids, acylcarnitines and biogenic amines, based on PITC- (phenylisothiocyanate) derivation in the presence of an internal standard followed by an FIA-MS / MS (acylcarnitines) and LC / MS (amino acids and biogenic amines) using a spectrometer AB SCIEX 4000 QTrap® (AB SCIEX, Darmstadt, Germany) with Electrosprayl Ionization (Ramsay SL 2007).

Protein analysis

Quadriceps muscles were homogenized in RIPA buffer [50 mM Tris pH 7.5, 1 % Nonident P40, 0.5 % Sodium Deoxycholate, 0.1 % SDS, 150 mM NaCl, 5 mM EDTA, 1 mM PMSF and protease inhibitor cocktail (45 µg/mL; Roche)]. Homogenates were separated in polyacrylamide gels and blotted to Hybond nitrocellulose membranes (Amersham Biosciences). Membranes were decorated using the following antibodies: anti-AR (C-terminal, #3299, IGBMC), anti-HK2 (2867 Cell Signaling), anti-ACC (3662, Cell Signaling), anti-

phospho-ACC Ser79 (3661, Cell Signaling). Secondary antibodies conjugated to horseradish peroxidase (Jackson ImmunoResearch, 1/10000) were detected using an enhanced chemiluminescence detection system (ECLplus, GE Healthcare) and an ImageQuant LAS 4000 biomolecular imager (GE Healthcare). GAPDH (2118, Cell Signaling) and beta-TUBULIN (Tub2a1, IGBMC) were used as loading controls, and GAPDH immunoblots are presented. Protein quantification was assessed by the FIJI/ImageJ distribution software (https://imagej.net/ImageJ) (Schneider et al., 2012).

Mitochondria respiration analysis

10 mg of gastrocnemius muscles were collected and placed in S solution [2.77 mM CaK_2EGTA, 7.23 mM K_2EGTA, 6.04 mM Na_2ATP, 6.56 mM $MgCl_2$, 20 mM taurine, 0.5 mM DTT, 50 mM potassium-methane sulfonate (160 mM ionic strength), 20 mM imidazole (pH 7.1), 5.7 mM Na_2ATP and 15 mM creatine-phosphate]. Fibers were separated under a binocular microscope in solution S at 4°C, and permeabilized for 30 min in solution S containing 50 µg/mL of saponin. Then, fibers were rinsed with agitation for 10 min at 4 °C in the buffer S. After being placed twice 5 min with agitation at 4 °C in MirO5 (EGTA 0.5 mM, $MgCl_2$ 3 mM, Potassium lactobionate 60 mM, Taurine 20 mM, KH_2PO_4 10 mM, HEPES 20 mM, Sucrose 110 mM, 2 mg/ml BSA) to wash out adenine nucleotides and creatine phosphate, respiration of permeabilized fibers was measured by high-resolution respiratory using Oxygraph-2K (OROBOROS INSTRUMENTS, Innsburk, Austria) at 37 °C in 2.1 mL glass chambers containing MirO5 medium. Control and $AR^{skm-/y}$ mice were processed in parallel. Mitochondrial respiration was assessed in MirO5 supplemented with 5 mM pyruvate and 2 mM malate substrates to activate mitochondrial complex I. After stabilization of mitochondrial respiration, 10 mM succinate were added to activate complex II. Maximal respiration rate was then recorded. 0.5 µM rotenone were finally added to inactivate mitochondrial complex I and measure complex II specific activity. Respiration rates were expressed in pmol / s and reported to 1 mg of sample. Mitochondrial H_2O_2 production was measured in parallel with mitochondrial respiration with the Amplex Red reagent (10 µM), which reacted with H_2O_2 in a 1:1 stoichiometry catalyzed by Horse Radish Peroxidase (1 U/mL).

Chromatin immunoprecipitation

For ChIP-seq analysis, libraries were prepared from AR- (C-terminal, #3299, IGBMC) and H3K4me2- (39141, ACTIVE MOTIF) immunoprecipitated DNA from skeletal muscle nuclear extracts as described (Joshi et al., 2017). ChIP-seq libraries were sequenced with an Illumina

Hiseq 4000 as paired-end 100 bp reads, and mapped to the mm10 reference genome using Bowtie 2 (Langmead and Salzberg, 2012). Uniquely mapped reads were retained for further analysis. MACS2 algorithm (https://github.com/taoliu/MACS/) (Zhang et al., 2008) was used for the peak calling with non-immunoprecipitated chromatin as control. All peaks with a FDR greater than 0.1 were excluded from further analysis. The genome-wide intensity profiles were visualized using the IGV genome browser (http://software.broadinstitute.org/software/igv/) (Thorvaldsdottir et al., 2013). HOMER was used to annotate peaks and for motif searches (Heinz et al., 2010). Genomic features (promoter/TSS, 5' UTR, exon, intron, 3' UTR, TTS and intergenic regions) were defined and calculated using Refseq and HOMER according to the distance to the nearest TSS. Venn diagrams were generated with Venny (Oliveros, 2007-2015). *De novo* identified motifs were referred to as follow: R = purine (G or A); Y = pyrimidine (T or C). Further bioinformatics analyses were performed with bedtools (https://bedtools.readthedocs.io/en/latest/index.html) (Quinlan and Hall, 2010): fasta sequences were obtained from bed files with GetFastaBed, location intersections were performed with Intersect interval and Multiple intersect, and gene centric analyses of peak distribution were performed with WindowBed. The mm10 RefSeq Genes annotation available from the UCSC table browser was used to define all genomic features except enhancers. Multiple TSSs of genes were included in the analysis.

Bioinformatics parameters: Parameters were set as default, with the exception of the following:

Bowtie parameters: --very-fast-local

MACS2 parameters: callpeak -- gsize 1.87e9 --format BAMPE -- bw 300 -- qvalue 0.01 -- nolambda -- mfold [5 ; 50] -- slocal 1000 --llocal 10000 --broad (only for broad peak calling)

Homer parameters: -len 15

Cell culture

C2C12 myoblasts, obtained from ATCC (CRL-1772), were grown in Dulbecco's modified Eagle medium (DMEM), supplemented with 1 g/L glucose and 20 % fetal calf serum. To induce myogenesis, cells were grown in DMEM, supplemented with 1 g/L glucose and 2 % horse serum for 4 days. Cells were treated with 1 µM Flutamide (S1908, Selleckchem), 1 µM 5α-Androstan-17β-ol-3-one (DHT, A8380, Sigma-Aldrich) or ethanol as vehicle, 24 h prior measurement of mitochondrial activity. Glucose uptake was measured with the Glucose Uptake Colorimetric Assay Kit (MAK083, Sigma-Aldrich). Cellular metabolic rates were determined using an XF96 analyzer (Seahorse Bioscience); as described (Duteil et al., 2016). Immediately before the measurement, cells were washed with unbuffered DMEM. Plates were placed into

the XF96 instrument for measurement of ECAR with the glycolysis stress kit (103017-100, Seahorse) (glucose, 10 mM; oligomycin, 1 mM; and 2-DG, 50 mM).

Quantification and statistical analysis

Data are represented as mean + SEM. Significance was calculated with GraphPad Prism (www.graphpad.com, GraphPad Software) using two-tailed Student's t test, one-way ANOVA or two-way ANOVA when appropriate.

Acknowledgements

We are grateful to Jean-Marc Bornert and Anastasia Bannwarth for providing excellent technical assistance. We thank the IGBMC animal house facility, cell culture and imaging facilities, the Mouse Clinical Institute (ICS, Illkirch, France) and the GenomEast platform, a member of the 'France Génomique' consortium (ANR-10-INBS-0009).

Author contributions: D.M. and D.D. generated the original hypothesis. K.G. and D.D. performed cell culture experiments. K.G., M.S., S.S-C, C.C., A.C., D.R. and D.D. performed molecular and histological characterizations of mice. N.M. performed ultrastructure analyses. A.-I.R. and D.D. performed bioinformatics analyses. K.G., M.S., J.Z., D.D. and D.M. took primary responsibility for data analysis and writing the manuscript. All authors edited the manuscript.

Funding

INSERM; CNRS; Unistra; IGBMC; Agence Nationale de la Recherche [ANR-10-BLAN-1108, AndroGluco; ANR-16-CE11-0009, AR2GR]; AFM strategic programme 15352; INSERM young researcher grant (to D.D.); ANR-10-LABX-0030-INRT, a French State fund managed by the ANR under the frame program Investissements d'Avenir [ANR-10-IDEX-0002-02]; A.-I.R. is an IGBMC International PhD Program fellow supported by LabEx INRT funds; D.R. was supported by ANR-16-CE11-0009, AR2GR; M.S. by AFM (15352); K.G. by the Association pour la Recherche à l'IGBMC (ARI), C.C. by AFM and ARI. Funding for open access charge: Agence Nationale de la Recherche.

Conflict of interest statement. None declared.

References

- Biancalana, V., Rendu, J., Chaussenot, A., Mecili, H., Bieth, E., Fradin, M., Mercier, S., Michaud, M., Nougues, M.C., Pasquier, L., et al. (2021). A recurrent RYR1 mutation associated with early-onset hypotonia and benign disease course. Acta Neuropathol Commun *9*, 155. 10.1186/s40478-021-01254-y.
- Bookout, A.L., Cummins, C.L., Mangelsdorf, D.J., Pesola, J.M., and Kramer, M.F. (2006). High-throughput real-time quantitative reverse transcription PCR. Curr Protoc Mol Biol *Chapter 15*, Unit 15 18. 10.1002/0471142727.mb1508s73.
- Chambon, C., Duteil, D., Vignaud, A., Ferry, A., Messaddeq, N., Malivindi, R., Kato, S., Chambon, P., and Metzger, D. (2010). Myocytic androgen receptor controls the strength but not the mass of limb muscles. Proc Natl Acad Sci U S A *107*, 14327-14332. 10.1073/pnas.1009536107.
- Chattopadhyay, M.K., and Tabor, H. (2013). Polyamines are critical for the induction of the glutamate decarboxylase-dependent acid resistance system in Escherichia coli. J Biol Chem *288*, 33559-33570. 10.1074/jbc.M113.510552.
- Copland, J.A., Pardini, A.W., Wood, T.G., Yin, D., Green, A., Bodenburg, Y.H., Urban, R.J., and Stuart, C.A. (2007). IGF-1 controls GLUT3 expression in muscle via the transcriptional factor Sp1. Biochim Biophys Acta *1769*, 631-640. 10.1016/j.bbaexp.2007.08.002.
- Davuluri, G., Allawy, A., Thapaliya, S., Rennison, J.H., Singh, D., Kumar, A., Sandlers, Y., Van Wagoner, D.R., Flask, C.A., Hoppel, C., et al. (2016). Hyperammonaemia-induced skeletal muscle mitochondrial dysfunction results in cataplerosis and oxidative stress. J Physiol *594*, 7341-7360. 10.1113/JP272796.
- De Gendt, K., and Verhoeven, G. (2012). Tissue- and cell-specific functions of the androgen receptor revealed through conditional knockout models in mice. Mol Cell Endocrinol *352*, 13-25. 10.1016/j.mce.2011.08.008.
- de Hoon, M.J., Imoto, S., Nolan, J., and Miyano, S. (2004). Open source clustering software. Bioinformatics *20*, 1453-1454. 10.1093/bioinformatics/bth078.
- Dubois, V., Laurent, M.R., Sinnesael, M., Cielen, N., Helsen, C., Clinckemalie, L., Spans, L., Gayan-Ramirez, G., Deldicque, L., Hespel, P., et al. (2014). A satellite cell-specific knockout of the androgen receptor reveals myostatin as a direct androgen target in skeletal muscle. FASEB J *28*, 2979-2994. 10.1096/fj.14-249748.
- Duteil, D., Chambon, C., Ali, F., Malivindi, R., Zoll, J., Kato, S., Geny, B., Chambon, P., and Metzger, D. (2010). The transcriptional coregulators TIF2 and SRC-1 regulate energy homeostasis by modulating mitochondrial respiration in skeletal muscles. Cell Metab *12*, 496-508. 10.1016/j.cmet.2010.09.016.
- Duteil, D., Tosic, M., Lausecker, F., Nenseth, H.Z., Muller, J.M., Urban, S., Willmann, D., Petroll, K., Messaddeq, N., Arrigoni, L., et al. (2016). Lsd1 Ablation Triggers Metabolic Reprogramming of Brown Adipose Tissue. Cell Rep *17*, 1008-1021. 10.1016/j.celrep.2016.09.053.
- Fan, W., Yanase, T., Nomura, M., Okabe, T., Goto, K., Sato, T., Kawano, H., Kato, S., and Nawata, H. (2005). Androgen receptor null male mice develop late-onset obesity caused by decreased energy expenditure and lipolytic activity but show normal insulin sensitivity with high adiponectin secretion. Diabetes *54*, 1000-1008. 10.2337/diabetes.54.4.1000.
- Fernando, S.M., Rao, P., Niel, L., Chatterjee, D., Stagljar, M., and Monks, D.A. (2010). Myocyte androgen receptors increase metabolic rate and improve body composition by reducing fat mass. Endocrinology *151*, 3125-3132. 10.1210/en.2010-0018.

- Ferry, A., Schuh, M., Parlakian, A., Mgrditchian, T., Valnaud, N., Joanne, P., Butler-Browne, G., Agbulut, O., and Metzger, D. (2014). Myofiber androgen receptor promotes maximal mechanical overload-induced muscle hypertrophy and fiber type transition in male mice. Endocrinology *155*, 4739-4748. 10.1210/en.2014-1195.
- Figueiredo, P.A., Powers, S.K., Ferreira, R.M., Amado, F., Appell, H.J., and Duarte, J.A. (2009). Impact of lifelong sedentary behavior on mitochondrial function of mice skeletal muscle. J Gerontol A Biol Sci Med Sci *64*, 927-939. 10.1093/gerona/glp066.
- Fraysse, B., Vignaud, A., Fane, B., Schuh, M., Butler-Browne, G., Metzger, D., and Ferry, A. (2014). Acute effect of androgens on maximal force-generating capacity and electrically evoked calcium transient in mouse skeletal muscles. Steroids *87*, 6-11. 10.1016/j.steroids.2014.05.005.
- Giorgetti, E., Yu, Z., Chua, J.P., Shimamura, R., Zhao, L., Zhu, F., Venneti, S., Pennuto, M., Guan, Y., Hung, G., and Lieberman, A.P. (2016). Rescue of Metabolic Alterations in AR113Q Skeletal Muscle by Peripheral Androgen Receptor Gene Silencing. Cell Rep *17*, 125-136. 10.1016/j.celrep.2016.08.084.
- Goto, M., Miyahara, I., Hirotsu, K., Conway, M., Yennawar, N., Islam, M.M., and Hutson, S.M. (2005). Structural determinants for branched-chain aminotransferase isozyme-specific inhibition by the anticonvulsant drug gabapentin. J Biol Chem *280*, 37246-37256. 10.1074/jbc.M506486200.
- Haizlip, K.M., Harrison, B.C., and Leinwand, L.A. (2015). Sex-based differences in skeletal muscle kinetics and fiber-type composition. Physiology (Bethesda) *30*, 30-39. 10.1152/physiol.00024.2014.
- Handschin, C., Chin, S., Li, P., Liu, F., Maratos-Flier, E., Lebrasseur, N.K., Yan, Z., and Spiegelman, B.M. (2007). Skeletal muscle fiber-type switching, exercise intolerance, and myopathy in PGC-1alpha muscle-specific knock-out animals. J Biol Chem *282*, 30014-30021. 10.1074/jbc.M704817200.
- Hawley, J.A., Lundby, C., Cotter, J.D., and Burke, L.M. (2018). Maximizing Cellular Adaptation to Endurance Exercise in Skeletal Muscle. Cell Metab *27*, 962-976. 10.1016/j.cmet.2018.04.014.
- Heinz, S., Benner, C., Spann, N., Bertolino, E., Lin, Y.C., Laslo, P., Cheng, J.X., Murre, C., Singh, H., and Glass, C.K. (2010). Simple combinations of lineage-determining transcription factors prime cis-regulatory elements required for macrophage and B cell identities. Mol Cell *38*, 576-589. 10.1016/j.molcel.2010.05.004.
- Hoehn, K.L., Turner, N., Swarbrick, M.M., Wilks, D., Preston, E., Phua, Y., Joshi, H., Furler, S.M., Larance, M., Hegarty, B.D., et al. (2010). Acute or chronic upregulation of mitochondrial fatty acid oxidation has no net effect on whole-body energy expenditure or adiposity. Cell Metab *11*, 70-76. 10.1016/j.cmet.2009.11.008.
- Joshi, S., Ueberschlag-Pitiot, V., Metzger, D., and Davidson, I. (2017). Improved Protocol for Chromatin Immunoprecipitation from Mouse Skeletal Muscle. J Vis Exp. 10.3791/56504.
- Kamei, Y., Hatazawa, Y., Uchitomi, R., Yoshimura, R., and Miura, S. (2020). Regulation of Skeletal Muscle Function by Amino Acids. Nutrients *12*. 10.3390/nu12010261.
- Kelly, D.M., and Jones, T.H. (2013). Testosterone: a metabolic hormone in health and disease. J Endocrinol *217*, R25-45. 10.1530/JOE-12-0455.
- Kim, J., Park, J., Kim, N., Park, H.Y., and Lim, K. (2019). Inhibition of androgen receptor can decrease fat metabolism by decreasing carnitine palmitoyltransferase I levels in skeletal muscles of trained mice. Nutr Metab (Lond) *16*, 82. 10.1186/s12986-019-0406-z.

- Kuo, T., Harris, C.A., and Wang, J.C. (2013). Metabolic functions of glucocorticoid receptor in skeletal muscle. Mol Cell Endocrinol *380*, 79-88. 10.1016/j.mce.2013.03.003.
- Langmead, B., and Salzberg, S.L. (2012). Fast gapped-read alignment with Bowtie 2. Nat Methods *9*, 357-359. 10.1038/nmeth.1923.
- Lin, H.Y., Xu, Q., Yeh, S., Wang, R.S., Sparks, J.D., and Chang, C. (2005). Insulin and leptin resistance with hyperleptinemia in mice lacking androgen receptor. Diabetes *54*, 1717-1725. 10.2337/diabetes.54.6.1717.
- Liu, Y., Dong, W., Shao, J., Wang, Y., Zhou, M., and Sun, H. (2017). Branched-Chain Amino Acid Negatively Regulates KLF15 Expression via PI3K-AKT Pathway. Front Physiol *8*, 853. 10.3389/fphys.2017.00853.
- Livak, K.J., and Schmittgen, T.D. (2001). Analysis of relative gene expression data using real-time quantitative PCR and the 2(-Delta Delta C(T)) Method. Methods *25*, 402-408. 10.1006/meth.2001.1262.
- Love, M.I., Huber, W., and Anders, S. (2014). Moderated estimation of fold change and dispersion for RNA-seq data with DESeq2. Genome Biol *15*, 550. 10.1186/s13059-014-0550-8.
- Lubahn, D.B., Joseph, D.R., Sullivan, P.M., Willard, H.F., French, F.S., and Wilson, E.M. (1988). Cloning of human androgen receptor complementary DNA and localization to the X chromosome. Science *240*, 327-330. 10.1126/science.3353727.
- MacLean, H.E., Chiu, W.S., Notini, A.J., Axell, A.M., Davey, R.A., McManus, J.F., Ma, C., Plant, D.R., Lynch, G.S., and Zajac, J.D. (2008). Impaired skeletal muscle development and function in male, but not female, genomic androgen receptor knockout mice. FASEB J *22*, 2676-2689. 10.1096/fj.08-105726.
- Mann, G., Mora, S., Madu, G., and Adegoke, O.A.J. (2021). Branched-chain Amino Acids: Catabolism in Skeletal Muscle and Implications for Muscle and Whole-body Metabolism. Front Physiol *12*, 702826. 10.3389/fphys.2021.702826.
- Moon, J.S., Jin, W.J., Kwak, J.H., Kim, H.J., Yun, M.J., Kim, J.W., Park, S.W., and Kim, K.S. (2011). Androgen stimulates glycolysis for de novo lipid synthesis by increasing the activities of hexokinase 2 and 6-phosphofructo-2-kinase/fructose-2,6-bisphosphatase 2 in prostate cancer cells. Biochem J *433*, 225-233. 10.1042/BJ20101104.
- Muraleedharan, V., and Jones, T.H. (2010). Testosterone and the metabolic syndrome. Ther Adv Endocrinol Metab *1*, 207-223. 10.1177/2042018810390258.
- Nicolaisen, T.S., Klein, A.B., Dmytriyeva, O., Lund, J., Ingerslev, L.R., Fritzen, A.M., Carl, C.S., Lundsgaard, A.M., Frost, M., Ma, T., et al. (2020). Thyroid hormone receptor alpha in skeletal muscle is essential for T3-mediated increase in energy expenditure. FASEB J *34*, 15480-15491. 10.1096/fj.202001258RR.
- Oliveros, J.C. (2007-2015). Venny. An interactive tool for comparing lists with Venn's diagrams. .
- Ophoff, J., Callewaert, F., Venken, K., De Gendt, K., Ohlsson, C., Gayan-Ramirez, G., Decramer, M., Boonen, S., Bouillon, R., Verhoeven, G., and Vanderschueren, D. (2009a). Physical activity in the androgen receptor knockout mouse: evidence for reversal of androgen deficiency on cancellous bone. Biochem Biophys Res Commun *378*, 139-144. 10.1016/j.bbrc.2008.11.016.
- Ophoff, J., Van Proeyen, K., Callewaert, F., De Gendt, K., De Bock, K., Vanden Bosch, A., Verhoeven, G., Hespel, P., and Vanderschueren, D. (2009b). Androgen signaling in myocytes contributes to the maintenance of muscle mass and fiber type regulation but

not to muscle strength or fatigue. Endocrinology *150*, 3558-3566. 10.1210/en.2008-1509.

- Pitteloud, N., Mootha, V.K., Dwyer, A.A., Hardin, M., Lee, H., Eriksson, K.F., Tripathy, D., Yialamas, M., Groop, L., Elahi, D., and Hayes, F.J. (2005). Relationship between testosterone levels, insulin sensitivity, and mitochondrial function in men. Diabetes Care *28*, 1636-1642. 10.2337/diacare.28.7.1636.
- Porter, C., Hurren, N.M., Cotter, M.V., Bhattarai, N., Reidy, P.T., Dillon, E.L., Durham, W.J., Tuvdendorj, D., Sheffield-Moore, M., Volpi, E., et al. (2015). Mitochondrial respiratory capacity and coupling control decline with age in human skeletal muscle. Am J Physiol Endocrinol Metab *309*, E224-232. 10.1152/ajpendo.00125.2015.
- Pradat, P.F., Bernard, E., Corcia, P., Couratier, P., Jublanc, C., Querin, G., Morelot Panzini, C., Salachas, F., Vial, C., Wahbi, K., et al. (2020). The French national protocol for Kennedy's disease (SBMA): consensus diagnostic and management recommendations. Orphanet J Rare Dis *15*, 90. 10.1186/s13023-020-01366-z.
- Quinlan, A.R., and Hall, I.M. (2010). BEDTools: a flexible suite of utilities for comparing genomic features. Bioinformatics *26*, 841-842. 10.1093/bioinformatics/btq033.
- Rana, K., Chiu, M.W., Russell, P.K., Skinner, J.P., Lee, N.K., Fam, B.C., Zajac, J.D., and MacLean, H.E. (2016). Muscle-specific androgen receptor deletion shows limited actions in myoblasts but not in myofibers in different muscles in vivo. J Mol Endocrinol *57*, 125-138. 10.1530/JME-15-0320.
- Robinson, M.D., McCarthy, D.J., and Smyth, G.K. (2010). edgeR: a Bioconductor package for differential expression analysis of digital gene expression data. Bioinformatics *26*, 139-140. 10.1093/bioinformatics/btp616.
- Rovito, D., Rerra, A.I., Ueberschlag-Pitiot, V., Joshi, S., Karasu, N., Dacleu-Siewe, V., Rayana, K.B., Ghaibour, K., Parisotto, M., Ferry, A., et al. (2021). Myod1 and GR coordinate myofiber-specific transcriptional enhancers. Nucleic Acids Res *49*, 4472-4492. 10.1093/nar/gkab226.
- Saeed, A.I., Bhagabati, N.K., Braisted, J.C., Liang, W., Sharov, V., Howe, E.A., Li, J., Thiagarajan, M., White, J.A., and Quackenbush, J. (2006). TM4 microarray software suite. Methods Enzymol *411*, 134-193. 10.1016/S0076-6879(06)11009-5.
- Sakakibara, I., Yanagihara, Y., Himori, K., Yamada, T., Sakai, H., Sawada, Y., Takahashi, H., Saeki, N., Hirakawa, H., Yokoyama, A., et al. (2021). Myofiber androgen receptor increases muscle strength mediated by a skeletal muscle splicing variant of Mylk4. iScience *24*, 102303. 10.1016/j.isci.2021.102303.
- Sato, K., Iemitsu, M., Aizawa, K., and Ajisaka, R. (2008). Testosterone and DHEA activate the glucose metabolism-related signaling pathway in skeletal muscle. Am J Physiol Endocrinol Metab *294*, E961-968. 10.1152/ajpendo.00678.2007.
- Schiaffino, S. (2010). Fibre types in skeletal muscle: a personal account. Acta Physiol (Oxf) *199*, 451-463. 10.1111/j.1748-1716.2010.02130.x.
- Schneider, C.A., Rasband, W.S., and Eliceiri, K.W. (2012). NIH Image to ImageJ: 25 years of image analysis. Nat Methods *9*, 671-675.
- Schuler, M., Ali, F., Chambon, C., Duteil, D., Bornert, J.M., Tardivel, A., Desvergne, B., Wahli, W., Chambon, P., and Metzger, D. (2006). PGC1alpha expression is controlled in skeletal muscles by PPARbeta, whose ablation results in fiber-type switching, obesity, and type 2 diabetes. Cell Metab *4*, 407-414. 10.1016/j.cmet.2006.10.003.

- Schuler, M., Ali, F., Metzger, E., Chambon, P., and Metzger, D. (2005). Temporally controlled targeted somatic mutagenesis in skeletal muscles of the mouse. Genesis *41*, 165-170. 10.1002/gene.20107.
- Stuart, C.A., Wen, G., Peng, B.H., Popov, V.L., Hudnall, S.D., and Campbell, G.A. (2000). GLUT-3 expression in human skeletal muscle. Am J Physiol Endocrinol Metab *279*, E855-861. 10.1152/ajpendo.2000.279.4.E855.
- Thorvaldsdottir, H., Robinson, J.T., and Mesirov, J.P. (2013). Integrative Genomics Viewer (IGV): high-performance genomics data visualization and exploration. Brief Bioinform *14*, 178-192. 10.1093/bib/bbs017.
- Troncoso, M.F., Pavez, M., Wilson, C., Lagos, D., Duran, J., Ramos, S., Barrientos, G., Silva, P., Llanos, P., Basualto-Alarcon, C., et al. (2021). Testosterone activates glucose metabolism through AMPK and androgen signaling in cardiomyocyte hypertrophy. Biol Res *54*, 3. 10.1186/s40659-021-00328-4.
- Ueberschlag-Pitiot, V., Stantzou, A., Messeant, J., Lemaitre, M., Owens, D.J., Noirez, P., Roy, P., Agbulut, O., Metzger, D., and Ferry, A. (2017). Gonad-related factors promote muscle performance gain during postnatal development in male and female mice. Am J Physiol Endocrinol Metab *313*, E12-E25. 10.1152/ajpendo.00446.2016.
- Vaz, C.V., Marques, R., Alves, M.G., Oliveira, P.F., Cavaco, J.E., Maia, C.J., and Socorro, S. (2016). Androgens enhance the glycolytic metabolism and lactate export in prostate cancer cells by modulating the expression of GLUT1, GLUT3, PFK, LDH and MCT4 genes. J Cancer Res Clin Oncol *142*, 5-16. 10.1007/s00432-015-1992-4.
- Wakabayashi, T. (2002). Megamitochondria formation - physiology and pathology. J Cell Mol Med *6*, 497-538. 10.1111/j.1582-4934.2002.tb00452.x.
- Wang, J., Duncan, D., Shi, Z., and Zhang, B. (2013). WEB-based GEne SeT AnaLysis Toolkit (WebGestalt): update 2013. Nucleic Acids Res *41*, W77-83. 10.1093/nar/gkt439.
- Xu, M., Kitaura, Y., Ishikawa, T., Kadota, Y., Terai, C., Shindo, D., Morioka, T., Ota, M., Morishita, Y., Ishihara, K., and Shimomura, Y. (2017). Endurance performance and energy metabolism during exercise in mice with a muscle-specific defect in the control of branched-chain amino acid catabolism. PLoS One *12*, e0180989. 10.1371/journal.pone.0180989.
- Zhang, Y., Liu, T., Meyer, C.A., Eeckhoute, J., Johnson, D.S., Bernstein, B.E., Nusbaum, C., Myers, R.M., Brown, M., Li, W., and Liu, X.S. (2008). Model-based analysis of ChIP-Seq (MACS). Genome Biol *9*, R137. 10.1186/gb-2008-9-9-r137.

Figure S1.

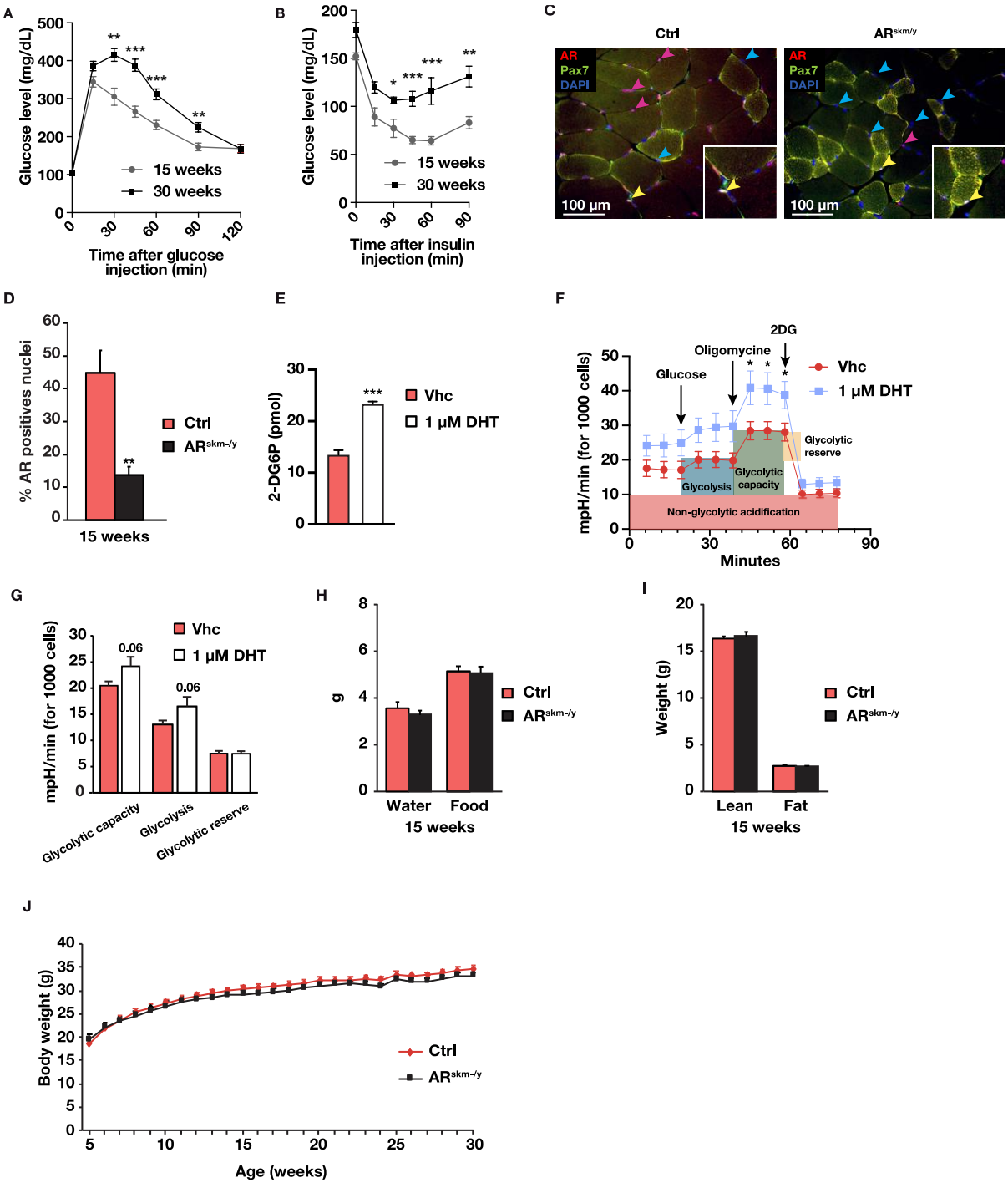

Figure S1: Role of AR in glucose metabolism *A-B. Glucose tolerance test (IPGTT) (A) and insulin sensitive test (IPIST) (B) of C57/Bl6 mice at 15 and 30 weeks of age. C-D. Immunofluorescent detection of the androgen receptor (AR, red) and PAX7 (green) (C) and corresponding percentage of AR-positive relative to total DAPI-positive nuclei (D) in*

*gastrocnemius muscles of 15-week-old control (Ctrl) and $AR^{skm-/y}$ mice. Red arrowheads: AR-positive nuclei, blue arrowheads: AR-negative nuclei, yellow arrowheads: PAX7- and AR-positive nuclei. Scale bar: 100 µm. E-G. Glucose uptake (E), representative extracellular acidification rate (ECAR) (F) and deduced maximal glycolytic capacity, glycolysis and glycolytic reserve (G) of C2C12 myotubes treated with 1 µM of 5α-Androstan-17β-ol-3-one (DHT) or vehicle (Vhc). H-J. Water and food consumption (H), total body lean and fat content (I) and body mass (J) of Ctrl and $AR^{skm-/y}$ mice at indicated ages. A, B: n=14, C-D: n= 4 mice, 5 fields / mouse, E: n=3, F-H: n=6, H-J: n=10 mice. A, B, F, J: mean ±SEM; D, E, G-I: mean + SEM. *, p<0.05; **, p<0.01; ***, p < 0.001.*

Figure S2.

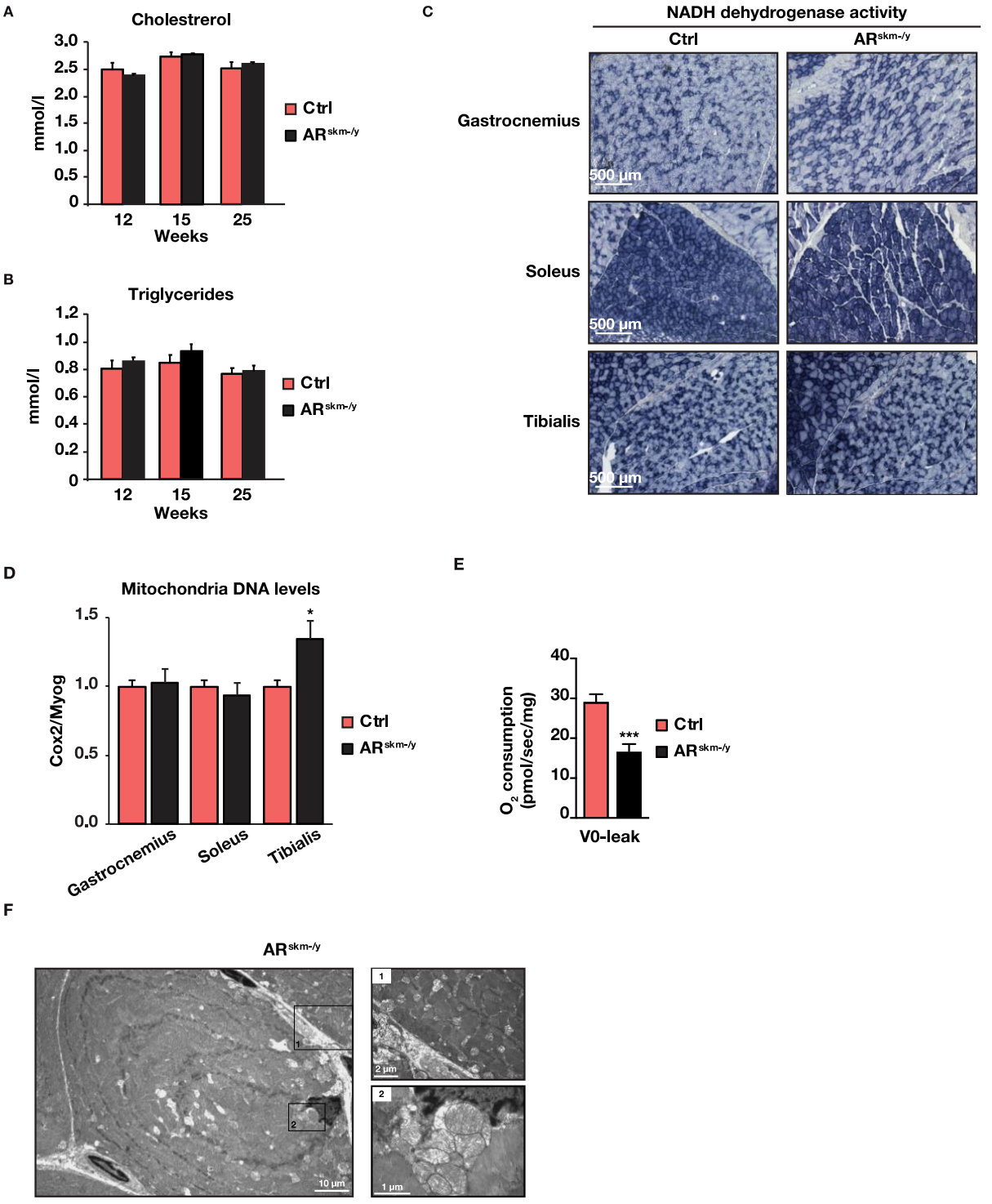

Figure S2: Role of AR in oxidative metabolism *A-B. Blood cholesterol (A) and triglycerides (B) content in control (Ctrl) and AR$^{skm-/y}$ mice at indicated ages. C. Histochemical staining of NADH dehydrogenase activity in gastrocnemius, soleus and tibialis muscles of 15-week-old Ctrl and AR$^{skm-/y}$ mice. The scale bar represents 500 µm. D. Quantification of mitochondrial*

content in gastrocnemius, soleus and tibialis muscles of 15-week-old Ctrl and $AR^{skm-/y}$ mice by qPCR amplification of the Cox2 mitochondrial gene and the Myog nuclear gene. E. Oxygen consumption in saponin-skinned gastrocnemius fibers of 15-week-old Ctrl and $AR^{skm-/y}$ mice in the absence of ADP (V0-leak). F. Ultrastructure of quadriceps muscles from 15-week-old Ctrl and $AR^{skm-/y}$ mice. Scale bar: 10 µm, inlets: 1 and 2 µm.

Figure S3.

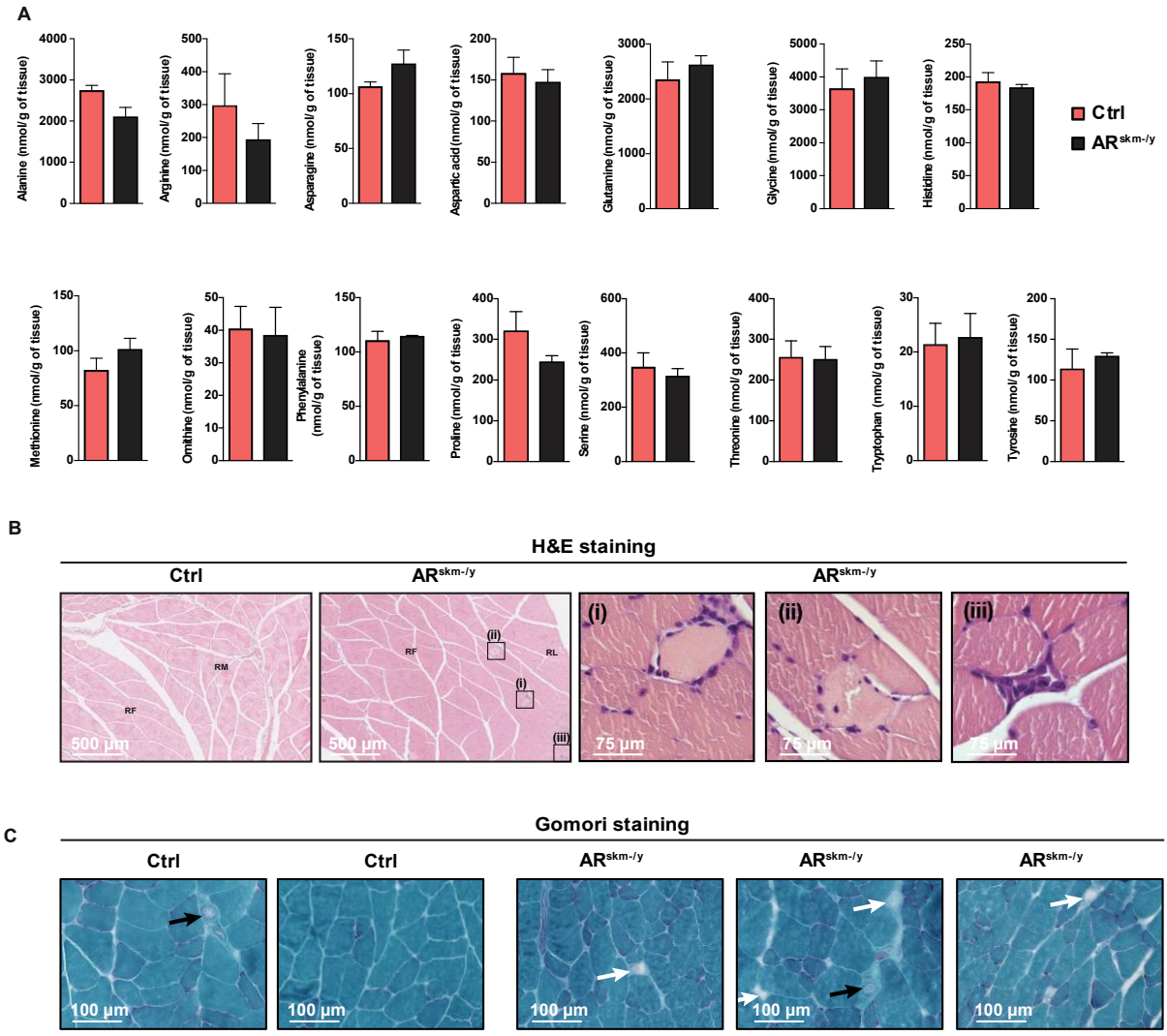

Figure S3: Role of AR in amino acid metabolism *A. Levels of indicated amino acids in gastrocnemius muscles of 15-week-old control (Ctrl) and AR$^{skm-/y}$ mice. B-C. Hematoxylin and eosin (H&E, B), and Gomori's trichrome staining (C) of quadriceps and gastrocnemius muscles of 15-week-old Ctrl and AR$^{skm-/y}$ mice, respectively. B: (i) metabolic necrosis characterized by fibers with a pale cytoplasm, (ii) sarcolemmal membrane disruptions, and (iii) phagocytic necrosis where macrophages have degraded necrotic myofibers. C: Black arrow points to blood vessels and white arrow highlights necrotic fiber. Scale bars: B: 500 µm, inlet: 75 µm; C: 100 µm. A: n=3, B, C: n=6.*

Figure S4.

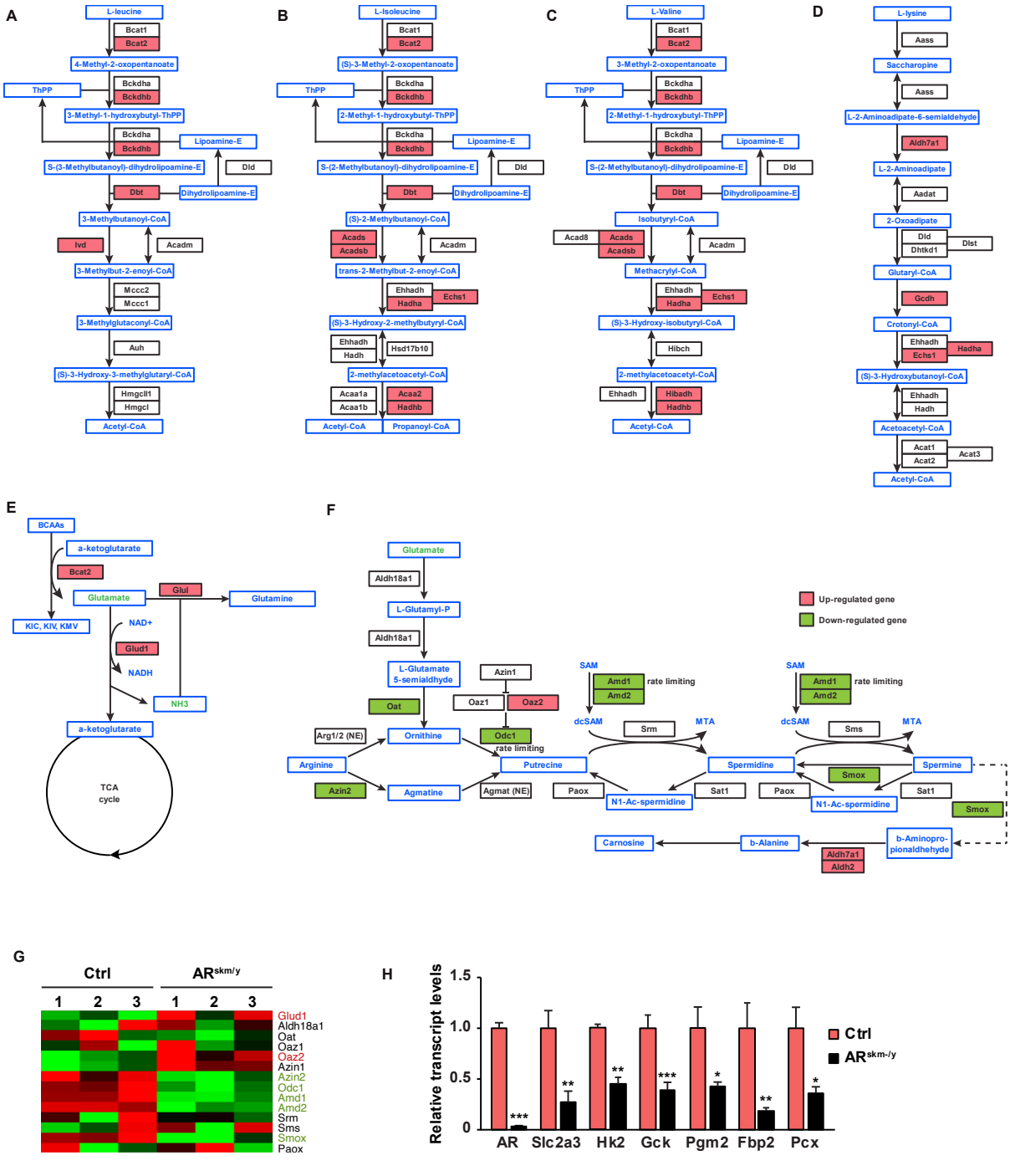
A
L-leucine
Bcat1
Bcat2
4-Methyl-2-oxopentanoate
ThPP
Bckdha
Bckdhb
3-Methyl-1-hydroxybutyl-ThPP
Lipoamine-E
S-(3-Methylbutanoyl)-dihydrolipoamine-E
Dld
Dbt
Dihydrolipoamine-E
3-Methylbutanoyl-CoA
Ivd
Acadm
3-Methylbut-2-enoyl-CoA
Mccc2
Mccc1
3-Methylglutaconyl-CoA
Auh
(S)-3-Hydroxy-3-methylglutaryl-CoA
Hmgcll1
Hmgcl
Acetyl-CoA
B
L-Isoleucine
(S)-3-Methyl-2-oxopentanoate
2-Methyl-1-hydroxybutyl-ThPP
S-(2-Methylbutanoyl)-dihydrolipoamine-E
(S)-2-Methylbutanoyl-CoA
Acads
Acadsb
trans-2-Methylbut-2-enoyl-CoA
Ehhadh
Hadha
Echs1
(S)-3-Hydroxy-2-methylbutyryl-CoA
Hsd17b10
2-methylacetoacetyl-CoA
Acaa1a
Acaa1b
Acaa2
Hadhb
Propanoyl-CoA
C
L-Valine
3-Methyl-2-oxopentanoate
2-Methyl-1-hydroxybutyl-ThPP
S-(2-Methylbutanoyl)-dihydrolipoamine-E
Isobutyryl-CoA
Acad8
Methacrylyl-CoA
(S)-3-Hydroxy-isobutyryl-CoA
Hibch
2-methylacetoacetyl-CoA
Hibadh
D
L-lysine
Aass
Saccharopine
L-2-Aminoadipate-6-semialdehyde
Aldh7a1
L-2-Aminoadipate
Aadat
2-Oxoadipate
Dld
Dhtkd1
Dlst
Glutaryl-CoA
Gcdh
Crotonyl-CoA
(S)-3-Hydroxybutanoyl-CoA
Acetoacetyl-CoA
Acat1
Acat2
Acat3
E
BCAAs
a-ketoglutarate
Bcat2
Glutamate
Glul
Glutamine
KIC, KIV, KMV
NAD+
Glud1
NADH
NH3
TCA cycle
F
Glutamate
Aldh18a1
L-Glutamyl-P
L-Glutamate 5-semialdhyde
Azin1
Oaz1
Oaz2
Oat
Arg1/2 (NE)
Ornithine
Odc1
rate limiting
Arginine
Azin2
Agmatine
Agmat (NE)
Putrecine
SAM
Amd1
Amd2
dcSAM
Srm
MTA
Paox
N1-Ac-spermidine
Spermidine
Sat1
Sms
Spermine
Smox
Carnosine
b-Alanine
b-Aminopro-pionaldhehyde
Aldh7a1
Aldh2
Up-regulated gene
Down-regulated gene
G
Ctrl
AR skm/y
1 2 3 1 2 3
Glud1
Aldh18a1
Oat
Oaz1
Oaz2
Azin1
Azin2
Odc1
Amd1
Amd2
Srm
Sms
Smox
Paox
H
Relative transcript levels
1.5
1.0
0.5
0
Ctrl
AR skm-/y
AR
Slc2a3
Hk2
Gck
Pgm2
Fbp2
Pcx

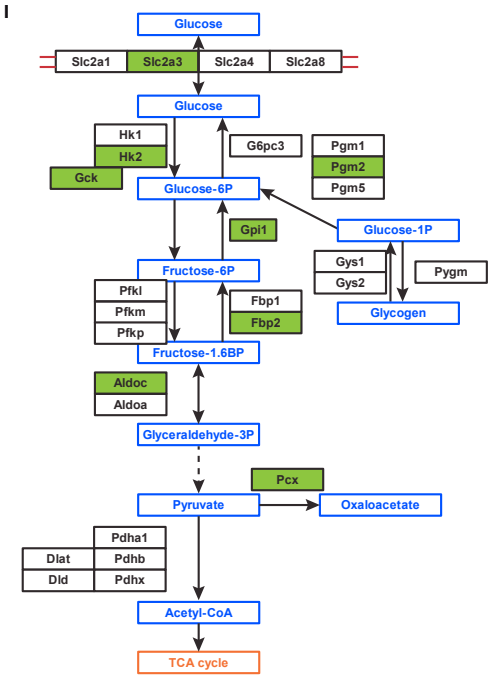
I
Glucose
Slc2a1
Slc2a3
Slc2a4
Slc2a8
Glucose
Hk1
Hk2
Gck
G6pc3
Pgm1
Pgm2
Pgm5
Glucose-6P
Gpi1
Glucose-1P
Gys1
Gys2
Pygm
Glycogen
Fructose-6P
Pfkl
Pfkm
Pfkp
Fbp1
Fbp2
Fructose-1.6BP
Aldoc
Aldoa
Glyceraldehyde-3P
Pcx
Pyruvate
Oxaloacetate
Pdha1
Dlat
Pdhb
Dld
Pdhx
Acetyl-CoA
TCA cycle

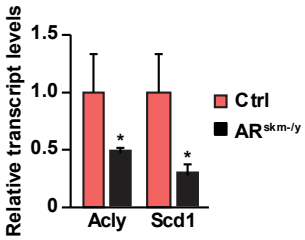
J
Relative transcript levels
1.5
1.0
0.5
0
Ctrl
AR skm-/y
*
*
Acly
Scd1

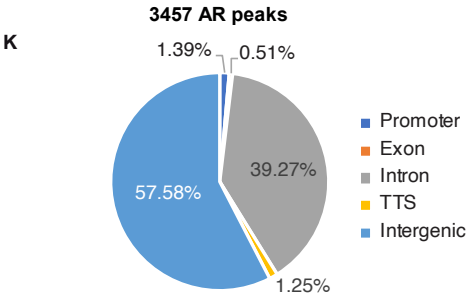
K
3457 AR peaks
1.39%
0.51%
39.27%
57.58%
1.25%
Promoter
Exon
Intron
TTS
Intergenic

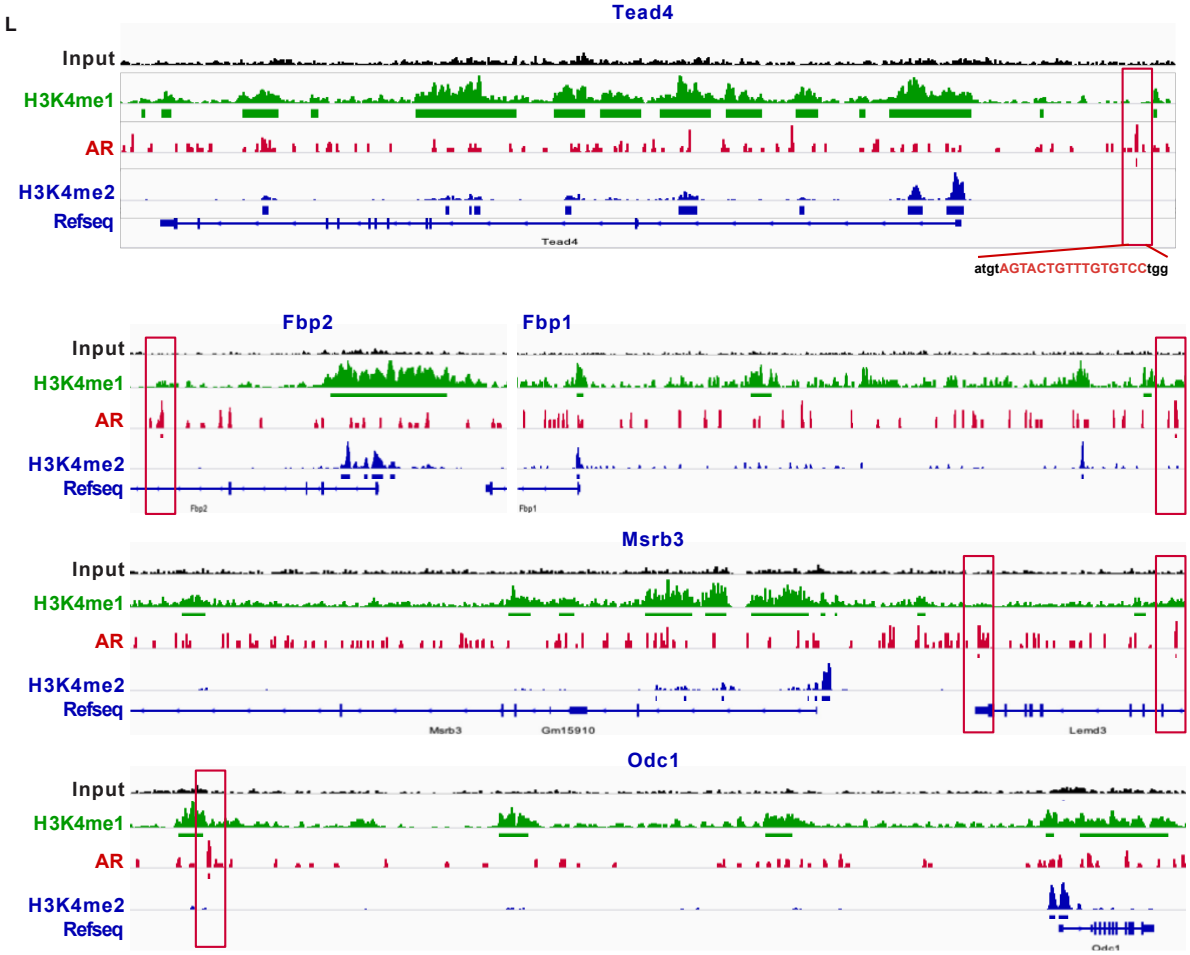
L
Tead4
Input
H3K4me1
AR
H3K4me2
Refseq
Tead4
atgtAGTACTGTTTGTGTCCtgg
Fbp2
Fbp1
Input
H3K4me1
AR
H3K4me2
Refseq
Fbp2
Fbp1
Msrb3
Input
H3K4me1
AR
H3K4me2
Refseq
Msrb3
Gm15910
Lemd3
Odc1
Input
H3K4me1
AR
H3K4me2
Refseq

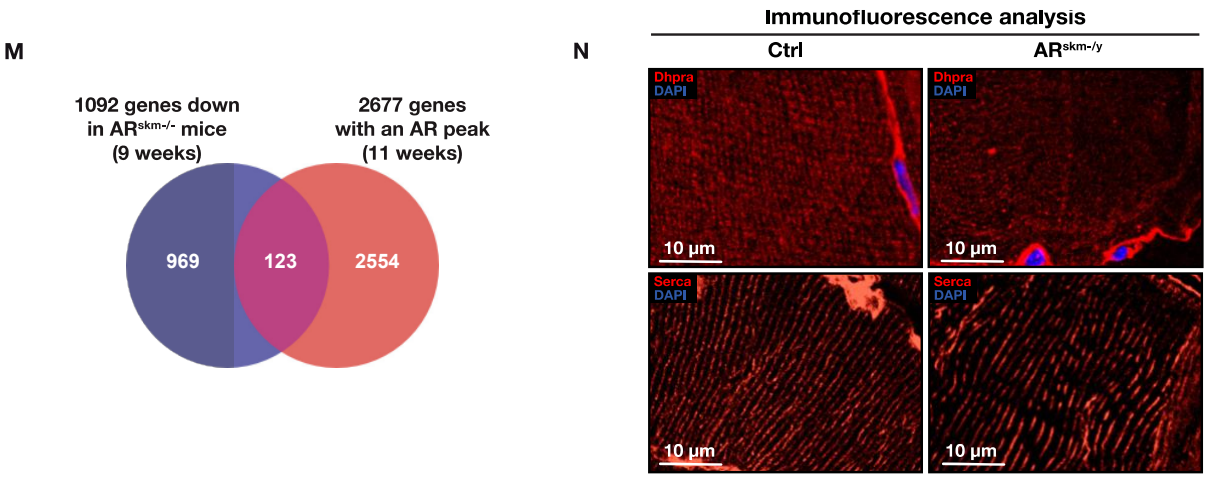

Figure S4: Analysis of AR functional targets in skeletal muscle *A-F. Schematic representation of the genes involved in L-leucine (A), L-isoleucine (B) L-valine (C), and L-lysine (D) degradation, in glutamate transamination (E), and in polyamine biosynthesis (F). Genes up- and down-regulated upon AR ablation are shown in red and green, respectively. G. Heatmap depicting the mean centered normalized expression of genes involved in polyamine metabolism obtained by RNA-seq analysis performed in gastrocnemius muscle of 9-week-old Ctrl and AR$^{skm-/y}$ mice. Genes significantly down- and up-regulated in AR$^{skm-/y}$ mice are marked in green and red, respectively. H. Relative transcript levels of genes encoding glycolytic enzymes in gastrocnemius muscles of 15-week-old control and AR$^{skm-/y}$ mice. I. Schematic representation of glycolysis. Genes down-regulated upon AR ablation are marked in green. J. Relative transcript levels of genes encoding enzymes involved in fatty acid metabolism in gastrocnemius muscles of 15-week-old control and AR$^{skm-/y}$ mice. K. Pie chart depicting the peak distribution of AR in the genome of skeletal muscles. L. Localization of AR, H3K4me1 and H3K4me2 at the indicated loci. M. Overlap between genes with AR peaks at 11 weeks and those down-regulated in 9-week-old AR$^{skm-/y}$ mice. N. DHPRA and SERCA1 immunofluorescent detection of 15-week-old control and AR$^{skm-/y}$ mice. Nuclei are stained with DAPI. Scale bar: 10 µm. H, J: n=6 mice; N: n=3 mice, 10 fields / mouse Mean + SEM. *, p<0.05; **, p<0.01; ***, p < 0.001.*

Table S1: Gene centric analysis of AR cistrome using the coordinates of genes down-regulated in $AR^{skm-/y}$ mice. See **TableS1.xlsx**

Name	Forward primer	Reverse primer
18S	5'-TCGTCTTCGAAACTCCGACT-3'	5'-CGCGGTTCTATTTTGTTGGT-3'
36b4	5'-AGATTCGGGATATGCTGTTGG-3'	5'-AAAGCCTGGAAGAAGGAGGTC-3'
Gapdh	5'-AGCTCACTGGCATGGCCTTC-3'	5'-ACGCCTGCTTCACCACCTTC-3'
Hprt	5'-GTTGGATACAGGCCAGACTTTGTTG-3'	5'-GATTCAACTTGCGCTCATCTTAGGC-3'
Ar	5'-CTGCCTCCGAAGTGTGGTAT-3'	5'-GCCAGAAGCTTCATCTCCAC-3'
Cd36	5'-TCTGACATTTGCAGGTCTATCT-3'	5'-ATCTCTACCATGCCAAGGAGCT-3'
Lpl	5'-GGATGGACGGTAAGAAGTGATTC-3'	5'-ATCCAAGGGTAGCAGACAGGT-3'
Pnpla2	5'-CAACGCCACTCACATCTACG-3'	5'-ACCAGGTTGAAGGAGGGATG-3'
Acox1	5'-AAGAATGTCGGATGGCTTGC-3'	5'-CGGCAGGTCATTCAAGTACG-3'
Acads	5'-TCGCTGGTCCCTTCGTAGAT-3'	5'-TGGGATGGGCTTCAAAATAG-3'
Acadl	5'-TTGGTGGGGACTTGCTCTCA-3'	5'-CTGTTCTTTTGTGCCGTAAT-3'
Echs1	5'-TGCTCACTGGTGGGGATAAG-3'	5'-AGGAGGATTTCTGGCTGTCC-3'
Bcat2	5'-TGCTGATGGTGGAGTGGAAT-3'	5'-ATCCTGTCCATGTTGAGCCA-3'
Hadhb	5'-TTTGGTACAGTTATTCAGGA-3'	5'-CAGCCACGACAGCATCACAC-3'
Glud1	5'-AATGTGGGCCTGCACTCTAT-3'	5'-ATGTCACAGTCAGCCTCCAA-3'
Aldh18a1	5'-CGTGGAGATGAAAACCGACC-3'	5'-GGCCCACTCTAGACTTGGTT-3'
Oat	5'-ATGTAAGCTCGCTCGTCGTT-3'	5'-GAAGGCAGCAACATTTGGAT-3'
Odc1	5'-CATCCAAAGGCAAAGTTGGA-3'	5'-CATGGAAGCTCACACCAATG-3'
Smox	5'-TCTGCACAGAGATGCTTCGACAGT-3'	5'-TTGAGCCCACCTGTGTGTAGGAAT-3'
Amd1	5'-TCATGAAGCCTTCTCACCAAGGGT-3'	5'-TCGGCTCTCTGGGAAATCCAAAGT-3'
Msrb3	5'-AGGCCATCGAGTTCACAGAT-3'	5'-CTCTCTTTGATGCCGCTTCC-3'
Slc2a3	5'-TGGTCCTTATGTGTGGCCAT-3'	5'-GCATTTCAACAGACTCCGCT-3'
Hk2	5'-TACCACACACCCTACAGCAG-3'	5'-CTCGGGAATGGCGTAGATCT-3'
Gck	5'-AGAATGTGGAGCTGGTGGAA-3'	5'-CAGCTCGCCCATGTACTTTC-3'
Pgm2	5'-CCAAAATCTTGCGGGCCATA-3'	5'-CCAGAACAAAGGGACAGCAC-3'
Fbp2	5'-GCTCAACTCGATGCTGACTG-3'	5'-AGCATGTTGATGACCAGGGA-3'
Pcx	5'-TGGCCAACAGAGGTGAGATT-3'	5'-TCCTTGGCCACCTTGATGAT-3'
Acly	5'-GCCAAGACCATCCTCTCACT-3'	5'-GGTCTTCCCAACTTCTCCCA-3'
Scd1	5'-ATGTCTGACCTGAAAGCCGA-3'	5'-GAAGGTGCTAACGAACAGGC-3'
Myog	5'-CCTTAAAGCAGAGAGCATCC-3'	5'-GGAATTCGAGGCATATTATGA-3'
Cox2	5'-CAGTCCCCTCCCTAGGACTT-3'	5'-TCAGAGCATTGGCCATAGAA-3'

Table S2. Primers used for qPCR analysis.

Chapter II

Objectives and contribution to this part

Skeletal muscles have a remarkable capacity of regeneration upon injury which relies of the capacity of its stem cell population to proliferate and differentiate. In this part, we investigated the role of the androgen receptor in muscle stem cells homeostasis and function in physiological conditions and after injury.

To identify AR role in satellite cells (SatC), we generated a mouse model in which AR is selectively ablated in SatC (hereafter $AR^{Sat-/Y}$). After AR knock-out, I performed histological analysis on muscle sections. My analysis showed SatC niche defects in the absence of AR. To decipher the target genes of AR in SatC, I optimized a protocol to efficiently dissociate skeletal muscles of adult mice to isolate SatC via fluorescent activated cell sorting. Following isolation, I took advantage of a new technique named Cut&Run developed to analyze a limited number of cells. After several trials, I was able to perform the experiment using antibodies directed against AR and H3K4me2 histone mark on SatC isolated from non-injured wild-type tibialis of 8-week-old male mice. Bio-informatic analysis revealed that AR is recruited on main genes involved in SatC quiescence, including *Pax7*, *Myf5*, *Klf7* and *Itgb1*. Moreover, RTqPCR analysis on total tibialis muscles showed the downregulation of the aforementioned genes upon AR ablation.

In the meantime, I investigated the regeneration capacity of SatC *in vivo* by inducing muscle injury via the injection of cardiotoxin in the tibialis interior of adult male mice via histological and transcriptomic analysis. Our data show that AR-deficient SatC fail to undergo asymmetric division to maintain the stem cell population, enter differentiation, and generate dystrophic myofibers upon injury. Transcriptomic and Cut&Run analysis revealed AR direct target genes in the process of muscle regeneration which are mainly implicated in “cell cycle”, “myoblast fusion” and “myofiber structure”. At the end of regeneration process, number of SatC significantly decline in mutant muscles compared to control and their reactivity is impaired upon a second muscle damage.

In this project, I was responsible of getting knowledge of the bibliography, managing the mouse model, planning, and performing the experiments. I completed the majority of the results shown in this part. For preparing the manuscript, I took charge of the writing and received help from Joe Rizk, Dr. Delphine Duteil and Dr. Daniel Metzger.

Manuscript in preparation

Androgens control satellite cell homeostasis and function and myofiber regeneration after muscle injury

Kamar Ghaibour[1-4], Arnaud Ferry[5], Delphine Duteil[1-4#], Daniel Metzger[1-4#].

[1] Department of functional genomics and cancer, Institut de Genetique et de Biologie Moleculaire et Cellulaire (IGBMC), Illkirch, France.

[2] Inserm, U1258, Illkirch, 67404, France.

[3] CNRS, UMR7104, Illkirch, 67404, France.

[4] Université de Strasbourg.

[5] Centre de Recherche en Myologie, UMRS974-Sorbonne Université-INSERM U974-Association Institut de Myologie, France.

Corresponding authors

Abstract

Satellite cell (SatC) are muscle stem cells required for tissue regeneration upon damage. They reside in a particular microenvironment called niche that is essential for their quiescence, maintenance, and activation. However, our knowledge of niche regulation and SatC differentiation is still incomplete. Here we show that the androgen receptor (AR) in SatC is a crucial factor involved in niche integrity, cell quiescence, as well as expansion and self-renewal during muscle regeneration. We demonstrate that AR directly controls the expression of various genes involved in SatC dormancy, including Pax7, in physiological conditions. In the absence of AR, SatC quit their niches and fuse to existing fibers. During muscle regeneration, AR deficient SatC preferably undergo symmetric differentiation, which leads to the decline in stem cell number at the end of the regeneration process. Moreover, AR-deficient newly generated myofibers exhibit dystrophic characteristics and misshaped cytoskeleton and sarcomeres, which affect their contraction force. Therefore, AR represents a potential therapeutic target for pathological conditions of the muscles in which the stem cell niche is compromised.

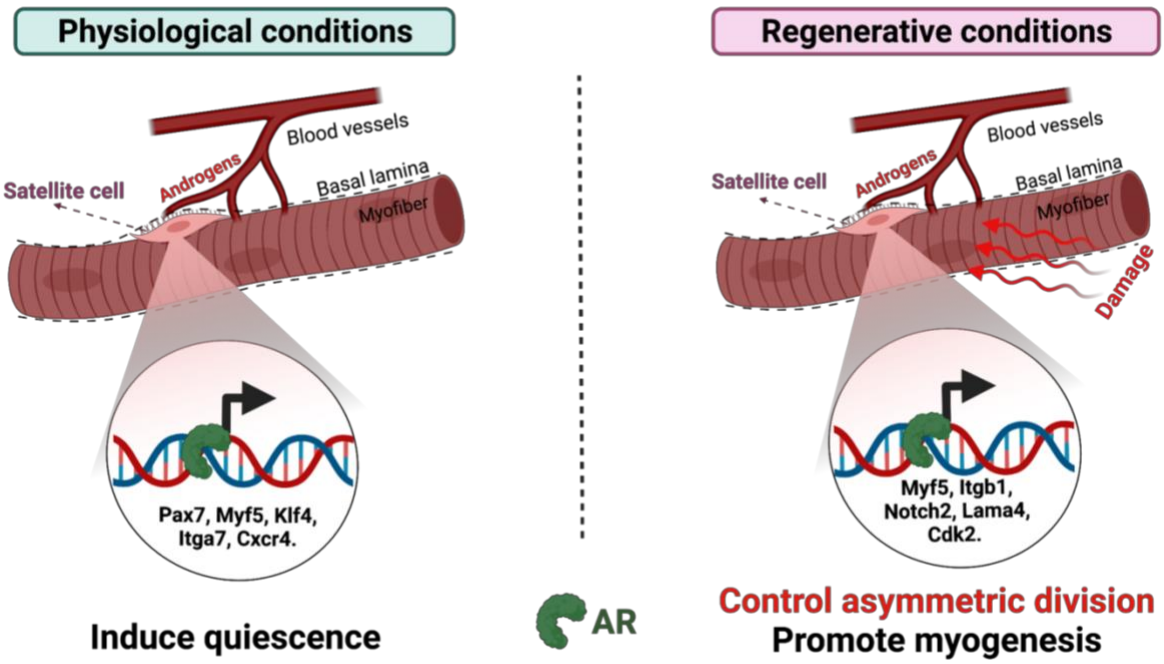

Introduction

Accounting for one-third of the mammalian body mass[1], skeletal muscle (SkM) is predominantly made up of cylindrical multinuclear cells, termed myofibers[2]. It is a highly adaptable tissue that responds to environmental and physiological demands, and is subjected to various aggressions. Fortunately, it has high regenerative capacities during post-natal life, which depend on the proliferation, differentiation and fusion of muscle progenitors[3]. Unlike its *de novo* embryonic development, that essentially originates from paraxial mesoderm-derived structures, *ad integrum* muscle growth and repair during post-embryonic life depends on the recruitment of undifferentiated progenitors, called satellite cells (SatC)[4].

SatC reside in a quiescent state in a niche located between the myofiber sarcolemma and the surrounding extracellular matrix, known as the basal lamina. Quiescent SatC are characterized by the expression of the Paired Box (PAX) 7 transcription factor. In response to increased mechanical load or injury, SatC become activated, re-enter the cell cycle, and undergo either symmetric division to expand the stem cell population, or asymmetric division to generate (i) SatC that maintain the pool of stem cells [5] and (ii) muscle progenitors that will give rise to nascent muscle fibers[6].

De novo myofiber formation is orchestrated by a cascade of transcription factors named myogenic regulatory factors (MRFs), among which myogenic regulatory factor 5 (MYF5) and myoblast determination protein 1 (MYOD1) commit SatC to the myogenic lineage by onsetting their asymmetrical division, transition into myoblasts, formation of myocytes expressing myogenin (MYOG), and subsequent fusion with other differentiating myocytes or with existing myofibers[6]. Of note, MYF5 is a key feature of SatC asymmetric division, which can distinguish stem cells from committed progenitors, as $PAX7^{+}/MYF5^{-}$ cells restore the pool of SatC, and $PAX7^{+}/MYF5^{+}$ committed cells differentiate and give rise to myocytes [6]. It has been recently shown that impaired SatC asymmetric division contributes to progressive muscle wasting observed in Duchenne muscle dystrophy[7]. While dystrophin (DMD) deficiency in muscle fibers makes them more susceptible to damage, lack of DMD expression in SatC results in loss of polarity and reduced asymmetric division capacity, leading to exhaustion of the SatC pool and impaired muscle regeneration efficiency[7]. Although SatC are the main modulators of myofiber formation, muscle regeneration is a highly time-orchestrated process that involves various additional cell types, including immune, endothelial, fibrogenic cells and adipogenic progenitors, working together to reconstitute muscle tissue within approximately a month [8,9].

Of note, to date, the molecular mechanisms that control the expression of key determinants of SatC renewal and commitment remain elusive.

Among many factors that maintain the homeostasis of SatC niche are hormones, including androgens. Androgens exert highly pleiotropic functions in mammals, such as the development of sexual organs and characteristics, as well as the control of muscle mass and strength[10]. At puberty, they also play a major role in regulating SatC homeostasis and differentiation, since they mediate cell transition from proliferative to quiescence state via the Notch signaling[11]. In addition, high doses of testosterone (the main mammalian androgen) have been shown to enhance SatC proliferation and differentiation[12] and to increase regenerating fiber cross-sectional areas after muscle injury in both young and old mice[13]. Oppositely, removal of endogenous androgens by gonadectomy results in activated SatC in the absence of stimuli and delayed muscle weight gain following cardiotoxin-induced muscle injury[14].

Androgens effects are mediated by the androgen receptor (AR), a member of the ligand-dependent nuclear receptors' superfamily. AR is expressed in SatC and its expression in isolated muscle stem cells increases when incubated with supraphysiological testosterone and/or 5-alpha-dihydrotestosterone (DHT) concentrations[15]. In a previous study, we showed that androgen-dependent postnatal hypertrophy of hindlimb muscle fibers is AR-independent. However, AR deficiency in hindlimb myocytes impairs sarcomeres' myofibrillar organization and decreases muscle strength, demonstrating that myocytic AR controls critical pathways required for maximum muscle force production[10]. To date, only one study aimed at unraveling the role of androgens via their receptor in muscle progenitors. Using *Myod1*-Cre mice, Dubois et al. ablated AR in SatC, as well as in SatC-derived myoblasts and myocytes, and showed that AR controls muscle mass and strength via direct regulation of myostatin, a member of the beta transforming growth factor (TGFB) superfamily[16]. However, endogenous androgen molecular deteminants via their receptor AR in SatC homeostasis and myofiber formation is still unknown.

In this study, we show that AR is a key player for maintaining SatC niche integrity and homeostasis. It promotes SatC quiescence by controlling the expression of PAX7 and other genes essential for cell dormancy. We further demonstrate that in case of muscle injury, AR stimulates SatC proliferation and asymmetric division that maintains the stem cell population, and that AR-deficient regenerating myofibers exhibit dystrophic characteristics. Thus, AR

presents is a potential therapeutic target for myopathies in which the SatC niche is compromised.

Results

AR controls satellite cell quiescence and niche integrity

Immunofluorescence analysis on tibialis anterior (TA) muscles isolated from 8-week-old wild-type mice showed that AR is mainly expressed in nuclei of PAX7-positive SatC (**Fig. S1A**). To determine the role of AR in SatC homeostasis at adult stage, we generated $AR^{Sat-/Y}$ male mice in which AR is selectively ablated in PAX7-expressing cells at adulthood (see Materials and Methods) (**Fig. S1B to S1D**). Hematoxylin and eosin (H&E) staining of TA muscles of $AR^{L2/Y}$ mice (harboring loxP sites flanking exon 1 of the AR gene, **Fig. S1B**, hereafter control) and of $AR^{Sat-/Y}$ ones, had a similar histology up to 4 months after AR ablation (**Fig. S1E**), with similar fiber number and cross section area (CSA) (**Fig. S1F and S1G, respectively)**. Moreover, flow cytometry analysis indicated that the percentage of SatC was similar in control and $AR^{Sat-/Y}$ TA muscles, one month after AR ablation (**Fig. 1A**). In agreement with these results, immunofluorescent detection of PAX7, together with 2-alpha laminin (LAMA2), the basal lamina major component, unveiled that the number of PAX7-expressing cells was similar in $AR^{Sat-/Y}$ and control TA muscles, even though PAX7 signal intensity was reduced in AR-deficient SatC (**Fig. 1B, green arrows and 1C**). RT-qPCR analysis on FACS-isolated SatC revealed a 2-fold decline in *Pax7* transcript levels in $AR^{Sat-/Y}$ muscles (**Fig. 1D**), which was confirmed by RT-qPCR analyses on total TA muscles, one week after AR ablation in SatC **(Fig. S1H)**. Since PAX7 controls SatC quiescence[10,11], we investigated the transcript levels of genes involved in cell dormancy [e.g. Myf, Kruppel Like Factor 7 (*Klf7*)[12] and beta 1 integrin (*Itgb1,* also named *Cd29*)][13], in niche integrity and cell adherence to the host fiber (e.g. *Cd34)*[14], as well as stemness potential (e.g. *Cxcr4)*[15-17] and its cognate target cluster of differentiation 9 (*Cd9*)[17]. The transcript levels of *Myf5*, *Klf7*, *Cxcr4*, *CD9* and *Itgb1* were similar in TA muscles of mutant mice than those of controls, one-week after AR invalidation (**Fig. S1H),** but were decreased three weeks later (**Fig. S1I**).

In agreement with these results, flow cytometry analysis revealed that CD34 and CXCR4 protein levels were lower in SatC of $AR^{Sat-/Y}$ hind-limb muscles compared to control (**Fig. 1E**), indicating that SatC quiescence might be impaired one month after AR ablation. Remarkably, LAMA2 staining unveiled interruptions in the basal lamina of $AR^{Sat-/Y}$ muscles (**Fig. 1B, white arrows**), indicating that SatC niche integrity might be altered. To further characterize the SatC compartment, an immunofluorescent detection of LAMA2, PAX7 and DMD was performed. Whereas PAX7-positive nuclei of TA muscles of control mice were located between the LAMA2-stained basal lamina and the DMD-marked sarcolemma (**Fig. S1J)**, as described[18],

one month after AR ablation, up to 80 % of PAX7-positive nuclei were detached from the lamina, some of which were mis-oriented, placed in a DMD-negative contact zone with the myofiber, and some of which were located within the sarcolemma (**Fig. 1F, S1J, yellow arrows, and Fig 1G**). Together, despite similar number of Pax7+ cells, the majority of SatC express reduced transcript levels of stemness markers, are no longer located in their niche, and reside within the adjacent muscle fiber, one month after AR ablation.

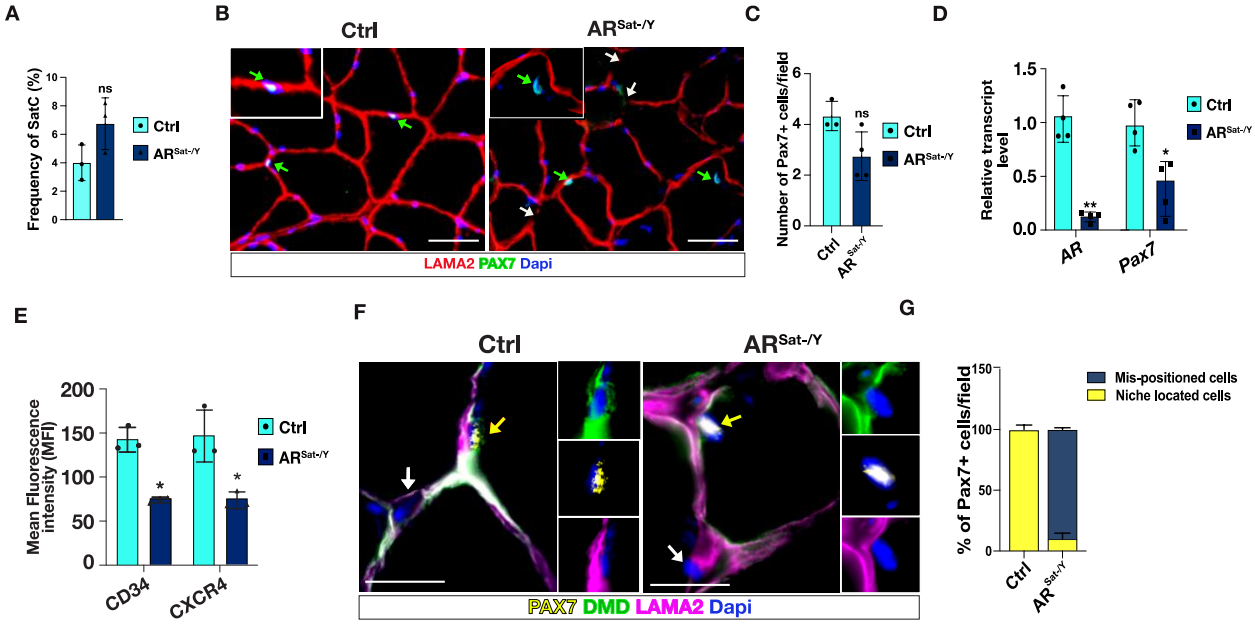

Figure 1:* AR controls satellite cell quiescence and niche integrity**. ***A. *Percentage of SatC determined by via flow cytometry analysis performed on control (Ctrl) and AR$^{Sat-/Y}$ TA one month after AR ablation. N=3 mice per condition.* ***B.*** *Immunofluorescent detection of PAX7 and laminin a2 (LAMA2) on tibialis muscle sections from control (Ctrl) and AR$^{Sat-/Y}$ mice one month after AR ablation. Nuclei were stained with DAPI. Green and white arrows point at cells expressing PAX7 and LAMA2 interruptions in myofibers, respectively. Scale bar = 50 µm.* ***C.*** *Quantification of PAX7+ cells per field. n=4 mice per group and 5 fields counted per animal.* ***D.*** *Relative transcript levels of Ar and Pax7 in FACS-isolated SatC from control (Ctrl) and mutant (AR$^{Sat-/Y}$) hind-limb muscles one month after AR ablation. N=4 mice per group.* ***E.*** *Flow cytometry analysis of CD34 and CXCR4 protein levels in SatC isolated form control (Ctrl) and AR$^{Sat-/Y}$ hind-limb muscles one month after AR ablation. N=3 mice per condition.* ***F.*** *Immunofluorescent detection of PAX7, DMD and LAMA2 on tibialis muscle sections from control (Ctrl) and AR$^{Sat-/Y}$ mice one month after AR ablation. Nuclei were stained with DAPI. Yellow and white arrows point at PAX7-expressing cells and PAX7-negative nuclei, respectively. Scale bar = 25 µm.* ***G.*** *Percentage of PAX7-positive cells location in niche or mis-positioned in tibialis of control (Ctrl) and AR$^{Sat-/Y}$ mice one month after AR ablation. Quantitative data are presented as mean ± SEM; Student's t-test: *p< 0.05, **p< 0.01 and ns, not significant.*

AR in resting SatC controls a vast gene network

To decipher the molecular mechanisms by which AR controls SatC homeostasis, we performed a "cleavage under targets and release using nuclease" (Cut&Run)[17] analysis with antibodies directed against AR followed by massive parallel sequencing, on FACS-isolated SatC from TA of 9-week-old control mice. Bio-informatic analysis revealed 7,840 peaks corresponding to 5,536 gene. These peaks were mainly located in intron and intergenic regions (**Fig. 2A**), and HOMER motif search revealed that ~80 % of AR-bound DNA segments contain oxosteroid receptor response elements [AR half-sites, AR response elements (ARE) or progesterone receptor response element (PRE)] (**Fig. 2B**). Moreover, Cut&Run analysis for dimethylated lysine 4 of histone 3 (H3K4me2) **(Fig. S2A**), a hallmark for active promoters, revealed that 3707 AR target genes have a H3K4me2 peak at their promoter region (-1000 bp to 100 bp from TSS), indicating that they are transcribed (**Fig. 2C**). KEGG pathway analysis on these genes unveiled that many of which are involved in Hippo signaling, which is implicated in myogenesis[18,19], pluripotency of stem cells, ECM-receptor interaction, adherence junctions, and in focal adhesion (**Fig. 2D**). Interestingly, *Pax7*, *Myf5*, *Myod1*, *Myog*, *Itgb1*, *Klf7*, *Cxcr4* and *Ar* itself were identified as AR direct targets in SatC (**Fig. 2E and S2B**). To determine whether PAX7 is also an AR target in human myoblasts, we treated LHCNM2 cells with vehicle or 100 nM of DHT for 24 h, and observed AR translocation to the nuclei associated with increased PAX7 signal intensity after DHT treatment **(Fig. 2F)**.

To determine whether AR might collaborate with MRFs to control the expression of target genes, we performed a seqMINER analysis of the AR binding profile in SatC with that of PAX7 in C2C12 mouse myoblasts [20]. We found that 970 AR peaks (12 %) are also bound by PAX7 **(Fig. 2G)**. Interestingly, the genes on which AR and PAX7 co-localize are associated with cell junction (58 genes, enrichment score 4.48, 84 % expressed in SatC), such as *Cxcr4*, *Itga9*, *Itgb3*, *Lama1*, *Lama4* and *Lamc2*, and implicated in cell differentiation (64 genes, enrichment score 3.15, 84 % expressed in SatC) including *Bmp3*, *Bmp6*, *Camk1*, *Dkk2*, *Kdm1a* and *Wnt5b,* as exemplified in **Fig. 2H**. Together, our data indicate that AR controls the expression of key genes required for the maintenance of SatC quiescence, at least in part in collaboration with PAX7.

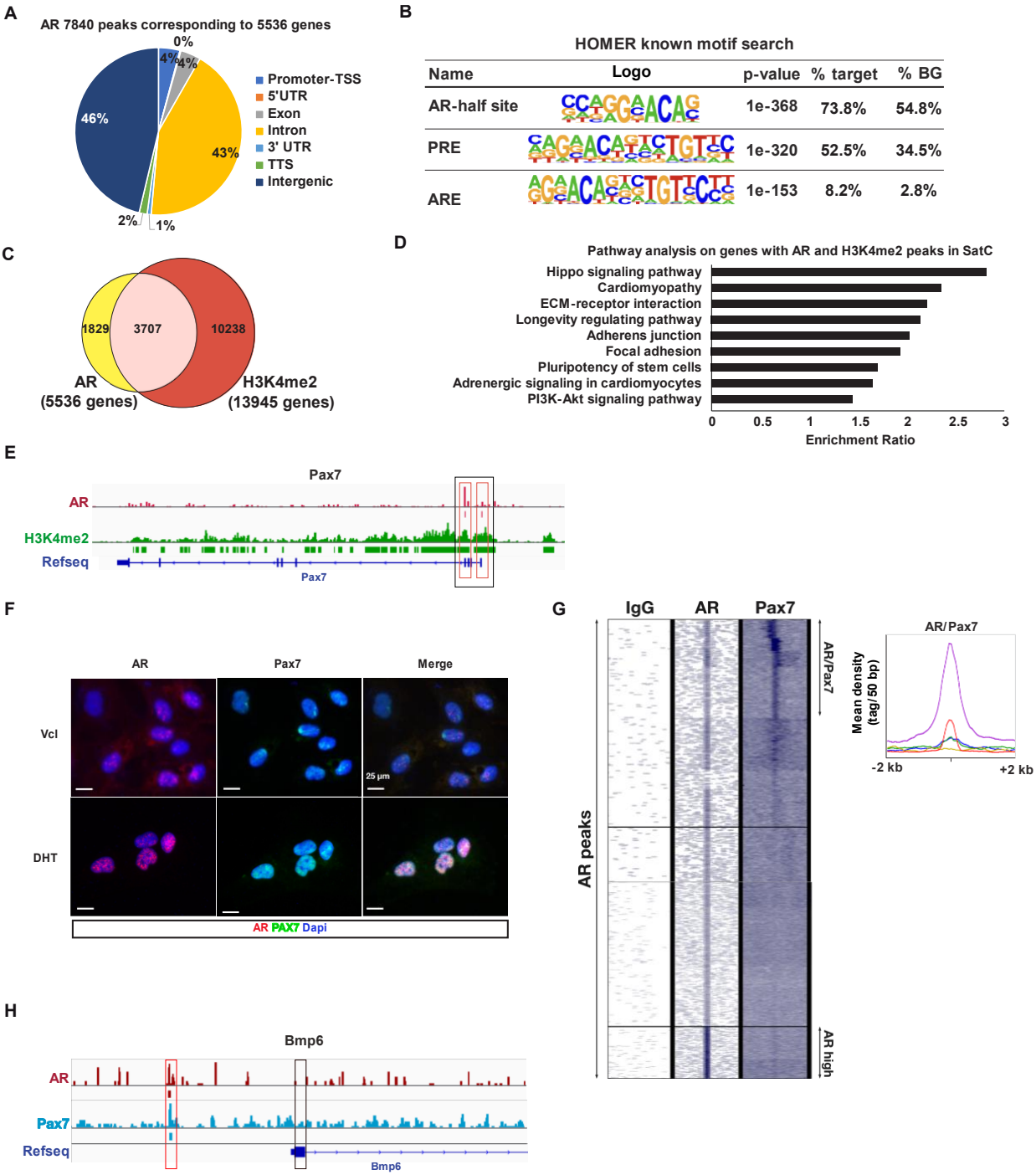

Figure 2: **AR in resting SatC controls a vast gene network.** ***A.*** *Pie chart depicting peak distribution of AR in the genome of FACS-isolated SatC from TA of control mice revealed after performing Cut&Run analysis.* ***B.*** *HOMER known motif analysis of AR-bound genome sequences in FACS-isolated SatC from control TA muscles.* ***C.*** *Overlap between genes bound by AR and H3K4me2 in FACS-isolated SatC from TA of control mice.* ***D.*** *KEGG Pathway analysis of genes with AR and H3K4me2 in FACS-isolated SatC from TA of control mice.* ***E.*** *Localization of H3K4me2 and AR at the Pax7 locus. The AR binding site and the corresponding genome sequence identified at the Pax7 promoter are highlighted with red boxes. Transcription start site (TSS) is highlighted with a black box.* ***F.*** *Immunofluorescent detection of AR and PAX7 on immortalized LHCN-M2 myoblasts treated with vehicle Vcl or 100 nM DHT for 24 h. Scale bar = 25 µm.* ***G.*** *Overlap between genes harboting AR peaks in FACS-isolated SatC*

*from TA of control mice and of genes with PAX7 peaks identified by chromatin immunoprecipitation in C2C12 myoblasts. Rabbit IgG was used as a negative control for AR Cut&Run analysis. **H.** Localization of AR and PAX7 at the Bmp6 locus. AR and PAX7 binding sites and the corresponding genome sequence are highlighted with a red box. Transcription start site (TSS) is highlighted with a black box.*

Muscle regeneration is impaired in $AR^{Sat-/Y}$ mice

To determine whether AR plays a role in SatC activation and myofiber formation, we experimentally induced injury in TA muscles of 8-week-old control and $AR^{Sat-/Y}$ male mice by cardiotoxin (Ctx) injection. Immunofluorescent analysis of AR, 5 (D5) and 7 (D7) days after muscle damage showed that AR is expressed in up to 95 % of PAX7-positive cells of control muscles (**Fig. 3A, yellow arrows and 3B**), and that ~80 % of SatC are AR-deficient in $AR^{Sat-/Y}$ mice (**Fig. 3A, green arrows and 3B**). Hematoxylin and eosin (H&E) staining 3 days after injury (D3) showed similar cellular infiltration (**Fig. S3A**, **green arrows**) and myofiber necrosis (**Fig. S3A**, **blue arrows**) in $AR^{Sat-/Y}$ and control muscles. Of note, no regenerating fibers were observed in both genotypes at D3 (**Fig. S3A**). Moreover, gomori trichrome staining demonstrated similar fibrosis emergence in $AR^{Sat-/Y}$ and control mice muscles at D3 (**Fig. S3B**).

At D5, whereas newly formed myofiber histology was similar between control and $AR^{Sat-/Y}$ muscles (**Fig. 3C**), we observed persistent myofiber necrosis characterized by membrane disruptions and pale sarcoplasm in $AR^{Sat-/Y}$ mice muscles (**Fig. 3C, blue arrows**). Moreover, immunofluorescent detection of LAMA2 revealed that whilst the shape of regenerating myofibers was mainly polygonal in control mice, it was elongated with lamina disruptions in $AR^{Sat-/Y}$ mice (**Fig. S3C, green arrows**), despite similar CSA with control littermates (**Fig. S3D**). DMD staining furtherly confirmed the malformation of regenerating fibers in $AR^{Sat-/Y}$ mice TA muscles **(Fig. S3E, white arrows)**, highlighted by DMD protein accumulation within the regenerative area **(Fig. S3E, green arrows).** Notably, we observed similar fibrosis emergence, as demonstrated by gomori trichrome staining at D5 in $AR^{Sat-/Y}$ and control TA muscles **(Fig. 3D, green dashes)**. In addition, staining of perilipin (PLIN1), a protein that coats lipid vesicles, revealed that presence of adipocytes between myofibers of $AR^{Sat-/Y}$ mice at D5 (**Fig. 3E, white arrows**). Moreover, flow cytometry analyses at D5 revealed similar percentage of immune, endothelial, as well as fibro-adipogenic progenitors (FAPs) and SatC in $AR^{Sat-/Y}$ and control muscles (**Fig. S3F**). of note, adipocyte quantification was not possible with flow cytometry since cells are larger to pass through the machine's nozzle.

At D7, H&E staining revealed massive infiltration (F**ig. 3C**, **green arrows**) in $AR^{Sat-/Y}$ mice

compared to controls, as well as lipid accumulation (**Fig. 3C**, **yellow arrows**). Moreover, we observed increased fibrosis at D7 in $AR^{Sat-/Y}$ TA muscles compared to controls **(Fig. 3D, green dashes)**. Of note, PBS injected (Vcl) $AR^{Sat-/Y}$ muscles did not exhibit any histological defects **(Fig. 3C-D and Fig. S3A-B).** PLIN1 staining indicated a higher number of adipocytes between myofibers of $AR^{Sat-/Y}$ than those of control mice at D7 (**Fig. 3E, white arrows**). Furthermore, LAMA2-detection unveiled the presence of elongated and malformed myofibers (**Fig. 3F, green arrows**), laminin accumulations (**Fig. 3F**, **orange arrows**) and inclusions within regenerating fibers (**Fig. 3F, white arrows**) in $AR^{Sat-/Y}$ mice TA muscles one week after injury. Additionally, CSA showed higher number of small fibers in $AR^{Sat-/Y}$ TA compared to control at D7 **(Fig. 3G).** In agreement, DMD staining unveiled myofiber deformity **(Fig. S3E, white arrows)** and DMD aggregates in $AR^{Sat-/Y}$ mice TA muscles **(Fig. S3E, green arrows).**

To further characterize the structural defects of regenerating myofibers of $AR^{Sat-/Y}$ mice, we performed immunofluorescent detection of sarcomeric alpha actinin (ACTN1) and DMD at D7. Our analysis of transversal sections unveiled a misalignment of sarcomeres and uneven distribution of ACTN1 throughout newly formed mutant fibers compared to the regular structure observed in control ones (**Fig. 3H, upper panel, red arrows**). Moreover, a similar analysis performed on longitudinal sections revealed that while ACTN1 formed a stairs-shape in regenerating fibers of control mice (**Fig. 3H, lower panel, magenta arrows**), sarcomeres were misaligned and Z-line were unparalleled in $AR^{Sat-/Y}$ myofibers (**Fig. 3H, lower panel, orange arrows**). In agreement, ultrastructure analysis uncovered misshaped sarcomeres (**Fig. 3I, green arrows**) and lack of protein content (**Fig. 3I, red arrows**) in $AR^{Sat-/Y}$ mice at D7. Moreover, we also detected enlarged mitochondria (**Fig. 3I, black arrows**), and significant enlargement of centro-nuclei of myofibers (**Fig. 3I**, **white arrow**), including necrotic ones (**Fig. 3I**, **yellow arrow**), as well as unparalleled T tubules to the Z-lines (**Fig. 3I, blue arrows**) and slanted triad structure (**Fig. 3I, magenta arrows**) in $AR^{Sat-/Y}$ mice TA muscles, 7 days after injury. Of note, control TA muscles demonstrated proper myofiber formation and structure at D7 (**Fig. 3I**). Since we observed greater infiltration in $AR^{Sat-/Y}$ TA muscles than in control via H&E staining at D7 (**Fig. 3C**), we characterized the stromal response in injured muscles by flow cytometry. This analysis unveiled that the infiltration in $AR^{Sat-/Y}$ TA muscles was mainly due to the presence of immune cells, primarily pro-inflammatory natural killer cells, at the expense of FAPs, and SatC (**Fig. 3J and S3G**). Together, our data show that AR deficiency in SatC and their progeny leads to the impairment of the regeneration process characterized by structural defects in both contractile and non-contractile cytoskeletons, accompanied with increased number of adipocytes, immune infiltration, and fibrosis.

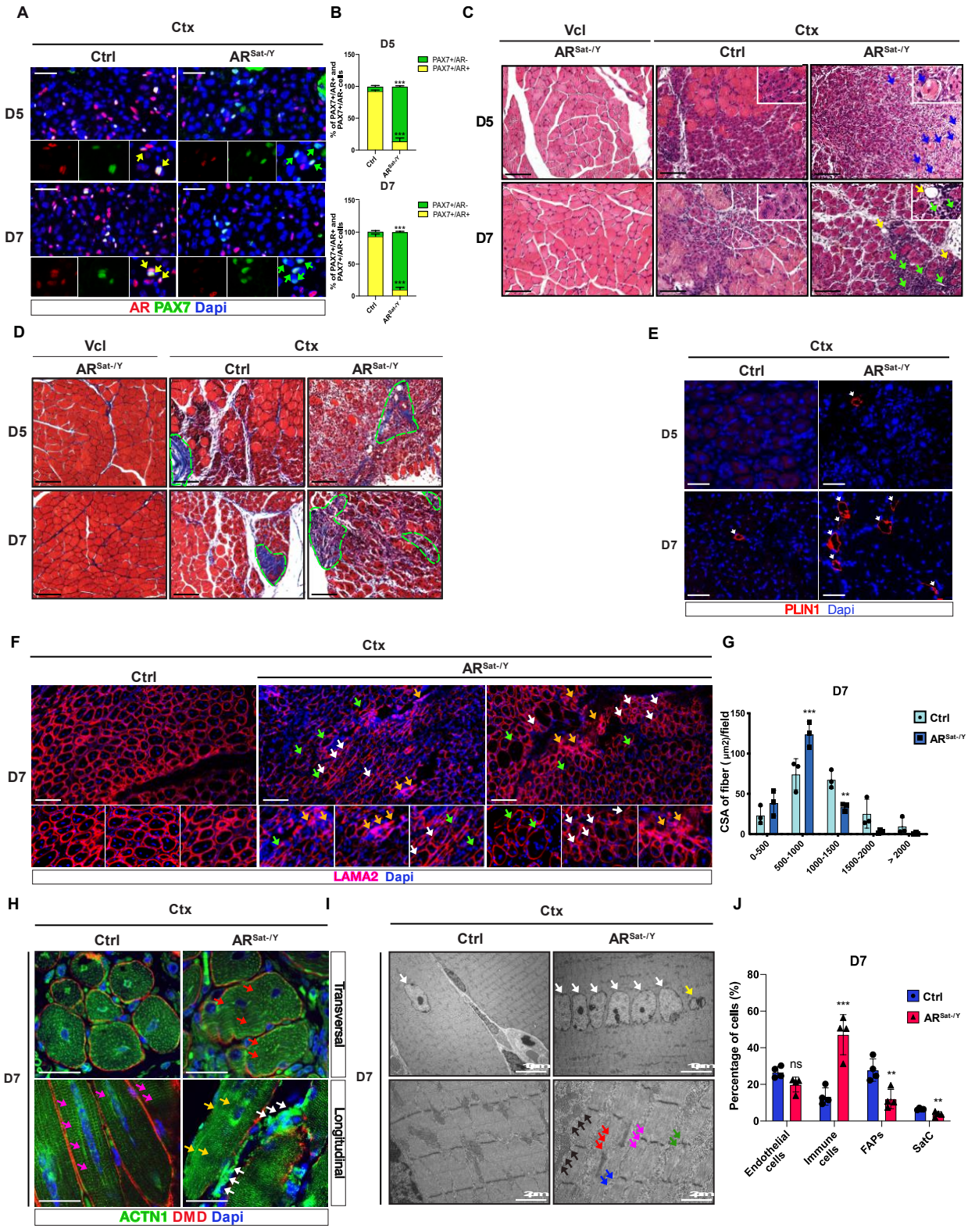

Figure 3: **Muscle regeneration is impaired in AR$^{Sat-/Y}$ mice.** ***A.*** *Immunofluorescent detection of AR and PAX7 on tibialis muscle sections from control (Ctrl) and AR$^{Sat-/Y}$ mice 5 (D5) and 7 (D7) days after cardiotoxin (Ctx) injection. Nuclei were stained with DAPI. Yellow and green arrows point at PAX7+/AR+ and PAX7+/AR- cells, respectively. N=3 mice per group and 4*

images were analyzed per animal. Scale bar = 50 μm. ***B.*** *Percentage of PAX7+/AR+ and PAX7+/AR- cells from control (Ctrl) and $AR^{Sat-/Y}$ mice at D5 and D7. N=3 mice per group and 4 images were analyzed per animal.* ***C.*** *H&E staining on tibialis muscle sections of control (Ctrl) and $AR^{Sat-/Y}$ mice at D5 and D7 after PBS (Vcl) or cardiotoxin (Ctx) injection. Blue, green, and yellow arrows point at necrotic myofibers, stromal cell infiltration, and adipocyte accumulation, respectively. Scale bar = 100 μm.* ***D.*** *Trichrome staining (Gomori) on tibialis muscle sections of control (Ctrl) and $AR^{Sat-/Y}$ mice at D5 and D7 after PBS (Vcl) or cardiotoxin (Ctx) injection. Green dashes circulate fibrosis. Scale bar = 100 μm.* ***E.*** *Perilipin (PLIN1-red) on tibialis muscle sections of control (Ctrl) and $AR^{Sat-/Y}$ mice at D5 and D7. Nuclei were stained with DAPI. White arrows point at PLIN1-expressing lipid vesicles. Scale bar = 50 μm.* ***F.*** *Immunofluorescent detection Laminin−α2 (LAMA2) on tibialis muscle sections from control (Ctrl) and $AR^{Sat-/Y}$ mice at D7. Nuclei were stained with DAPI. Orange, white and green arrows point at LAMA2 protein accumulations, LAMA2 inclusions within the regenerating fibers and elongated misshaped myofibers, respectively. Scale bar = 50 μm.* ***G.*** *Cross-sections area analysis of DMD-stained TA sections of control (Ctrl) and $AR^{Sat-/Y}$ mice at D7. N=3 mice per group.* ***H.*** *Immunofluorescent detection of DMD and alpha-actinin (ACTN1) on tibialis muscle sections from control (Ctrl) and $AR^{Sat-/Y}$ mice at D7. Nuclei were stained with DAPI. Magenta, red, orange and white arrows point at stairs-shaped ACTN1 in control fibers, mis-distributed ACTN1 organization in mutant fibers, lack of ACTN1 protein in mutant myofibers, and ACTN1-expressing cells accumulating at the membrane of mutant myofibers. Scale bar = 25 μm.* ***I.*** *Ultrastructural analysis of TA of control (Ctrl) and $AR^{Sat-/Y}$ mice at D7. White and yellow arrows point at centro-nuclei and necrotic centro-nucleus, respectively. Green, red, black, blue and magenta show mis-shaped sarcomeres, lack of protein content, enlarged mitochondria, unparalleled T-tubules to the Z-line, and oblique triad structure, respectively. Scale bars (upper panel, 10 μm, lower panel, 2 μm).* ***J.*** *Percentage of resident and recruited immune, endothelial, fibro-adipogenic progenitors and SatC revealed by flow cytometry analysis performed on control (Ctrl) and mutant ($AR^{Sat-/Y}$) TA at D7. N=4 animals per condition. Quantitative data are presented as mean ± SEM; Student's t-test: **p< 0.01, ***p< 0.001 and ns, not significant.*

Cellular division and differentiation are altered in AR-deficient SatC after injury

Flow cytometry analysis revealed that although the percentage of SatC was similar at D5 in control and mutant mice **(Fig. S3F)**, it was 2-fold lower at D7 in $AR^{Sat-/Y}$ mice than to control littermates (**Fig. 3J and S3G)**. To further examine our observations regarding SatC number, we proceeded with a co-labeling of PAX7 and DMD to visualize cell localization. In agreement with the previous analysis, the number of PAX7-positive cells was similar between control and $AR^{Sat-/Y}$ mice at D5 (**Fig. 4A-B**). It remained noticeably unchanged in control mice between D5 and D7 (**Fig. 4A-B**), but decreased by 60 % between D5 and D7 in $AR^{Sat-/Y}$ TA muscles (**Fig. 4A-B**). Interestingly, the number of cells positive for deoxynucleotidyl transferase dUTP nick end labeling (TUNEL) assay that detects extensive DNA degradation during late stage of cell death[21] was similar at D5 and D7 in $AR^{Sat-/Y}$ and control TA muscles (**Fig. S4A, white**

arrows and S4B), although it significantly decreased in D7 compared to D5 in both genotypes. To determine whether the decrease in SatC number in $AR^{Sat-/Y}$ TA muscles is due to defects in their proliferation, we proceeded with a PAX7 and KI67 co-staining. Our data show that the number of proliferative SatC (PAX7+/KI67+) was 60 % and 30 % lower in TA muscles of $AR^{Sat-/Y}$ compared to those of control mice at D5 and D7, respectively (**Fig. 4C, yellow arrows, 4D and 4E**). Moreover, the number of MYOG-expressing myocytes was decreased by 2-fold at D5, but increased by 2-fold at D7 in TA muscles of $AR^{Sat-/Y}$ compared to those of controls (**Fig. S4C, green arrows and S4D**). To determine whether SatC self-renewal is altered after AR deficiency, we performed a co-staining of PAX7 and MYOG. Our analysis revealed that the percentage of $PAX7^{+}/MYOG^{+}$ committed cells was 2-fold higher at D5 in $AR^{Sat-/Y}$ muscles compared to control (**Fig. 4F, yellow arrows, 4G and 4H**), whereas that of $PAX7^{-}/MYOG^{+}$ myocytes was decreased (**Fig. 4F, white arrows, 4G and 4H)** and that of $PAX7^{+}/MYOG^{-}$ self-renewal fraction was similar (**Fig. 4F to 4H)**. Nevertheless, at D7, the proportion of each cell type was different than at D5, as the percentage of $PAX7^{+}/MYOG^{+}$ committed cells was similar (**Fig. 4F, yellow arrows, 4G and 4H**), and that of $PAX7^{-}/MYOG^{+}$ myocytes was higher by 2-fold in mutant muscles compared to control (**Fig. 4F, white arrows, 4G and 4H)** at the expense of $PAX7^{+}/MYOG^{-}$ self-renewal fraction (**Fig. 4F to 4H)**. Together, our results show that proliferation is impaired in AR-deficient SatC and indicate that mutant cells fail to maintain the stem cell population and commit to the myogenic lineage during muscle regeneration.

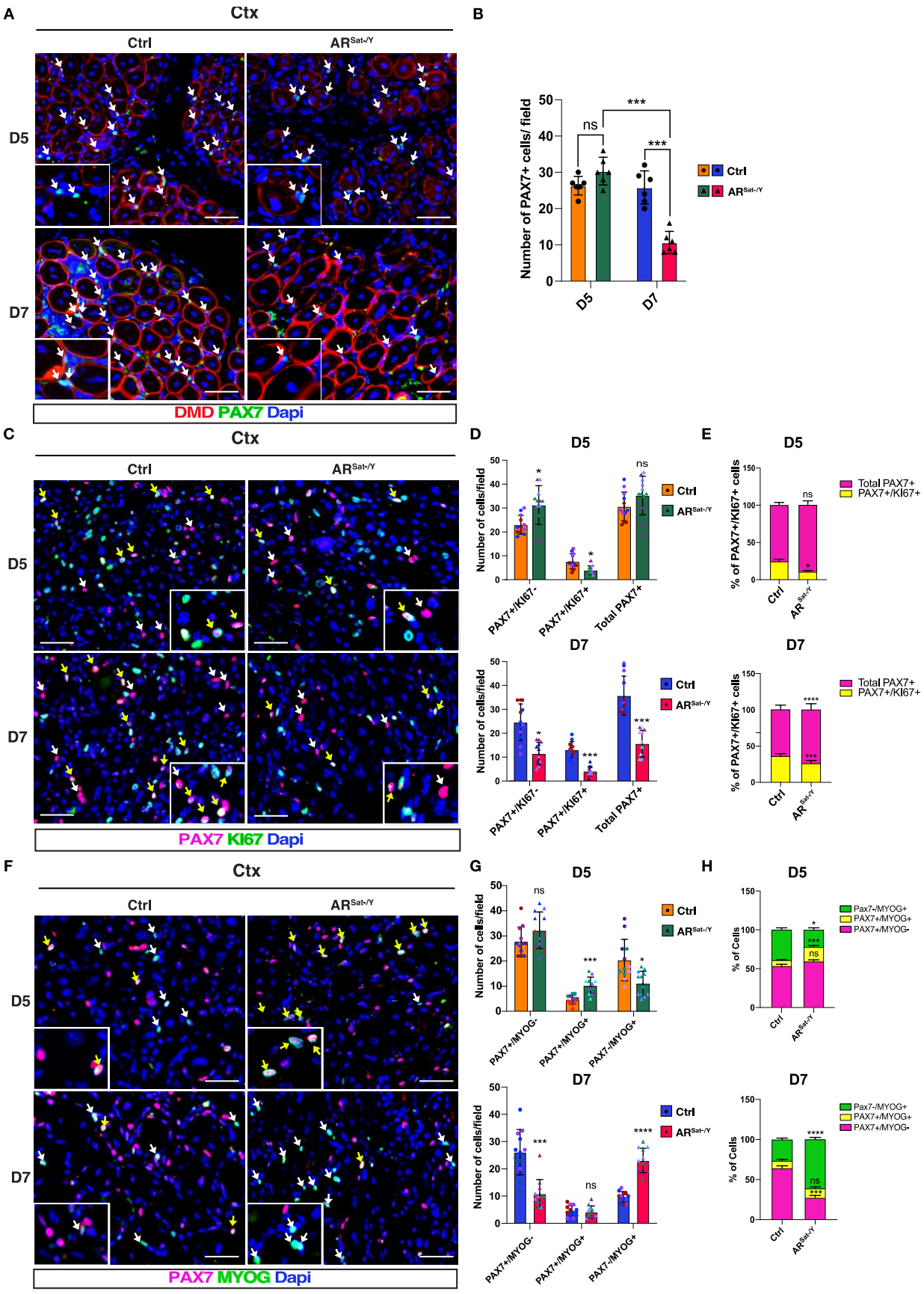

.

Figure 4: **Cellular division and differentiation are altered in AR-deficient SatC after injury.** ***A.*** *Immunofluorescent detection of DMD and PAX7 on tibialis muscle sections from*

control (Ctrl) and $AR^{Sat-/Y}$ mice 5 (D5) and 7 (D7) days after cardiotoxin (Ctx) injection. Nuclei were stained with DAPI. White arrows point at PAX7+ nuclei. Scale bar = 50 µm. ***B.*** *Quantification of PAX7+ cells per field from TA of control (Ctrl) and $AR^{Sat-/Y}$ mice at D5 and D7. N=6 mice per group and 4 images were analyzed per animal.* ***C.*** *Immunofluorescent detection of PAX7 and KI67 on tibialis muscle sections from control (Ctrl) and $AR^{Sat-/Y}$ mice at D5 and D7. Nuclei were stained with DAPI. Yellow and white arrows point at PAX7+/KI67+ and PAX7+/KI67- nuclei, respectively. Scale bar = 50 µm.* ***D.*** *Quantification of PAX7+/KI67-, PAX7+/KI67+ and total PAX7+ cells per field from TA of control (Ctrl) and $AR^{Sat-/Y}$ mice at D5 and D7. N=3 mice per group and 4 images were analyzed per animal. Data from a given animal are shown by the same color.* ***E.*** *Percentage of proliferative PAX7+/KI67+ cells out of total PAX7+ population in the tibialis of control (Ctrl) and $AR^{Sat-/Y}$ mice at D5 and D7. N=3 mice per group and 4 images were analyzed per animal.* ***F.*** *Immunofluorescent detection of PAX7 and MYOG on tibialis muscle sections from control (Ctrl) and $AR^{Sat-/Y}$ mice at D5 and D7. Nuclei were stained with DAPI. Yellow and white arrows point at PAX7+/MYOG+ and PAX7-/MYOG+ nuclei, respectively. Scale bar = 50 µm.* ***G.*** *Quantification of number of PAX7+/MYOG-, PAX7+/MYOG+ and PAX7-/MYOG+ cells per field from TA of control (Ctrl) and $AR^{Sat-/Y}$ mice at D5 and D7. N=3 mice per group and 4 images were analyzed per animal. Data from a given animal are shown by the same color.* ***H.*** *Percentage of PAX7+/MYOG-, PAX7+/MYOG+ and PAX7-/MYOG+ cells in TA of control (Ctrl) and $AR^{Sat-/Y}$ mice at D5 and D7. N=3 mice per group and 4 images were analyzed per animal. Quantitative data are presented as mean ± SEM; Student's t-test: *p< 0.05, **p< 0.01, ***p<0.001 and ****p<0.0001, ns, not significant.*

Myofiber cytoskeleton organization and ECM establishment are AR-dependent

To decipher the molecular mechanisms by which AR controls SatC activation and differentiation, we performed a Cut&Run analysis with antibodies direct against AR and H3K4me2 on FACS-isolated SatC from TA of control mice at D5. Our analysis uncovered 5,880 and 47,646 peaks for AR and H3K4me2, respectively, mainly located at intron and intergenic regions **(Fig. 5A and S5A)**. HOMER *de novo* motif search revealed that AR is bound to DNA via AREs at ~50 % of the sites **(Fig. 5B)**. Interestingly, a seqMINER analysis revealed that only 375 (~6 %) of AR peaks in SatC of non-injured of TA sample (NT) were in common with those identified at D5 **(Fig. 5C)**. Among these common locations, we found *AR*, *Cxcr4*, *Klf9,* and *Lamc2* loci. Noteworthy, the 5,880 AR peaks at D5 are associated with 3,853 genes, 55% (2,146) of which have a H3K4me2 peak at promoter **(Fig. 5D).** Pathway analysis unveiled that AR targets are associated with cell stemness (e.g., pluripotency of stem cells, Hippo signaling pathway), and muscle growth and contraction (e.g., axon guidance, adherens junction, Pi3k-Akt signaling pathway, cAMP signaling pathway, adrenergic signaling in cardiomyocytes) **(Fig. 5E)**. Even though AR was bound to a number of genes, RT-qPCR analyses revealed that the expression of genes involved in SatC stemness and activation are similar between TA muscles of control and $AR^{Sat-/Y}$ mice at D5 **(Fig. S5B)**. However, we

observed a significant decrease in transcript levels of *Pax7*, *Myog*, *Cxcr4*, *Cd34*, *Cd9* and the troponin 1 (*Tnnt1,* also named *Tropo1*) at D7 **(Fig. S5C)**. Therefore, we performed a transcriptome analysis of TA at D7 that unraveled 2045 down- and 1541 upregulated genes (reads more than 50 and p-adjusted less than 0.01**)** in $AR^{Sat-/Y}$ compared to control **(Fig. S5D)**. Of note, the expression of *Pax7*, *Myod1*, *Myf5* and *Myog* was decreased in TA of $AR^{Sat-/Y}$ mice, as well as those of main membrane proteins involved in myoblast fusion, including Myomixer (*Mymx*), Myomaker (*Mymk*), *Cd9* and *Cd81*. Remarkably, immunofluorescence analysis on longitudinal sections showed ACTN1-expressing cells accumulated on the membrane of centro-nucleated myofibers of $AR^{Sat-/Y}$ muscles 7 days after injury, highlighting defects in myocyte fusion after AR ablation (**Fig. 3H, lower panel, white arrows**).

KEGG pathway analysis on down-regulated genes at D7 did not reveal a transcriptomic signature of muscle differentiation, but identified genes involved in cell cycle (*Ccna2*, *Ccnb1*, *Ccnb2*, *Ccnd3*, *Cdk1-2-4-6*, *Cdkn1a-1c-2a*, *Mcm3-4-5-6*), as well as various components of actin cytoskeleton (*Actb*, *Actn1-4*, *Cxcl12*, *Cxcr4*) and the extracellular matrix (*Itga5*, *Itgb7*, *Lama2-4*, *Lamb1-c1-c2*, *Sdc1*, *Tnc* and various collagens) **(Fig. 5F and 5G)**. Of note, key genes of muscle development, such as *Lama4*, *Lamc2*, *Myf5*, *Myh3*, *Notch2*, *Mymk*, *Mymx*, *Cd9*, *Cd81, Tgfb1* and *Tuba1a* harbored AR peaks on their loci. Moreover, down-regulated genes at D7 in $AR^{Sat-/Y}$ mice were associated with immune response ("Natural killer cell mediated cytotoxicity", "Chemokine signaling pathway", "NF-kappa B signaling pathway") (**Fig. 5F**), whereas up-regulated ones account for cell metabolism ("Carbon metabolism", "Valine, leucine and isoleucine degradation" "TCA cycle", "Oxidative phosphorylation" …) (**Fig. 5H**), which might be due to alteration in SatC microenvironment. In agreement, flow cytometry analysis revealed increased number of immune cells and reduced number of FAPs in muscles of $AR^{Sat-/Y}$ mice (**Fig. 3J)**. Together, our data show that at D5 of regeneration AR is re-allocated to new sites, thereby activating a vast gene network required for SatC proliferation, myogenesis, myoblast fusion, and the establishment of myofiber structure.

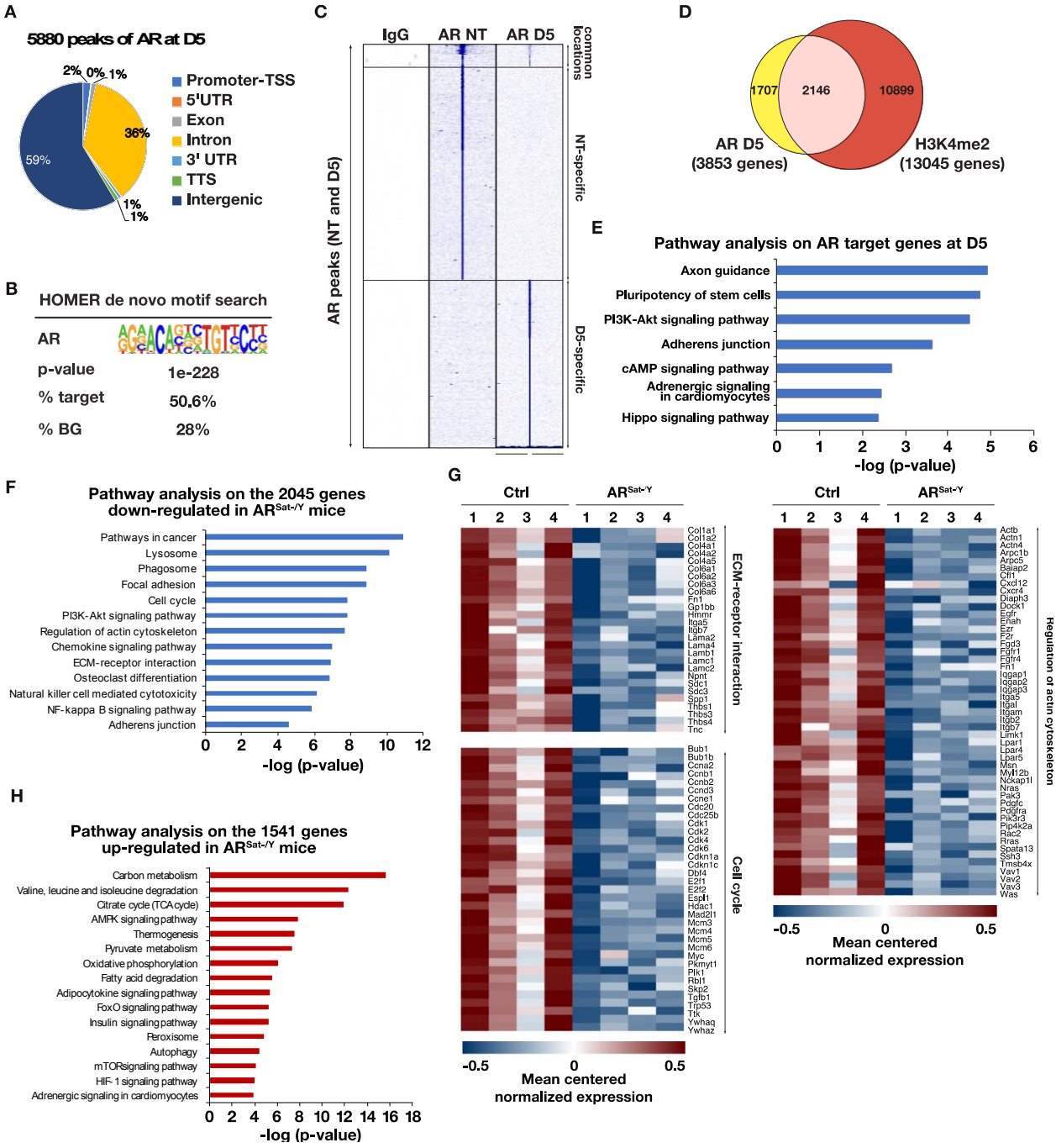

Figure 5: **Myofiber cytoskeleton organization and ECM establishment are AR-dependent**
A. *Pie chart depicting peak distribution of AR in the genome of FACS-isolated SatC from TA at D5.* ***B.*** *HOMER known motif analysis of AR-bound genome sequences in FACS-sorted SatC from control TA at D5. BG refers to estimated background.* ***C.*** *Overlap between genes harboring AR peaks in FACS-isolated SatC from control TA of non-injured and D5 of regeneration. Rabbit IgG was used as a negative control.* ***D.*** *Overlap between genes with AR peaks and those with H3K4me2 peaks in FACS-isolated SatC from TA of control mice at D5 after injury.* ***E.*** *KEGG Pathway analysis of genes with AR peaks in FACS-isolated SatC from TA of control mice at D5.* ***F.*** *KEGG Pathway analysis of down-regulated genes in AR$^{Sat-/Y}$ TA compared to control obtained by RNA-seq analysis performed at D7. N=4 mice per group.* ***G.*** *Heatmap depicting the mean centered normalized expression of indicated down-regulated genes selected by pathway analysis in TA muscles of AR$^{Sat-/Y}$ mice at D7. N=4 mice per group.*

H. *KEGG Pathway analysis of up-regulated genes in $AR^{Sat-/Y}$ TA compared to control obtained by RNA-seq analysis performed 7 days after injury. N=4 mice per group.*

AR ablation in SatC affects myofiber formation and contraction after injury

To determine whether AR ablation has long-term effects on stem cell population and/or myofiber formation, we characterized TA muscles of control and $AR^{Sat-/Y}$ mice at D28. Whereas control muscles contained regenerative fibers organized in fasciculus devoid of infiltration, $AR^{Sat-/Y}$ mice harbored major infiltration **(Fig. 6A, black arrows)**. Perilipin (PLIN1) staining showed an accumulation of adipocytes between myofibers of $AR^{Sat-/Y}$ mice (**Fig. 6B**). Of note, LAMA2 immunostaining further unveiled structural abnormalities of AR-depleted myofibers **(Fig. 6C)**, which were associated with a decrease in average of regenerating fiber CSA in $AR^{Sat-/Y}$ muscles when compared to control **(Fig. S6A, B)**. In addition, ultrastructure analysis showed the presence of necrotic centro-nuclei (**Fig. 6E, yellow arrow**), misorientation of sarcomeres (**Fig. 6E, green arrows**), as well as unparalleled T tubules to the Z-lines (**Fig. 6E, blue arrows**) and aslant triad structure (**Fig. 6E**, **magenta arrows**) in $AR^{Sat-/Y}$ muscles, while control ones exhibited proper muscle structure **(Fig. 6E)**. Interestingly, PAX7 and LAMA2 co-staining demonstrated a 2-fold decrease in SatC number in mutant TA compared to control ones **(Fig. 6C, white arrows and 6D).** To further characterize newly regenerated fibers after AR ablation in SatC, *in situ* contractile properties were analyzed at D28. The maximal tetanic force of isolated regenerative single fibers in response to stimulation frequencies was lower in TA of mutant mice than of control at 25 to 125 Hz **(Fig. 6F)**, whereas specific tetanic force normalized to muscle weight was similar **(Fig. 6G)**.

Taken together, our findings demonstrate that AR is essential for the maintenance of SatC number and for myofiber sarcomere organization, ensuring proper contractile force after muscle recovery.

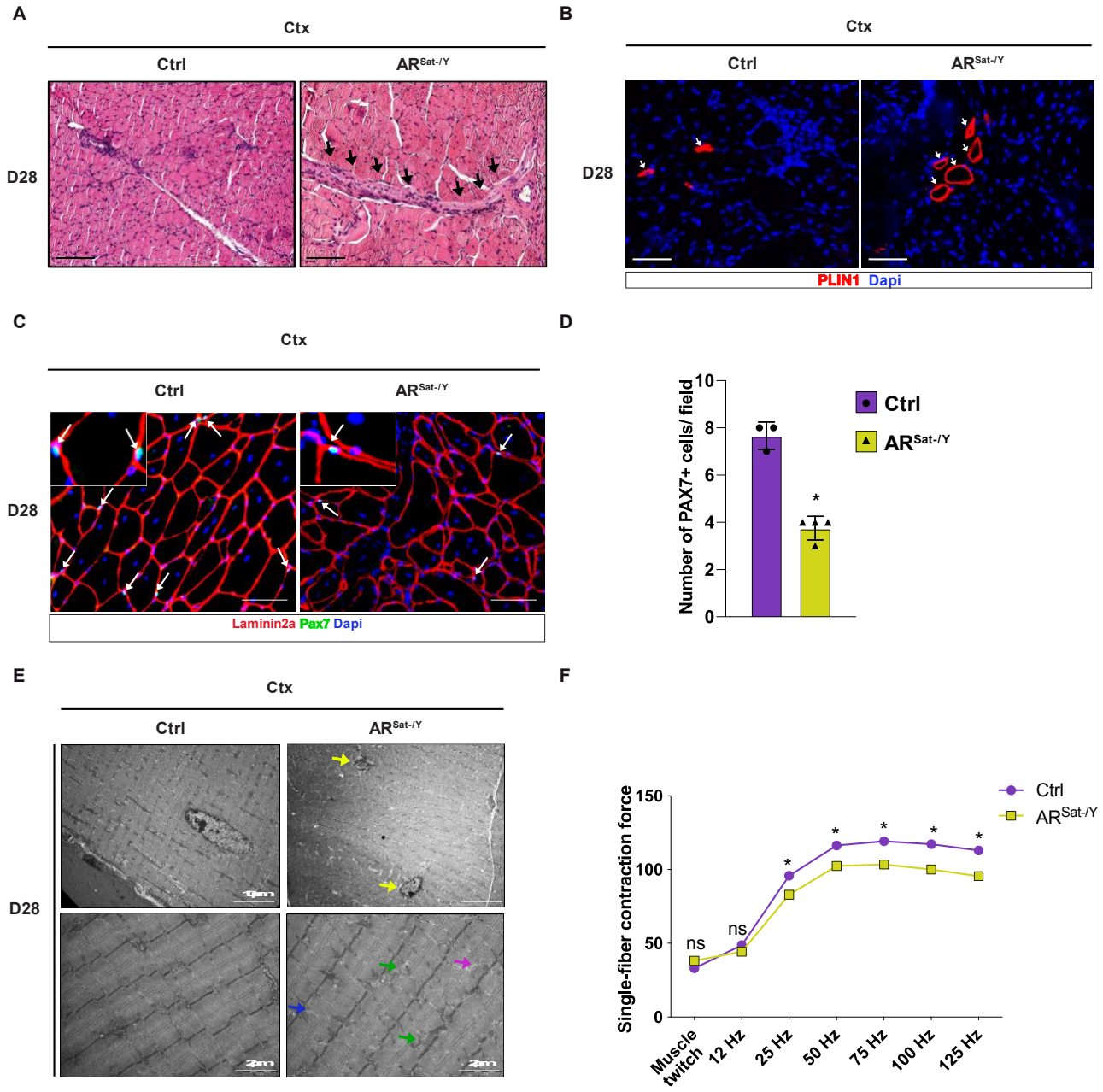

Figure 6: AR ablation in SatC impacts terminal muscle regeneration phase. A. *H&E staining of TA sections of control (Ctrl) and AR$^{Sat-/Y}$ mice at D28. Black arrows point at infiltration. Scale bar = 100 µm.* ***B.*** *Immunofluorescent detection of perilipin (PLIN1, red) on TA sections from control (Ctrl) and AR$^{Sat-/Y}$ mice at D28. Nuclei were stained with DAPI. White arrows point at PLIN1+ lipid droplets. Scale bar = 25 µm.* ***C.*** *Immunofluorescent detection of PAX7 and Laminin–α2 (LAMA2) on TA sections from control (Ctrl) and AR$^{Sat-/Y}$ mice at D28. Nuclei were stained with DAPI. White arrows point at PAX7+ nuclei. Scale bar = 25 µm.* ***D.*** *Quantification of PAX7+ cells per field, n=3-4 control and mutant mice. 3 fields were counted per animal.* ***E.*** *Ultrastructural analysis of TA of control (Ctrl) and AR$^{Sat-/Y}$ mice at D28. Yellow, green, blue and magenta arrows show necrotic nuclei, misorientation of sarcomeres, unparalleled T-tubules to the Z-line, and oblique triad structure. Scale bars: upper panel = 10 µm, lower panel = 2 µm.* ***F.*** *In situ single-fiber isometric force of TA from control (Ctrl) and AR$^{Sat-/Y}$ mice at D28 after a series of stimulation frequencies from 12 to 125 Hz, n = 6–7,*

*respectively. Quantitative data presented as mean ± SEM; Student's t-test: *p< 0.05 and ns, not significant.*

Loss of AR in SatC impairs their proliferative capacities and myofiber formation upon a second muscle injury

Since at the final stage of the regeneration process, we noticed a significant decrease in SatC number in $AR^{Sat-/Y}$ TA muscles compared to control, we questioned whether the remaining stem cells are capable to efficiently sustain a second round of muscle regeneration. To this end, we experimentally induced a second injury with Ctx injection in TA muscles of $AR^{Sat-/Y}$ and control mice at D28 and harvested these tissues 7 days after the second injection (hereafter D28+7). Histological analysis via H&E staining showed that whereas control muscles at D28+7 exhibited a more advanced regeneration pattern at D7 **(Fig. 7A and 3C),** $AR^{Sat-/Y}$ TA muscles at D28+7 exhibited similar histological pattern than at D7, characterized by cellular infiltration **(Fig. 7A, green arrows)** and misshaped myofibers **(Fig. 7A, blue arrows)**. DMD detection at D28+7 confirmed the dystrophic characteristics of $AR^{Sat-/Y}$ TA muscles manifested by misshaped fibers and the augmentation of the proportion of small fibers compared to average ones **(Fig. 7B)**. Moreover, the number of $PAX7^{+}$ cells was 60 % lower in $AR^{Sat-/Y}$ compared to control muscles **(Fig. 7B-C)**. Interestingly, we noticed that the phenotype generated after inducing a second injury (D28+7) recapitulates the one from (D7) regarding the number of SatC and myofiber structure **(Fig. 7C)**. Moreover, KI67 detection along with PAX7 showed that SatC of $AR^{Sat-/Y}$ were not proliferative at D28+7, while the majority of those of control were PAX7+/KI67+ **(Fig. 7D)**.

Thus, after a second round of injury, the healing process is accelerated in control muscles, but not in mutant ones in which SatC proliferation is further affected.

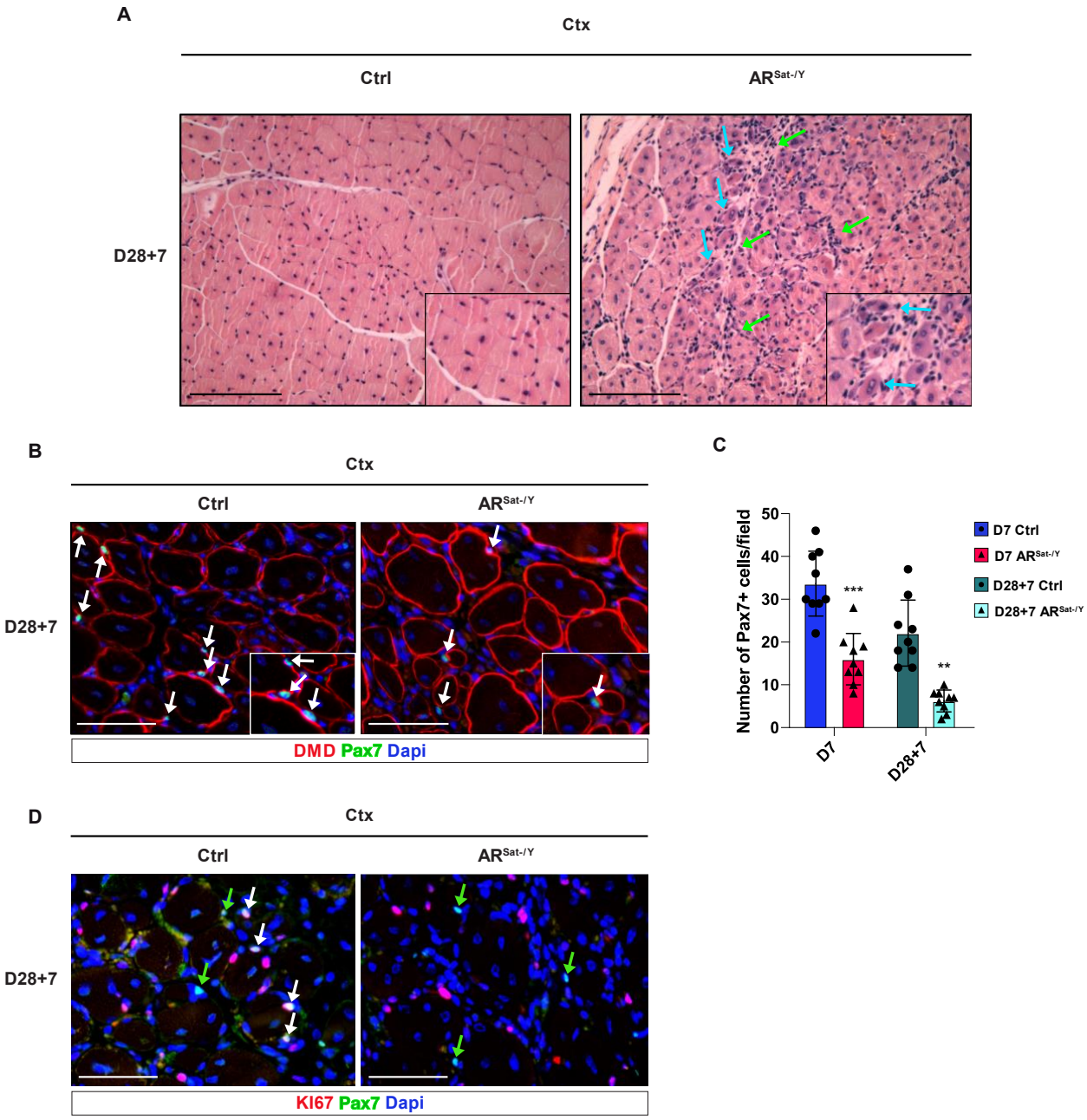

Figure 7: **Number and quality restored after injury permit to survive a second muscle damage.** ***A.*** *H&E staining on tibialis muscle sections of control (Ctrl) and $AR^{Sat-/Y}$ mice at D28+7 timepoint. Blue and green arrows point at infiltration and misshaped regenerating fiber. Scale bar = 100 µm.* ***B.*** *Immunofluorescent detection of PAX7 and Laminin−α2 (LAMA2) on TA sections from control (Ctrl) and $AR^{Sat-/Y}$ mice at D28+7 timepoint. Nuclei were stained with DAPI. White arrows point at PAX7+ nuclei. Scale bar = 25 µm.* ***C.*** *Quantification of PAX7+ cells per field, n=3, 4 control and mutant mice, respectively, and 3 fields were counted per animal.* ***D.*** *Immunofluorescent detection of PAX7 and KI67 on tibialis muscle sections from control (Ctrl) and $AR^{Sat-/Y}$ mice at D28. Nuclei were stained with DAPI. White and green arrows point at PAX7+/KI67+ and PAX7+/KI67- nuclei, respectively. Scale bar = 50 µm. Quantitative data are presented as mean ± SEM; Student's t-test: **p< 0.01, ***p<0.001 and ****p<0.0001, ns, not significant.*

Discussion

In this study, we analyzed endogenous androgens effects, mediated by their receptor, on satellite cells (SatC) and skeletal muscle healing capacity after injury. We show that androgens not only maintain the anatomical integrity of the healthy male muscles as reported[22], but also underpin molecular pathways that maintain its stem cell's niche, modulate its regeneration, and influence its physiological functions after healing.

To determine the role of AR in SatC under physiological conditions, we first compared the histology and structure of TA muscles and stem cell niche anatomy from control and $AR^{Sat-/Y}$ mice. Our results show that whilst muscle fibers exhibited no histological defects in the absence of AR in SatC, stem cell niche anatomy was affected. The most striking abnormality that we highlighted, and that has not yet to our knowledge been described, is the disruption of the standard anatomical position of AR-deficient SatC. Interestingly, Our CUT&RUN analysis performed on dormant FACS-isolated SatC uncovered more than 7000 AR binding sites, mainly located at intergenic regions, that coordinate the expression of major transcription factors involved in quiescence, such as *Pax7*, *Myf5*, *Myod1*, *Myog*, *Cxcr4*, *Itgb1* as well as *Klf7*. *Klf7* was shown to act under the Notch signaling to guard SatC in a quiescent state[20]. Moreover, *Itgb1* was reported to be crucial for SatC dormancy and proliferation after activation[24]. Indeed, *Itgb1* deficient SatC exit their quiescence and enter symmetric differentiation, which eventually leads to the exhaustion of the stem cell population.

Importantly, we unraveled a putative cooperation between AR and PAX7 to control the expression of various genes implicated in cell junctions, including laminin and cell differentiation like Bmp and Wnt signaling. AR deficiency in SatC leads to stemness potential impairment combined to loss of mechanical anchoring to the basal lamina impacting niche integrity. Corrupted SatC quit their compartment and fuse with adjacent muscle fiber beyond the DMD layer. This phenomenon was previously observed in M-cad knock-out SatC mouse model, in which the authors demonstrated DMD lacking SatC niche fusing with fiber[18].

Despite the large number of analyses describing the role of androgens in skeletal muscle recovery after injury, a comprehensive picture of the molecular determinants that confer AR's specificity of action in SatC remains blurry. To unravel the impact of AR ablation in SatC during various levels of skeletal muscle regeneration after acute injury, we compared the histology and structure of control and $AR^{Sat-/Y}$ TA muscles 3, 5, 7, and 28 days after injury. Our results show that the organization of the necrotic area and histology of damaged muscles

are similar in control and mutant mice 3 days after injury (D3). Noteworthy, at D3 we did not observe any emerging myofibers in the injured area, which could explain the histological similarities between the two genotypes. From day 5 (D5) to 28 (D28), our results revealed a distinguishable phenotype in $AR^{Sat-/Y}$ TA muscles. Although regenerative marks such as decreasing in the interstitial space and the emergence of newly formed myofibers were portrayed, the histology of the newly emerging skeletal muscle 5, 7 and 28 days after injury indicates that muscle regeneration mechanisms that normally maintain and/or repair muscle tissue are severely perturbed in $AR^{Sat-/Y}$ mice.

Given SatC chief role in modulating the healing progression, we investigated the kinetics of their proliferation and commitment to the myogenic lineage, 5 and 7 days after injury. Our analysis showed that proliferation and primary steps of SatC differentiation in mutant mice were not similar to controls, suggesting that the initial of $AR^{Sat-/Y}$ skeletal muscles are impacted. This indicates that AR in SatC modulates their cell specific functions and regulates the expression of specific gene networks implicated either in their cell cycle or in their differentiation capacities. Intriguingly, we noticed that whilst control muscles harbored similar number of SatC at D5 and D7, mutant ones lost at D7 up to 60 % of the SatC that they initially contained at D5.

Evano et al., demonstrated that SatC rather undergo symmetric division and asymmetric division at D3 and D5 of muscle regeneration, respectively[25]. Interestingly, we observed similar number of SatC at D5 between mutant and control muscles, that is the outcome of events taking place at D3, indicating that the recruitment and symmetric division of these cells are not impaired at this stage. However, we noticed a significant decline in SatC number at D7, referring that the self-renewing asymmetric division, initially occurring at D5, might be compromised. In addition, our data revealed that SatC of $AR^{Sat-/Y}$ mutant muscles cannot sustain proliferation and rather undergo myogenic differentiation to generate MYOG-expressing myocytes. In the long run defects in SatC self-renewal led to decline of SatC number, which was confirmed by histological analysis followed by quantification of PAX7-expressing cell number at D28. Using an integrative approach combining cistromic and transcriptomic analysis, we identified gene networks involved in various cell functions that are directly regulated by AR in SatC at D7, including cell cycle (e.g., *Cdk1-2-4-6*, *Myc*, *E2f1-2*), ECM-receptor interaction (e.g. *Col1a1-2*, *Lama2-4*, *Tnc*), and regulation of actin cytoskeleton (e.g. *Actb*, *Cxcr4*, *Itga5*). Importantly, our cutting-edge cistrome data unveiled a major re-allocation of AR binding sites when SatC shift from quiescent to activated state. Of note, about

6 % of AR target genes were conserved that were associated with genes like *Ar*, *Cxcr4*, *Klf9* and *Lamac2*. Intriguingly, ARE was more conserved in activated SatC than in quiescent ones. In activated SatC, we found 5500 DNA segments on which AR bound to its AREs controlling various pathways required for myogenesis (*Cxcr4*, *Klf9* and *Lamc2).*

In addition, DMD and LAMA2 labeling and ultrastructural analysis revealed emerging myofibers harboring misshaped cytoskeletons and malformed sarcomeres in $AR^{Sat-/Y}$, with lower CSA mean to those of control mice, which led us to question the contractibility of these muscles. To this end, we examined maximal tetanic force of isolated regenerative single fibers in response to stimulation frequencies which was significantly lower in TA of mutant mice than of control littermates at the final stages of the regeneration process (D28).

Interestingly, when inducing a second injury in TA muscles, we noticed an amplified proliferation defects in SatC of $AR^{Sat-/Y}$ muscles. Nevertheless, we observed striking histology of control muscles which were better than those of D7, indicating that SatC at the injured site where already on alert state (G-alert), which led them to enter activation and regenerate fibers even faster than when we induced single injury. SatC in G-alert were already described in the literature as a state of minor activation that muscle stem cells keep after recent injury[26].

Not only fiber proprieties were affected, but muscle microenvironment was also influenced by AR ablation in SatC. Indeed, our flow cytometry analysis showed an increase in immune natural killer cells and a decrease in macrophages and FAPs in $AR^{Sat-/Y}$ mice muscles when compared to controls, which indicates a strong influence of AR in SatC to re-arrange muscle microenvironment during muscle healing. Many of these cell populations were shown to play important roles in SatC activation and myogenic potential, like macrophages[27], FAPs[28,29], and natural killers[30].

Previously, Dubois et al. aimed at unravelling the role of AR in SatC and their progeny during muscle formation; however, contrarily to our study, they induced AR ablation during embryonic development and studied the outcome in 12-week-old mice (in adulthood). In our analysis, we induce AR knock-out in adulthood and study muscle regeneration capacity upon injury. In agreement with Dubois et al., our data showed reduced CSA and force contractile defects of newly emerging myofibers in $AR^{Sat-/Y}$ mice compared to control. However, we did not observe impaired muscle mass in mutant mice compared to control, which might be due to the injury site that covers only a third of the TA muscle. In addition, Dubois et al., reported that myostatin levels were decreased after AR ablation in skeletal muscles. Our transcriptomic

data showed that myostatin transcript level increases in mutant TA muscles compared to control littermates. Although, since we performed our analysis in total muscle tissue, we cannot discriminate whether this augmentation occurs in the regenerative fibers, SatC or another cell type.

Taken together, in this study, we show that androgen signaling is essential for niche integrity and that AR directly controls the expression of key genes involved in SatC quiescence. Upon muscle damage, AR is reallocated to new sites to stimulate the expression of genes supporting cell proliferation, myogenesis, and myoblast fusion. It also supports the reconstitution of the stem cell population by promoting the asymmetric division of cells that reside in G-alert status at the end of the regeneration process.

Materials and methods

Mice

Mice were maintained in a temperature- and humidity-controlled animal facility, with a 12-hours light/dark cycle. Water and standard rodent chow (2800 kcal/kg, Usine d'Alimentation Rationelle, Villemoisson-sur-Orge, France) were provided *ad libitum*. Breeding and maintenance of mice were performed according to institutional guidelines. All experiments were done in an accredited animal house, in compliance with French and EU regulations on the use of laboratory animals for research. Intended manipulations were submitted to the Ethical committee (Com'Eth, Strasbourg, France) for approval and to the French Research Ministry for ethical evaluation and authorization according to the 2010/63/EU directive (APAFIS #22281). Animals were killed by cervical dislocation, and tissues were immediately collected, weighed, and frozen in liquid nitrogen or processed for biochemical and histological analysis.

Generation of $AR^{Sat-/Y}$ mice

$AR^{L2/Y}$ mice[31] were intercrossed with Pax7-$CreER^{T2}$ mice that express the tamoxifen (Tam) dependent $CreER^{T2}$ recombinase, selectively in satellite cells[32] to generate control ($AR^{L2/Y}$) and Pax7-$CreER^{T2}$/$AR^{L2/Y}$ mice. Seven-week-old $AR^{L2/Y}$ male mice and sex-matched Pax7-$CreER^{T2}$/$AR^{L2/Y}$ littermates were intraperitoneally injected with Tam (1 mg/mouse/day) for five days to generate control and $AR^{Sat-/Y}$ mutant mice, respectively. All mice were on a C57/Bl6J background. Primers used for genotyping are listed in **Table 1**.

Muscle injury and sample processing

Seven days after Tam treatment, tibialis anterior muscles (TA) were injected with 50 µl of cardiotoxin (0.06 mg/ml) from Naja mossambica snake (Latoxan laboratory, Ref: L8102) using a Hamilton precision syringe. 0, 3 ,5, 7, 14 and 28 days after injection, TA muscles were dissected and either snap frozen in liquid nitrogen for molecular analyses or processed for histological analyses by immersion in nitrogen-chilled isopentane (Sigma) and kept at −80 °C, or fixation overnight in 4% paraformaldehyde. Frozen muscles were sectioned with cryostat (Leica CM1520) to prepare frozen sections (10 µm) that were used for immunostaining. Fixed tissues were cut with microtome (Leica RM, 2145, 0737/09.1998) to make paraffin sections (5 µm), which were stained with Haematoxylin and Eosin (H&E, Surgipath), Gomori's one-step trichrome staining kit (Polysciences) or used for immunostaining.

Immunostaining on cells and frozen sections

Cells or frozen muscle sections (10 µm) were fixed for 10 min in 4% paraformaldehyde, permeabilized with 0.1% Triton-X-100 (Sigma)/PBS for 15 min at room temperature (RT), rinsed with wash buffer (0.05% Triton-X 100/PBS), treated with blocking buffer [5% fetal calf Serum (Genetex)] for 1 – 2h at RT, before incubation with primary antibodies diluted in 0.1% Triton-X-100 (Sigma)/PBS overnight at 4 °C. Primary antibodies against following antigens were diluted as follows: Pax7 (Rabbit; thermo fisher, Ref: PA1-117, 1:400); Pax7 (Mouse; DSHB, Ref: AB_528428, 1:50), Myod1 (Cell signaling, Ref: D8G3, 1:200); laminin 2a (sigma aldrich, Ref: L0663-.1ML, 1:500); Dystrophin (sigma, Ref: D8168, 1:400); eMyHC (DSHB, Ref: F1.652, 1:20); Myf5 (R&D systems, Ref: MAB4027 1:400), Ki67 (R&D systems, Ref: 14-5698-82, 1:500) ; M-cadherin (bioreagent, Ref: orb101714, 1:400). Mouse, rat or rabbit IgGs were used as controls. Cells or muscle sections were rinsed with wash buffer, and incubated with appropriate Alexa-Fluor-conjugated secondary antibodies (1:1000, Invitrogen) with different fluorescent wavelengths (488, 555 or 647 nm) in permeabilization buffer for 45 min at RT. After wash, slides were then mounted with Fluoromount-G contaning Dapi (Invitrogen, Ref: 00-4959-52) and coverslips (VWR).

Immunostaining on paraffin sections

5 µm paraffin sections were deparaffinized (histosol 2x 10 min, 100 % ethanol x2 5 min, 70 % ethanol x2 5 min) and rehydrated (water 5 min), and antigen retrieval was performed by boiling the samples for 20 min in tris-hydroxymethyl-aminomethane (Tris buffer) of pH 9. Sections were blocked for 1 h (PBS with 0.1% Tween 20 and 5% FCS) and incubated overnight at 4 °C with primary antibodies directed against: AR (abcam, Ref: ab108341, 1:500); Pax7 (Rabbit; thermo fisher, Ref: PA1-117, 1:400); Pax7 (Mouse; DSHB, Ref: AB_528428, 1:50); Myogenin (abcam, Ref: ab1835, 1:400); alpha-actinin (abcam, Ref: ab9465, 1:400); Dystrophin (IGBMC, 1:1000), Ki67 (R&D systems, Ref: 14-5698-82, 1:500). Slides were rinsed with wash buffer and incubated with appropriate Alexa-Fluor-conjugated secondary antibodies (1:1000, Invitrogen) with various fluorescent wavelengths (488, 555 or 647 nm) in permeabilization buffer for 45 min at RT. After wash, slides were mounted with Fluoromount-G containing Dapi (Invitrogen, Ref: 00-4959-52) and coverslips (VWR).

Ultrastructural analysis of muscle sections

Tibialis muscle samples of 1 mm^2 were fixed by immersion in 2.5 % glutaraldehyde and 2.5 % paraformaldehyde in cacodylate buffer (0.1 M, pH 7.4), washed in cacodylate buffer for 30 minutes and kept at 4 °C. Post-fixation was performed with 1 % osmium tetraoxide in 0.1 M cacodylate buffer for 1h at 4 °C and dehydration through graded alcohol (50, 70, 90 and 100 %) and propylene oxide for 30 minutes each. Samples were oriented longitudinally or transversally and embedded in Epon 812. Ultrathin sections were cut at 70 nm and contrasted with uranyl acetate and lead citrate and examined at 70 kV with a Morgagni 268D electron microscope. Images were captured digitally by a Mega View III camera (Soft Imaging System).

FACS sorting of satellite cells

FACS sorting of satellite cells was performed as described[33]. In brief, hind limb muscles were dissected from wild-type and $AR^{Sat-/Y}$ mice, minced into small pieces, digested with 1,25 U/ml Dispase II (Stemcell technologies, Cat:07913) and 500 µg/ml Collagenase, Type I, powder (ThermoFisher scientific, Ref: 17018029), and filtered through 100 µm, 70 µm, and 40 µm cell strainers (Corning Life Sciences). After centrifuge at 400 g for 5 minutes, cell pellets were collected and resuspended in FACS buffer (DMEM w/o phenol red, 4,5 glucose g/l, 2% BSA, 2 mM EDTA). Immunofluorescence was performed using fluorescence-coupled primary antibodies directed against: CD11b PE-Cy7 (eBioscience, 25-0112-82, 1:100), CD45 PE (eBioscience, 12-0451-83, 1:100), CD31 PE (eBioscience, 12-0311-82, 1:100), Integrin-α7 FITC (MBL, K0046-4, 1:50), CXCR4 APC (eBioscience, 17-9991-82, 1:100), and CD34 eFluor405 (eBioscience, 48-0341-82, 1:33). Cells were gated based on the forward scatter (FSC) and side scatter (SSC) parameters to exclude cellular debris and cell doublets. CD11b, CD45, and CD31 markers were used to exclude leukocytes and endothelial cells. CD11b/CD45/CD31-negative cells were further selected for the expression of CD34 and Integrin-α7 markers. Finally, double positive cells were gated for the expression of CXCR4. Sorted cells were proceeded for RNA extraction.

For microenvironment analysis, after muscle digestion and filtration, mono-nucleated cells were incubated with fluorescence-coupled primary antibodies directed against: CD45 Alexa eFluor700 (eBioscience, 56-0451-82, 1:100), CD31 PE (eBioscience, 12-0311-82, 1:100), SCA-1 PE-Cy7 (eBioscience, 25-5981-82, 1:100), and Integrin-α7 (ITGA7) FITC (MBL, K0046-4, 1:50). Cells were gated based on the forward scatter (FSC) and side scatter (SSC) parameters to exclude

cellular debris and cell doublets. CD45-positive and CD31-positive cells were chosen to count immune and endothelial cells, respectively. After eliminating CD45 and CD31expressing populations, SCA1-positive cells were selected to analyze fibro-adipogenic progenitor cells (FAPs). Finally, SCA1-negative and ITGA7-positive cells were gated as satellite cells.

Cut&Run analysis on FACS sorted satellite cells

Cut&Run was performed as described (Janssens and Henikoff, 2019). Briefly, FACS sorted satellite cells were centrifuged for 10 min at 500 g. After discarding the solution, cell pellet was incubated with nuclear extraction buffer for 20 min on ice. Nuclei were washed and incubated with Concanavalin beads (BioMag Plus Concanavalin A, Cat: 86057-3) for 10 min at 4 °C. After washing, nuclei/beads complexes were incubated with primary antibodies [anti-AR (abcam, Ref: ab108341, 1:100), anti-H3K4me2 (1:100) or H3K27ac (1:100)] over-night at 4 °C with gentle agitation. Nuclei/beads complexes were precipitated and incubated with protein A-micrococcal nuclease (pA-MN-IGBMC) for 1h at 4 °C with agitation. To initiate cleavage, 3 µl of 100 mM of $CaCl_2$ were added and the mix was incubated 30 min on ice. Reaction was ceased with a stop buffer (200 mM NaCl, 20 mM EDTA, 4 mM EGTA, 50 µg/ml RNaseA, 40 µg/ml glycogen, 25 pg/ml yeast spike-in DNA) and incubated for 20 min at 37°C. Samples were proceeded for DNA extraction.

Libraries were prepared from immunoprecipitated DNA as described [18,19] and sequenced with an Illumina Hiseq 4000 as single-end 50 bp reads. Reads overlapping with the ENCODE blacklist region (V2) were removed, the remaining reads were separated into 2 groups: fragment size <120 bp (without nucleosome, in general for transcription factors) and fragment size >150 bp (with nucleosomes, normally for histone markers), and mapped to the mm10 reference genome using Bowtie 2 (v2.3.4.3) [20]. Bigwig files were generated with bamCoverage (deeptools 3.3.0: bamCoverage --normalizeUsing RPKM --binSize 20). Uniquely mapped reads were retained for further analysis. Raw bedgraph files were generated with genomeCoverageBed (bedtools v2.26.0). SEACR 1.3 algorithm (stringent) was used for the peak calling with IgG-immunoprecipitated sample as control. The genome-wide intensity profiles were visualized using the IGV genome browser (http://software.broadinstitute.org/software/igv/) [21]. HOMER was used to annotate peaks and for motif searches [22]. Genomic features (promoter/TSS, 5' UTR, exon, intron, 3' UTR, TTS and intergenic regions) were defined and calculated using Refseq and HOMER according to the distance to the nearest TSS. Venn diagrams were generated with Venny [23]. Clustering analyses

were done with the seqMINER software (41), and clustering normalization was done with the K-Means linear option. Further bioinformatics analyses were performed with bedtools (https://bedtools.readthedocs.io/en/latest/index.html) [24]: fasta sequences were obtained from bed files with GetFastaBed, location intersections were performed with Intersect interval and Multiple intersect, and gene centric analyses of peak distribution were performed with WindowBed. Bioinformatics parameters: Parameters were set as default.

Cell culture

LHCN-M2 myoblast cells were a kind gift from Laporte laboratory at IGBMC. Cells were cultured in DMEM (4,5 g/l glucose, 20% FCS, 20 µg/l gentamicin). After reaching 70 % confluency, cells were treated with a vehicle (0,001 % Ethanol) or 100 nM of DHT (Sigma, Ref: A8380-1G). 24 h after treatment, cells were fixed with 4 % PFA for 10 min at RT, then processed for IF as described previously.

DNA Extraction by Phenol/Chloroform

Tail samples were digested overnight at 55 °C in a solution containing 25 µl Proteinase K (20 mg/ml) and 500 µl Digestion Buffer (100 mM NaCl, 10 mM Tris-HCl pH 8, 25 mM EDTA pH 8, 0.5% SDS, Viagen Biotech, CA90010). 1 ml of Phenol/Chloroform (1:1) was added to each sample, and tubes were mixed by back inversing. Phases were then separated by spinning for 5 min at 11000 g. The upper phase was transferred into a new tube to which 200 µl of chloroform were added. Tubes were vortexed and centrifuged for 5 min at 11000 g. To precipitate DNA, 2 volumes of 100% ethanol were added to the upper phase, and tubes were centrifuged for 5 min at 11000 g. For washing, 100% ethanol was eliminated, and 1 volume of 70% ethanol was added. DNA pellets, obtained after another 5-min centrifugation at 11000 g, were resuspended in 150 µl of sterile water. DNA concentrations were measured with a Nanodrop (Thermoscientific, Nanodrope 2000c). DNA was stored at 4°C.

PCR Analysis and Agarose Gel Electrophoresis

Polymerase Chain Reaction (PCR) was performed using PCR Hot-Start II Invitrogen™ Platinum™ kit (Thermo Scientific™ F140WH, 15183133) in 96 well-plates (Applied biosystems). For each DNA sample (2 µl), 24.1 µl water, 3 µl (10×) PCR Buffer (Invitrogen, 14000013), 0.3 µl deoxynucleotide triphosphate (dNTP) (Invitrogen, R72501), 0.1 µl of forward primer (100 µM), 0.1 µl of reverse primer (100 µM) and 0.5 µl of DNA Taq Polymerase (Invitrogen, 15966005)

were added. Primers are described in Table 1. The PCR plate was processed in a Thermal Cycler (SimpliAmp Thermal Cycler Roche A37834) with the following program: Activation: 95°C for 1.5 min; Amplification: 95°C for 30 s, 55°C for 30 s, 72°C for 30 s for 35 cycles; Elongation: 72°C for 7 min; Cooling: 4°C for 30 s. For visualization of PCR amplification, a 2% agarose gel was prepared by mixing 8 g of agarose and to 400 ml of Tris-Acetate-EDTA (TAE) buffer (40 mM Tris-acetate, 1 mM EDTA). The flask was heated in the microwave for 5-6 min. After a 15-min cooling, 20 µl of Ethidium Bromide (Euromedex, EU0070) (0.5 µg/ml) were added to the melted agarose and poured into a gel tray to polymerize. After 1 h, the gel tray was placed in a migration chamber in 1× TAE. 6 µl of DNA gel loading dye (6×) (10 mM Tris-HCl (pH 7.6), 0.03 % bromophenol blue, 0.03 % xylene cyanol FF, 60 % glycerol, 60 mM EDTA) were added to the DNA samples. 15 µl of each DNA sample were loaded in each well. 10 µl of the DNA size marker (Invitrogen, 15628019) were loaded along with experimental samples. The gel was run at 200 V, 400 mA for 45 min. When electrophoresis had completed, gel photos were taken under UV light.

RNA extraction

Muscles were homogenized in TRIzol reagent (Life Technologies, Darmstadt, Germany), 1 ml TRIzol/150 mg of muscle tissue. RNA was isolated using a standard phenol/chloroform extraction protocol, and quantified by spectrophotometry (Nanodrop, Thermo Fisher). Quantitative PCR was prepared by reverse transcription of 2 µg of total RNA using SuperScript IV (Life Technologies) and oligo(dT) primers according to the supplier's protocol. cDNA was diluted hundred times and quantitative PCR was performed with a Lightcycler 480 II (Roche) using the SYBR® Green PCR kit (Roche) according to the supplier's protocol (2 µl cDNA, 4.8 µl water, 5 µl Syber Green 2x mix and 0.2 µl of 100 µM primer mix). Primers are described in **Table 2**. TBP, 36b4 and 18S were used as internal controls. Data were analyzed using the standard curve[34] and ΔΔCt[35] methods. Primer efficiency was calculated as Eff = 100*10^((-1/The Slope Value)-1). As similar data were obtained with the various analyses, results obtained with 36b4 and the standard curve method are presented.

For RNA-seq, RNA integrity was confirmed by Bioanalyzer, cDNA library prepared, and sequenced by the standard Illumina protocol (HiSeq 4000, single-end, 50 bp) following the manufacturer's instructions. Image analysis and base calling were performed using RTA 2.7.7 and bcl2fastq 2.17.1.14. Adapter dimer reads were removed using DimerRemover. FastQC 0.11.2 (http://www.bioinformatics.babraham.ac.uk/projects/fastqc/) was used to evaluate the quality of

the sequencing. Reads were mapped to the mouse mm10 genome (NCBI Build 38) using Bowtie2 2.3.4.3 (http://bowtie-bio.sourceforge.net/bowtie2/index.shtml/). Only uniquely aligned reads were retained for further analyses. Quantification of gene expression was performed using HTSeq 0.11.0. For comparison among datasets, the transcripts with more than 100 raw reads were considered. Differentially expressed genes (DEGs) were identified using the Bioconductor libraries EdgeR and DESeq (ref). A p-adj < 0.01 and a fold change excluding values between 0.77 and 1.3 were used as a threshold for DEGs that were further submitted for pathway analysis in WebGestalt using the Over-Representation Analysis (ORA) method and a significant level of FDR < 0.05. Heatmaps were generated by centering and normalizing expression values with Cluster 3.0 and importing them to MultiExperiment Viewer (MeV, http://mev.tm4.org/#/welcome) (ref). Genes were clustered according to the hierarchical method (HCL clustering) using gene tree, the Pearson correlation and average linkage.

Contractile Measurements

In situ isometric tibialis anterior muscle force in response to nerve stimulation was performed as described[36], and muscle masses were measured to calculate specific maximal force. Specific maximal tetanic force (mN/mm^5) was calculated by dividing the force by the estimated cross-sectional area of the muscle. Assuming muscles have a cylindrical shape and a density of 1.06 mg mm−3, the muscle cross-sectional area corresponds to the wet weight of the muscle divided by its fiber length (Lf). L0 is the fiber length at which maximal tetanic force is observed. All data provided by the muscle lever were recorded and analyzed on a microcomputer, using the PowerLab/4SP system (AD Instruments).

Acknowledgments:

We are grateful to Mohamed AbouElmaaty, Daniela Rovito, and Sirine Souali-Crispo for their great scientific feedback. We thank Anastasia Bannwarth for providing excellent technical assistance. We thank Valerie Schreiber for sharing her Cut&Run experience and for providing the pA-MN restriction enzyme. We thank the IGBMC animal house facility, the cell culture, the Mouse Clinical Institute (ICS, Illkirch, France), the imaging, the electron microscopy, the flow cytometry, and the GenomEast platform, a member of the ‘France Génomique’ consortium (ANR-10-INBS-0009).

Table 1

Gene	**Forward**	**Reverse**
Cre	5’ TTCCCGCAGAACCTGAAGATGTTCG 3’	5’ GGGTGTTATAAGCAATCCCCAGAAATGC 3’
ARL2	5’ CTGGTTGCTAAGGGACTTCGG 3’	5’ GCCCACACAAACAGTCAGCCCA 3’
ARL-(1)	5’ CTGGTTGCTAAGGGACTTCGG 3’	5’ GCCCACACAAACAGTCAGCCCA 3’
ARL-(2)	5’ TGTTTTCACTGTCACTGCAGC 3’	5’ GCCCACACAAACAGTCAGCCCA 3’

Table 2

Gene	**Forward**	**Reverse**
Pax7	5’ TAAGAGAGAGAACCCCGGGA 3’	5’ GATGCCATCGATGCTGTGTT 3’
CD34	5’ GCACAGAACTTCCCAGCAAA 3’	5’ AGCAGAACTCCAGAGGTGAC 3’
Cxcr4	5’ GTAGAGCGAGTGTTGCCATG 3’	5’ TGAAGTAGATGGTGGGCAGG 3’
Klf7	5’ AGTGAGTTTGCGTTCCCCTT 3’	5’ AGGGGACTTCACGGGAGTAA 3’
Itgb1	5’ GGACGCTGCGAAAAGATGAA 3’	5’ CCACAATTTGGCCCTGCTTG 3’
Myf5	5’ TCTGACGGCATGCCTGAAT 3’	5’ CTCGGATGGCTCTGTAGACG 3’
AR	5’ CTGCCTCCGAAGTGTGGTAT 3’	5’ GCCAGAAGCTTCATCTCCAC 3’
Myod1	5’ AGCACTACAGTGGCGACTCA 3’	5’ GCTCCACTATGCTGGACAGG 3’
Myogenin	5’ CACCCTGCTCAACCCCAAC 3’	5’ CAGCCCCACTTAAAAGCCC 3’
36b4	5’ AGATTCGGGATATGCTGTTGG 3’	5’ AAAGCCTGGAAGAAGGAGGTC 3’
Cd9	5’ TTGTCGAGTCCCTTCTGTCC 3’	5’ TCTGAGAGTCGAATCGGAGC 3’
Cd81	5’ GTCTGCTGGGGACGTTCT 3’	5’ TGCTTCACATCCTTGGCGAT 3’
Dtnb	5’ ACAATGGCCTTAACACGCTG 3’	5’ AAACACGGTCAACTTGGGTG 3’
TBP	5’ GTCCCGTGGCTCTCTTATTCTC 3’	5’ ATATAATCCCAAGCGATTTGC 3’
18s	5’ TCGTCTTCGAAACTCCGACT 3’	5’ CGCGGTTCTATTTTGTTGGT 3’

References

1. Sartori R, Romanello V, Sandri M. Mechanisms of muscle atrophy and hypertrophy: implications in health and disease. *Nat Commun*. 2021;12(1):330. doi:10.1038/s41467-020-20123-1

2. Relaix F, Bencze M, Borok MJ, et al. Perspectives on skeletal muscle stem cells. *Nat Commun*. 2021;12(1):692. doi:10.1038/s41467-020-20760-6

3. Yamakawa H, Kusumoto D, Hashimoto H, Yuasa S. Stem Cell Aging in Skeletal Muscle Regeneration and Disease. *Int J Mol Sci*. 2020;21(5):1830. doi:10.3390/ijms21051830

4. Bentzinger CF, Wang YX, Rudnicki MA. Building Muscle: Molecular Regulation of Myogenesis. *Cold Spring Harb Perspect Biol*. 2012;4(2):a008342-a008342. doi:10.1101/cshperspect.a008342

5. Relaix F, Zammit PS. Satellite cells are essential for skeletal muscle regeneration: the cell on the edge returns centre stage. *Development*. 2012;139(16):2845-2856. doi:10.1242/dev.069088

6. Chen W, Datzkiw D, Rudnicki MA. Satellite cells in ageing: use it or lose it. *Open Biol*. 2020;10(5):200048. doi:10.1098/rsob.200048

7. Dumont NA, Bentzinger CF, Sincennes M, Rudnicki MA. Satellite Cells and Skeletal Muscle Regeneration. In: Terjung R, ed. *Comprehensive Physiology*. 1st ed. Wiley; 2015:1027-1059. doi:10.1002/cphy.c140068

8. Brun CE, Dumont NA. Déficits intrinsèques des cellules satellites dans la dystrophie musculaire de Duchenne. *médecine/sciences*. 2016;32(10):800-802. doi:10.1051/medsci/20163210003

9. Fang XB, Song ZB, Xie MS, Liu YM, Zhang WX. Synergistic effect of glucocorticoids and IGF-1 on myogenic differentiation through the Akt/GSK-3β pathway in C2C12 myoblasts. *Int J Neurosci*. 2020;130(11):1125-1135. doi:10.1080/00207454.2020.1730367

10. Chambon C, Duteil D, Vignaud A, et al. Myocytic androgen receptor controls the strength but not the mass of limb muscles. *Proc Natl Acad Sci*. 2010;107(32):14327-14332. doi:10.1073/pnas.1009536107

11. Kim JH, Han GC, Seo JY, et al. Sex hormones establish a reserve pool of adult muscle stem cells. *Nat Cell Biol*. 2016;18(9):930-940. doi:10.1038/ncb3401

12. Nnodim JO. Testosterone mediates satellite cell activation in denervated rat levator ani muscle. *Anat Rec*. 2001;263(1):19-24. doi:10.1002/ar.1072

13. Serra C, Tangherlini F, Rudy S, et al. Testosterone Improves the Regeneration of Old and Young Mouse Skeletal Muscle. *J Gerontol A Biol Sci Med Sci*. 2013;68(1):17-26. doi:10.1093/gerona/gls083

14. MacKrell JG, Yaden BC, Bullock H, et al. Molecular Targets of Androgen Signaling that Characterize Skeletal Muscle Recovery and Regeneration. *Nucl Recept Signal*. 2015;13(1):nrs.13005. doi:10.1621/nrs.13005

15. Sinha-Hikim I, Taylor WE, Gonzalez-Cadavid NF, Zheng W, Bhasin S. Androgen Receptor in Human Skeletal Muscle and Cultured Muscle Satellite Cells: Up-Regulation by Androgen Treatment. *J Clin Endocrinol Metab*. 2004;89(10):5245-5255. doi:10.1210/jc.2004-0084

16. Dubois V, Laurent MR, Sinnesael M, et al. A satellite cell-specific knockout of the androgen receptor reveals myostatin as a direct androgen target in skeletal muscle. *FASEB J*. 2014;28(7):2979-2994. doi:10.1096/fj.14-249748

17. Meers MP, Bryson TD, Henikoff JG, Henikoff S. Improved CUT&RUN chromatin profiling tools. *eLife*. 2019;8:e46314. doi:10.7554/eLife.46314

18. Park GH, Jeong H, Jeong MG, et al. Novel TAZ modulators enhance myogenic differentiation and muscle regeneration: Myogenic stimulation by novel TAZ modulators. *Br J Pharmacol*. 2014;171(17):4051-4061. doi:10.1111/bph.12755

19. Judson RN, Tremblay AM, Knopp P, et al. The Hippo pathway member Yap plays a key role in influencing fate decisions in muscle satellite cells. *J Cell Sci*. 2012;125(24):6009-6019. doi:10.1242/jcs.109546

20. Lilja KC, Zhang N, Magli A, et al. Pax7 remodels the chromatin landscape in skeletal muscle stem cells. Asakura A, ed. *PLOS ONE*. 2017;12(4):e0176190. doi:10.1371/journal.pone.0176190

21. Kalyuzhny AE. Combination of TUNEL Assay with Immunohistochemistry for Simultaneous Detection of DNA Fragmentation and Oxidative Cell Damage. In: Didenko VV, ed. *DNA Damage Detection In Situ, Ex Vivo, and In Vivo*. Vol 682. Methods in Molecular Biology. Humana Press; 2011:15-27. doi:10.1007/978-1-60327-409-8_2

22. Dalbo VJ, Roberts MD, Mobley CB, et al. Testosterone and trenbolone enanthate increase mature myostatin protein expression despite increasing skeletal muscle hypertrophy and satellite cell number in rodent muscle. *Andrologia*. 2017;49(3):e12622. doi:10.1111/and.12622

23. Wang X, Shen QW, Wang J, et al. KLF7 Regulates Satellite Cell Quiescence in Response to Extracellular Signaling. *Stem Cells*. 2016;34(5):1310-1320. doi:10.1002/stem.2346

24. Rozo M, Li L, Fan CM. Targeting β1-integrin signaling enhances regeneration in aged and dystrophic muscle in mice. *Nat Med*. 2016;22(8):889-896. doi:10.1038/nm.4116

25. Evano B, Khalilian S, Le Carrou G, Almouzni G, Tajbakhsh S. Dynamics of Asymmetric and Symmetric Divisions of Muscle Stem Cells In Vivo and on Artificial Niches. *Cell Rep*. 2020;30(10):3195-3206.e7. doi:10.1016/j.celrep.2020.01.097

26. Rodgers JT, King KY, Brett JO, et al. mTORC1 controls the adaptive transition of quiescent stem cells from G0 to GAlert. *Nature*. 2014;510(7505):393-396. doi:10.1038/nature13255

27. Loreti M, Sacco A. The jam session between muscle stem cells and the extracellular matrix in the tissue microenvironment. *Npj Regen Med*. 2022;7(1):16. doi:10.1038/s41536-022-00204-z

28. Joe AWB, Yi L, Natarajan A, et al. Muscle injury activates resident fibro/adipogenic progenitors that facilitate myogenesis. *Nat Cell Biol*. 2010;12(2):153-163. doi:10.1038/ncb2015

29. Biferali B, Proietti D, Mozzetta C, Madaro L. Fibro–Adipogenic Progenitors Cross-Talk in Skeletal Muscle: The Social Network. *Front Physiol*. 2019;10:1074. doi:10.3389/fphys.2019.01074

30. Larouche JA, Fraczek PM, Kurpiers SJ, et al. Neutrophil and natural killer cell imbalances prevent muscle stem cell–mediated regeneration following murine volumetric muscle loss. *Proc Natl Acad Sci*. 2022;119(15):e2111445119. doi:10.1073/pnas.2111445119

31. Shiina H, Matsumoto T, Sato T, et al. Premature ovarian failure in androgen receptor-deficient mice. *Proc Natl Acad Sci*. 2006;103(1):224-229. doi:10.1073/pnas.0506736102

32. Murphy MM, Lawson JA, Mathew SJ, Hutcheson DA, Kardon G. Satellite cells, connective tissue fibroblasts and their interactions are crucial for muscle regeneration. *Development*. 2011;138(17):3625-3637. doi:10.1242/dev.064162

33. Günther S, Kim J, Kostin S, Lepper C, Fan CM, Braun T. Myf5-Positive Satellite Cells Contribute to Pax7-Dependent Long-Term Maintenance of Adult Muscle Stem Cells. *Cell Stem Cell*. 2013;13(5):590-601. doi:10.1016/j.stem.2013.07.016

34. Larionov A, Krause A, Miller W. [No title found]. *BMC Bioinformatics*. 2005;6(1):62. doi:10.1186/1471-2105-6-62

35. Livak KJ, Schmittgen TD. Analysis of Relative Gene Expression Data Using Real-Time Quantitative PCR and the 2−ΔΔCT Method. *Methods*. 2001;25(4):402-408. doi:10.1006/meth.2001.1262

36. Lahoute C, Sotiropoulos A, Favier M, et al. Premature Aging in Skeletal Muscle Lacking Serum Response Factor. Andreu AL, ed. *PLoS ONE*. 2008;3(12):e3910. doi:10.1371/journal.pone.0003910

Supplementary data

Figure S1.

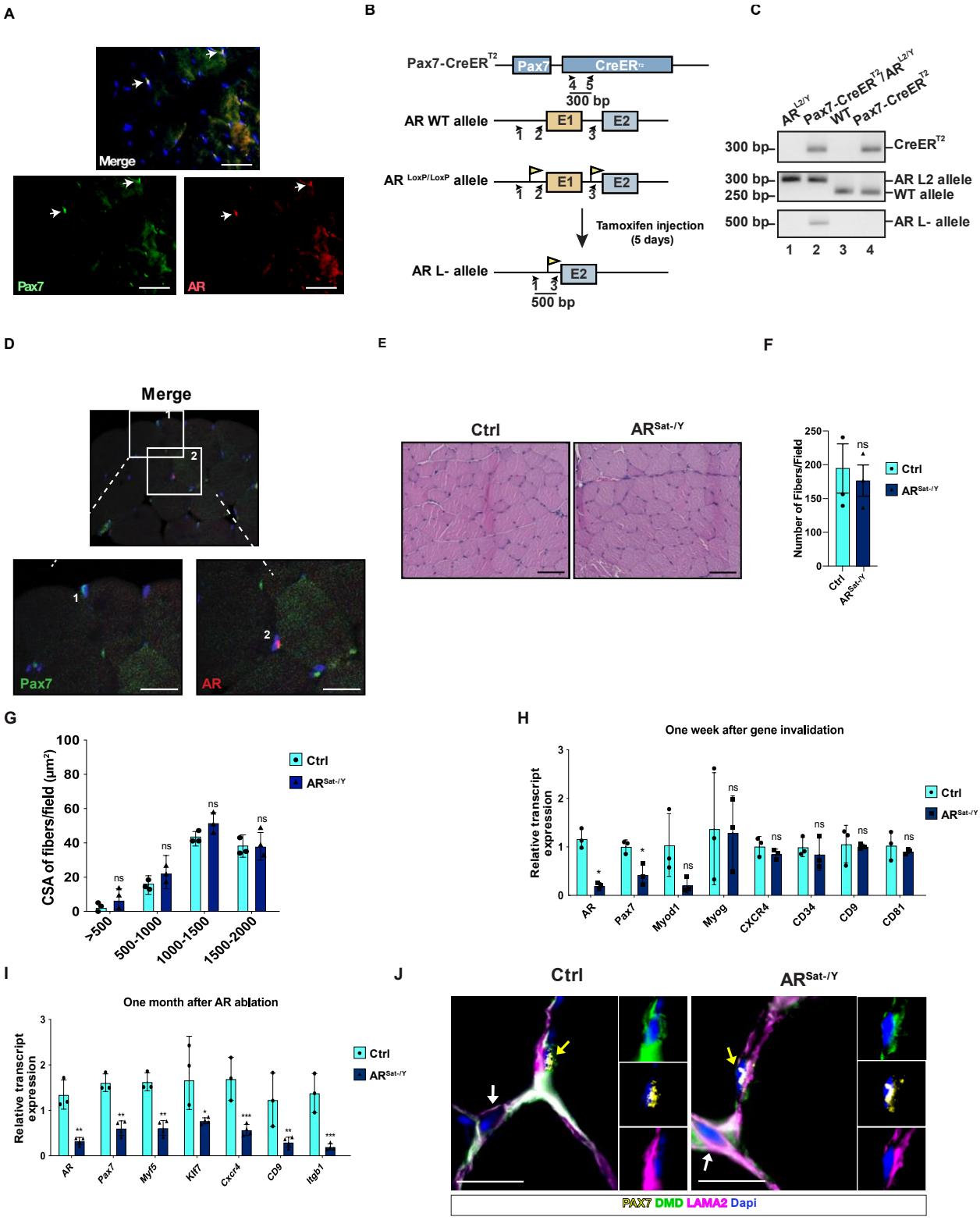

Figure S1: **AR controls satellite cell quiescence in physiological conditions**. ***A.*** *Immunofluorescent detection of androgen receptor (AR-red) and PAX7 (green) on tibialis muscle sections from control (Ctrl) mice one month after AR ablation. Nuclei were stained with DAPI. White arrows show cells co-expressing PAX7 and AR. Scale bar = 50 µm.* ***B.*** *Scheme depicting the generation of $AR^{Sat-/Y}$ mice.* ***C.*** *Polymerase chain reaction analysis performed on $AR^{L2/Y}$, Pax7-$CreER^{T2}$/ $AR^{L2/Y}$, Wild-Type (WT) and Pax7-$CreER^{T2}$ mice TA to identify $CreER^{T2}$, $AR^{L2/Y}$, WT and AR^{L-}alleles.* ***D.*** *Immunofluorescent detection of androgen receptor (AR)-red and PAX7-green on tibialis muscle sections from $AR^{Sat-/Y}$ mice one month after AR ablation. Nuclei were stained with DAPI. Scale bar 25 = µm.* ***E.*** *Hematoxylin and Eosin staining of tibialis muscle sections of control (Ctrl) and $AR^{Sat-/Y}$ mice one month after AR ablation. Scale bar = 50 µm.* ***F.*** *Quantification of number of muscle fibers per field. N=3 mice per group, 5 fields were analyzed per animal.* ***G.*** *Cross-sections area analysis of Laminin-α2-stained (LAMA2)-myofiber of tibialis muscle sections of control (Ctrl) and $AR^{Sat-/Y}$ mice one month after AR ablation. N=3 mice per group, 5 fields were analyzed per animal.* ***H.*** *Relative transcript levels of genes involved in satellite cell homeostasis in TA of control (Ctrl) and $AR^{Sat-/Y}$ mice one week after AR ablation. N=3 per group.* ***I.*** *Relative transcript levels of genes indispensable for satellite cell homeostasis in TA of control (Ctrl) and $AR^{Sat-/Y}$ mice (N= 3-4, respectively) one month after AR ablation.* ***J.*** *Immunofluorescent detection of PAX7, DMD and LAMA2 on tibialis muscle sections from control (Ctrl) and $AR^{Sat-/Y}$ mice one month after AR ablation. Nuclei were stained with DAPI. Yellow and white arrows point at PAX7-expressing cells and PAX7-negative nuclei, respectively. Scale bar = 25 µm. Quantitative data are presented as mean ± SEM; Student's t-test: *p< 0.05, **p< 0.01, ***p< 0.001 and ns, not significant.*

Figure S2.

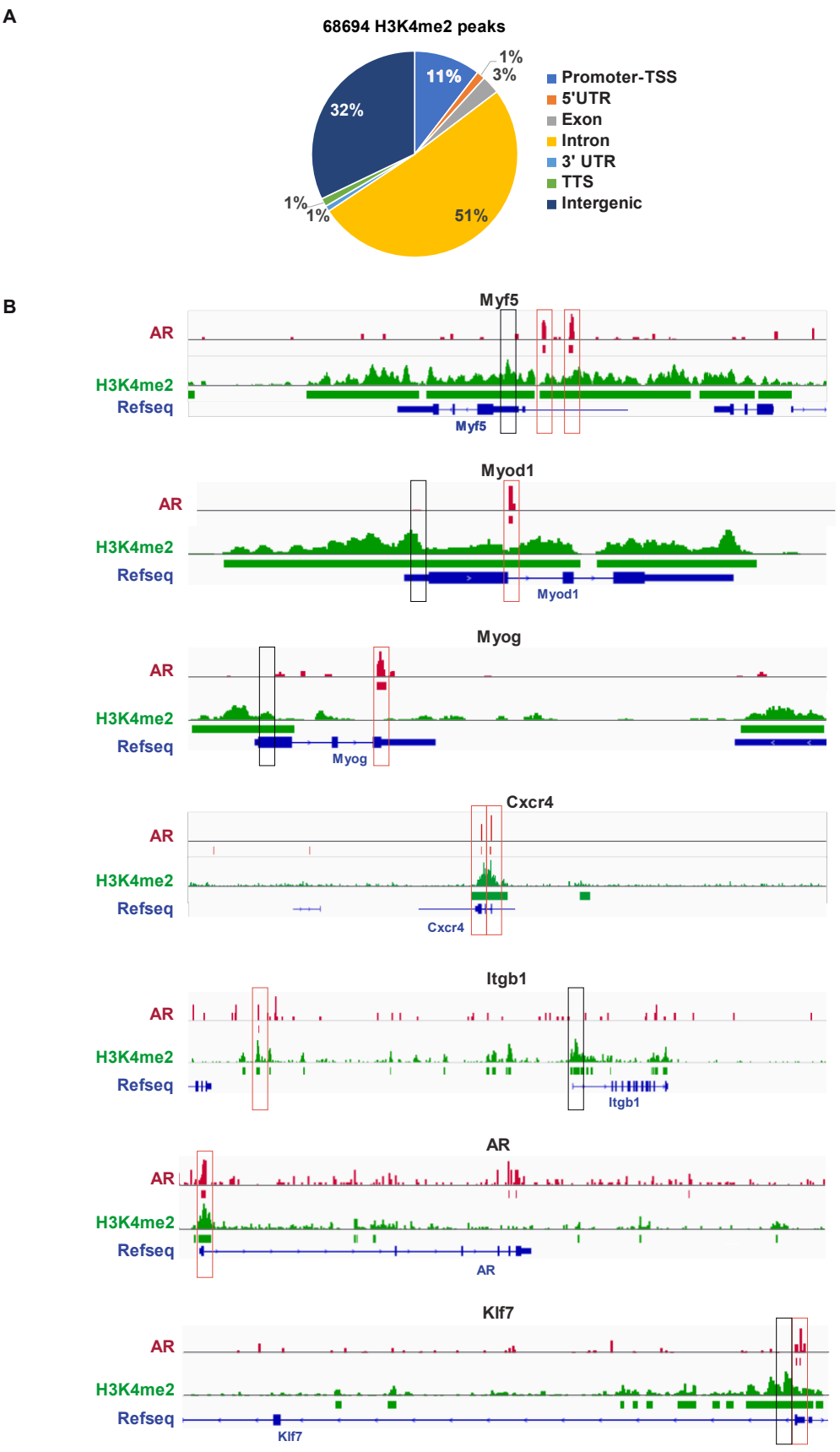
A
68694 H3K4me2 peaks
11%
1%
3%
32%
1%
1%
51%
Promoter-TSS
5'UTR
Exon
Intron
3' UTR
TTS
Intergenic
B
Myf5
AR
H3K4me2
Refseq
Myf5
Myod1
AR
H3K4me2
Refseq
Myod1
Myog
AR
H3K4me2
Refseq
Myog
Cxcr4
AR
H3K4me2
Refseq
Cxcr4
Itgb1
AR
H3K4me2
Refseq
Itgb1
AR
AR
H3K4me2
Refseq
AR
Klf7
AR
H3K4me2
Refseq
Klf7

Figure S2: **AR in resting SatC controls a vast gene network.** ***A.*** *Pie chart depicting the peak distribution of H3K4me2 revealed in FACS-isolated satellite cells from TA of control mice.* ***B.*** *Localization of H3K4me2 and AR at the Myf5, MyoD1, Myog, Cxcr4, Integrin β1 (Itgb1), AR, and Klf7 loci. The AR binding site and the corresponding DNA sequence identified at the aforementioned genes loci are highlighted with red boxes. Transcription start site (TSS) are highlighted with black boxes when different from AR binding site.*

Figure S3.

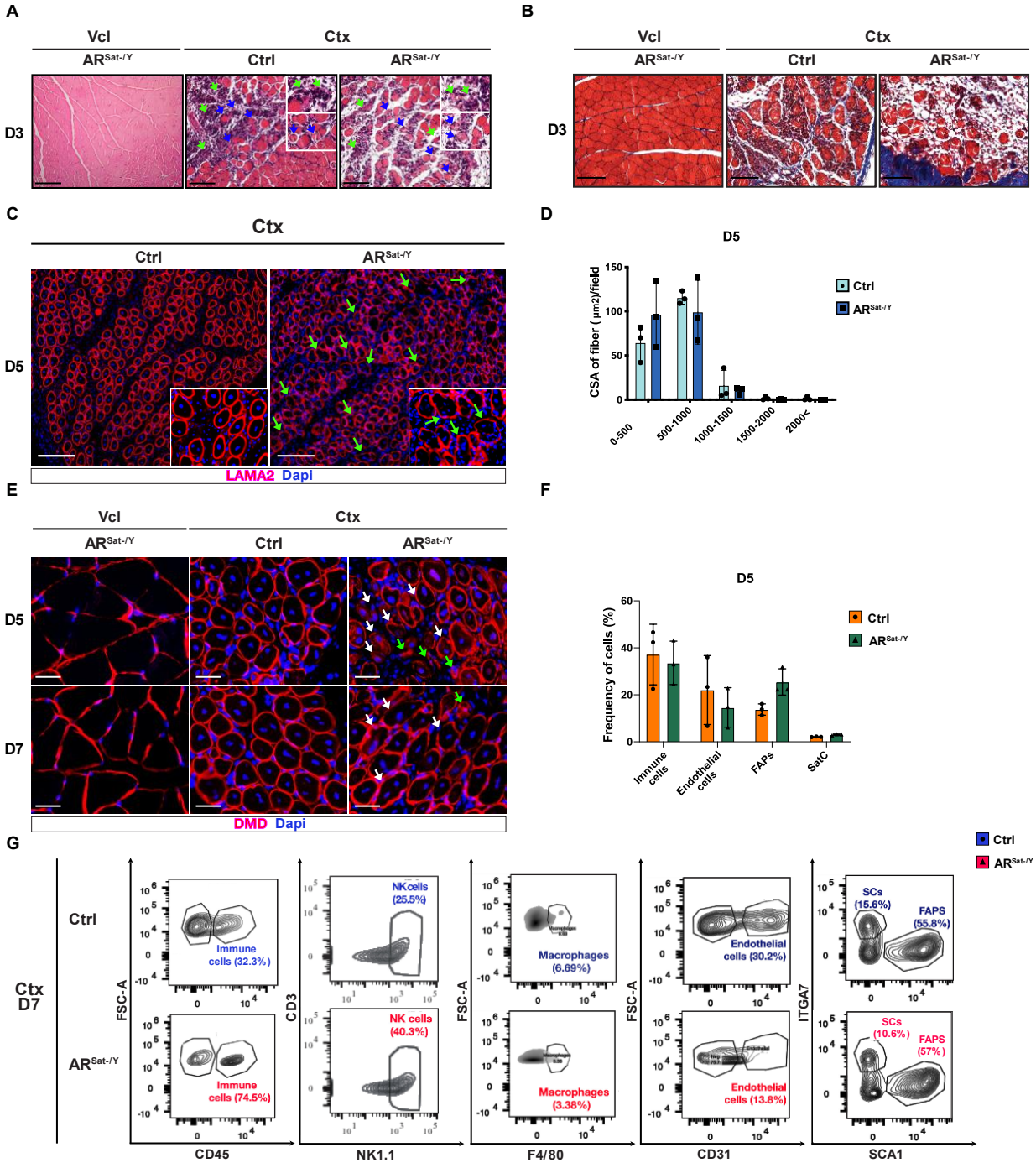

Figure S3: **Muscle regeneration is impaired in AR$^{Sat-/Y}$ mice.** ***A.*** *H&E staining on tibialis muscle sections of control (Ctrl) and AR$^{Sat-/Y}$ mice at D3 of treatment with PBS (Vcl) or cardiotoxin (Ctx). Blue and green arrows point at necrotic myofibers and stromal cell infiltration, respectively. Scale bar = 100 µm.* ***B.*** *Trichrome staining (Gomori) on tibialis muscle sections of control (Ctrl) and AR$^{Sat-/Y}$ mice at D3 of treatment with PBS (Vcl) or cardiotoxin (Ctx). Green arrows point at*

fibrosis. Scale bar = 100 µm. ***C.*** *Immunofluorescent detection Laminin–α2 (LAMA2) on TA sections from control (Ctrl) and* $AR^{Sat-/Y}$ *mice at D5 after Ctx injection. Nuclei were stained with DAPI. Green arrows point at elongated misshaped myofibers. Scale bar = 50 µm.* ***D.*** *Cross-sections area analysis of DMD-stained TA sections of control (Ctrl) and* $AR^{Sat-/Y}$ *mice at D5 after Ctx injection. N=3 animals per group and 3 images were analyzed per muscle.* ***E.*** *Immunofluorescent detection of DMD on TA sections from control (Ctrl) and* $AR^{Sat-/Y}$ *mice at D5 and D7. Nuclei were stained with DAPI. White and green arrows point at mis-shaped myofibers and protein accumulations, respectively. Scale bar = 50 µm.* ***F.*** *Percentage of resident and recruited immune, endothelial, fibro-adipogenic progenitors (FAPs) and SatC revealed via flow cytometry analysis performed on control (Ctrl) and* $AR^{Sat-/Y}$ *TA at D5. N=3 mice per condition.* ***G.*** *Flow cytometry gating strategy of CD45+ immune, CD3+/NK1.1+ natural killers, F4-80+ macrophages, endothelial CD31+, Sca1+ fibro-adipogenic progenitor and Integrin α7 (ITGA7)+ cells recruited in TA of control (Ctrl-blue) and* $AR^{Sat-/Y}$ *(red) mice at D7. Quantitative data are presented as mean ± SEM; Student's t-test: ns, not significant.*

Figure S4.

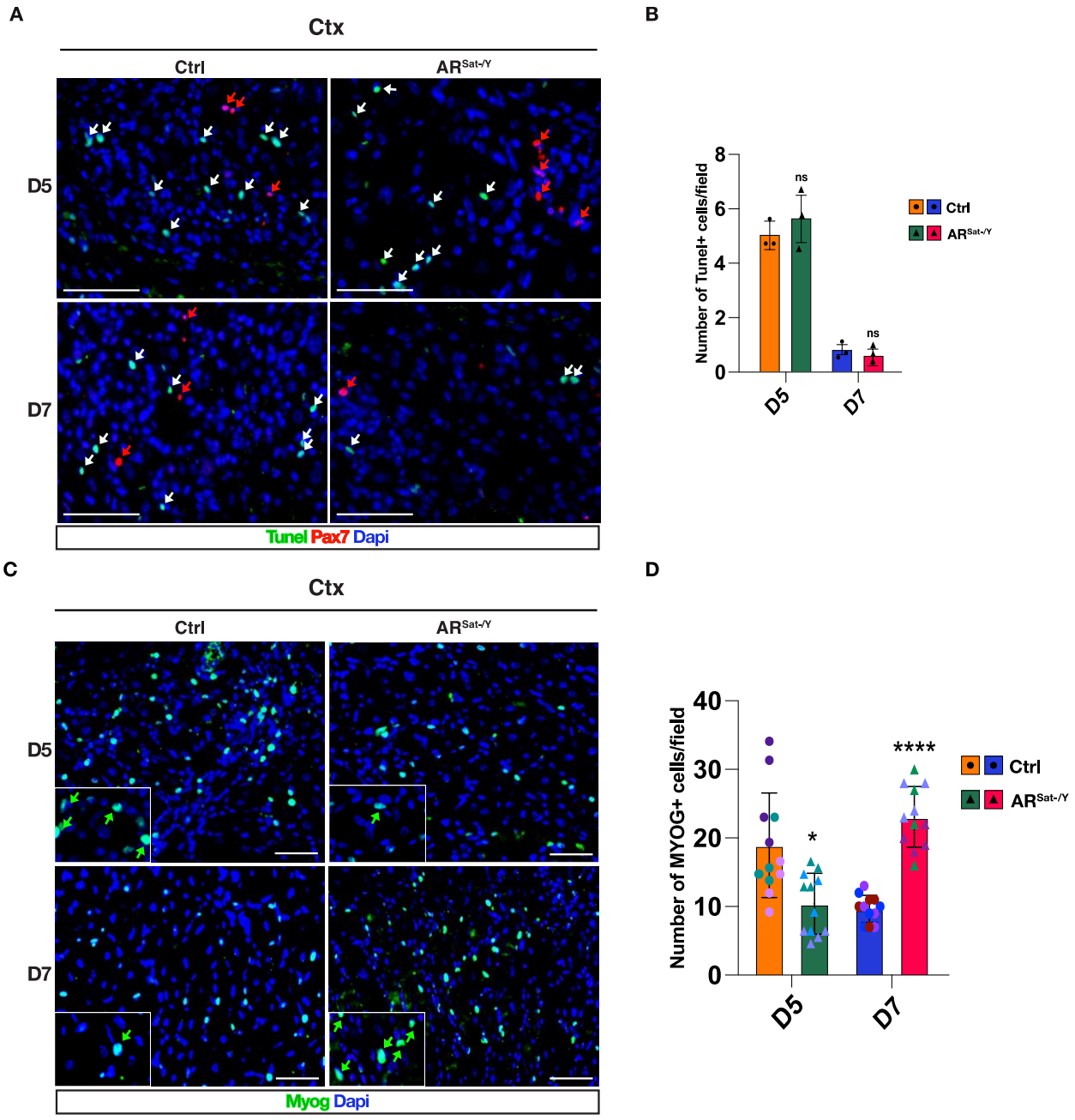

Figure S4: **Cellular division and differentiation are altered in AR-deficient SatC after injury.** ***A.*** *Immunofluorescent detection of Tunel and PAX7 on tibialis muscle sections from control (Ctrl) and AR$^{Sat-/Y}$ mice at D5 and D7. Nuclei were stained with DAPI. Red and white arrows point at Tunel+ and PAX7+ cells, respectively. Scale bar = 50 µm.* ***B.*** *Quantification of number of Tunel+ cells per field from control (Ctrl) and AR$^{Sat-/Y}$ mice at D5 and D7. N=3 animals per group and 3 images were analyzed per animal.* ***C.*** *Immunofluorescent detection of MYOG on tibialis muscle sections from control (Ctrl) and AR$^{Sat-/Y}$ mice at D5 and D7. Nuclei were stained with DAPI. White*

arrows point at MYOG+ cells. Scale bar = 50 μm. ***D.*** *Quantification of number of MYOG+ cells per field from control (Ctrl) and* $AR^{Sat-/Y}$ *mice at D5 and D7. N=3 animals per group and 3 images were analyzed per animal. Data from a given animal are shown by the same color. Quantitative data presented as mean ± SEM; Student's t-test: *p< 0.05, ****p<0.0001 and ns, not significant.*

Figure S5.

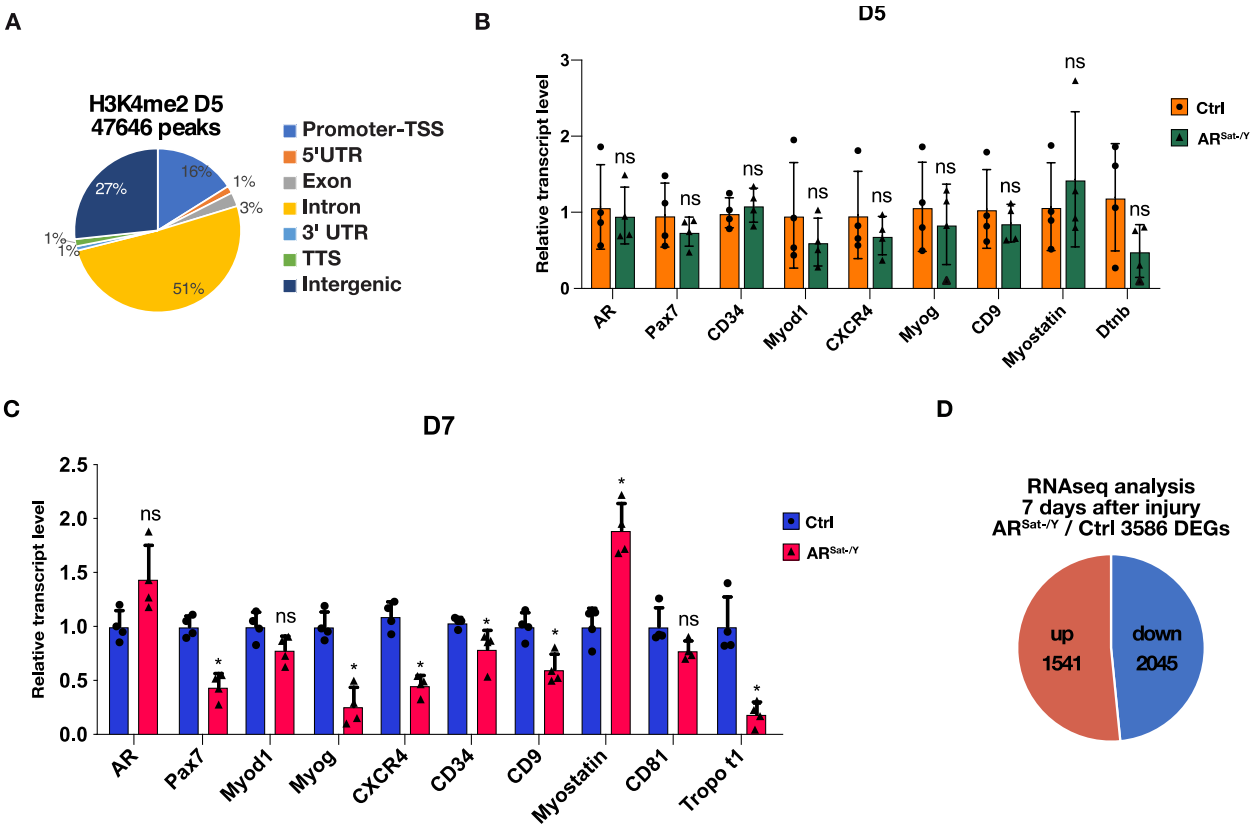

Figure S5: **Myofiber cytoskeleton organization and ECM establishment are AR-dependent**. ***A.*** *Pie chart depicting peak distribution of H3k4me2 in the genome of FACS-isolated SatC from TA at D5.* ***B.*** *Relative transcript levels of genes involved in satellite cell homeostasis and differentiation in control (Ctrl) and* $AR^{Sat-/Y}$ *mice TA at D5. N=4 mice per group.* ***C.*** *Relative transcript levels of genes involved in SatC cell homeostasis and differentiation in control (Ctrl) and* $AR^{Sat-/Y}$ *mice TA at D7. N=4 mice per group.* ***D.*** *Pie chart depicting differentially expressed genes revealed in* $AR^{Sat-/Y}$ *total TA compared to control obtained by RNA-seq analysis performed at D7. Quantitative data are presented as mean ± SEM; Student's t-test: *p< 0.05 and ns, not significant.*

Figure S6.

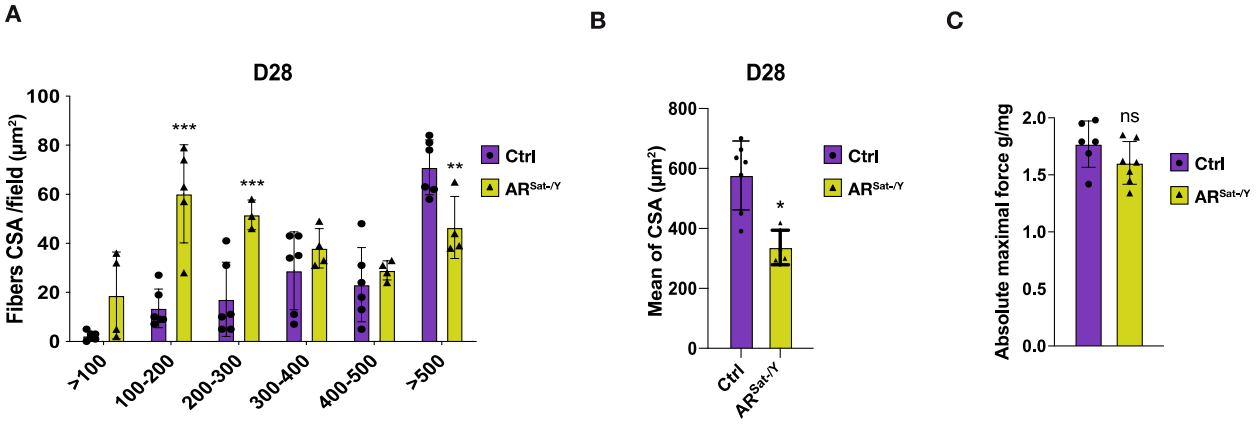

Figure S6: AR ablation in satellite cells impacts terminal muscle regeneration phase. ***A.*** *Mean of cross-sections area on Laminin-α2-stained (LAMA2)-myofibers of TA sections of control (Ctrl) and $AR^{Sat-/Y}$ mice at D28 (n = 6, 4), respectively.* ***B.*** *Cross-sections area analysis on Laminin-α2-stained (LAMA2)-myofibers of TA sections of control (Ctrl) and $AR^{Sat-/Y}$ mice at D28 days, (n = 6, 4), respectively.* ***C.*** *In situ maximal isometric force (mN) normalized to muscle weight on TA of control (Ctrl) and $AR^{Sat-/Y}$ mice at D28, n = 6–7, respectively. Quantitative data are presented as mean ± SEM; Student's t-test: *p< 0.05, **p< 0.01, ***p< 0.001 and ns, not significant.*

General Discussion and Conclusion

Skeletal muscles (Skm) in mammals represent up to 40% of the body mass. Their properties of excitability, contractility, and elasticity, allow them to generate force and movement, enabling individuals to move within their environment. Skm has an essential metabolic function since it is a major site of glucose and fatty acid utilization, which constitute the core of energy storing and spending required for contraction. Moreover, Skm exhibit a remarkable regeneration capacity sustained by a stem cell population named the satellite cells (SatC). However, despite its physiological importance, the mechanisms concerning skeletal muscle's functions, particularly in adulthood, remain poorly understood.

Androgens play significant roles in regulating body mass, brain, and their prominent influence on skeletal muscles has been a subject of interest in the scientific community. Although an uncountable number of papers have been published on this matter, the specific molecular targets of androgens in skeletal muscles remain unknown.

This thesis work aims at characterizing the molecular mechanisms by which androgens, via their receptor (AR), influence the two major components of skeletal muscles, the myofibers, and the SatC population, in physiological and pathological conditions.

Tissue-specific cistrome of the androgen receptor (AR)

Despite many genome-wide analyses in cellular and animal models, a comprehensive picture of the intertwined tissue-specific-AR binding has remained elusive.

Our analysis of chromatin immune precipitation followed by sequencing (ChIP-seq) in adult hind-limb skeletal muscles and Cut&Run data in FACS-isolated SatC of non-injured and injured tibialis muscles propose a specific target gene signature of AR, defined by cell type and even cell status. For instance, our ChIP-seq data in hind-limb muscles show that AR is located at the intergenic regions aligned with the enhancer histone mark H3K4me1 that defines zones of weak activation. AR in muscle fibers controls a set of genes mainly involved in metabolic processes, cell adhesion, calcium flux, as well as the contractile and non-contractile cytoskeleton. However, AR ChIP-seq performed in bulbocavernosus muscles unraveled 700 peaks corresponding to ~500 genes involved in “calcium regulation,” “muscle contraction,” and “pluripotency of stem cells”. Homer motif search showed oxo steroid hormones as first proposed motif, suggesting that AR binds to its androgen response elements (ARE) in perineal muscles.

Interestingly, in quiescent SatC isolated from non-injured tibialis muscles, two-thirds of AR peaks are located on active promoter regions highlighted by the H3k4me2 histone mark. Approximately 50 % of these AR-bound DNA segments contain oxosteroid receptors response elements like [AR half-sites and AR full-sites (ARE)]. In quiescent SatC, AR regulates genes implicated in myogenesis, the pluripotency of stem cells, ECM-receptor interaction, adherence junctions, and focal adhesion. Moreover, Cut&Run analysis in SatC isolated from injured tibialis muscles at D5 demonstrates that AR is mainly located in intron and intergenic regions. Its targets are associated with cell stemness (pluripotency of stem cells, Hippo signaling), and muscle growth and contraction (axon guidance, adherence junction, Pi3k-Akt signaling pathway, cAMP signaling pathway, adrenergic signaling in cardiomyocytes). Surprisingly, we found that the gene signature of AR in quiescent SatC is entirely different from activated ones since only 375 (~6 %) of AR peaks were in common between D5 and non-injured samples.

Interestingly, ChIP-seq data identifying AR cistrome in the prostate from our laboratory, show that AR is located at active enhancer and promoter regions and controls a large set of genes involved in cancer signaling (data not shown).

Our findings in various tissues and cell types suggest a high specificity regulation of AR cistrome according to cell function and status. Unraveling AR cistrome in these main androgen-sensitive organs and cell types could open new perspectives to identify tissue-specific gene targets or develop androgen receptor modulators (SARM), which have agonist effects in muscles myofiber and SatC but are inactive in the reproductive systems. However, to have a complete picture, it will be interesting in the future to perform ChIP analysis on myofiber single nuclei isolated from injured tibialis muscles to reveal gene targets regulated by AR in regenerative fibers.

The controversial status of myostatin regulation by androgens in skeletal muscles

Myostatin (MSTN) is an essential regulator of muscles, and its invalidation in rodents results in a significant increase in tissue mass (Lee, 2004). The hypertrophy observed in MSTN knock-out mice is more pronounced in males than in females (McPherron et al., 1997), and the decrease in muscle mass when MSTN is overexpressed in mice is more significant in males than females (Reisz-Porszasz et al., 2003). These studies suggest that androgens and MSTN signaling pathways might interfere. In limb muscles, supraphysiological levels of androgens inhibit the MSTN/SMAD and FOXO3 catabolic pathway (Seo et al., 2019). Moreover, our transcriptomic analysis performed on tibialis muscles 7 days upon injury showed that MSTN transcript levels are increased in $AR^{Sat-/Y}$ compared to control mice. These data suggest that AR negatively influence the expression of MSTN in skeletal muscles.

Intriguingly, a former Ph.D. student in our laboratory found a decrease in MSTN expression in tibialis muscles of $AR^{Sat-/Y}$ compared to control mice under physiological conditions (data not shown). Her results agree with findings from Dubois and colleagues showing that AR regulates MSTN in SatC and their progeny (Dubois et al., 2014). Our Cut&Run analysis in SatC shows the recruitment of AR on the MSTN locus only when cells are in a quiescent state but not activated (data not shown). Since no negative expression effect was reported for AR, we hypothesize that AR induces the expression of MSTN in dormant SatC.

Taken together, after gathering the different published controversial results combined with our data, we theorize that androgens negatively regulate the expression of MSTN in muscle fibers but positively influence its expression in quiescent SatC. Androgens in myofibers induce hypertrophy, which aligns with MSTN inhibition since the latter causes muscle atrophy. Whereas the data obtained in our lab accompanied with our AR cistrome in quiescent SatC indicate that androgens via AR positively regulates MSTN expression, which is in agreement with Dubois et al. Interestingly, MSTN promotes the expression of the cyclin-dependent kinase (CDK) inhibitor p21 (Thomas et al., 2000), which inhibits cell activation (McCroskery et al., 2003) and ensures their dormancy. Moreover, MSTN secreted by myoblasts and myofibers

negatively regulates the cell cycle of SatC (Langley et al., 2002). These observations further highlight the cell-type specificity of androgens' actions, as discussed in the previous paragraph.

Additional experiments could be performed to test our hypothesis *in vitro* or *in vivo*. LHCNM2 myoblasts could be treated with androgens agonists or inhibitors to unravel MSTN transcript level. Another possibility would be to administrate AR agonists or inhibitors to $AR^{Sat-/Y}$ mice and investigate myostatin expression.

Unraveling the paradoxical effect of AR on limb muscle mass

It has been shown that androgens level decline in humans with andropause (Kevorkian, 2007; Mastrogiacomo et al., 1982) or in rodents following castration (Axell et al., 2006) results in a decrease in limb muscle mass. However, our laboratory previously reported that removal of mycotic AR in myofibers using an HSA-Cre (E16,5) mouse model does not affect limb muscle mass or fiber CSA (Chambon et al., 2010). Conversely, using a muscle creatine kinase (MCK)-Cre (E12,5-13,5) mouse model deficient in postmitotic myocyte-AR, a study by Ophoff and colleagues shows a similar pattern of force production but a decline in limb muscle in mutant mice compared to control littermates. They suggested that muscle mass reduction is due to decreased fiber number but not CSA (Ophoff et al., 2009). Furthermore, another study using the same previous mouse model showed a decrease in limb muscle mass upon AR ablation due to defects in myoblast proliferation (MacLean et al., 2008). Conversely, myoblast AR knock-out mouse model using the Myod1-Cre (E10,5) exhibits a decrease in force production in limb muscles, but no changes in muscle mass or fiber CSA compared to control (Dubois et al., 2014). Noteworthy, all the previous mice models performed AR ablation during embryogenesis.

It has been shown that AR promotes the expression of myogenic genes and myoblast fusion *in vitro* (Vlahopoulos et al., 2005). In addition, SBMA patients with an AR PolyQ mutation exhibit impaired myotube fusion and altered contractile structures in their myofibers. Our results show that ablation of AR in SatC ($AR^{Sat-/Y}$) in adulthood does not induce loss of tibialis muscle mass or myofiber CSA in physiological conditions. However, when tibialis muscles of $AR^{Sat-/Y}$ were challenged with injury in adulthood, they did not show a difference in muscle mass. Still, they exhibited reduced fiber CSA mean and force production compared to control littermates, as well as fiber misshaped cytoskeleton and misaligned sarcomeres. Our transcriptome analysis on $AR^{Sat-/Y}$ tibialis muscles at D7 showed that the main genes involved in the cell cycle (e.g., *Cdk1-2-4-6*, *Myc*, *E2f1-2*) and myoblast fusion (Myomaker, Myomerger, *Cd9*) are down-regulated upon AR ablation compared to control. Additionally, immunostaining of alpha-actinin unraveled the presence of myoblasts clumps on the periphery of newly regenerating fibers of $AR^{Sat-/Y}$ tibialis muscles at D7, suggesting defects in myoblast fusion.

These data imply that AR controls essential functions occurring in little time frame during myofiber formation, explaining the reason why we find contradicting results among different mice models. We hypothesize that AR does not control muscle mass and myofiber

CSA during embryogenesis as reported in Myod1-Cre mouse model by (Dubois et al., 2014). However, in adulthood, after sex hormones peak at puberty, elevated levels of circulating androgens are present. This is where AR becomes mandatory for proper myofiber regeneration upon injury affecting its sarcomere structure, cytoskeleton organization, and CSA. Muscle mass upon injury is challenging to investigate since with a classical Ctx injury only one-third of the muscle is affected. However, SBMA mice phenotype could shed the light on AR role during myofiber formation, since exercise induces muscle load and regeneration, and SBMA rodents exhibit reduced muscle mass and fiber CSA compared to controls upon exercise(Giorgetti et al., 2016).

To further investigate our hypothesis and unravel the exact time frame in which the presence of AR is mandatory, regeneration and androgen administration experiments could be performed on both HSA- and MCK-AR knock-out mice. During my Ph.D., Using the HSA-Cre model, I analyzed muscle regeneration and myofiber formation capacity in myocytic-AR knocked-out mice ($AR^{Skm-/Y}$). Seven days upon cardiotoxin treatment, newly formed fibers exhibited chaotic myocytes fusion, misshaped fibers, and misaligned sarcomeres, indicating the importance of AR presence at the time of HSA gene expression (Figure 1). I did not have the time to investigate fiber CSA, but it is in our schedule. A similar analysis could be performed on the MCK-Cre mouse model to help unravel once and for all the truth behind AR's influence on limb muscle mass.

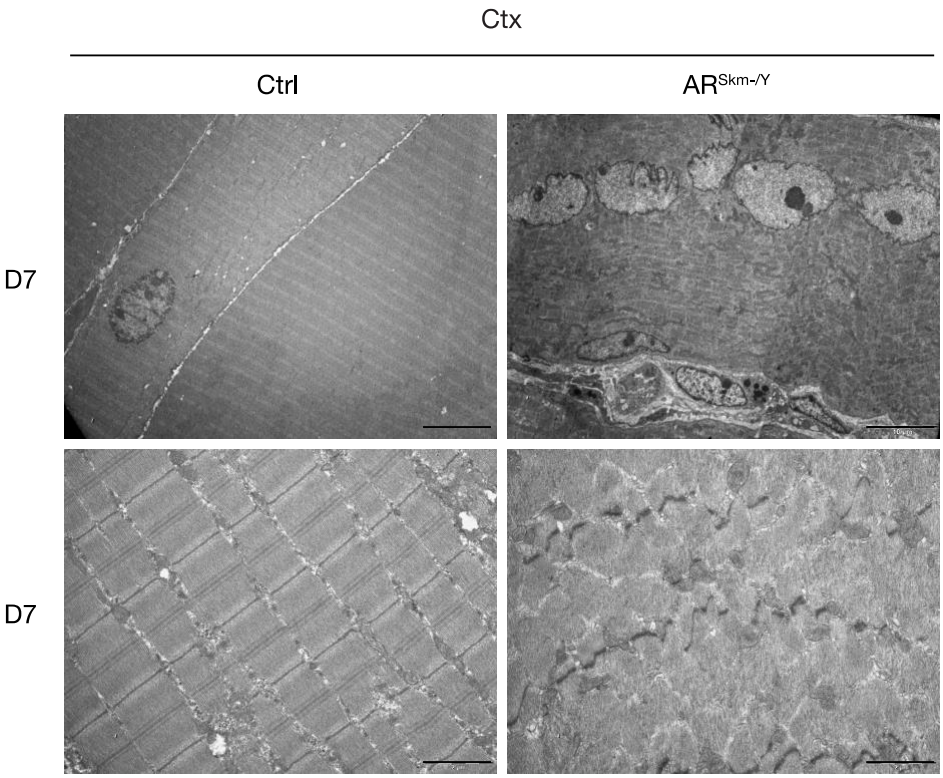

Figure 1: Ultrastructural analysis of tibialis muscle sections 7 days (D7) upon cardiotoxin (Ctx) injection.

Scale bars: upper panel = 10 µm and lower panel = 2 µm.

Androgens, aging, skeletal muscles, and satellite cells

Impact of aging and decline of androgen levels on muscles and satellite cells

Since the advancement in age is concomitated with androgen concentration decline in bloodstream, our data from wild-type mice show that AR protein levels also decrease in skeletal muscles from 15-week of age. We wondered how these changes affect muscle integrity and its stem cell population. It has been shown that SatC number and niche quality decline with age (Henze et al., 2020; McCormick & Vasilaki, 2018), and depletion of SatC from muscles of old mice did not affect the CSA of myofibers (Fry et al. 2015). To verify these findings, we FACS-isolated quiescent SatC from hind-limb muscles of 8- and 35-week-old wild-type mice (Figure 2), and our results show a significant decrease in the percentage of stem cells with aging. However, H&E staining of the same mice samples did not show any defects in aged mice's hind-limb muscles compared to younger ones (data not shown). This suggests that the decrease of androgens and AR in muscles only directly affects SatC number and homeostasis but does not have a short-term effect on muscle integrity.

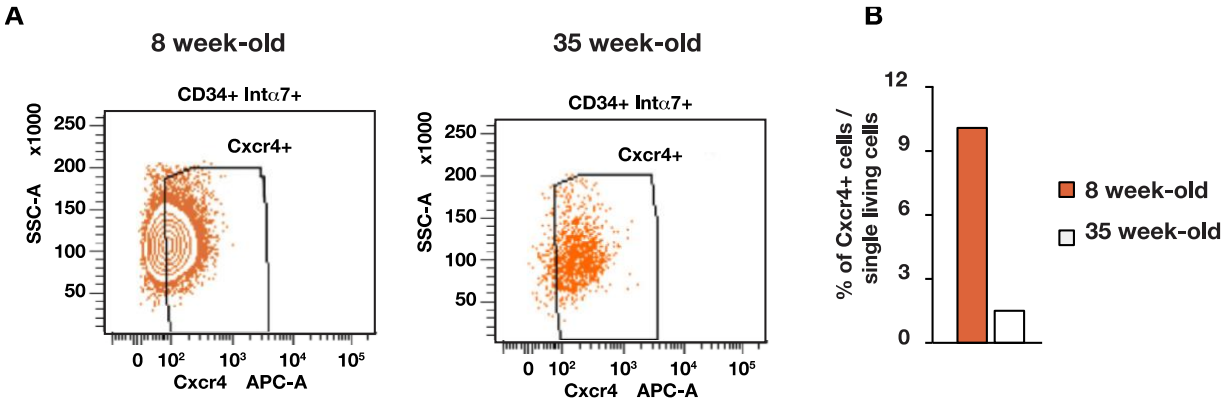

Figure 2: FACS analysis of SatC population isolated from hind-limb muscles of 8- and 35-week-old mice.

A. *Flow cytometry gating of satellite cells population expressing CXCR4 isolated from 8- and 35-week-old mice limb muscles after selecting cells expressing CD34 and Itga7.* ***B.*** *Percentage of CXCR4+ cells out of single living cells. n = 2 per condition.*

However, what happens with advanced aging when muscles are deprived for a more extended period of androgens and AR? To answer this question, we analyzed the tibialis, gastrocnemius, and quadriceps muscles of 60-week-old mice. H&E staining of quadriceps and tibialis demonstrated the presence of centri-nucleated fibers and excessive regeneration in the tibialis and quadriceps of aged mice (Figure 3 – blue arrows). In addition, some mice samples also showed condensed cytoplasm in regenerating fibers (Figure 3 – black arrow) and signs of necrotic fibers exhibiting pale cytoplasm (Figure 3 – yellow arrow). These data suggest that muscle integrity is compromised with age, but even the reduced number of survived SatC can still form new fibers and rescue tissue function.

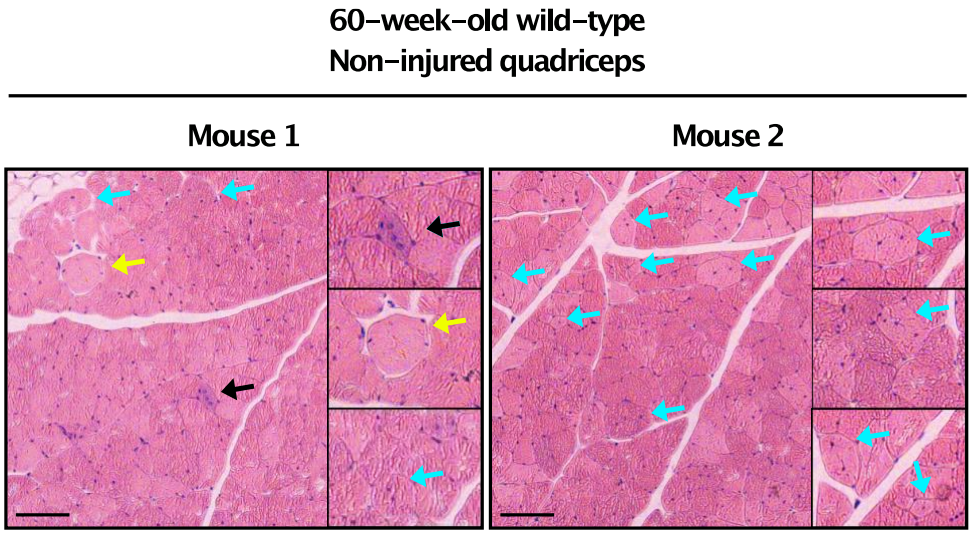

Figure 3: H&E staining on quadriceps muscles sections isolated from two mice.

Black, yellow, and blue arrows point at defects in regeneration, pale cytoplasm necrotic fiber and centri-nucleated regenerative fibers, respectively. Scale bars: 100 µm.

Moreover, trichrome staining on quadriceps muscle of 60-week-old mice sections unraveled increased interstitial fibrosis and collagen accumulation within myofiber sarcolemma (data not shown). Additionally, ultrastructural analysis unraveled the presence of malformed mitochondria emptied of their content (Figure 4 – red arrows) and T-tubule protein accumulation in the sarcolemma (Figure 4 – yellow arrows), which confirms compromised myofiber integrity with age.

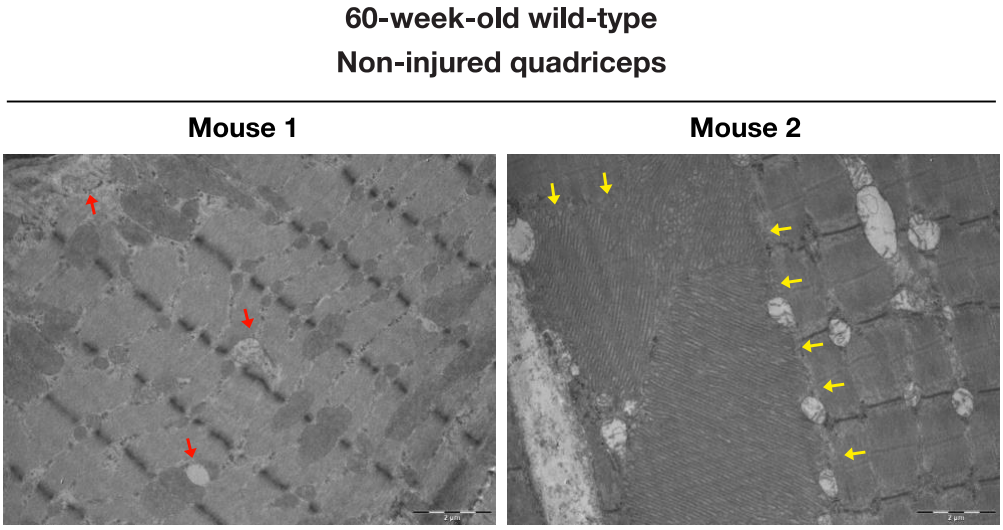

Figure 4: Ultrastructural analysis of tibialis muscles isolated from 60-week-old mice.

Red, and yellow arrows point at defects in mitochondria and t-tubules accumulations, respectively. Scale bars: 2 µm.

To deliver more insights into the homeostasis and function of geriatric SatC, we plan to perform a Cut&Run analysis of FACS-isolated muscle stem cells from old mice's hind-limb muscles. Combining our current Cut&Run data with the genome-wide accessibility and comparing AR cistrome from geriatric SatC, we wish to figure out the mechanisms by which old stem cells adapt to their new environment and low androgens levels to keep regenerating new fibers.

Impact of aging and AR ablation on satellite cells in $AR^{Sat-/Y}$ mice

Since we observed a decrease in *Pax7* transcript levels in SatC of $AR^{Sat-/Y}$ mice muscles and a decline in the number of stem cells at the end of the regeneration process upon injury compared to control littermates, we questioned whether these conditions, combined with aging, would generate MYOSCO-like phenotype. To this end, we analyzed tibialis muscle histology of 52-week-old $AR^{Sat-/Y}$ mice and control littermates. H&E staining on both ARL2/Y and $AR^{Sat-/Y}$ showed minor necrosis in both phenotypes (Figure 5 - upper panel - black arrows). However, we observed an important intrafibrillar lipid accumulation in muscles of $AR^{Sat-/Y}$, which was not observed in $AR^{L2/Y}$ sections (Figure 5 - upper panel - yellow arrows). Our observations were confirmed with immunostaining using an antibody directed against perilipin (Figure 5 - lower panel - green). The main characteristic of MYOSCO muscle histology is the substitution of myofibers by fibro-adipose tissue in the absence of major necrosis (Feichtinger et al., 2019), as discussed in section **4.1.1.**

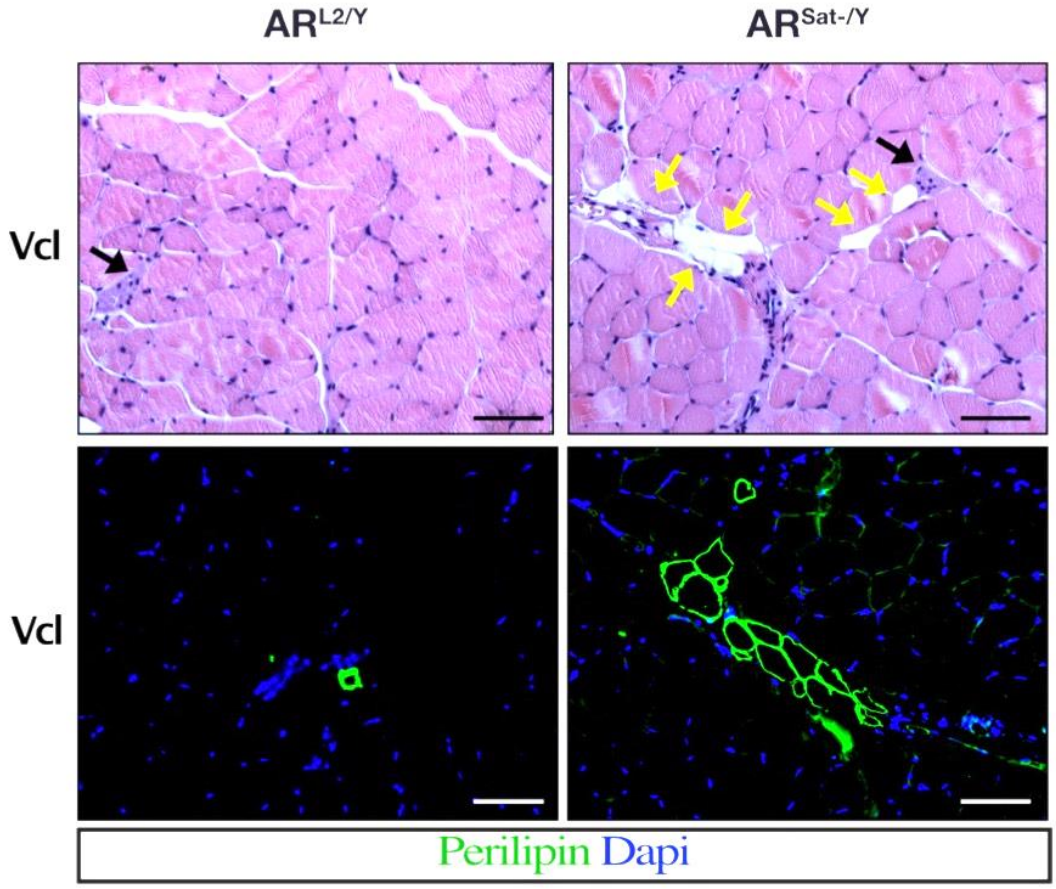

Figure 5: Histological analysis of 52-week-old $AR^{Sat-/Y}$ and control mice muscles.

Upper panel, Hematoxylin and Eosin (H&E) staining on tibialis muscle sections of control ($AR^{L2/Y}$) and mutant ($AR^{Sat-/Y}$) mice 7 (D7) days after PBS treatment (vehicle-Vcl). Yellow and black arrows point at lipid accumulations and necrotic myofibers, respectively. Lower panel, immunofluorescent detection of lipid droplets using an antibody directed against perilipin (green) and nuclei were stained with Dapi (blue) on tibialis muscle sections of control ($AR^{L2/Y}$) and mutant ($AR^{Sat-/Y}$) mice. Scale bars: 50 µm.

To test the regenerating capacity of these muscles, we induced tibialis injury with cardiotoxin and analysis sections at D7. H&E staining showed that while control muscles regenerated properly with similar capacity to younger ones (data not shown), mutant ones exhibited excessive infiltration into the injured site (Figure 6 – upper panel – blue arrows), as well as misshaped centro-nucleated fibers (Figure 6 – upper panel – red arrows). Moreover, perilipin staining demonstrated a significant increase in lipid droplet accumulation within the interfibrillar area of $AR^{Sat-/Y}$ muscles compared to control (Figure 6 - lower panel - green). Notably, the number of PAX7 expressing cells declined in mutant muscle sections compared to control (data not shown).

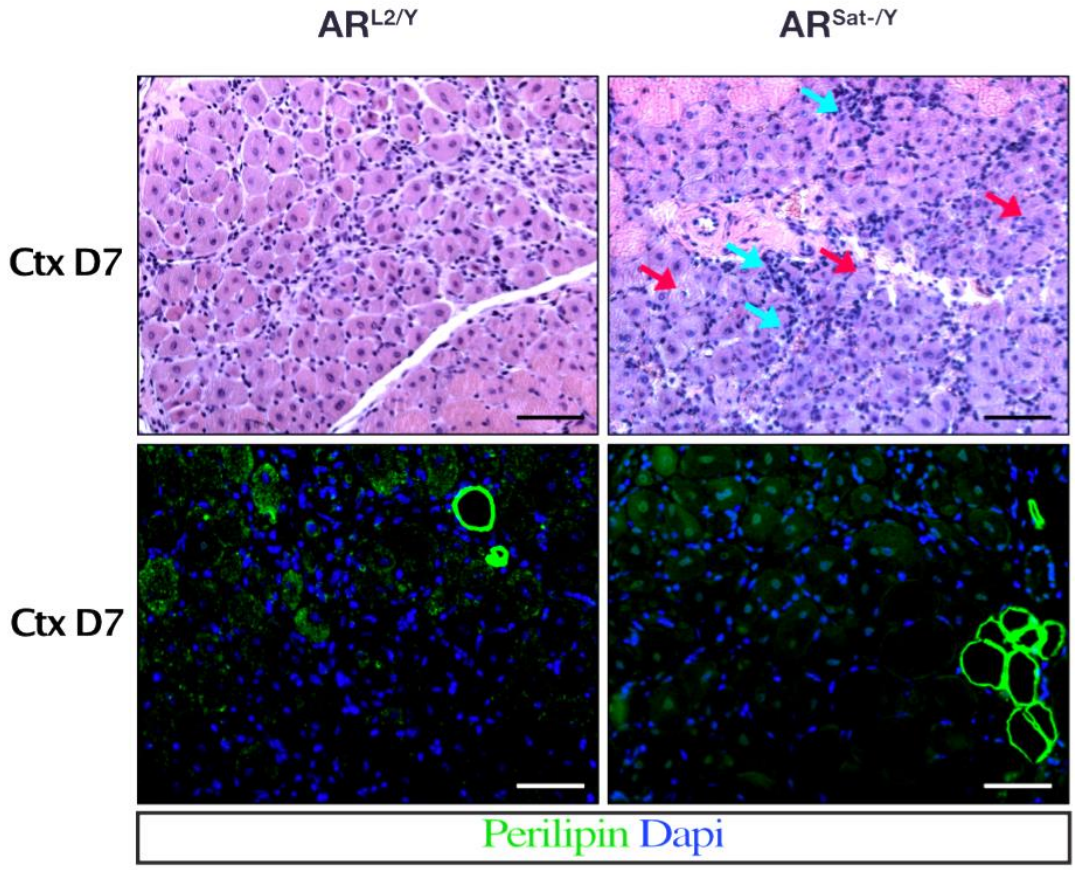

Figure 6: Histological analysis of 52-week-old $AR^{Sat-/Y}$ and control mice muscles 7 days (D7) upon cardiotoxin (Ctx) treatment.

Upper panel, Hematoxylin and Eosin (H&E) staining on tibialis muscle sections of control ($AR^{L2/Y}$) and mutant ($AR^{Sat-/Y}$) mice 7 (D7) days after cardiotoxin (Ctx) injection. Blue and red arrows point at stromal cell infiltration and necrotic myofibers, respectively. Lower panel, immunofluorescent detection of lipid droplets using an antibody directed against perilipin (green) and nuclei were stained with Dapi (blue) on tibialis muscle sections of control ($AR^{L2/Y}$) and mutant ($AR^{Sat-/Y}$) mice at D7. Scale bars: 50 µm.

Interestingly, SatC can generate brown adipocytes under pathological conditions (Sanna et al., 2009; Tosic et al., 2018). Since only $AR^{Sat-/Y}$ muscles exhibited important adipocyte infiltration compared to control and wild-type aged mice, we hypothesized that androgens might have a role in conserving the myogenic potential of these cells. To test our hypothesis, we cultured C2C12 myoblasts in an adipogenesis-inducing medium for 7 days in the presence or absence of 5-alpha-dihydrotestosterone (an endogenous androgen – DHT). Our analysis by Oil-red-O staining showed the accumulation of lipids in the cytoplasm of myofibers generated in the absence of DHT; however, the presence of androgens blocked lipid droplet formation (Figure 7A). Immunofluorescence detection of MYHs showed that DHT favored the formation of multinucleated myotubes to the detriment of adipocytes (Figure 7B). Moreover, RT-qPCR analysis showed that key genes involved in adipogenesis, such as *Apoc1*, *Retn*, *Pparg,* and *Ucp1,* were downregulated (Figure 7C), and genes of myogenesis, including *Mef2c* and *Myh4,* were upregulated (Figure 7C) in cells incubated with DHT and that their levels of expression resembled those of cells cultured with myogenic medium (Figure 7C).

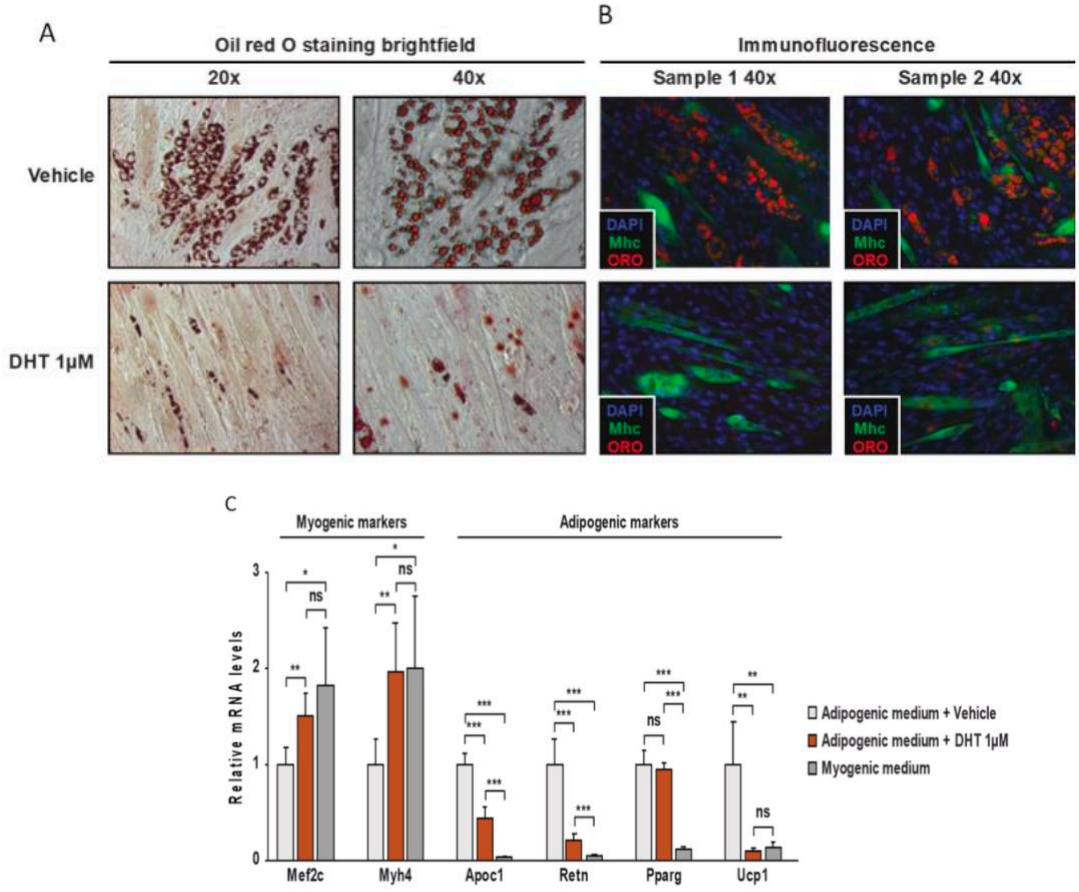

Figure 7: DHT promotes myogenesis to the detriment of adipogenesis.

A-B. *Histological analysis of C2C12 cells non-differentiated or treated with adipogenic medium in the presence or absence of DHT,* ***(A)*** *Oil-red-o staining (lipid droplets in red) and* ***(B)*** *immunofluorescence assay using antibodies directed against Dystrophine (Dmd, green) and Myosine heavy chain slow (Mhc1, red). Nuclei were counterstained with DAPI (blue) and lipid accumulation was detected by Oil_Red-O staining (white).* ***C.*** *Relative transcription level analysis for myogenic or adipogenic markers for C2C12 cells, non- differentiated or treated with adipogenic medium in the presence or absence of DHT, and for MM treated C2C12 cells.*

These data indicate that androgens, via their receptor, conserve not only SatC homeostasis and functions but also their identity and myogenic potential, blocking their adipogenic differentiation. However, to verify this hypothesis, a cell tracing mouse model could be intercrossed with $AR^{Sat-/Y}$ mice to follow the differentiation of SatC and attest to the expression of the transgene in the infiltrated adipocytes.

Intriguingly, a decline of androgens with age did not have a major impact on SatC myogenic potential, most probably since low levels of circulating androgens are still present in these mice, which appears to be enough for SatC's commitment. However, when we removed AR, the impact was more pronounced. Therefore, it would be very interesting to perform a Cut&Run analysis using antibodies directed against various histone marks of these AR ablated geriatric SatC to investigate genome accessibility and compare it to younger muscle stem cells. These findings could elucidate the effect of androgens levels decline with aging on SatC homeostasis and myogenic potential.

General conclusion

Aged muscles exhibit metabolic defects, malformed mitochondria, accumulation of T-tubules, necrotic fibers, adipocytes, fibrosis accumulation between the fibers, and decreased number of SatC. In addition, Androgen levels decline with age in males. To decipher whether the decline of androgen is the origin of muscle defects observed with age, we generated two mouse models in which AR is either selectively ablated in muscle myofibers during embryonic development ($AR^{Skm-/Y}$), Chambon et al., 2010) or in satellite cells via tamoxifen administration to adult *Pax7*-$CreER^{T2}$ mice (Hutcheson & Kardon, 2009) harboring LoxP floxed AR alleles ($AR^{Sat-/Y}$).

Our data from 15-week-old $AR^{Skm-/Y}$ mice showed that AR is responsible for the metabolic activity of muscles. Indeed, our ChIP analysis shows that AR directly controls the expression of major key players of glycolysis including hexokinase II (HK II). AR ablation led to a decline in the metabolic activity of the muscles and the emergence of earlier type II diabetes in mice. Moreover, 15-week-old $AR^{Skm-/Y}$ mice muscles exhibited malformed mitochondria with empty content, misaligned sarcomeres and misshaped triad structure, fiber necrosis, regeneration pattern, and decline in force production capacity when compared to control. Those defects are in line with what we observe in geriatric muscles. When we performed Ctx injection, mutant regenerative muscles displayed myoblast fusion defects, and regenerating fiber exhibited severe structure impairment.

Our results from $AR^{Sat-/Y}$ mice showed that AR is mandatory for primary gene expression involved in cell dormancy, including *Pax7* in physiological conditions. AR deficient SatC could not keep their quiescent state; instead, they become activated and fuse with neighboring fibers. Chronic activation and fusion of SatC lead to the exhaustion of the stem cell population, which could explain the phenotype we observe in aged muscles. When challenged with Ctx injection, mutant SatC showed impaired proliferation and asymmetric division capacity, which led to the decline of the number of stem cells at the end of the regeneration process. Upon activation, our cistrome analysis showed AR re-allocation to new sites compared to the ones revealed in quiescent SatC. Indeed, our data show that AR controls genes responsible for myogenesis, cell cycle, focal adhesion, and pluripotency of stem cells. Regenerating tibialis muscles deficient of AR exhibited similar defects to those observed in $AR^{Skm-/Y}$ and geriatric ones, including fiber mitochondrial defects, misshaped cytoskeleton, myoblast fusion defects, and contraction force decline compared to control as well as adipocytes and fibrosis emergence.

Thus, the phenotypes of $AR^{Skm-/Y}$ and $AR^{Sat-/Y}$ mice models perfectly recapitulate the defects of male geriatric muscles observed in both myofibers and the SatC population. Here we conclude that androgens and AR levels decline with aging are the main reasons for muscle atrophy and function defects elderlies suffer from. Furthermore, our results on AR cistrome in muscle fibers and SatC shed light on the molecular determinants controlled via AR and androgens. These findings could open new strategies to develop more efficient SARMs and/or specific AR target agonist for muscle injury and/or atrophy with aging.

Annexes

Published in **Nucleic Acids Research (NAR).** 2021 May 7;49(8):4472-4492.
DOI: 10.1093/nar/gkab226.

Myod1 and GR coordinate myofiber-specific transcriptional enhancers

Daniela Rovito [1], Anna-Isavella Rerra [1], Vanessa Ueberschlag-Pitiot [1], Shilpy Joshi [1], Nezih Karasu [1], Vanessa Dacleu-Siewe [1], Khalil Ben Rayana [1], **Kamar Ghaibour [1]**, Maxime Parisotto [1], Arnaud Ferry [2], Scott A Jelinsky [3], Gilles Laverny [1], Bruno P Klaholz [1], Tom Sexton [1], Isabelle M L Billas [1], Delphine Duteil [1], Daniel Metzger [1]

Affiliations:

[1]Université de Strasbourg, CNRS UMR7104, INSERM U1258, IGBMC, F-67400 Illkirch, France.
[2]Centre de Recherche en Myologie, UMRS974-Sorbonne Université-INSERM U974-Association Institut de Myologie, France.
[3]Department of Inflammation and Immunology, Pfizer Research, Cambridge, MA, USA.

References

1. Abou-Khalil, R., Le Grand, F., Pallafacchina, G., Valable, S., Authier, F.-J., Rudnicki, M. A., Gherardi, R. K., Germain, S., Chretien, F., Sotiropoulos, A., Lafuste, P., Montarras, D., & Chazaud, B. (2009). Autocrine and Paracrine Angiopoietin 1/Tie-2 Signaling Promotes Muscle Satellite Cell Self-Renewal. *Cell Stem Cell*, *5*(3), 298–309. https://doi.org/10.1016/j.stem.2009.06.001

2. Addison, O., Drummond, M. J., Lastayo, P. C., Dibble, L. E., Wende, A. R., McClain, D. A., & Marcus, R. L. (2014). Intramuscular fat and inflammation differ in older adults: The impact of frailty and inactivity. *The Journal of Nutrition, Health & Aging*, *18*(5), 532–538. https://doi.org/10.1007/s12603-014-0019-1

3. Ahrens, H. E., Huettemeister, J., Schmidt, M., Kaether, C., & von Maltzahn, J. (2018). Klotho expression is a prerequisite for proper muscle stem cell function and regeneration of skeletal muscle. *Skeletal Muscle*, *8*(1), 20. https://doi.org/10.1186/s13395-018-0166-x

4. Almeida, C. F., Fernandes, S. A., Ribeiro Junior, A. F., Keith Okamoto, O., & Vainzof, M. (2016). Muscle Satellite Cells: Exploring the Basic Biology to Rule Them. *Stem Cells International*, *2016*, 1–14. https://doi.org/10.1155/2016/1078686

5. Al-Qusairi, L., & Laporte, J. (2011). T-tubule biogenesis and triad formation in skeletal muscle and implication in human diseases. *Skeletal Muscle*, *1*(1), 26. https://doi.org/10.1186/2044-5040-1-26

6. Arnold, L., Henry, A., Poron, F., Baba-Amer, Y., van Rooijen, N., Plonquet, A., Gherardi, R. K., & Chazaud, B. (2007). Inflammatory monocytes recruited after skeletal muscle injury switch into antiinflammatory macrophages to support myogenesis. *Journal of Experimental Medicine*, *204*(5), 1057–1069. https://doi.org/10.1084/jem.20070075

7. Axell, A.-M., MacLean, H. E., Plant, D. R., Harcourt, L. J., Davis, J. A., Jimenez, M., Handelsman, D. J., Lynch, G. S., & Zajac, J. D. (2006). Continuous testosterone administration prevents skeletal muscle atrophy and enhances resistance to fatigue in orchidectomized male mice. *American Journal of Physiology-Endocrinology and Metabolism*, *291*(3), E506–E516. https://doi.org/10.1152/ajpendo.00058.2006

8. Baghdadi, M. B., Castel, D., Machado, L., Fukada, S., Birk, D. E., Relaix, F., Tajbakhsh, S., & Mourikis, P. (2018). Reciprocal signalling by Notch–Collagen V–CALCR retains muscle stem cells in their niche. *Nature*, *557*(7707), 714–718. https://doi.org/10.1038/s41586-018-0144-9

9. Baghdadi, M. B., & Tajbakhsh, S. (2018). Regulation and phylogeny of skeletal muscle regeneration. *Developmental Biology*, *433*(2), 200–209. https://doi.org/10.1016/j.ydbio.2017.07.026

10. Barraza-Flores, P., Bates, C. R., Oliveira-Santos, A., & Burkin, D. J. (2020). Laminin and Integrin in LAMA2-Related Congenital Muscular Dystrophy: From Disease to Therapeutics. *Frontiers in Molecular Neuroscience*, *13*, 1. https://doi.org/10.3389/fnmol.2020.00001

11. Barua, B., Winkelmann, D. A., White, H. D., & Hitchcock-DeGregori, S. E. (2012). Regulation of actin-myosin interaction by conserved periodic sites of tropomyosin. *Proceedings of the National Academy of Sciences*, *109*(45), 18425–18430. https://doi.org/10.1073/pnas.1212754109

12. Beauchamp, J. R., Heslop, L., Yu, D. S. W., Tajbakhsh, S., Kelly, R. G., Wernig, A., Buckingham, M. E., Partridge, T. A., & Zammit, P. S. (2000). Expression of Cd34 and Myf5 Defines the Majority of Quiescent Adult Skeletal Muscle Satellite Cells. *Journal of Cell Biology*, *151*(6), 1221–1234. https://doi.org/10.1083/jcb.151.6.1221

13. Bentzinger, C. F., Wang, Y. X., Dumont, N. A., & Rudnicki, M. A. (2013). Cellular dynamics in the muscle satellite cell niche. *EMBO Reports*, *14*(12), 1062–1072. https://doi.org/10.1038/embor.2013.182

14. Bentzinger, C. F., Wang, Y. X., & Rudnicki, M. A. (2012). Building Muscle: Molecular Regulation of Myogenesis. *Cold Spring Harbor Perspectives in Biology*, *4*(2), a008342–a008342. https://doi.org/10.1101/cshperspect.a008342

15. Bentzinger, C. F., Wang, Y. X., von Maltzahn, J., Soleimani, V. D., Yin, H., & Rudnicki, M. A. (2013). Fibronectin Regulates Wnt7a Signaling and Satellite Cell Expansion. *Cell Stem Cell*, *12*(1), 75–87. https://doi.org/10.1016/j.stem.2012.09.015

16. Bernet, J. D., Doles, J. D., Hall, J. K., Kelly Tanaka, K., Carter, T. A., & Olwin, B. B. (2014). P38 MAPK signaling underlies a cell-autonomous loss of stem cell self-renewal in skeletal muscle of aged mice. *Nature Medicine*, *20*(3), 265–271. https://doi.org/10.1038/nm.3465

17. Bhasin, S., Storer, T. W., Berman, N., Callegari, C., Clevenger, B., Phillips, J., Bunnell, T. J., Tricker, R., Shirazi, A., & Casaburi, R. (1996). The Effects of Supraphysiologic Doses of Testosterone on Muscle Size and Strength in Normal Men. *New England Journal of Medicine*, *335*(1), 1–7. https://doi.org/10.1056/NEJM199607043350101

18. Biferali, B., Proietti, D., Mozzetta, C., & Madaro, L. (2019). Fibro–Adipogenic Progenitors Cross-Talk in Skeletal Muscle: The Social Network. *Frontiers in Physiology*, *10*, 1074. https://doi.org/10.3389/fphys.2019.01074

19. Bigot, A., Duddy, W. J., Ouandaogo, Z. G., Negroni, E., Mariot, V., Ghimbovschi, S., Harmon, B., Wielgosik, A., Loiseau, C., Devaney, J., Dumonceaux, J., Butler-Browne, G., Mouly, V., & Duguez, S. (2015). Age-Associated Methylation Suppresses SPRY1 , Leading to a Failure of Re-quiescence and Loss of the Reserve Stem Cell Pool in Elderly Muscle. *Cell Reports*, *13*(6), 1172–1182. https://doi.org/10.1016/j.celrep.2015.09.067

20. Bjornson, C. R. R., Cheung, T. H., Liu, L., Tripathi, P. V., Steeper, K. M., & Rando, T. A. (2012). Notch Signaling Is Necessary to Maintain Quiescence in Adult Muscle Stem Cells. *Stem Cells*, *30*(2), 232–242. https://doi.org/10.1002/stem.773

21. Blake, E. (2022). Piezo1 regulates the regenerative capacity of skeletal muscles via orchestration of stem cell morphological states. *SCIENCE ADVANCES*, 14.

22. Blaszczyk, N., Masri, B. A., Mawji, N. R., Ueda, T., McAlinden, G., Duncan, C. P., Bruchovsky, N., Schweikert, H.-U., Schnabel, D., Jones, E. C., & Sadar, M. D. (2004). Osteoblast-Derived Factors Induce Androgen-Independent Proliferation and Expression of Prostate-Specific Antigen in Human Prostate Cancer Cells. *Clinical Cancer Research*, *10*(5), 1860–1869. https://doi.org/10.1158/1078-0432.CCR-0974-3

23. Blouin, K., Boivin, A., & Tchernof, A. (2008). Androgens and body fat distribution. *The Journal of Steroid Biochemistry and Molecular Biology*, *108*(3–5), 272–280. https://doi.org/10.1016/j.jsbmb.2007.09.001

24. Bouzakri, K., Koistinen, H., & Zierath, J. (2005). Molecular Mechanisms of Skeletal Muscle Insulin Resistance in Type 2 Diabetes. *Current Diabetes Reviews*, *1*(2), 167–174. https://doi.org/10.2174/1573399054022785

25. Brack, A. S., Conboy, M. J., Roy, S., Lee, M., Kuo, C. J., Keller, C., & Rando, T. A. (2007). Increased Wnt Signaling During Aging Alters Muscle Stem Cell Fate and Increases Fibrosis. *Science*, *317*(5839), 807–810. https://doi.org/10.1126/science.1144090

26. Brawer, M. K. (n.d.). *Testosterone Replacement in Men With Andropause: An Overview*. 7.

27. Breza, M., & Koutsis, G. (2019). Kennedy's disease (spinal and bulbar muscular atrophy): A clinically oriented review of a rare disease. *Journal of Neurology*, *266*(3), 565–573. https://doi.org/10.1007/s00415-018-8968-7

28. Brun, C. E., & Dumont, N. A. (2016). Déficits intrinsèques des cellules satellites dans la dystrophie musculaire de Duchenne. *Médecine/Sciences*, *32*(10), 800–802. https://doi.org/10.1051/medsci/20163210003

29. Brzoska, E., Kowalski, K., Markowska-Zagrajek, A., Kowalewska, M., Archacki, R., Plaskota, I., Stremińska, W., Jańczyk-Ilach, K., & Ciemerych, M. A. (2015). Sdf-1 (CXCL12) induces CD9 expression in stem cells engaged in muscle regeneration. *Stem Cell Research & Therapy*, *6*(1), 46. https://doi.org/10.1186/s13287-015-0041-1

30. Bua, E., Johnson, J., Herbst, A., Delong, B., McKenzie, D., Salamat, S., & Aiken, J. M. (2006). Mitochondrial DNA–Deletion Mutations Accumulate Intracellularly to Detrimental Levels in Aged Human Skeletal Muscle Fibers. *The American Journal of Human Genetics*, *79*(3), 469–480. https://doi.org/10.1086/507132

31. Buckingham, M., Bajard, L., Chang, T., Daubas, P., Hadchouel, J., Meilhac, S., Montarras, D., Rocancourt, D., & Relaix, F. (2003). The formation of skeletal muscle: From somite to limb. *Journal of Anatomy*, *202*(1), 59–68. https://doi.org/10.1046/j.1469-7580.2003.00139.x

32. Burkin, D. J., & Kaufman, S. J. (1999). The α7β1 integrin in muscle development and disease. *Cell and Tissue Research*, *296*(1), 183–190. https://doi.org/10.1007/s004410051279

33. Burzyn, D., Kuswanto, W., Kolodin, D., Shadrach, J. L., Cerletti, M., Jang, Y., Sefik, E., Tan, T. G., Wagers, A. J., Benoist, C., & Mathis, D. (2013). A Special Population of Regulatory T Cells Potentiates Muscle Repair. *Cell*, *155*(6), 1282–1295. https://doi.org/10.1016/j.cell.2013.10.054

34. Cadot, B., Gache, V., & Gomes, E. R. (2015). Moving and positioning the nucleus in skeletal muscle – one step at a time. *Nucleus*, *6*(5), 373–381. https://doi.org/10.1080/19491034.2015.1090073

35. Calderón, J. C., Bolaños, P., & Caputo, C. (2014). The excitation–contraction coupling mechanism in skeletal muscle. *Biophysical Reviews*, *6*(1), 133–160. https://doi.org/10.1007/s12551-013-0135-x

36. Cardamone, M., Darras, B., & Ryan, M. (2008). Inherited Myopathies and Muscular Dystrophies. *Seminars in Neurology*, *28*(2), 250–259. https://doi.org/10.1055/s-2008-1062269

37. Castets, P., Ham, D. J., & Rüegg, M. A. (2020). The TOR Pathway at the Neuromuscular Junction: More Than a Metabolic Player? *Frontiers in Molecular Neuroscience*, *13*, 162. https://doi.org/10.3389/fnmol.2020.00162

38. Chakkalakal, J. V., Jones, K. M., Basson, M. A., & Brack, A. S. (2012). The aged niche disrupts muscle stem cell quiescence. *Nature*, *490*(7420), 355–360. https://doi.org/10.1038/nature11438

39. Chambon, C., Duteil, D., Vignaud, A., Ferry, A., Messaddeq, N., Malivindi, R., Kato, S., Chambon, P., & Metzger, D. (2010). Myocytic androgen receptor controls the strength but not the mass of limb muscles. *Proceedings of the National Academy of Sciences*, *107*(32), 14327–14332. https://doi.org/10.1073/pnas.1009536107

40. Chambon, P. (2005). The Nuclear Receptor Superfamily: A Personal Retrospect on the First Two Decades. *Molecular Endocrinology*, *19*(6), 1418–1428. https://doi.org/10.1210/me.2005-0125

41. Chapman, M. A., Mukund, K., Subramaniam, S., Brenner, D., & Lieber, R. L. (2017). Three distinct cell populations express extracellular matrix proteins and increase in number during skeletal muscle fibrosis. *American Journal of Physiology-Cell Physiology*, *312*(2), C131–C143. https://doi.org/10.1152/ajpcell.00226.2016

42. Chargé, S. B. P., & Rudnicki, M. A. (2004). Cellular and Molecular Regulation of Muscle Regeneration. *Physiological Reviews*, *84*(1), 209–238. https://doi.org/10.1152/physrev.00019.2003

43. Charrin, S., Latil, M., Soave, S., Polesskaya, A., Chrétien, F., Boucheix, C., & Rubinstein, E. (2013). Normal muscle regeneration requires tight control of muscle cell fusion by tetraspanins CD9 and CD81. *Nature Communications*, *4*(1), 1674. https://doi.org/10.1038/ncomms2675

44. Chen, H., Li, Z., Dong, L., Wu, Y., Shen, H., & Chen, Z. (2019). Lipid metabolism in chronic obstructive pulmonary disease. *International Journal of Chronic Obstructive Pulmonary Disease*, *Volume 14*, 1009–1018. https://doi.org/10.2147/COPD.S196210

45. Chen, W., Datzkiw, D., & Rudnicki, M. A. (2020a). Satellite cells in ageing: Use it or lose it. *Open Biology*, *10*(5), 200048. https://doi.org/10.1098/rsob.200048

46. Chen, W., Datzkiw, D., & Rudnicki, M. A. (2020b). Satellite cells in ageing: Use it or lose it. *Open Biology*, *10*(5), 200048. https://doi.org/10.1098/rsob.200048

47. Cho, D. S., & Doles, J. D. (2017). Single cell transcriptome analysis of muscle satellite cells reveals widespread transcriptional heterogeneity. *Gene*, *636*, 54–63. https://doi.org/10.1016/j.gene.2017.09.014

48. Christov, C., Chretien, F., Abou-Khalil, R., Bassez, G., Vallet, G., Bassaglia, Y., Shinin, V., Tajbakhsh, S., Chazaud, B., & Gherardi, R. K. (2007). Muscle Satellite Cells and Endothelial Cells: Close Neighbors and Privileged Partners□D. *Molecular Biology of the Cell*, *18*, 13.

49. Conboy, I. M., Conboy, M. J., Smythe, G. M., & Rando, T. A. (2003). Notch-Mediated Restoration of Regenerative Potential to Aged Muscle. *Science*, *302*(5650), 1575–1577. https://doi.org/10.1126/science.1087573

50. Cornelison, D. D. W., Filla, M. S., Stanley, H. M., Rapraeger, A. C., & Olwin, B. B. (2001). Syndecan-3 and Syndecan-4 Specifically Mark Skeletal Muscle Satellite Cells

and Are Implicated in Satellite Cell Maintenance and Muscle Regeneration. *Developmental Biology*, *239*(1), 79–94. https://doi.org/10.1006/dbio.2001.0416

51. Cosgrove, B. D., Gilbert, P. M., Porpiglia, E., Mourkioti, F., Lee, S. P., Corbel, S. Y., Llewellyn, M. E., Delp, S. L., & Blau, H. M. (2014). Rejuvenation of the muscle stem cell population restores strength to injured aged muscles. *Nature Medicine*, *20*(3), 255–264. https://doi.org/10.1038/nm.3464

52. Cossu, G., & Tajbakhsh, S. (2007). Oriented Cell Divisions and Muscle Satellite Cell Heterogeneity. *Cell*, *129*(5), 859–861. https://doi.org/10.1016/j.cell.2007.05.029

53. Dalbo, V. J., Roberts, M. D., Mobley, C. B., Ballmann, C., Kephart, W. C., Fox, C. D., Santucci, V. A., Conover, C. F., Beggs, L. A., Balaez, A., Hoerr, F. J., Yarrow, J. F., Borst, S. E., & Beck, D. T. (2017a). Testosterone and trenbolone enanthate increase mature myostatin protein expression despite increasing skeletal muscle hypertrophy and satellite cell number in rodent muscle. *Andrologia*, *49*(3), e12622. https://doi.org/10.1111/and.12622

54. Dalbo, V. J., Roberts, M. D., Mobley, C. B., Ballmann, C., Kephart, W. C., Fox, C. D., Santucci, V. A., Conover, C. F., Beggs, L. A., Balaez, A., Hoerr, F. J., Yarrow, J. F., Borst, S. E., & Beck, D. T. (2017b). Testosterone and trenbolone enanthate increase mature myostatin protein expression despite increasing skeletal muscle hypertrophy and satellite cell number in rodent muscle. *Andrologia*, *49*(3), e12622. https://doi.org/10.1111/and.12622

55. Daneshvar, N., Tatsumi, R., Peeler, J., & Anderson, J. E. (2020). Premature satellite cell activation before injury accelerates myogenesis and disrupts neuromuscular junction maturation in regenerating muscle. *American Journal of Physiology-Cell Physiology*, *319*(1), C116–C128. https://doi.org/10.1152/ajpcell.00121.2020

56. Davey, R. A., & Grossmann, M. (n.d.). *Androgen Receptor Structure, Function and Biology: From Bench to Bedside*. 13.

57. Davidyan, A., Pathak, S., Baar, K., & Bodine, S. C. (2021). Maintenance of muscle mass in adult male mice is independent of testosterone. *PLOS ONE*, *16*(3), e0240278. https://doi.org/10.1371/journal.pone.0240278

58. de Meeûs d'Argenteuil, C., Boshuizen, B., Oosterlinck, M., van de Winkel, D., De Spiegelaere, W., de Bruijn, C. M., Goethals, K., Vanderperren, K., & Delesalle, C. J. G. (2021). Flexibility of equine bioenergetics and muscle plasticity in response to different types of training: An integrative approach, questioning existing paradigms. *PLOS ONE*, *16*(4), e0249922. https://doi.org/10.1371/journal.pone.0249922

59. Dell'Orso, S., Juan, A. H., Ko, K.-D., Naz, F., Gutierrez-Cruz, G., Feng, X., & Sartorelli, V. (2019). Single-cell analysis of adult skeletal muscle stem cells in homeostatic and regenerative conditions. *Development*, dev.174177. https://doi.org/10.1242/dev.174177

60. Deschenes, M. R., Roby, M. A., Eason, M. K., & Harris, M. B. (2010). Remodeling of the neuromuscular junction precedes sarcopenia related alterations in myofibers. *Experimental Gerontology*, *45*(5), 389–393. https://doi.org/10.1016/j.exger.2010.03.007

61. Diel, P., Baadners, D., Schlüpmann, K., Velders, M., & Schwarz, J. P. (2008). C2C12 myoblastoma cell differentiation and proliferation is stimulated by androgens and

associated with a modulation of myostatin and Pax7 expression. *Journal of Molecular Endocrinology*, *40*(5), 231–241. https://doi.org/10.1677/JME-07-0175

62. Domingues-Faria, C., Vasson, M.-P., Goncalves-Mendes, N., Boirie, Y., & Walrand, S. (2016). Skeletal muscle regeneration and impact of aging and nutrition. *Ageing Research Reviews*, *26*, 22–36. https://doi.org/10.1016/j.arr.2015.12.004

63. Duan, D., Goemans, N., Takeda, S., Mercuri, E., & Aartsma-Rus, A. (2021). *Duchenne muscular dystrophy*. 19.

64. Duarte-Guterman, P., Lieblich, S. E., Wainwright, S. R., Chow, C., Chaiton, J. A., Watson, N. V., & Galea, L. A. M. (2019). Androgens Enhance Adult Hippocampal Neurogenesis in Males but Not Females in an Age-Dependent Manner. *Endocrinology*, *160*(9), 2128–2136. https://doi.org/10.1210/en.2019-00114

65. Dubois, V., Laurent, M. R., Sinnesael, M., Cielen, N., Helsen, C., Clinckemalie, L., Spans, L., Gayan-Ramirez, G., Deldicque, L., Hespel, P., Carmeliet, G., Vanderschueren, D., & Claessens, F. (2014a). A satellite cell-specific knockout of the androgen receptor reveals myostatin as a direct androgen target in skeletal muscle. *The FASEB Journal*, *28*(7), 2979–2994. https://doi.org/10.1096/fj.14-249748

66. Dubois, V., Laurent, M. R., Sinnesael, M., Cielen, N., Helsen, C., Clinckemalie, L., Spans, L., Gayan-Ramirez, G., Deldicque, L., Hespel, P., Carmeliet, G., Vanderschueren, D., & Claessens, F. (2014b). A satellite cell-specific knockout of the androgen receptor reveals myostatin as a direct androgen target in skeletal muscle. *The FASEB Journal*, *28*(7), 2979–2994. https://doi.org/10.1096/fj.14-249748

67. Dubois, V., Laurent, M. R., Sinnesael, M., Cielen, N., Helsen, C., Clinckemalie, L., Spans, L., Gayan-Ramirez, G., Deldicque, L., Hespel, P., Carmeliet, G., Vanderschueren, D., & Claessens, F. (2014c). A satellite cell-specific knockout of the androgen receptor reveals myostatin as a direct androgen target in skeletal muscle. *The FASEB Journal*, *28*(7), 2979–2994. https://doi.org/10.1096/fj.14-249748

68. Dumont, N. A., Bentzinger, C. F., Sincennes, M., & Rudnicki, M. A. (2015). Satellite Cells and Skeletal Muscle Regeneration. In R. Terjung (Ed.), *Comprehensive Physiology* (1st ed., pp. 1027–1059). Wiley. https://doi.org/10.1002/cphy.c140068

69. El Hokayem, J., Amadei, C., Obeid, J.-P., & Nawaz, Z. (2017). Ubiquitination of nuclear receptors. *Clinical Science*, *131*(10), 917–934. https://doi.org/10.1042/CS20160708

70. Eliazer, S., Muncie, J. M., Christensen, J., Sun, X., D'Urso, R. S., Weaver, V. M., & Brack, A. S. (2019). Wnt4 from the Niche Controls the Mechano-Properties and Quiescent State of Muscle Stem Cells. *Cell Stem Cell*, *25*(5), 654-665.e4. https://doi.org/10.1016/j.stem.2019.08.007

71. Escriva, H., Delaunay, F., & Laudet, V. (2000). Ligand binding and nuclear receptor evolution. *BioEssays*, *22*(8), 717–727. https://doi.org/10.1002/1521-1878(200008)22:8<717::AID-BIES5>3.0.CO;2-I

72. Evano, B., Khalilian, S., Le Carrou, G., Almouzni, G., & Tajbakhsh, S. (2020). Dynamics of Asymmetric and Symmetric Divisions of Muscle Stem Cells In Vivo and on Artificial Niches. *Cell Reports*, *30*(10), 3195-3206.e7. https://doi.org/10.1016/j.celrep.2020.01.097

73. Evano, B., & Tajbakhsh, S. (2018). Skeletal muscle stem cells in comfort and stress. *Npj Regenerative Medicine*, *3*(1), 24. https://doi.org/10.1038/s41536-018-0062-3

74. Fang, X.-B., Song, Z.-B., Xie, M.-S., Liu, Y.-M., & Zhang, W.-X. (2020). Synergistic effect of glucocorticoids and IGF-1 on myogenic differentiation through the Akt/GSK-3β pathway in C2C12 myoblasts. *International Journal of Neuroscience*, *130*(11), 1125–1135. https://doi.org/10.1080/00207454.2020.1730367

75. Faus, H., & Haendler, B. (2006). Post-translational modifications of steroid receptors. *Biomedicine & Pharmacotherapy*, *60*(9), 520–528. https://doi.org/10.1016/j.biopha.2006.07.082

76. Feichtinger, R. G., Mucha, B. E., Hengel, H., Orfi, Z., Makowski, C., Dort, J., D'Anjou, G., Nguyen, T. T. M., Buchert, R., Juenger, H., Freisinger, P., Baumeister, S., Schoser, B., Ahting, U., Keimer, R., Nguyen, C.-T. E., Fabre, P., Gauthier, J., Miguet, M., … Dumont, N. A. (2019). Biallelic variants in the transcription factor PAX7 are a new genetic cause of myopathy. *Genetics in Medicine*, *21*(11), 2521–2531. https://doi.org/10.1038/s41436-019-0532-z

77. Florkowska, A., Meszka, I., Zawada, M., Legutko, D., Proszynski, T. J., Janczyk-Ilach, K., Streminska, W., Ciemerych, M. A., & Grabowska, I. (2020). Pax7 as molecular switch regulating early and advanced stages of myogenic mouse ESC differentiation in teratomas. *Stem Cell Research & Therapy*, *11*(1), 238. https://doi.org/10.1186/s13287-020-01742-3

78. Fonseca, G. W. P. D., Dworatzek, E., Ebner, N., & Von Haehling, S. (2020). Selective androgen receptor modulators (SARMs) as pharmacological treatment for muscle wasting in ongoing clinical trials. *Expert Opinion on Investigational Drugs*, *29*(8), 881–891. https://doi.org/10.1080/13543784.2020.1777275

79. Franco, M., Roswall, P., Cortez, E., Hanahan, D., & Pietras, K. (2011). Pericytes promote endothelial cell survival through induction of autocrine VEGF-A signaling and Bcl-w expression. *Blood*, *118*(10), 2906–2917. https://doi.org/10.1182/blood-2011-01-331694

80. Fruchart, J.-C., Santos, R. D., Aguilar-Salinas, C., Aikawa, M., Al Rasadi, K., Amarenco, P., Barter, P. J., Ceska, R., Corsini, A., Després, J.-P., Duriez, P., Eckel, R. H., Ezhov, M. V., Farnier, M., Ginsberg, H. N., Hermans, M. P., Ishibashi, S., Karpe, F., Kodama, T., … Libby, P. (2019). The selective peroxisome proliferator-activated receptor alpha modulator (SPPARMα) paradigm: Conceptual framework and therapeutic potential: A consensus statement from the International Atherosclerosis Society (IAS) and the Residual Risk Reduction Initiative (R3i) Foundation. *Cardiovascular Diabetology*, *18*(1), 71. https://doi.org/10.1186/s12933-019-0864-7

81. Fry, C. S., Drummond, M. J., Glynn, E. L., Dickinson, J. M., Gundermann, D. M., Timmerman, K. L., Walker, D. K., Dhanani, S., Volpi, E., & Rasmussen, B. B. (2011). Aging impairs contraction-induced human skeletal muscle mTORC1 signaling and protein synthesis. *Skeletal Muscle*, *1*(1), 11. https://doi.org/10.1186/2044-5040-1-11

82. Fu, S., Lin, X., Yin, L., & Wang, X. (2021). Androgen receptor regulates the proliferation of myoblasts under appropriate or excessive stretch through IGF-1 receptor mediated p38 and ERK1/2 pathways. *Nutrition & Metabolism*, *18*(1), 85. https://doi.org/10.1186/s12986-021-00610-y

83. Fu, X., Wang, H., & Hu, P. (2015). Stem cell activation in skeletal muscle regeneration. *Cellular and Molecular Life Sciences*, *72*(9), 1663–1677. https://doi.org/10.1007/s00018-014-1819-5

84. Fukada, S., Uezumi, A., Ikemoto, M., Masuda, S., Segawa, M., Tanimura, N., Yamamoto, H., Miyagoe-Suzuki, Y., & Takeda, S. (2007). Molecular Signature of Quiescent Satellite Cells in Adult Skeletal Muscle. *Stem Cells*, *25*(10), 2448–2459. https://doi.org/10.1634/stemcells.2007-0019

85. Galpin, A. J., Raue, U., Jemiolo, B., Trappe, T. A., Harber, M. P., Minchev, K., & Trappe, S. (2012). Human skeletal muscle fiber type specific protein content. *Analytical Biochemistry*, *425*(2), 175–182. https://doi.org/10.1016/j.ab.2012.03.018

86. Ganassi, M., Badodi, S., Ortuste Quiroga, H. P., Zammit, P. S., Hinits, Y., & Hughes, S. M. (2018). Myogenin promotes myocyte fusion to balance fibre number and size. *Nature Communications*, *9*(1), 4232. https://doi.org/10.1038/s41467-018-06583-6

87. Ganassi, M., Muntoni, F., & Zammit, P. S. (2022). Defining and identifying satellite cell-opathies within muscular dystrophies and myopathies. *Experimental Cell Research*, *411*(1), 112906. https://doi.org/10.1016/j.yexcr.2021.112906

88. García-Prat, L., Muñoz-Cánoves, P., & Martinez-Vicente, M. (2016). Dysfunctional autophagy is a driver of muscle stem cell functional decline with aging. *Autophagy*, *12*(3), 612–613. https://doi.org/10.1080/15548627.2016.1143211

89. Gattazzo, F., Laurent, B., Relaix, F., Rouard, H., & Didier, N. (2020). Distinct Phases of Postnatal Skeletal Muscle Growth Govern the Progressive Establishment of Muscle Stem Cell Quiescence. *Stem Cell Reports*, *15*(3), 597–611. https://doi.org/10.1016/j.stemcr.2020.07.011

90. Gavassini, B. F., Carboni, N., Nielsen, J. E., Danielsen, E. R., Thomsen, C., Svenstrup, K., Bello, L., Maioli, M. A., Marrosu, G., Ticca, A. F., Mura, M., Marrosu, M. G., Soraru, G., Angelini, C., Vissing, J., & Pegoraro, E. (2011). Clinical and molecular characterization of limb-girdle muscular dystrophy due to LAMA2 mutations. *Muscle & Nerve*, *44*(5), 703–709. https://doi.org/10.1002/mus.22132

91. Germain, P., Staels, B., Dacquet, C., Spedding, M., & Laudet, V. (2006). Overview of Nomenclature of Nuclear Receptors. *Pharmacological Reviews*, *58*(4), 685–704. https://doi.org/10.1124/pr.58.4.2

92. Germani, A., Di Carlo, A., Mangoni, A., Straino, S., Giacinti, C., Turrini, P., Biglioli, P., & Capogrossi, M. C. (2003). Vascular Endothelial Growth Factor Modulates Skeletal Myoblast Function. *The American Journal of Pathology*, *163*(4), 1417–1428. https://doi.org/10.1016/S0002-9440(10)63499-2

93. Giordani, L., He, G. J., Negroni, E., Sakai, H., Law, J. Y. C., Siu, M. M., Wan, R., Corneau, A., Tajbakhsh, S., Cheung, T. H., & Le Grand, F. (2019). High-Dimensional Single-Cell Cartography Reveals Novel Skeletal Muscle-Resident Cell Populations. *Molecular Cell*, *74*(3), 609-621.e6. https://doi.org/10.1016/j.molcel.2019.02.026

94. Giorgetti, E., Yu, Z., Chua, J. P., Shimamura, R., Zhao, L., Zhu, F., Venneti, S., Pennuto, M., Guan, Y., Hung, G., & Lieberman, A. P. (2016). Rescue of Metabolic Alterations in AR113Q Skeletal Muscle by Peripheral Androgen Receptor Gene Silencing. *Cell Reports*, *17*(1), 125–136. https://doi.org/10.1016/j.celrep.2016.08.084

95. Glass, C. K., & Rosenfeld, M. G. (2000). The coregulator exchange in transcriptional functions of nuclear receptors. *Genes & Development*, *14*(2), 121–141. https://doi.org/10.1101/gad.14.2.121

96. Gollapudi, S. K., Michael, J. J., & Chandra, M. (2014). Striated Muscle Dynamics. In *Reference Module in Biomedical Sciences* (p. B9780128012383003000). Elsevier. https://doi.org/10.1016/B978-0-12-801238-3.00251-8

97. Green, H. J., Reichmann, H., & Pette, D. (1982). A comparison of two ATPase based schemes for histochemical muscle fibre typing in various mammals. *Histochemistry*, *76*(1), 21–31. https://doi.org/10.1007/BF00493282

98. Gronemeyer, H., Gustafsson, J.-Å., & Laudet, V. (2004). Principles for modulation of the nuclear receptor superfamily. *Nature Reviews Drug Discovery*, *3*(11), 950–964. https://doi.org/10.1038/nrd1551

99. Grounds, M. D. (1998). Age-associated Changes in the Response of Skeletal Muscle Cells to Exercise and Regenerationa. *Annals of the New York Academy of Sciences*, *854*(1 TOWARDS PROLO), 78–91. https://doi.org/10.1111/j.1749-6632.1998.tb09894.x

100. Grounds, M. D. (2008). Complexity of Extracellular Matrix and Skeletal Muscle Regeneration. In *Skeletal Muscle Repair and Regeneration* (Vol. 3, pp. 269–302). Springer Netherlands. https://doi.org/10.1007/978-1-4020-6768-6_13

101. Günther, S., Kim, J., Kostin, S., Lepper, C., Fan, C.-M., & Braun, T. (2013). Myf5-Positive Satellite Cells Contribute to Pax7-Dependent Long-Term Maintenance of Adult Muscle Stem Cells. *Cell Stem Cell*, *13*(5), 590–601. https://doi.org/10.1016/j.stem.2013.07.016

102. Hameed, M., Orrell, R. W., Cobbold, M., Goldspink, G., & Harridge, S. D. R. (2003). Expression of IGF-I splice variants in young and old human skeletal muscle after high resistance exercise. *The Journal of Physiology*, *547*(1), 247–254. https://doi.org/10.1113/jphysiol.2002.032136

103. Hara, M., Yuasa, S., Shimoji, K., Onizuka, T., Hayashiji, N., Ohno, Y., Arai, T., Hattori, F., Kaneda, R., Kimura, K., Makino, S., Sano, M., & Fukuda, K. (2011). G-CSF influences mouse skeletal muscle development and regeneration by stimulating myoblast proliferation. *Journal of Experimental Medicine*, *208*(4), 715–727. https://doi.org/10.1084/jem.20101059

104. Henderson, C. A., Gomez, C. G., Novak, S. M., Mi-Mi, L., & Gregorio, C. C. (2017). Overview of the Muscle Cytoskeleton. In R. Terjung (Ed.), *Comprehensive Physiology* (1st ed., pp. 891–944). Wiley. https://doi.org/10.1002/cphy.c160033

105. Henze, H., Jung, M. J., Ahrens, H. E., Steiner, S., & von Maltzahn, J. (2020). Skeletal muscle aging – Stem cells in the spotlight. *Mechanisms of Ageing and Development*, *189*, 111283. https://doi.org/10.1016/j.mad.2020.111283

106. Heredia, J. E., Mukundan, L., Chen, F. M., Mueller, A. A., Deo, R. C., Locksley, R. M., Rando, T. A., & Chawla, A. (2013). Type 2 Innate Signals Stimulate Fibro/Adipogenic Progenitors to Facilitate Muscle Regeneration. *Cell*, *153*(2), 376–388. https://doi.org/10.1016/j.cell.2013.02.053

107. Hickey, M. S., Carey, J. O., Azevedo, J. L., Houmard, J. A., Pories, W. J., Israel, R. G., & Dohm, G. L. (1995). Skeletal muscle fiber composition is related to adiposity and in vitro glucose transport rate in humans. *American Journal of Physiology-Endocrinology and Metabolism*, *268*(3), E453–E457. https://doi.org/10.1152/ajpendo.1995.268.3.E453

108. Hnia, K., Ramspacher, C., Vermot, J., & Laporte, J. (2015). Desmin in muscle and associated diseases: Beyond the structural function. *Cell and Tissue Research*, *360*(3), 591–608. https://doi.org/10.1007/s00441-014-2016-4

109. Hughes, I. A., Davies, J. D., Bunch, T. I., Pasterski, V., Mastroyannopoulou, K., & MacDougall, J. (2012). Androgen insensitivity syndrome. *The Lancet*, *380*(9851), 1419–1428. https://doi.org/10.1016/S0140-6736(12)60071-3

110. Illa, I., Leon-Monzon, M., & Dalakas, M. C. (1992). Regenerating and denervated human muscle fibers and satellite cells express neural cell adhesion molecule recognized by monoclonal antibodies to natural killer cells. *Annals of Neurology*, *31*(1), 46–52. https://doi.org/10.1002/ana.410310109

111. Irintchev, A., Zeschnigk, M., Starzinski-Powitz, A., & Wernig, A. (1994). Expression pattern of M-cadherin in normal, denervated, and regenerating mouse muscles. *Developmental Dynamics*, *199*(4), 326–337. https://doi.org/10.1002/aja.1001990407

112. Ishii, K., Sakurai, H., Suzuki, N., Mabuchi, Y., Sekiya, I., Sekiguchi, K., & Akazawa, C. (2018). Recapitulation of Extracellular LAMININ Environment Maintains Stemness of Satellite Cells In Vitro. *Stem Cell Reports*, *10*(2), 568–582. https://doi.org/10.1016/j.stemcr.2017.12.013

113. Jejurikar, S. S., Henkelman, E. A., Cederna, P. S., Marcelo, C. L., Urbanchek, M. G., & Kuzon, W. M. (2006). Aging increases the susceptibility of skeletal muscle derived satellite cells to apoptosis. *Experimental Gerontology*, *41*(9), 828–836. https://doi.org/10.1016/j.exger.2006.06.053

114. Jiao, Q., Pruznak, A. M., Huber, D., Vary, T. C., & Lang, C. H. (2009). Castration differentially alters basal and leucine-stimulated tissue protein synthesis in skeletal muscle and adipose tissue. *American Journal of Physiology-Endocrinology and Metabolism*, *297*(5), E1222–E1232. https://doi.org/10.1152/ajpendo.00473.2009

115. Joe, A. W. B., Yi, L., Natarajan, A., Le Grand, F., So, L., Wang, J., Rudnicki, M. A., & Rossi, F. M. V. (2010). Muscle injury activates resident fibro/adipogenic progenitors that facilitate myogenesis. *Nature Cell Biology*, *12*(2), 153–163. https://doi.org/10.1038/ncb2015

116. Jordan, C. L., & DonCarlos, L. (2008). Androgens in health and disease: An overview. *Hormones and Behavior*, *53*(5), 589–595. https://doi.org/10.1016/j.yhbeh.2008.02.016

117. Judson, R. N., Tremblay, A. M., Knopp, P., White, R. B., Urcia, R., De Bari, C., Zammit, P. S., Camargo, F. D., & Wackerhage, H. (2012). The Hippo pathway member Yap plays a key role in influencing fate decisions in muscle satellite cells. *Journal of Cell Science*, *125*(24), 6009–6019. https://doi.org/10.1242/jcs.109546

118. Kalyuzhny, A. E. (2011). Combination of TUNEL Assay with Immunohistochemistry for Simultaneous Detection of DNA Fragmentation and Oxidative Cell Damage. In V. V. Didenko (Ed.), *DNA Damage Detection In Situ, Ex Vivo, and In Vivo* (Vol. 682, pp. 15–27). Humana Press. https://doi.org/10.1007/978-1-60327-409-8_2

119. Kanayama, G., Kaufman, M. J., & Pope, H. G. (2018). Public health impact of androgens: *Current Opinion in Endocrinology & Diabetes and Obesity*, *25*(3), 218–223. https://doi.org/10.1097/MED.0000000000000404

120. Kim, J., Park, J., Kim, N., Park, H., & Lim, K. (2019). Inhibition of androgen receptor can decrease fat metabolism by decreasing carnitine palmitoyltransferase I levels in

skeletal muscles of trained mice. *Nutrition & Metabolism*, *16*(1), 82. https://doi.org/10.1186/s12986-019-0406-z

121. Kim, J.-H., Han, G.-C., Seo, J.-Y., Park, I., Park, W., Jeong, H.-W., Lee, S. H., Bae, S., Seong, J., Yum, M.-K., Hann, S.-H., Kwon, Y.-G., Seo, D., Choi, M. H., & Kong, Y.-Y. (2016a). Sex hormones establish a reserve pool of adult muscle stem cells. *Nature Cell Biology*, *18*(9), 930–940. https://doi.org/10.1038/ncb3401

122. Kim, J.-H., Han, G.-C., Seo, J.-Y., Park, I., Park, W., Jeong, H.-W., Lee, S. H., Bae, S., Seong, J., Yum, M.-K., Hann, S.-H., Kwon, Y.-G., Seo, D., Choi, M. H., & Kong, Y.-Y. (2016b). Sex hormones establish a reserve pool of adult muscle stem cells. *Nature Cell Biology*, *18*(9), 930–940. https://doi.org/10.1038/ncb3401

123. Kitamoto, T., & Hanaoka, K. (2010). *Notch3* Null Mutation in Mice Causes Muscle Hyperplasia by Repetitive Muscle Regeneration. *Stem Cells*, *28*(12), 2205–2216. https://doi.org/10.1002/stem.547

124. Kitzmann, M., & Fernandez, A. (2001). Crosstalk between cell cycle regulators and the myogenic factor MyoD in skeletal myoblasts: *Cellular and Molecular Life Sciences*, *58*(4), 571–579. https://doi.org/10.1007/PL00000882

125. Klose, A., Liu, W., Paris, N. D., Forman, S., Krolewski, J. J., Nastiuk, K. L., & Chakkalakal, J. V. (2018). Castration induces satellite cell activation that contributes to skeletal muscle maintenance. *JCSM Rapid Communications*, *1*(1), 1–16. https://doi.org/10.1002/j.2617-1619.2018.tb00004.x

126. K.M. Reeves, E., Rayavarapu, S., M. Damsker, J., & Nagaraju, K. (2012). Glucocorticoid Analogues: Potential Therapeutic Alternatives for Treating Inflammatory Muscle Diseases. *Endocrine, Metabolic & Immune Disorders-Drug Targets*, *12*(1), 95–103. https://doi.org/10.2174/187153012799279045

127. Koch, A. J., Pereira, R., & Machado, M. (n.d.). *The creatine kinase response to resistance exercise*. 10.

128. Kostallari, E., Baba-Amer, Y., Alonso-Martin, S., Ngoh, P., Relaix, F., Lafuste, P., & Gherardi, R. K. (2015). Pericytes in the myovascular niche promote post-natal myofiber growth and satellite cell quiescence. *Development*, dev.115386. https://doi.org/10.1242/dev.115386

129. Kottlors, M., & Kirschner, J. (2010). Elevated satellite cell number in Duchenne muscular dystrophy. *Cell and Tissue Research*, *340*(3), 541–548. https://doi.org/10.1007/s00441-010-0976-6

130. Krook, A., Björnholm, M., Galuska, D., Jiang, X. J., Fahlman, R., Myers, M. G., Wallberg-Henriksson, H., & Zierath, J. R. (2000). Characterization of signal transduction and glucose transport in skeletal muscle from type 2 diabetic patients. *Diabetes*, *49*(2), 284–292. https://doi.org/10.2337/diabetes.49.2.284

131. Kuang, S., Kuroda, K., Le Grand, F., & Rudnicki, M. A. (2007). Asymmetric Self-Renewal and Commitment of Satellite Stem Cells in Muscle. *Cell*, *129*(5), 999–1010. https://doi.org/10.1016/j.cell.2007.03.044

132. Kuroda, K., Tani, S., Tamura, K., Minoguchi, S., Kurooka, H., & Honjo, T. (1999). Delta-induced Notch Signaling Mediated by RBP-J Inhibits MyoD Expression and Myogenesis. *Journal of Biological Chemistry*, *274*(11), 7238–7244. https://doi.org/10.1074/jbc.274.11.7238

133. Lahoute, C., Sotiropoulos, A., Favier, M., Guillet-Deniau, I., Charvet, C., Ferry, A., Butler-Browne, G., Metzger, D., Tuil, D., & Daegelen, D. (2008). Premature Aging in Skeletal Muscle Lacking Serum Response Factor. *PLoS ONE*, *3*(12), e3910. https://doi.org/10.1371/journal.pone.0003910

134. Lalevée, S., Ferry, C., & Rochette-Egly, C. (2010). Phosphorylation Control of Nuclear Receptors. In P. J. Higgins (Ed.), *Transcription Factors* (Vol. 647, pp. 251–266). Humana Press. https://doi.org/10.1007/978-1-60761-738-9_15

135. Langlois, A., Forterre, A., Pinget, M., & Bouzakri, K. (2021). Impact of moderate exercise on fatty acid oxidation in pancreatic β-cells and skeletal muscle. *Journal of Endocrinological Investigation*, *44*(9), 1815–1825. https://doi.org/10.1007/s40618-021-01551-2

136. Larionov, A., Krause, A., & Miller, W. (2005). [No title found]. *BMC Bioinformatics*, *6*(1), 62. https://doi.org/10.1186/1471-2105-6-62

137. Larivière, L., Seizl, M., & Cramer, P. (2012). A structural perspective on Mediator function. *Current Opinion in Cell Biology*, *24*(3), 305–313. https://doi.org/10.1016/j.ceb.2012.01.007

138. Larouche, J. A., Fraczek, P. M., Kurpiers, S. J., Yang, B. A., Davis, C., Castor-Macias, J. A., Sabin, K., Anderson, S., Harrer, J., Hall, M., Brooks, S. V., Jang, Y. C., Willett, N., Shea, L. D., & Aguilar, C. A. (2022). Neutrophil and natural killer cell imbalances prevent muscle stem cell–mediated regeneration following murine volumetric muscle loss. *Proceedings of the National Academy of Sciences*, *119*(15), e2111445119. https://doi.org/10.1073/pnas.2111445119

139. Latroche, C., Weiss-Gayet, M., Muller, L., Gitiaux, C., Leblanc, P., Liot, S., Ben-Larbi, S., Abou-Khalil, R., Verger, N., Bardot, P., Magnan, M., Chrétien, F., Mounier, R., Germain, S., & Chazaud, B. (2017). Coupling between Myogenesis and Angiogenesis during Skeletal Muscle Regeneration Is Stimulated by Restorative Macrophages. *Stem Cell Reports*, *9*(6), 2018–2033. https://doi.org/10.1016/j.stemcr.2017.10.027

140. Leduc-Gaudet, J.-P., Picard, M., Pelletier, F. S.-J., Sgarioto, N., Auger, M.-J., Vallée, J., Robitaille, R., St-Pierre, D. H., & Gouspillou, G. (2015). Mitochondrial morphology is altered in atrophied skeletal muscle of aged mice. *Oncotarget*, *6*(20), 17923–17937. https://doi.org/10.18632/oncotarget.4235

141. Leikina, E., Gamage, D. G., Prasad, V., Goykhberg, J., Crowe, M., Diao, J., Kozlov, M. M., Chernomordik, L. V., & Millay, D. P. (2018). Myomaker and Myomerger Work Independently to Control Distinct Steps of Membrane Remodeling during Myoblast Fusion. *Developmental Cell*, *46*(6), 767-780.e7. https://doi.org/10.1016/j.devcel.2018.08.006

142. Lepper, C., Conway, S. J., & Fan, C.-M. (2009). Adult satellite cells and embryonic muscle progenitors have distinct genetic requirements. *Nature*, *460*(7255), 627–631. https://doi.org/10.1038/nature08209

143. Lepper, C., Partridge, T. A., & Fan, C.-M. (2011). An absolute requirement for Pax7-positive satellite cells in acute injury-induced skeletal muscle regeneration. *Development*, *138*(17), 3639–3646. https://doi.org/10.1242/dev.067595

144. Levin, E. R. (2008). Rapid signaling by steroid receptors. *American Journal of Physiology-Regulatory, Integrative and Comparative Physiology*, *295*(5), R1425–R1430. https://doi.org/10.1152/ajpregu.90605.2008

145. Li, Y., Schwartz, R. J., Waddell, I. D., Holloway, B. R., & Reid, M. B. (1998). Skeletal muscle myocytes undergo protein loss and reactive oxygen-mediated NF-κB activation in response to tumor necrosis factorα. *The FASEB Journal*, *12*(10), 871–880. https://doi.org/10.1096/fasebj.12.10.971

146. Lilja, K. C., Zhang, N., Magli, A., Gunduz, V., Bowman, C. J., Arpke, R. W., Darabi, R., Kyba, M., Perlingeiro, R., & Dynlacht, B. D. (2017). Pax7 remodels the chromatin landscape in skeletal muscle stem cells. *PLOS ONE*, *12*(4), e0176190. https://doi.org/10.1371/journal.pone.0176190

147. Liu, J., Burkin, D. J., & Kaufman, S. J. (2008). Increasing $\alpha_7\beta_1$-integrin promotes muscle cell proliferation, adhesion, and resistance to apoptosis without changing gene expression. *American Journal of Physiology-Cell Physiology*, *294*(2), C627–C640. https://doi.org/10.1152/ajpcell.00329.2007

148. Liu, J., Huang, Z.-P., Nie, M., Wang, G., Silva, W. J., Yang, Q., Freire, P. P., Hu, X., Chen, H., Deng, Z., Pu, W. T., & Wang, D.-Z. (2020). Regulation of myonuclear positioning and muscle function by the skeletal muscle-specific CIP protein. *Proceedings of the National Academy of Sciences*, *117*(32), 19254–19265. https://doi.org/10.1073/pnas.1922911117

149. Liu, W., Klose, A., Forman, S., Paris, N. D., Wei-LaPierre, L., Cortés-Lopéz, M., Tan, A., Flaherty, M., Miura, P., Dirksen, R. T., & Chakkalakal, J. V. (2017). Loss of adult skeletal muscle stem cells drives age-related neuromuscular junction degeneration. *ELife*, *6*, e26464. https://doi.org/10.7554/eLife.26464

150. Liu, W., Zeng, M., & Fu, N. (2021). Functions of nuclear receptors SUMOylation. *Clinica Chimica Acta*, *516*, 27–33. https://doi.org/10.1016/j.cca.2021.01.007

151. Livak, K. J., & Schmittgen, T. D. (2001). Analysis of Relative Gene Expression Data Using Real-Time Quantitative PCR and the $2^{-\Delta\Delta CT}$ Method. *Methods*, *25*(4), 402–408. https://doi.org/10.1006/meth.2001.1262

152. Lluís, F., Perdiguero, E., Nebreda, A. R., & Muñoz-Cánoves, P. (2006). Regulation of skeletal muscle gene expression by p38 MAP kinases. *Trends in Cell Biology*, *16*(1), 36–44. https://doi.org/10.1016/j.tcb.2005.11.002

153. Lluri, G., Langlois, G. D., McClellan, B., Soloway, P. D., & Jaworski, D. M. (2006). Tissue inhibitor of metalloproteinase-2 (TIMP-2) regulates neuromuscular junction development via a β1 integrin-mediated mechanism. *Journal of Neurobiology*, *66*(12), 1365–1377. https://doi.org/10.1002/neu.20315

154. Lopes, F., Miguet, M., Mucha, B. E., Gauthier, J., Saillour, V., Nguyen, C.-T. É., Vanasse, M., Ellezam, B., Michaud, J. L., Soucy, J.-F., & Campeau, P. M. (2018). *MYOD1* involvement in myopathy. *European Journal of Neurology*, *25*(12), e123–e124. https://doi.org/10.1111/ene.13782

155. Loreti, M., & Sacco, A. (2022). The jam session between muscle stem cells and the extracellular matrix in the tissue microenvironment. *Npj Regenerative Medicine*, *7*(1), 16. https://doi.org/10.1038/s41536-022-00204-z

156. Loveland, J. L., Giraldo-Deck, L. M., Lank, D. B., Goymann, W., Gahr, M., & Küpper, C. (2021). Functional differences in the hypothalamic-pituitary-gonadal axis are associated with alternative reproductive tactics based on an inversion polymorphism. *Hormones and Behavior*, *127*, 104877. https://doi.org/10.1016/j.yhbeh.2020.104877

157. Low, S., Barnes, J. L., Zammit, P. S., & Beauchamp, J. R. (2018). Delta-Like 4 Activates Notch 3 to Regulate Self-Renewal in Skeletal Muscle Stem Cells. *Stem Cells*, *36*(3), 458–466. https://doi.org/10.1002/stem.2757

158. Lubahn, D. B., Joseph, D. R., Sar, M., Tan, J., Higgs, H. N., Larson, R. E., French, F. S., & Wilson, E. M. (1988). The Human Androgen Receptor: Complementary Deoxyribonucleic Acid Cloning, Sequence Analysis and Gene Expression in Prostate. *Molecular Endocrinology*, *2*(12), 1265–1275. https://doi.org/10.1210/mend-2-12-1265

159. Lukjanenko, L., Karaz, S., Stuelsatz, P., Gurriaran-Rodriguez, U., Michaud, J., Dammone, G., Sizzano, F., Mashinchian, O., Ancel, S., Migliavacca, E., Liot, S., Jacot, G., Metairon, S., Raymond, F., Descombes, P., Palini, A., Chazaud, B., Rudnicki, M. A., Bentzinger, C. F., & Feige, J. N. (2019). Aging Disrupts Muscle Stem Cell Function by Impairing Matricellular WISP1 Secretion from Fibro-Adipogenic Progenitors. *Cell Stem Cell*, *24*(3), 433-446.e7. https://doi.org/10.1016/j.stem.2018.12.014

160. MacKrell, J. G., Yaden, B. C., Bullock, H., Chen, K., Shetler, P., Bryant, H. U., & Krishnan, V. (2015). Molecular Targets of Androgen Signaling that Characterize Skeletal Muscle Recovery and Regeneration. *Nuclear Receptor Signaling*, *13*(1), nrs.13005. https://doi.org/10.1621/nrs.13005

161. MacLean, H. E., Chiu, W. S. M., Notini, A. J., Axell, A.-M., Davey, R. A., McManus, J. F., Ma, C., Plant, D. R., Lynch, G. S., & Zajac, J. D. (2008). Impaired skeletal muscle development and function in male, but not female, genomic *androgen receptor* knockout mice. *The FASEB Journal*, *22*(8), 2676–2689. https://doi.org/10.1096/fj.08-105726

162. Mahdy, M. A. A. (2019). Skeletal muscle fibrosis: An overview. *Cell and Tissue Research*, *375*(3), 575–588. https://doi.org/10.1007/s00441-018-2955-2

163. Makieva, S., Saunders, P. T. K., & Norman, J. E. (2014). Androgens in pregnancy: Roles in parturition. *Human Reproduction Update*, *20*(4), 542–559. https://doi.org/10.1093/humupd/dmu008

164. Malena, A., Pennuto, M., Tezze, C., Querin, G., D'Ascenzo, C., Silani, V., Cenacchi, G., Scaramozza, A., Romito, S., Morandi, L., Pegoraro, E., Russell, A. P., Sorarù, G., & Vergani, L. (2013). Androgen-dependent impairment of myogenesis in spinal and bulbar muscular atrophy. *Acta Neuropathologica*, *126*(1), 109–121. https://doi.org/10.1007/s00401-013-1122-9

165. Mann, G., Mora, S., Madu, G., & Adegoke, O. A. J. (2021). Branched-chain Amino Acids: Catabolism in Skeletal Muscle and Implications for Muscle and Whole-body Metabolism. *Frontiers in Physiology*, *12*, 702826. https://doi.org/10.3389/fphys.2021.702826

166. Manna, P. R., Stetson, C. L., Slominski, A. T., & Pruitt, K. (2016). Role of the steroidogenic acute regulatory protein in health and disease. *Endocrine*, *51*(1), 7–21. https://doi.org/10.1007/s12020-015-0715-6

167. Martínez-Reyes, I., & Chandel, N. S. (2020). Mitochondrial TCA cycle metabolites control physiology and disease. *Nature Communications*, *11*(1), 102. https://doi.org/10.1038/s41467-019-13668-3

168. Marzetti, E., Wohlgemuth, S. E., Lees, H. A., Chung, H.-Y., Giovannini, S., & Leeuwenburgh, C. (2008). Age-related activation of mitochondrial caspase-

independent apoptotic signaling in rat gastrocnemius muscle. *Mechanisms of Ageing and Development*, *129*(9), 542–549. https://doi.org/10.1016/j.mad.2008.05.005

169. Mauro, A. (1961). SATELLITE CELL OF SKELETAL MUSCLE FIBERS. *The Journal of Biophysical and Biochemical Cytology*, *9*(2), 493–495. https://doi.org/10.1083/jcb.9.2.493

170. McClung, J. M., Reinardy, J. L., Mueller, S. B., McCord, T. J., Kontos, C. D., Brown, D. A., Hussain, S. N. A., Schmidt, C. A., Ryan, T. E., & Green, T. D. (2015). Muscle cell derived angiopoietin-1 contributes to both myogenesis and angiogenesis in the ischemic environment. *Frontiers in Physiology*, *6*. https://doi.org/10.3389/fphys.2015.00161

171. McClure, M. J., Ramey, A. N., Rashid, M., Boyan, B. D., & Schwartz, Z. (2019). Integrin-α7 signaling regulates connexin 43, M-cadherin, and myoblast fusion. *American Journal of Physiology-Cell Physiology*, *316*(6), C876–C887. https://doi.org/10.1152/ajpcell.00282.2018

172. McCormick, R., & Vasilaki, A. (2018). Age-related changes in skeletal muscle: Changes to life-style as a therapy. *Biogerontology*, *19*(6), 519–536. https://doi.org/10.1007/s10522-018-9775-3

173. McCroskery, S., Thomas, M., Maxwell, L., Sharma, M., & Kambadur, R. (2003). Myostatin negatively regulates satellite cell activation and self-renewal. *Journal of Cell Biology*, *162*(6), 1135–1147. https://doi.org/10.1083/jcb.200207056

174. Medler, S. (2019). Mixing it up: The biological significance of hybrid skeletal muscle fibers. *Journal of Experimental Biology*, *222*(23), jeb200832. https://doi.org/10.1242/jeb.200832

175. Meers, M. P., Bryson, T. D., Henikoff, J. G., & Henikoff, S. (2019). Improved CUT&RUN chromatin profiling tools. *ELife*, *8*, e46314. https://doi.org/10.7554/eLife.46314

176. Millay, D. P., Sutherland, L. B., Bassel-Duby, R., & Olson, E. N. (2014). Myomaker is essential for muscle regeneration. *Genes & Development*, *28*(15), 1641–1646. https://doi.org/10.1101/gad.247205.114

177. Miniou, P. (1999). Gene targeting restricted to mouse striated muscle lineage. *Nucleic Acids Research*, *27*(19), 27e–227. https://doi.org/10.1093/nar/27.19.e27

178. Moebius Syndrome Research Consortium, Di Gioia, S. A., Connors, S., Matsunami, N., Cannavino, J., Rose, M. F., Gilette, N. M., Artoni, P., de Macena Sobreira, N. L., Chan, W.-M., Webb, B. D., Robson, C. D., Cheng, L., Van Ryzin, C., Ramirez-Martinez, A., Mohassel, P., Leppert, M., Scholand, M. B., Grunseich, C., … Engle, E. C. (2017). A defect in myoblast fusion underlies Carey-Fineman-Ziter syndrome. *Nature Communications*, *8*(1), 16077. https://doi.org/10.1038/ncomms16077

179. Montarras, D., L'honoré, A., & Buckingham, M. (2013). Lying low but ready for action: The quiescent muscle satellite cell. *FEBS Journal*, *280*(17), 4036–4050. https://doi.org/10.1111/febs.12372

180. Montarras, D., Morgan, J., Collins, C., Relaix, F., Zaffran, S., Cumano, A., Partridge, T., & Buckingham, M. (2005). Direct Isolation of Satellite Cells for Skeletal Muscle Regeneration. *Science*, *309*(5743), 2064–2067. https://doi.org/10.1126/science.1114758

181. Motohashi, N., & Asakura, A. (2014). Muscle satellite cell heterogeneity and self-renewal. *Frontiers in Cell and Developmental Biology*, *2*. https://doi.org/10.3389/fcell.2014.00001

182. Mourikis, P., Sambasivan, R., Castel, D., Rocheteau, P., Bizzarro, V., & Tajbakhsh, S. (2012). A Critical Requirement for Notch Signaling in Maintenance of the Quiescent Skeletal Muscle Stem Cell State. *Stem Cells*, *30*(2), 243–252. https://doi.org/10.1002/stem.775

183. Mukund, K., & Subramaniam, S. (2020). Skeletal muscle: A review of molecular structure and function, in health and disease. *WIREs Systems Biology and Medicine*, *12*(1). https://doi.org/10.1002/wsbm.1462

184. Murphy, M. M., Lawson, J. A., Mathew, S. J., Hutcheson, D. A., & Kardon, G. (2011). Satellite cells, connective tissue fibroblasts and their interactions are crucial for muscle regeneration. *Development*, *138*(17), 3625–3637. https://doi.org/10.1242/dev.064162

185. Musarò, A. (2014). The Basis of Muscle Regeneration. *Advances in Biology*, *2014*, 1–16. https://doi.org/10.1155/2014/612471

186. Myers, J. B., & Meacham, R. B. (2003). Androgen replacement therapy in the aging male. *Reviews in Urology*, *5*(4), 216–226.

187. Nnodim, J. O. (2001). Testosterone mediates satellite cell activation in denervated rat levator ani muscle. *The Anatomical Record*, *263*(1), 19–24. https://doi.org/10.1002/ar.1072

188. Ohlendieck, K. (2010). Proteomics of skeletal muscle glycolysis. *Biochimica et Biophysica Acta (BBA) - Proteins and Proteomics*, *1804*(11), 2089–2101. https://doi.org/10.1016/j.bbapap.2010.08.001

189. Ono, Y., Masuda, S., Nam, H., Benezra, R., Miyagoe-Suzuki, Y., & Takeda, S. (2012). Slow-dividing satellite cells retain long-term self-renewal ability in adult muscle. *Journal of Cell Science*, *125*(5), 1309–1317. https://doi.org/10.1242/jcs.096198

190. Ontell, M., Feng, K. C., Klueber, K., Dunn, R. F., & Taylor, F. (1984). Myosatellite cells, growth, and regeneration in murine dystrophic muscle: A quantitative study. *The Anatomical Record*, *208*(2), 159–174. https://doi.org/10.1002/ar.1092080203

191. Ophoff, J., Van Proeyen, K., Callewaert, F., De Gendt, K., De Bock, K., Vanden Bosch, A., Verhoeven, G., Hespel, P., & Vanderschueren, D. (2009). Androgen Signaling in Myocytes Contributes to the Maintenance of Muscle Mass and Fiber Type Regulation But Not to Muscle Strength or Fatigue. *Endocrinology*, *150*(8), 3558–3566. https://doi.org/10.1210/en.2008-1509

192. Oustanina, S., Hause, G., & Braun, T. (2004). Pax7 directs postnatal renewal and propagation of myogenic satellite cells but not their specification. *The EMBO Journal*, *23*(16), 3430–3439. https://doi.org/10.1038/sj.emboj.7600346

193. Palomero, J., Vasilaki, A., Pye, D., McArdle, A., & Jackson, M. J. (2013). Aging increases the oxidation of dichlorohydrofluorescein in single isolated skeletal muscle fibers at rest, but not during contractions. *American Journal of Physiology-Regulatory, Integrative and Comparative Physiology*, *305*(4), R351–R358. https://doi.org/10.1152/ajpregu.00530.2012

194. Pannérec, A., Marazzi, G., & Sassoon, D. (2012). Stem cells in the hood: The skeletal muscle niche. *Trends in Molecular Medicine*, *18*(10), 599–606. https://doi.org/10.1016/j.molmed.2012.07.004

195. Park, G. H., Jeong, H., Jeong, M.-G., Jang, E. J., Bae, M. A., Lee, Y.-L., Kim, N. J., Hong, J.-H., & Hwang, E. S. (2014). Novel TAZ modulators enhance myogenic differentiation and muscle regeneration: Myogenic stimulation by novel TAZ modulators. *British Journal of Pharmacology*, *171*(17), 4051–4061. https://doi.org/10.1111/bph.12755

196. Perandini, L. A., Chimin, P., Lutkemeyer, D. da S., & Câmara, N. O. S. (2018). Chronic inflammation in skeletal muscle impairs satellite cells function during regeneration: Can physical exercise restore the satellite cell niche? *The FEBS Journal*, *285*(11), 1973–1984. https://doi.org/10.1111/febs.14417

197. Perdiguero, E., Ruiz-Bonilla, V., Serrano, A. L., & Muñoz-Cánoves, P. (2007). Genetic Deficiency of p38α Reveals its Critical Role in Myoblast Cell Cycle Exit:The p38α-JNK Connection. *Cell Cycle*, *6*(11), 1298–1303. https://doi.org/10.4161/cc.6.11.4315

198. Peter, J. B., Barnard, R. J., Edgerton, V. R., Gillespie, C. A., & Stempel, K. E. (1972). Metabolic profiles of three fiber types of skeletal muscle in guinea pigs and rabbits. *Biochemistry*, *11*(14), 2627–2633. https://doi.org/10.1021/bi00764a013

199. Petrany, M. J., & Millay, D. P. (2019). Cell Fusion: Merging Membranes and Making Muscle. *Trends in Cell Biology*, *29*(12), 964–973. https://doi.org/10.1016/j.tcb.2019.09.002

200. Piasecki, M., Ireland, A., Stashuk, D., Hamilton-Wright, A., Jones, D. A., & McPhee, J. S. (2016). Age-related neuromuscular changes affecting human vastus lateralis. *The Journal of Physiology*, *594*(16), 4525–4536. https://doi.org/10.1113/JP271087

201. Pinti, M., Cevenini, E., Nasi, M., De Biasi, S., Salvioli, S., Monti, D., Benatti, S., Gibellini, L., Cotichini, R., Stazi, M. A., Trenti, T., Franceschi, C., & Cossarizza, A. (2014). Circulating mitochondrial DNA increases with age and is a familiar trait: Implications for "inflamm-aging": Innate immunity. *European Journal of Immunology*, *44*(5), 1552–1562. https://doi.org/10.1002/eji.201343921

202. Porpiglia, E., Samusik, N., Ho, A. T. V., Cosgrove, B. D., Mai, T., Davis, K. L., Jager, A., Nolan, G. P., Bendall, S. C., Fantl, W. J., & Blau, H. M. (2017). High-resolution myogenic lineage mapping by single-cell mass cytometry. *Nature Cell Biology*, *19*(5), 558–567. https://doi.org/10.1038/ncb3507

203. Pratt, W. B., & Toft, D. O. (1997). *Steroid Receptor Interactions with Heat Shock Protein and Immunophilin Chaperones*. *18*(3), 55.

204. Przewoźniak, M., Czaplicka, I., Czerwińska, A. M., Markowska-Zagrajek, A., Moraczewski, J., Stremińska, W., Jańczyk-Ilach, K., Ciemerych, M. A., & Brzoska, E. (2013). Adhesion Proteins—An Impact on Skeletal Myoblast Differentiation. *PLoS ONE*, *8*(5), e61760. https://doi.org/10.1371/journal.pone.0061760

205. Quinn, M. E., Goh, Q., Kurosaka, M., Gamage, D. G., Petrany, M. J., Prasad, V., & Millay, D. P. (2017). Myomerger induces fusion of non-fusogenic cells and is required for skeletal muscle development. *Nature Communications*, *8*(1), 15665. https://doi.org/10.1038/ncomms15665

206. Rahate, K., Bhatt, L. K., & Prabhavalkar, K. S. (2020). SERCA stimulation: A potential approach in therapeutics. *Chemical Biology & Drug Design*, *95*(1), 5–15. https://doi.org/10.1111/cbdd.13620

207. Ramaswamy, K. S., Palmer, M. L., van der Meulen, J. H., Renoux, A., Kostrominova, T. Y., Michele, D. E., & Faulkner, J. A. (2011). Lateral transmission of force is impaired in skeletal muscles of dystrophic mice and very old rats: Lateral transmission of force in skeletal muscles of mice and rats. *The Journal of Physiology*, *589*(5), 1195–1208. https://doi.org/10.1113/jphysiol.2010.201921

208. Rasmussen, M., & Jin, J.-P. (2021). Troponin Variants as Markers of Skeletal Muscle Health and Diseases. *Frontiers in Physiology*, *12*, 747214. https://doi.org/10.3389/fphys.2021.747214

209. Ratajczak, M. Z., Kucia, M., Reca, R., Majka, M., Janowska-Wieczorek, A., & Ratajczak, J. (2004). Stem cell plasticity revisited: CXCR4-positive cells expressing mRNA for early muscle, liver and neural cells 'hide out' in the bone marrow. *Leukemia*, *18*(1), 29–40. https://doi.org/10.1038/sj.leu.2403184

210. Raue, U., Slivka, D., Jemiolo, B., Hollon, C., & Trappe, S. (2006). Myogenic gene expression at rest and after a bout of resistance exercise in young (18–30 yr) and old (80–89 yr) women. *Journal of Applied Physiology*, *101*(1), 53–59. https://doi.org/10.1152/japplphysiol.01616.2005

211. Rayagiri, S. S., Ranaldi, D., Raven, A., Mohamad Azhar, N. I. F., Lefebvre, O., Zammit, P. S., & Borycki, A.-G. (2018). Basal lamina remodeling at the skeletal muscle stem cell niche mediates stem cell self-renewal. *Nature Communications*, *9*(1), 1075. https://doi.org/10.1038/s41467-018-03425-3

212. Relaix, F., Bencze, M., Borok, M. J., Der Vartanian, A., Gattazzo, F., Mademtzoglou, D., Perez-Diaz, S., Prola, A., Reyes-Fernandez, P. C., Rotini, A., & Taglietti. (2021a). Perspectives on skeletal muscle stem cells. *Nature Communications*, *12*(1), 692. https://doi.org/10.1038/s41467-020-20760-6

213. Relaix, F., Bencze, M., Borok, M. J., Der Vartanian, A., Gattazzo, F., Mademtzoglou, D., Perez-Diaz, S., Prola, A., Reyes-Fernandez, P. C., Rotini, A., & Taglietti. (2021b). Perspectives on skeletal muscle stem cells. *Nature Communications*, *12*(1), 692. https://doi.org/10.1038/s41467-020-20760-6

214. Relaix, F., Montarras, D., Zaffran, S., Gayraud-Morel, B., Rocancourt, D., Tajbakhsh, S., Mansouri, A., Cumano, A., & Buckingham, M. (2006). Pax3 and Pax7 have distinct and overlapping functions in adult muscle progenitor cells. *Journal of Cell Biology*, *172*(1), 91–102. https://doi.org/10.1083/jcb.200508044

215. Relaix, F., Rocancourt, D., Mansouri, A., & Buckingham, M. (2005). A Pax3/Pax7-dependent population of skeletal muscle progenitor cells. *Nature*, *435*(7044), 948–953. https://doi.org/10.1038/nature03594

216. Relaix, F., & Zammit, P. S. (2012). Satellite cells are essential for skeletal muscle regeneration: The cell on the edge returns centre stage. *Development*, *139*(16), 2845–2856. https://doi.org/10.1242/dev.069088

217. Robinson-Rechavi, M., Maina, C. V., Gissendanner, C. R., Laudet, V., & Sluder, A. (2005). Explosive Lineage-Specific Expansion of the Orphan Nuclear Receptor HNF4 in Nematodes. *Journal of Molecular Evolution*, *60*(5), 577–586. https://doi.org/10.1007/s00239-004-0175-8

218. Rocheteau, P., Gayraud-Morel, B., Siegl-Cachedenier, I., Blasco, M. A., & Tajbakhsh, S. (2012). A Subpopulation of Adult Skeletal Muscle Stem Cells Retains All Template DNA Strands after Cell Division. *Cell*, *148*(1–2), 112–125. https://doi.org/10.1016/j.cell.2011.11.049

219. Rodgers, J. T., King, K. Y., Brett, J. O., Cromie, M. J., Charville, G. W., Maguire, K. K., Brunson, C., Mastey, N., Liu, L., Tsai, C.-R., Goodell, M. A., & Rando, T. A. (2014). MTORC1 controls the adaptive transition of quiescent stem cells from G0 to GAlert. *Nature*, *510*(7505), 393–396. https://doi.org/10.1038/nature13255

220. Rodríguez Cruz, P. M., Cossins, J., Beeson, D., & Vincent, A. (2020). The Neuromuscular Junction in Health and Disease: Molecular Mechanisms Governing Synaptic Formation and Homeostasis. *Frontiers in Molecular Neuroscience*, *13*, 610964. https://doi.org/10.3389/fnmol.2020.610964

221. Rose, A. J., & Richter, E. A. (2005). Skeletal Muscle Glucose Uptake During Exercise: How is it Regulated? *Physiology*, *20*(4), 260–270. https://doi.org/10.1152/physiol.00012.2005

222. Rossi, A. E., & Dirksen, R. T. (2006). Sarcoplasmic reticulum: The dynamic calcium governor of muscle. *Muscle & Nerve*, *33*(6), 715–731. https://doi.org/10.1002/mus.20512

223. Rozo, M., Li, L., & Fan, C.-M. (2016a). Targeting β1-integrin signaling enhances regeneration in aged and dystrophic muscle in mice. *Nature Medicine*, *22*(8), 889–896. https://doi.org/10.1038/nm.4116

224. Rozo, M., Li, L., & Fan, C.-M. (2016b). Targeting β1-integrin signaling enhances regeneration in aged and dystrophic muscle in mice. *Nature Medicine*, *22*(8), 889–896. https://doi.org/10.1038/nm.4116

225. Rudnicki, M. A., Schnegelsberg, P. N. J., Stead, R. H., Braun, T., Arnold, H.-H., & Jaenisch, R. (1993). MyoD or Myf-5 is required for the formation of skeletal muscle. *Cell*, *75*(7), 1351–1359. https://doi.org/10.1016/0092-8674(93)90621-V

226. Ryder, J. W., Yang, J., Galuska, D., Rincón, J., Björnholm, M., Krook, A., Lund, S., Pedersen, O., Wallberg-Henriksson, H., Zierath, J. R., & Holman, G. D. (2000). Use of a novel impermeable biotinylated photolabeling reagent to assess insulin- and hypoxia-stimulated cell surface GLUT4 content in skeletal muscle from type 2 diabetic patients. *Diabetes*, *49*(4), 647–654. https://doi.org/10.2337/diabetes.49.4.647

227. Sabourin, L. A., Girgis-Gabardo, A., Seale, P., Asakura, A., & Rudnicki, M. A. (1999). Reduced Differentiation Potential of Primary MyoD−/− Myogenic Cells Derived from Adult Skeletal Muscle. *The Journal of Cell Biology*, *144*, 13.

228. Saclier, M., Yacoub-Youssef, H., Mackey, A. L., Arnold, L., Ardjoune, H., Magnan, M., Sailhan, F., Chelly, J., Pavlath, G. K., Mounier, R., Kjaer, M., & Chazaud, B. (2013). Differentially Activated Macrophages Orchestrate Myogenic Precursor Cell Fate During Human Skeletal Muscle Regeneration. *Stem Cells*, *31*(2), 384–396. https://doi.org/10.1002/stem.1288

229. Sampath, S. C., Sampath, S. C., & Millay, D. P. (2018). Myoblast fusion confusion: The resolution begins. *Skeletal Muscle*, *8*(1), 3. https://doi.org/10.1186/s13395-017-0149-3

230. Sartori, R., Romanello, V., & Sandri, M. (2021). Mechanisms of muscle atrophy and hypertrophy: Implications in health and disease. *Nature Communications*, *12*(1), 330. https://doi.org/10.1038/s41467-020-20123-1

231. Saunders, M. A., Good, J. M., Lawrence, E. C., Ferrell, R. E., Li, W.-H., & Nachman, M. W. (2006). Human Adaptive Evolution at Myostatin (GDF8), a Regulator of Muscle Growth. *The American Journal of Human Genetics*, *79*(6), 1089–1097. https://doi.org/10.1086/509707

232. Scarth, M., & Bjørnebekk, A. (2021). Androgen abuse and the brain. *Current Opinion in Endocrinology, Diabetes & Obesity*, *28*(6), 604–614. https://doi.org/10.1097/MED.0000000000000675

233. Schakman, O., Gilson, H., & Thissen, J. P. (2008). Mechanisms of glucocorticoid-induced myopathy. *Journal of Endocrinology*, *197*(1), 1–10. https://doi.org/10.1677/JOE-07-0606

234. Scher, H. I., Fizazi, K., Saad, F., Taplin, M.-E., Sternberg, C. N., Miller, K., de Wit, R., Mulders, P., Chi, K. N., Shore, N. D., Armstrong, A. J., Flaig, T. W., Fléchon, A., Mainwaring, P., Fleming, M., Hainsworth, J. D., Hirmand, M., Selby, B., Seely, L., & de Bono, J. S. (2012). Increased Survival with Enzalutamide in Prostate Cancer after Chemotherapy. *New England Journal of Medicine*, *367*(13), 1187–1197. https://doi.org/10.1056/NEJMoa1207506

235. Scherz-Shouval R, Shvets E, Fass E, Shorer H, Gil L, Elazar Z. Reactive oxygen species are essential for autophagy and specifically regulate the activity of Atg4. EMBO J. 2007 Apr 4;26(7):1749-60. doi: 10.1038/sj.emboj.7601623. Epub 2007 Mar 8. Erratum in: EMBO J. 2019 May 15;38(10): PMID: 17347651; PMCID: PMC1847657.

236. Schiaffino, S., Rossi, A. C., Smerdu, V., Leinwand, L. A., & Reggiani, C. (2015). Developmental myosins: Expression patterns and functional significance. *Skeletal Muscle*, *5*(1), 22. https://doi.org/10.1186/s13395-015-0046-6

237. Schmalbruch, H., & Hellhammer, U. (1977). The number of nuclei in adult rat muscles with special reference to satellite cells. *The Anatomical Record*, *189*(2), 169–175. https://doi.org/10.1002/ar.1091890204

238. Schmidt, M., Schüler, S. C., Hüttner, S. S., von Eyss, B., & von Maltzahn, J. (2019). Adult stem cells at work: Regenerating skeletal muscle. *Cellular and Molecular Life Sciences*, *76*(13), 2559–2570. https://doi.org/10.1007/s00018-019-03093-6

239. Seale, P., Sabourin, L. A., Girgis-Gabardo, A., Mansouri, A., Gruss, P., & Rudnicki, M. A. (2000). Pax7 Is Required for the Specification of Myogenic Satellite Cells. *Cell*, *102*(6), 777–786. https://doi.org/10.1016/S0092-8674(00)00066-0

240. Seaton, A., Scullin, P., Maxwell, P. J., Wilson, C., Pettigrew, J., Gallagher, R., O'Sullivan, J. M., Johnston, P. G., & Waugh, D. J. J. (2008). Interleukin-8 signaling promotes androgen-independent proliferation of prostate cancer cells via induction of androgen receptor expression and activation. *Carcinogenesis*, *29*(6), 1148–1156. https://doi.org/10.1093/carcin/bgn109

241. Segalés, J., Perdiguero, E., & Muñoz-Cánoves, P. (2016). Regulation of Muscle Stem Cell Functions: A Focus on the p38 MAPK Signaling Pathway. *Frontiers in Cell and Developmental Biology*, *4*. https://doi.org/10.3389/fcell.2016.00091

242. Seo, J.-Y., Kim, J.-H., & Kong, Y.-Y. (n.d.). *Unraveling the Paradoxical Action of Androgens on Muscle Stem Cells*. 7.

243. Serra, C., Tangherlini, F., Rudy, S., Lee, D., Toraldo, G., Sandor, N. L., Zhang, A., Jasuja, R., & Bhasin, S. (2013a). Testosterone Improves the Regeneration of Old and Young Mouse Skeletal Muscle. *The Journals of Gerontology Series A: Biological Sciences and Medical Sciences*, *68*(1), 17–26. https://doi.org/10.1093/gerona/gls083

244. Serra, C., Tangherlini, F., Rudy, S., Lee, D., Toraldo, G., Sandor, N. L., Zhang, A., Jasuja, R., & Bhasin, S. (2013b). Testosterone Improves the Regeneration of Old and Young Mouse Skeletal Muscle. *The Journals of Gerontology Series A: Biological Sciences and Medical Sciences*, *68*(1), 17–26. https://doi.org/10.1093/gerona/gls083

245. Serrano, A. L., & Muñoz-Cánoves, P. (2010). Regulation and dysregulation of fibrosis in skeletal muscle. *Experimental Cell Research*, *316*(18), 3050–3058. https://doi.org/10.1016/j.yexcr.2010.05.035

246. Shang, M., Cappellesso, F., Amorim, R., Serneels, J., Virga, F., Eelen, G., Carobbio, S., Rincon, M. Y., Maechler, P., De Bock, K., Ho, P.-C., Sandri, M., Ghesquière, B., Carmeliet, P., Di Matteo, M., Berardi, E., & Mazzone, M. (2020). Macrophage-derived glutamine boosts satellite cells and muscle regeneration. *Nature*, *587*(7835), 626–631. https://doi.org/10.1038/s41586-020-2857-9

247. Shefer, G., Van de Mark, D. P., Richardson, J. B., & Yablonka-Reuveni, Z. (2006). Satellite-cell pool size does matter: Defining the myogenic potency of aging skeletal muscle. *Developmental Biology*, *294*(1), 50–66. https://doi.org/10.1016/j.ydbio.2006.02.022

248. Sheth, K. A., Iyer, C. C., Wier, C. G., Crum, A. E., Bratasz, A., Kolb, S. J., Clark, B. C., Burghes, A. H. M., & Arnold, W. D. (2018). Muscle strength and size are associated with motor unit connectivity in aged mice. *Neurobiology of Aging*, *67*, 128–136. https://doi.org/10.1016/j.neurobiolaging.2018.03.016

249. Shiina, H., Matsumoto, T., Sato, T., Igarashi, K., Miyamoto, J., Takemasa, S., Sakari, M., Takada, I., Nakamura, T., Metzger, D., Chambon, P., Kanno, J., Yoshikawa, H., & Kato, S. (2006). Premature ovarian failure in androgen receptor-deficient mice. *Proceedings of the National Academy of Sciences*, *103*(1), 224–229. https://doi.org/10.1073/pnas.0506736102

250. Shilagardi, K., Li, S., Luo, F., Marikar, F., Duan, R., Jin, P., Kim, J. H., Murnen, K., & Chen, E. H. (2013). Actin-Propelled Invasive Membrane Protrusions Promote Fusogenic Protein Engagement During Cell-Cell Fusion. *Science*, *340*(6130), 359–363. https://doi.org/10.1126/science.1234781

251. Shinin, V., Gayraud-Morel, B., Gomès, D., & Tajbakhsh, S. (2006). Asymmetric division and cosegregation of template DNA strands in adult muscle satellite cells. *Nature Cell Biology*, *8*(7), 677–682. https://doi.org/10.1038/ncb1425

252. Short, K. R., Bigelow, M. L., Kahl, J., Singh, R., Coenen-Schimke, J., Raghavakaimal, S., & Nair, K. S. (2005). Decline in skeletal muscle mitochondrial function with aging in humans. *Proceedings of the National Academy of Sciences*, *102*(15), 5618–5623. https://doi.org/10.1073/pnas.0501559102

253. Shukla, A., Narayanan, D. L., Asher, U., & Girisha, K. M. (2019). A novel bi-allelic loss-of-function variant in *MYOD1*: Further evidence for gene-disease association and

phenotypic variability in *MYOD1* -related myopathy. *Clinical Genetics*, *96*(3), 276–277. https://doi.org/10.1111/cge.13596

254. Shukla, G. C., Plaga, A. R., Shankar, E., & Gupta, S. (2016). Androgen receptor-related diseases: What do we know? *Andrology*, *4*(3), 366–381. https://doi.org/10.1111/andr.12167

255. Singh, P. (2013). Andropause: Current concepts. *Indian Journal of Endocrinology and Metabolism*, *17*(9), 621. https://doi.org/10.4103/2230-8210.123552

256. Singh, R., Artaza, J. N., Taylor, W. E., Braga, M., Yuan, X., Gonzalez-Cadavid, N. F., & Bhasin, S. (2006). Testosterone Inhibits Adipogenic Differentiation in 3T3-L1 Cells: Nuclear Translocation of Androgen Receptor Complex with β-Catenin and T-Cell Factor 4 May Bypass Canonical Wnt Signaling to Down-Regulate Adipogenic Transcription Factors. *Endocrinology*, *147*(1), 141–154. https://doi.org/10.1210/en.2004-1649

257. Sinha-Hikim, I., Roth, S. M., Lee, M. I., & Bhasin, S. (2003). Testosterone-induced muscle hypertrophy is associated with an increase in satellite cell number in healthy, young men. *Endocrinol Metab*, *285*, 10.

258. Sinha-Hikim, I., Taylor, W. E., Gonzalez-Cadavid, N. F., Zheng, W., & Bhasin, S. (2004a). Androgen Receptor in Human Skeletal Muscle and Cultured Muscle Satellite Cells: Up-Regulation by Androgen Treatment. *The Journal of Clinical Endocrinology & Metabolism*, *89*(10), 5245–5255. https://doi.org/10.1210/jc.2004-0084

259. Sinha-Hikim, I., Taylor, W. E., Gonzalez-Cadavid, N. F., Zheng, W., & Bhasin, S. (2004b). Androgen Receptor in Human Skeletal Muscle and Cultured Muscle Satellite Cells: Up-Regulation by Androgen Treatment. *The Journal of Clinical Endocrinology & Metabolism*, *89*(10), 5245–5255. https://doi.org/10.1210/jc.2004-0084

260. *Sj.emboj.7601623*. (n.d.). Retrieved June 2, 2022, from http://10.0.4.14/sj.emboj.7601623

261. Smith, C. K., Janney, M. J., & Allen, R. E. (1994). Temporal expression of myogenic regulatory genes during activation, proliferation, and differentiation of rat skeletal muscle satellite cells. *Journal of Cellular Physiology*, *159*(2), 379–385. https://doi.org/10.1002/jcp.1041590222

262. Smith, L. B., & Walker, W. H. (2014). The regulation of spermatogenesis by androgens. *Seminars in Cell & Developmental Biology*, *30*, 2–13. https://doi.org/10.1016/j.semcdb.2014.02.012

263. Song, M.-Y., Ruts, E., Kim, J., Janumala, I., Heymsfield, S., & Gallagher, D. (2004). Sarcopenia and increased adipose tissue infiltration of muscle in elderly African American women. *The American Journal of Clinical Nutrition*, *79*(5), 874–880. https://doi.org/10.1093/ajcn/79.5.874

264. Squire, J. (2019). Special Issue: The Actin-Myosin Interaction in Muscle: Background and Overview. *International Journal of Molecular Sciences*, *20*(22), 5715. https://doi.org/10.3390/ijms20225715

265. Stanford, K. I., & Goodyear, L. J. (2014). Exercise and type 2 diabetes: Molecular mechanisms regulating glucose uptake in skeletal muscle. *Advances in Physiology Education*, *38*(4), 308–314. https://doi.org/10.1152/advan.00080.2014

266. Summers, P. J., & Parsons, R. (1981). A QUANTITATIVE ASSESSMENT OF DYSTROPHIC MOUSE (129 ReJ dy/dy) MYOGENESIS IN VITRO. *Neuropathology and Applied Neurobiology*, *7*(4), 269–277. https://doi.org/10.1111/j.1365-2990.1981.tb00098.x

267. Tajbakhsh, S. (2013). Losing stem cells in the aged skeletal muscle niche. *Cell Research*, *23*(4), 455–457. https://doi.org/10.1038/cr.2013.3

268. Tan, M. E., Li, J., Xu, H. E., Melcher, K., & Yong, E. (2015). Androgen receptor: Structure, role in prostate cancer and drug discovery. *Acta Pharmacologica Sinica*, *36*(1), 3–23. https://doi.org/10.1038/aps.2014.18

269. Tanner, C. J., Barakat, H. A., Dohm, G. L., Pories, W. J., MacDonald, K. G., Cunningham, P. R. G., Swanson, M. S., & Houmard, J. A. (2002). Muscle fiber type is associated with obesity and weight loss. *American Journal of Physiology-Endocrinology and Metabolism*, *282*(6), E1191–E1196. https://doi.org/10.1152/ajpendo.00416.2001

270. Tatsumi, R., Sankoda, Y., Anderson, J. E., Sato, Y., Mizunoya, W., Shimizu, N., Suzuki, T., Yamada, M., Rhoads, R. P., Ikeuchi, Y., & Allen, R. E. (2009). Possible implication of satellite cells in regenerative motoneuritogenesis: HGF upregulates neural chemorepellent Sema3A during myogenic differentiation. *American Journal of Physiology-Cell Physiology*, *297*(2), C238–C252. https://doi.org/10.1152/ajpcell.00161.2009

271. Taylor, R. W., & Turnbull, D. M. (2005). Mitochondrial DNA mutations in human disease. *Nature Reviews Genetics*, *6*(5), 389–402. https://doi.org/10.1038/nrg1606

272. Tchernof, A., Brochu, D., Maltais-Payette, I., Mansour, M. F., Marchand, G. B., Carreau, A., & Kapeluto, J. (2018). Androgens and the Regulation of Adiposity and Body Fat Distribution in Humans. In R. Terjung (Ed.), *Comprehensive Physiology* (1st ed., pp. 1253–1290). Wiley. https://doi.org/10.1002/cphy.c170009

273. Termin, A., Staron, R. S., & Pette, D. (1989). Myosin heavy chain isoforms in histochemically defined fiber types of rat muscle. *Histochemistry*, *92*(6), 453–457. https://doi.org/10.1007/BF00524756

274. Thomas, M., Langley, B., Berry, C., Sharma, M., Kirk, S., Bass, J., & Kambadur, R. (2000). Myostatin, a Negative Regulator of Muscle Growth, Functions by Inhibiting Myoblast Proliferation. *Journal of Biological Chemistry*, *275*(51), 40235–40243. https://doi.org/10.1074/jbc.M004356200

275. Vasilaki, A., Pollock, N., Giakoumaki, I., Goljanek-Whysall, K., Sakellariou, G. K., Pearson, T., Kayani, A., Jackson, M. J., & McArdle, A. (2016). The effect of lengthening contractions on neuromuscular junction structure in adult and old mice. *AGE*, *38*(4), 259–272. https://doi.org/10.1007/s11357-016-9937-7

276. Verdijk, L. B., Snijders, T., Drost, M., Delhaas, T., Kadi, F., & van Loon, L. J. C. (2014). Satellite cells in human skeletal muscle; from birth to old age. *AGE*, *36*(2), 545–557. https://doi.org/10.1007/s11357-013-9583-2

277. Verma, M., Asakura, Y., Murakonda, B. S. R., Pengo, T., Latroche, C., Chazaud, B., McLoon, L. K., & Asakura, A. (2018). Muscle Satellite Cell Cross-Talk with a Vascular Niche Maintains Quiescence via VEGF and Notch Signaling. *Cell Stem Cell*, *23*(4), 530-543.e9. https://doi.org/10.1016/j.stem.2018.09.007

278. Vivian, J. L., Olson, E. N., & Klein, W. H. (2000). Thoracic Skeletal Defects in Myogenin- and MRF4-Deficient Mice Correlate with Early Defects in Myotome and Intercostal Musculature. *Developmental Biology*, *224*(1), 29–41. https://doi.org/10.1006/dbio.2000.9788

279. Vlahopoulos, S., Zimmer, W. E., Jenster, G., Belaguli, N. S., Balk, S. P., Brinkmann, A. O., Lanz, R. B., Zoumpourlis, V. C., & Schwartz, R. J. (2005). Recruitment of the Androgen Receptor via Serum Response Factor Facilitates Expression of a Myogenic Gene. *Journal of Biological Chemistry*, *280*(9), 7786–7792. https://doi.org/10.1074/jbc.M413992200

280. von Maltzahn, J., Jones, A. E., Parks, R. J., & Rudnicki, M. A. (2013). Pax7 is critical for the normal function of satellite cells in adult skeletal muscle. *Proceedings of the National Academy of Sciences*, *110*(41), 16474–16479. https://doi.org/10.1073/pnas.1307680110

281. Wagenmakers, A. J. M. (1998). Protein and Amino Acid Metabolism in Human Muscle. In E. A. Richter, B. Kiens, H. Galbo, & B. Saltin (Eds.), *Skeletal Muscle Metabolism in Exercise and Diabetes* (Vol. 441, pp. 307–319). Springer US. https://doi.org/10.1007/978-1-4899-1928-1_28

282. Wall, B. T., Gorissen, S. H., Pennings, B., Koopman, R., Groen, B. B. L., Verdijk, L. B., & van Loon, L. J. C. (2015). Aging Is Accompanied by a Blunted Muscle Protein Synthetic Response to Protein Ingestion. *PLOS ONE*, *10*(11), e0140903. https://doi.org/10.1371/journal.pone.0140903

283. Walters, K. A., Rodriguez Paris, V., Aflatounian, A., & Handelsman, D. J. (2019). Androgens and ovarian function: Translation from basic discovery research to clinical impact. *Journal of Endocrinology*, *242*(2), R23–R50. https://doi.org/10.1530/JOE-19-0096

284. Wang, C., Tian, L., Popov, V. M., & Pestell, R. G. (2011). Acetylation and nuclear receptor action. *The Journal of Steroid Biochemistry and Molecular Biology*, *123*(3–5), 91–100. https://doi.org/10.1016/j.jsbmb.2010.12.003

285. Wang, X., Shen, Q. W., Wang, J., Zhang, Z., Feng, F., Chen, T., Zhang, Y., Wei, H., Li, Z., Wang, X., & Wang, Y. (2016). KLF7 Regulates Satellite Cell Quiescence in Response to Extracellular Signaling. *Stem Cells*, *34*(5), 1310–1320. https://doi.org/10.1002/stem.2346

286. Welle, S., Thornton, C., Jozefowicz, R., & Statt, M. (1993). Myofibrillar protein synthesis in young and old men. *American Journal of Physiology-Endocrinology and Metabolism*, *264*(5), E693–E698. https://doi.org/10.1152/ajpendo.1993.264.5.E693

287. Westerblad, H., Bruton, J. D., & Katz, A. (2010). Skeletal muscle: Energy metabolism, fiber types, fatigue and adaptability. *Experimental Cell Research*, *316*(18), 3093–3099. https://doi.org/10.1016/j.yexcr.2010.05.019

288. White, J. P., Gao, S., Puppa, M. J., Sato, S., Welle, S. L., & Carson, J. A. (2013). Testosterone regulation of Akt/mTORC1/FoxO3a signaling in skeletal muscle. *Molecular and Cellular Endocrinology*, *365*(2), 174–186. https://doi.org/10.1016/j.mce.2012.10.019

289. Wozniak, A. C., & Anderson, J. E. (n.d.). *Nitric oxide-dependence of satellite stem cell activation and quiescence on normal skeletal muscle fibers*. 11.

290. Yablonka-Reuveni, Z. (n.d.). *The Skeletal Muscle Satellite Cell: StillYoung and Fascinating at 50*. 19.

291. Yablonka-Reuveni, Z., & Anderson, J. E. (2006). Satellite cells from dystrophic (Mdx) mice display accelerated differentiation in primary cultures and in isolated myofibers. *Developmental Dynamics*, *235*(1), 203–212. https://doi.org/10.1002/dvdy.20602

292. Yamakawa, H., Kusumoto, D., Hashimoto, H., & Yuasa, S. (2020). Stem Cell Aging in Skeletal Muscle Regeneration and Disease. *International Journal of Molecular Sciences*, *21*(5), 1830. https://doi.org/10.3390/ijms21051830

293. Yang, W., & Hu, P. (2018). Skeletal muscle regeneration is modulated by inflammation. *Journal of Orthopaedic Translation*, *13*, 25–32. https://doi.org/10.1016/j.jot.2018.01.002

294. Yin, H., Price, F., & Rudnicki, M. A. (2013). Satellite Cells and the Muscle Stem Cell Niche. *Physiological Reviews*, *93*(1), 23–67. https://doi.org/10.1152/physrev.00043.2011

295. Zammit, P. S. (2017). Function of the myogenic regulatory factors Myf5, MyoD, Myogenin and MRF4 in skeletal muscle, satellite cells and regenerative myogenesis. *Seminars in Cell & Developmental Biology*, *72*, 19–32. https://doi.org/10.1016/j.semcdb.2017.11.011

296. Zhou, S., Zhang, W., Cai, G., Ding, Y., Wei, C., Li, S., Yang, Y., Qin, J., Liu, D., Zhang, H., Shao, X., Wang, J., Wang, H., Yang, W., Wang, H., Chen, S., Hu, P., & Sun, L. (2020). Myofiber necroptosis promotes muscle stem cell proliferation via releasing Tenascin-C during regeneration. *Cell Research*, *30*(12), 1063–1077. https://doi.org/10.1038/s41422-020-00393-6

297. Zitzmann, M., & Nieschlag, E. (2003). Effects of androgen replacement on metabolism and physical performances in male hypogonadism. *Journal of Endocrinological Investigation*, *26*(9), 886–892. https://doi.org/10.1007/BF03345240

Résumé en Français

Introduction.

Les cellules satellites (CS) sont des cellules souches exprimant la boîte à paire 7 (Pax7) qui sont principalement responsables de l'homéostasie post-natale, de la croissance et du renouvellement des muscles squelettiques (Wang et Rudnicki 2011). Les CS résident dans un état quiescent dans un microenvironnement particulier (niche) situé à la périphérie des myofibres. Des découvertes récentes suggèrent que les SCs forment des sous-populations fonctionnellement hétérogènes caractérisées par d'autres marqueurs tels que Myf5 et MyoD, ainsi que Pax7. Ces cellules présentent des capacités variables d'activation, de division et d'auto-renouvellement (Kuang et al. 2007, Cho et Doles 2017).

Lors d'une lésion musculaire, les myofibres subissent une dégénérescence provoquant une infiltration de cellules inflammatoires suivie d'une activation des CS. Ces dernières se divisent et génèrent des myoblastes qui fusionnent pour former des fibres et/ou ? remplacer celles qui sont endommagées (Tedesco et al. 2010). Différents types de cellules harmonisent la régénération des myofibres, notamment les cellules endothéliales, les cellules immunitaires et les progéniteurs fibro-adipeux (FAP), via la libération de signaux extracellulaires, notamment des cytokines, des chimiokines et des facteurs de croissance (Wosczyna et Rando 2018 et De Micheli et al. 2020).

Bien que les CS soient abrités dans des niches, ils peuvent être affectés par des signaux paracrines, notamment des hormones. Par exemple, le pic d'hormones sexuelles à la puberté induit la quiescence des CS pour établir un pool de cellules souches (Kim et al. 2016), et en particulier, les androgènes ont été signalés pour initier la transition des CS d'un état prolifératif à un état quiescent via la signalisation Notch (Seo et al. 2019). De plus, la 5α-Dihydrotestostérone (DHT), un androgène endogène, favorise la myogenèse des myoblastes C2C12 en culture tissulaire (Diel et al. 2008). De plus, il a été signalé que les androgènes augmentent la masse et la force des muscles squelettiques chez les hommes hypogonadiques (Bhasin et al. 2000). En outre, l'ablation des AR dans les fibres musculaires a été signalée comme affectant la force musculaire (Chambon et al., 2010).

Les effets des androgènes sont médiés par le récepteur des androgènes (AR), un membre de la superfamille des récepteurs nucléaires ligand-dépendants (Davey et Grossmann, 2016). L'AR est exprimé dans les CS, et le traitement avec un ligand apparenté augmente ses niveaux et induit sa translocation nucléaire (Sinha-Hikim et al. 2004). Puisque les androgènes semblent jouer un rôle majeur dans la modulation des SC, l'objectif de ce projet est de caractériser les mécanismes par lesquels les androgènes via leur récepteur régulent l'homéostasie des cellules satellites et, par la suite, la régénération musculaire.

Résultats.

AR est exprimé in vivo dans les cellules satellites Pax7-positives.

Pour déterminer si AR est exprimé dans les cellules satellites (CS) pendant la régénération musculaire, nous avons induit une lésion musculaire en injectant 0,06 µg de cardiotoxine (Ctx) dans le tibialis antérieur de souris de type sauvage âgées de 8 semaines. Un test d'immunofluorescence (IF) sur des sections musculaires utilisant des anticorps dirigés contre AR et Pax7 a révélé que AR était exprimé dans les noyaux des cellules satellites Pax7-positives aux jours 5 (J5) et 7 (J7) post-lésion, et dans les noyaux des fibres régénératives aux jours 14 (J14) et 28 (J28).

Le knock-out de l'AR dans les cellules satellites retarde la régénération musculaire.

Pour évaluer le rôle potentiel de l'AR dans les CS, nous avons généré des souris chez lesquelles l'AR a été ablaté de manière sélective dans les cellules exprimant Pax7 à l'âge adulte (ci-après $AR^{sat-/Y}$), en croisant des souris exprimant la recombinase $CreER^{T2}$ inductible par le tamoxifène (Tam) sous le contrôle du promoteur Pax7 (Pax7-$CreER^{T2}$) avec des souris hébergeant des allèles AR floxés conditionnels (ARL2/L2). L'injection de Ctx a été effectuée sur 10 souris $AR^{sat-/Y}$ et 10 souris $AR^{L2/Y}$ (contrôle), et l'ablation de l'AR a été confirmée sur des sections de muscle $AR^{sat-/Y}$ par IF dans les noyaux positifs de Pax7.

Nous avons évalué l'efficacité de la régénération musculaire en observant la morphologie des fibres et l'inflammation sur des sections musculaires incluses en paraffine et colorées à l'hématoxyline et à l'éosine (H&E) 3, 5, 7, 14 et 28 jours après la lésion Ctx. Nous avons remarqué des défauts dans la néo-formation des fibres musculaires, leur orientation et le nombre de noyaux par fibre dans les sections musculaires $AR^{sat-/Y}$ par rapport à celles des souris témoins. Pour déterminer les défauts structurels des myofibres régénérées par les centri-nucléaires, nous avons effectué une analyse ultrastructurale 7 et 28 jours après la blessure, qui a démontré l'absence de matériel contractile, des mitochondries agrandies, et une augmentation de la taille et du nombre de noyaux par fibre dans les muscles mutants par rapport au contrôle. Notre observation a été confirmée par la coloration de l'alpha-actinine sarcomérique à J7, qui a mis en évidence une fusion aberrante des cellules musculaires à la périphérie de la fibre (données non présentées).

Pour caractériser davantage ces cellules en fusion, nous avons réalisé une coloration Pax7 à J5 et J7 après la lésion Ctx. Alors que la population de cellules exprimant Pax7 était similaire entre les souris témoins et les souris $AR^{sat-/Y}$ à J5, nos résultats ont montré que le nombre de CS a fortement diminué à J7 dans les muscles $AR^{sat-/Y}$ par rapport aux témoins. La capacité de prolifération des CS, déterminée par la coloration Ki67 avec Pax7, a montré que les cellules en prolifération étaient moins nombreuses dans les muscles blessés des souris témoins et $AR^{sat-/Y}$ à J5, et qu'elles étaient complètement absentes à J7 chez les souris mutantes. Puisque la prolifération des CS s'arrête lorsque les cellules subissent une différenciation suite à une division cellulaire asymétrique, nous nous demandons si ces processus sont affectés en l'absence d'AR. A cette fin, nous avons réalisé une coloration Myf5 qui a montré une augmentation du nombre de progéniteurs dans les muscles mutants par rapport aux contrôles à J7. De plus, la coloration Myog a montré une augmentation du nombre de myocytes dans les muscles $AR^{sat-/Y}$ par rapport aux muscles $AR^{L2/Y}$. Dans l'ensemble, nos données suggèrent que les AR contrôlent la division asymétrique et la prolifération des CS, la fusion des myoblastes et la structure sarcomérique des fibres régénératives.

Les AR contrôlent la prolifération et la différenciation des CS.

Pour valider nos observations en culture tissulaire, un tri cellulaire activé par fluorescence (FACS) a été réalisé à l'aide d'anticorps dirigés contre le cluster de différenciation 34 (CD34, un marqueur de cellules souches hématopoïétiques, endothéliales progénitrices et mésenchymateuses), l'intégrine 7 (Int7, un marqueur de muscles lisses, cardiaques et squelettiques) et le récepteur de chimiokine C-X-C de type 4 (CXCR4, un marqueur de lymphocytes, hématopoïétiques et de cellules satellites), comme décrit (Gunther et al. 2013). Les CS isolées des souris $AR^{L2/Y}$ et $AR^{sat-/Y}$ ont été cultivées dans un milieu de croissance contenant 4,5 g/l de glucose, 20 % de sérum de veau fœtal et 1 % d'extrait d'embryon

de poulet pendant cinq jours. L'ablation de l'AR dans les noyaux Pax7+ a été confirmée par immunofluorescence dans les cellules isolées des souris $AR^{sat-/Y}$. Après avoir été cultivées dans un milieu de croissance, les cellules témoins ont été entraînées dans la myogenèse par incubation avec un milieu myogénique pendant 7 jours. Les CS se sont différenciés, ont fusionné et ont formé des myotubes multinucléés exprimant la Dystrophine. De manière surprenante, les CS isolés des souris $AR^{sat-/Y}$ ne se sont pas attachés ou n'ont pas proliféré en culture, ce qui suggère que les AR contrôlent leur potentiel de souche et leur survie.

L'analyse FACS a également révélé une diminution de 50 % des niveaux d'expression de la protéine CD34 et de CXCR4, mais pas de Int7 dans les CS isolées à partir de 3 souris $AR^{sat-/Y}$ par rapport à 3 souris $AR^{L2/Y}$. Le CD34 a été rapporté pour conduire la prolifération des CS, tandis que l'axe CXCR4 a été montré pour induire l'expression du cluster de différenciation 9 (CD9), qui contrôle la fusion des myoblastes pendant la régénération musculaire.

De plus, l'analyse RT-qPCR effectuée sur les muscles totaux du tibialis a montré une diminution de Pax7, CXCR4 et CD9 chez les animaux mutants par rapport aux compagnons de portée témoins. Par conséquent, nous postulons que la perte de l'AR dans les CS nuit à leur potentiel de souche et à leur différenciation.

Discussion.

Dans l'ensemble, ces résultats identifient les androgènes comme des acteurs clés de l'homéostasie des CS et de la régénération musculaire. Après une blessure par Ctx, nous avons identifié des fibres régénératives mal formées chez $AR^{sat-/Y}$ par rapport à $AR^{L2/Y}$, ce qui pourrait être une conséquence de la fusion des myoblastes. De plus, nous avons distingué une diminution du nombre de CS pendant la formation musculaire des souris mutantes, suggérant une perte de la population de cellules souches. Nos analyses Cut&Run dans les CS triées par FACS et ChIP-qPCR ont révélé que AR a contrôle directement l'expression de Pax7, et la coloration Ki67 a démontré un manque de prolifération des cellules exprimant Pax7 dans le tibialis $AR^{sat-/Y}$ par rapport aux contrôles. En outre, l'analyse de Myf5 et Myog a montré un nombre plus élevé de progéniteurs myogéniques dans les muscles mutants par rapport à $AR^{L2/Y}$ à J7. Nous supposons donc que l'AR est le principal facteur contrôlant le potentiel de souche et la division asymétrique des CS, et la fusion des myoblastes filles.

De plus, notre analyse FACS a montré que l'ablation de l'AR dans les cellules souches musculaires Pax7+ avait un impact sur l'expression des protéines CD34 et CXCR4. Il a été démontré que le CD34, un marqueur de cellules souches mésenchymateuses, joue un rôle majeur dans la prolifération des CS et la fusion des myoblastes pendant la régénération musculaire (Alfaro et al. 2011 et Jankowski et al. 2002). De plus, nos données montrent que CXCR4, qui a été décrit pour réguler la migration des CS et la formation des myofibres après une blessure (Bae et al. 2008), est directement contrôlé par AR, comme cela a été montré dans les cellules du cancer du sein (Azariadis et al. 2017). L'axe CXCR4/Sdf1 induit l'expression de CD9, ce dernier contrôlant la fusion des myoblastes (Charrin et al., 2013). Ainsi, nous avons postulé que le potentiel de souche, la prolifération, la division asymétrique et la fusion des myoblastes des CS sont compromis lors de l'ablation des AR, ce qui pourrait avoir des conséquences sur la régénération musculaire. Nous prévoyons donc de réaliser une analyse Cut&Run dans les muscles squelettiques régénératifs afin de mieux dévoiler les mécanismes par lesquels les AR contrôlent la structure des fibres.

En résumé, nos données fournissent de nouvelle information sur le rôle potentiel de la signalisation des AR dans les CS et son effet sur la régénération des muscles squelettiques. La compréhension des fondements moléculaires par lesquels les androgènes régulent l'homéostasie des CS ouvre des perspectives innovantes pour le développement de stratégies thérapeutiques pour la régénération musculaire après une blessure causée par un traumatisme ou une dégénérescence dans les dystrophies musculaires et le vieillissement.

Références.

Alfaro, L. A., et al. (2011). "CD34 promotes satellite cell motility and entry into proliferation to facilitate efficient skeletal muscle regeneration." Stem Cells **29**(12): 2030-2041.

Azariadis, K., et al. (2017). "Androgen Triggers the Pro-Migratory CXCL12/CXCR4 Axis in AR-Positive Breast Cancer Cell Lines: Underlying Mechanism and Possible Implications for the Use of Aromatase Inhibitors in Breast Cancer." Cell Physiol Biochem **44**(1): 66-84.

Bae, G. U., et al. (2008). "Regulation of myoblast motility and fusion by the CXCR4-associated sialomucin, CD164." J Biol Chem **283**(13): 8301-8309.

Bhasin, S., et al. (2000). "Testosterone replacement and resistance exercise in HIV-infected men with weight loss and low testosterone levels." JAMA **283**(6): 763-770.

Cho, D. S. and J. D. Doles (2017). "Single cell transcriptome analysis of muscle satellite cells reveals widespread transcriptional heterogeneity." Gene **636**: 54-63.

Charrin, S., Latil, M., Soave, S., Polesskaya, A., Chrétien, F., Boucheix, C. and Rubinstein, E., 2013. Normal muscle regeneration requires tight control of muscle cell fusion by tetraspanins CD9 and CD81. *Nature Communications*, 4(1).

Davey, R. A. and M. Grossmann (2016). "Androgen Receptor Structure, Function and Biology: From Bench to Bedside." Clin Biochem Rev **37**(1): 3-15.

De Micheli, A. J., et al. (2020). "Single-Cell Analysis of the Muscle Stem Cell Hierarchy Identifies Heterotypic Communication Signals Involved in Skeletal Muscle Regeneration." Cell Rep **30**(10): 3583-3595 e3585.

Diel, P., et al. (2008). "C2C12 myoblastoma cell differentiation and proliferation is stimulated by androgens and associated with a modulation of myostatin and Pax7 expression." J Mol Endocrinol **40**(5): 231-241.

Gali Ramamoorthy, T., et al. (2015). "The transcriptional coregulator PGC-1beta controls mitochondrial function and anti-oxidant defence in skeletal muscles." Nat Commun **6**: 10210.

Gunther, S., et al. (2013). "Myf5-positive satellite cells contribute to Pax7-dependent long-term maintenance of adult muscle stem cells." Cell Stem Cell **13**(5): 590-601.

Jankowski, R. J., et al. (2002). "The role of CD34 expression and cellular fusion in the regeneration capacity of myogenic progenitor cells." J Cell Sci **115**(Pt 22): 4361-4374.

Kim, J. H., et al. (2016). "Erratum: Sex hormones establish a reserve pool of adult muscle stem cells." Nat Cell Biol **18**(10): 1109.

Kuang, S., et al. (2007). "Asymmetric self-renewal and commitment of satellite stem cells in muscle." Cell **129**(5): 999-1010.

Seo, J. Y., et al. (2019). "Unraveling the Paradoxical Action of Androgens on Muscle Stem Cells." Mol Cells **42**(2): 97-103.

Sinha-Hikim, I., et al. (2004). "Androgen receptor in human skeletal muscle and cultured muscle satellite

cells: up-regulation by androgen treatment." J Clin Endocrinol Metab **89**(10): 5245-5255.

Tedesco, F. S., et al. (2010). "Repairing skeletal muscle: regenerative potential of skeletal muscle stem cells." J Clin Invest **120**(1): 11-19.

Wang, Y. X. and M. A. Rudnicki (2011). "Satellite cells, the engines of muscle repair." Nat Rev Mol Cell Biol **13**(2): 127-133.

Wosczyna, M. N. and T. A. Rando (2018). "A Muscle Stem Cell Support Group: Coordinated Cellular Responses in Muscle Regeneration." Dev Cell **46**(2): 135-143.

Yang, W. and P. Hu (2018). "Skeletal muscle regeneration is modulated by inflammation." J Orthop Translat **13**: 25-32.

Kamar GHAIBOUR

Unravelling the Role of Androgens in Skeletal Muscle Progenitor Cells and Myofibers

Résumé

Les androgènes sont des hormones stéroïdes qui exercent des fonctions pléiotropes chez les mammifères, notamment sur la prolifération cellulaire, la mise en place des caractéristiques sexuelles et du comportement, le métabolisme, ainsi que le contrôle de la masse et de la force musculaire. Les effets de ces hormones sont relayés par le récepteur des androgènes (AR), qui appartient à la superfamille des récepteurs nucléaires.
Les muscles squelettiques sont principalement composés de myofibres contractiles et d'une population de progéniteurs musculaires résidant dans un état quiescent à leur périphérie, appelés cellules satellites (SatC).
Dans cette étude, nous montrons que AR contrôle les principales voies métaboliques dans la fibre musculaire, y compris la glycolyse et l'oxydation des acides gras. En l'absence d'AR, le muscle ne parvient pas utiliser le glucose, ce qui maintient ses niveaux sanguins à un niveau très élevé, mais catabolise les acides aminés, augmentant le stress oxydatif et la production d'ammoniac, ce qui a pour effet d'altérer les fonctions mitochondriales. Ainsi, notre étude révèle que AR contrôle le métabolisme des myofibres, protégeant les souris du développement du diabète de type 2.
De plus, nos données montrent qu'en l'absence de AR les SatC ne maintiennent pas leur quiescence dans des conditions homéostatiques et présentent des défauts dans leur niche. Nos données du cistrome de AR montrent que ce dernier contrôle l'expression des principaux gènes impliqués dans la dormance des SatC, notamment *Pax7* et *Klf7*. Une fois activées, la prolifération des SatC dépourvues de AR est dérégulée, conduisant à long terme à la perte de la population de cellules progénitrices. En outre, au cours de la régénération musculaire, les SatC génèrent des myofibres dystrophiques avec des défauts dans la capacité de contraction en l'absence de AR.
Dans l'ensemble, Cette étude nous a permis d'éclaircir les mécanismes moléculaires et cellulaire par lesquels AR régule l'homéostasie musculaire, et ouvriront de nouvelles vois dans le traitement de myopathies et maladies métaboliques.

Mots clés : Muscle squelettiques, myofibres, cellules satellites, quiescence, cellules souches, differenciation, régénération musculaire, metabolisme.

Résumé en anglais

Androgens are steroid hormones that exert pleiotropic functions in mammals, including cell proliferation, development of sexual characteristics and behavior, metabolism, as well as the control of muscle mass and strength. The effects of these hormones are mediated by the androgen receptor (AR), which belongs to the nuclear receptor superfamily.
Skeletal muscles (Skm) are mainly composed of contractile myofibers and a population of muscle progenitors residing in a quiescent state named satellite cells (SatC).
In this study, we unveil that AR control main metabolic pathways in Skm fiber, including glycolysis and fatty acid oxidation. In the absence of AR, Skm fails to utilize energy sources keeping blood glucose levels very high, but enhances amino acid consumption, that generates oxidative stress, ammonia production, thereby affecting mitochondrial functions. Thus, we establish that AR controls myofiber metabolism and homeostasis, protecting mice from the development of type-2 diabetes.
Moreover, our data in SatC show that in the absence of AR cells do not sustain quiescence in homeostatic conditions and exhibit defects in their niche. Our cutting-edge AR cistrome data show that it controls the expression of main genes involved in SatC dormancy including Pax7, and Klf7. Upon activation, AR deficient SatC showed deregulated proliferation leading in the long term to the loss of the stem cell population. In addition, SatC generated dystrophic myofibers with defects in contraction capacity in mutant mice.
Taken together, our data present AR as key regulator of skeletal muscle homeostasis in physiological and regenerative conditions through control of muscle progenitor cell integrity and myofiber metabolic activity.

Keywords: Skeletal muscles, muscle regeneration, satellite cells, myofibers, nuclear receptor, androgen receptor, androgens, ARE, quiescence, stem cells, differentiation, ChIP-seq, Cut&Run.